# A STUDY OF RF-OVER-FIBRE BASED ACTIVE RFID INDOOR LOCATION SYSTEM

*Yanchuan Huang*

*Supervisor:*

*Prof. P. V. Brennan*

A thesis submitted for the degree of
Doctor of Philosophy
of
University College London

Department of Electronic and Electrical Engineering
University College London
Feb. 2011

I, Yanchuan Huang, confirm that the work presented in this thesis is my own and has not been submitted in any form for another degree or diploma at any university. Where information has been derived from other sources, I confirm that this has been indicated in the thesis.

# Abstract

Location systems developed for indoor environments have attracted increasing interest, as a result of the rapidly growing location and navigation services provided by the Global Positioning System (GPS). Location information of people and objects can be used to cooperate with existing communication or database systems to provide abundant services to system operators and end users. For example, equipment tracking in hospitals ensure that location of the appropriate equipment can be provided simultaneously with necessary medical services; attendee tracking at conferences may encourage more efficient communications and networking; location of valuable assets in factories or warehouses aids logistics and protects these assets from theft. Since established global and terrestrial navigation systems cannot provide reliable location services in indoor environments, these demands are increasingly being met by wireless indoor location systems.

A review of the existing systems reveals that the current systems are able to provide either an accurate location service with sophisticated system design at higher cost or a less accurate location service by means of integrated systems supplemented by existing facilities.

This thesis presents a novel design of an indoor location system that is based on an RF-over-fibre backbone network, which is able to provide high location accuracy while the network infrastructure can be shared with multiple wireless systems. It is the first such demonstrator in this area. This research has been conducted by the author through a research project called The Intelligent Airport (TINA), which is the motivation for this research.

The TINA project seeks to develop a new seamless wireless/wired ubiquitous infrastructure with high levels of computational capability to meet the application requirements of future airport environments. In the TINA system, multiple wireless services are provided through an integrated system supported by an RF-over-Fibre network, which transports RF signals through optical fibres. The active RFID indoor

location unit is an essential part of the TINA system, which will facilitate the infrastructure to provide location-based services.

The thesis describes the detailed design of the active RFID indoor location system proposed for the TINA project, and a few key issues discovered during trials of the demonstration system developed. The overall system design, including ranging technique, TDOA location finding algorithm, and hardware implementation, is presented in this thesis. Particular contributions also include a numerical algorithm for solving target location from TDOA measurement and a technique to determine the chirp linearity requirement. The field trial results of the system design demonstrate the principals and their location performance. The system has the potential to be extended to other scenarios where RF-over-fibre networks are employed and accurate location ability is desired.

# Acknowledgements

I would like to express my sincere appreciation to Prof. Paul Brennan for his continuous and valuable supervision during the research. I am also very grateful to Dr. Chin-Pang Liu for the nice time we had working together, as well as the important technical assistance and guidance I received from him. Special thanks to Prof. Alwyn Seeds, Dr. Tab Ismail, Dr. Kenneth Tong, Dr. Thomas McCoy, and Dr. Richard Bullock for their great ideas and very useful advices.

I am also very appreciative to many friends for their help in the past few years, especially those in the Department of Electronic and Electrical Engineering at UCL, including Dr. Dai Jiang, Dr. Hongyu Wang, Dr. Marc Thomas, Dr. Pier F. Sammartino, Dr. Alessio Balleri, Waddah Al-Ashwal, Matthew Ash, and Chris Banahan, who have provided their hearty help in various ways.

The work contained in this thesis is a part of the Intelligent Airport research project, which is kindly funded by the Engineering and Physical Sciences Research Council. I would like to thank them for sponsoring this project too as otherwise this work would not have been possible.

No words can express my appreciation and gratitude to my parents, Mr. HUANG Sanwei and Mrs. HUANG Shunying, for their constant love and encouragement, which have been the most important support for me.

# Contents

# List of Figures

# List of Tables

# Acronym

| | |
|---|---|
| **ADC** | Analogue-to-Digital Converter |
| **AFPM** | Asymmetric Fabry-Perot Modulator |
| **AOA** | Angle Of Arrival |
| **AP** | Access Point |
| **ASIC** | Application-Specific Integrated Circuit |
| **AU** | Antenna Unit |
| **BPF** | Band-Pass Filter |
| **CDMA** | Code Division Multiple Access |
| **CEP** | Circular Error Probability |
| **CRLB** | Cramer-Rao Lower Bound |
| **DAQ** | Data Acquisition |
| **DDS** | Direct Digital Synthesizer |
| **DLL** | Dispersive Delay Line |
| **DLOS** | Direct Line Of Sight |
| **DSP** | Digital Signal Processor |
| **DSSS** | Direct Sequence Spread Spectrum |
| **ETSI** | European Telecommunications Standards Institute |
| **FFT** | Fast Fourier Transform |
| **FH** | Frequency Hopped |
| **FM** | Frequency Modulation |
| **FMCW** | Frequency Modulated Continuous Wave |
| **FPGA** | Field Programmable Gate Array |
| **FSV** | Fractional Slope Variation |
| **GPIB** | General Purpose Interface Bus |
| **GPS** | Global Positioning System |

| | |
|---|---|
| **GSM** | Global System for Mobile Communications |
| **HF** | High Frequency |
| **IF** | Intermediate Frequency |
| **ISM** | Industrial, Scientific and Medical (radio bands) |
| **LF** | Low Frequency |
| **LFM** | Linear Frequency Modulated |
| **LO** | Local Oscillator |
| **LOS** | Line-Of-Sight |
| **LS** | Least Square |
| **LTE** | Long Term Evolution |
| **MMF** | Multi-Mode Fibre |
| **ML** | Maximum Likelihood |
| **NLOS** | Non-Line-Of-Sight |
| **PLL** | Phase Lock Loop |
| **PN** | Pseudo-Noise |
| **RDOA** | Range Difference Of Arrival |
| **RF** | Radio Frequency |
| **RFID** | Radio Frequency Identification |
| **RMS** | Root Mean Square |
| **RMSE** | Root Mean Square Error |
| **RSS** | Received Signal Strength |
| **RTLS** | Real-Time Location System |
| **RVP** | Residual-Video-Phase |
| **RoF** | RF-over-Fibre |
| **SAR** | Synthetic-Aperture Radar |
| **SAW** | Surface Acoustic Wave |
| **SNR** | Signal to Noise Ratio |

| | |
|---|---|
| **SMS** | Short Message Service |
| **STD** | Standard Deviation |
| **STFT** | Short Time Fourier Transform |
| **TDOA** | Time Difference Of Arrival |
| **TF** | Time-Frequency |
| **TINA** | The INtelligent Airport |
| **TOA** | Time Of Arrival |
| **UHF** | Ultra High Frequency |
| **UT** | User Terminal |
| **UWB** | Ultra-Wideband |
| **VCO** | Voltage Controlled Oscillator |
| **WDM** | Wavelength Division Multiplexing |
| **WLAN** | Wireless Local Area Network |

# *Chapter 1*

## INTRODUCTION

The term ‘indoor location system’ usually refers to those wireless systems that attach small wireless tags (operating as either transmitters or receivers, or both) onto the objects to be located, or assign them to personnel. A wireless network of reference stations around the area to be covered communicate with the tags. By analyzing the received radio signal relative to the known reference stations, the 2-D/3-D position of the tag can be found.

These kinds of services have found application in a variety of areas. For example manufacturer warehouses, hospitals, sport stadia, conference centres, farms, and communication systems. Since the applications are diverse, there have been lots of ideas proposed on this topic and many names have been used to describe the same concept, such as real-time location system (RTLS), indoor positioning system, indoor localization system, and indoor location sensing/finding system.

The work presented in this thesis was undertaken through a broader project, namely the Intelligent Airport (TINA), whose goal is to develop an integrated wired and wireless communications infrastructure for the next generation airport services. The RF-over-fibre (RoF) based active RFID (radio frequency identification) indoor location system is designed to manage the personnel, passengers, and movable properties in an airport.

In this Chapter, we will firstly introduce the motivation and objectives of this research project. Set against the objectives, the main results and contributions of this thesis are then summarised in the Section 1.3. The outline of this thesis will also be given in the last section.

## 1.1 Global Positioning System

The Global Positioning System (GPS) is a global navigation satellite system that provides location information to the users anywhere on or near the earth. Indoor location systems have drawn increasing attention since the great success of civilian services of GPS in the last decade [1;2]. Having initially served as military aids, the GPS system operated by the U.S. Department of Defense has become a dual-use system available for both military and commercial applications since the removal of "Selectivity Availability" of non-degraded GPS signals in the year 2000 [3]. It is estimated by the market analyst firm Canalys that there are currently over 68 million GPS users globally now, reflecting the strong demand for the location-based services that it enables.

The location method of GPS is trilateration, which determines the location by intersecting at least three spherical surfaces whose centres and radii are given. The GPS satellites continuously transmit timing messages to the users on earth. A GPS receiver that sees four or more satellites is able to use the received timing messages to calculate the distances to these satellites.

The GPS location service is accessible all over the world, so long as there are line-of-sight paths between four or more GPS satellites and the receiver. However, in indoor scenarios satellite signals suffer attenuation by the construction and multipath reflection off the walls. The GPS service becomes unreliable and sometimes unavailable.

Also, location services for indoor applications require finer accuracy than the civilian GPS service can provide. It is reported by Vossiek et al. [4] that one metre location accuracy has not been readily achievable by satellite positioning system to date. Recently, progress has been made to enable indoor operation of GPS services using assisted GPS receivers [5], which also utilises the mobile network service to assist GPS operation in indoor environment.

However, to fulfill the growing interest in indoor location services, there have been even more efforts spent by researchers in developing self-contained systems for locating people and objects in indoor environments [6]. This thesis is one such effort in designing a dedicated location system for use in indoor environments.

## 1.2 TINA-The Intelligent Airport

Fuelled by the growth of international air traffic, airports are now amongst the most complex environments known. Airport terminals will increasingly require ubiquitous systems with computational ability to provide the necessary intelligent automation; to provide high quality services to passengers; stringent levels of safety and security that are as unobtrusive as possible; efficient processing of commercial goods and luggage; high quality information systems; airport transportation systems and appropriate support for in-house commercial ventures. The demand for indoor location service in airport is high, as most international airports are expecting a growing number of travelers who are potential users of location-based services.

The TINA project seeks to develop such a new seamless wireless/wired ubiquitous infrastructure with high levels of computational power to meet the application requirements of airport environments. While it is proposed to suit the increasingly critical demand of airport operators, it also provides a new opportunity for designing novel indoor location system. The RoF infrastructure it is based on has the potential to aid a compact but reliable indoor location system which has not been investigated before.

The active RFID indoor location unit is an essential part of the TINA system. The indoor location unit in TINA is able to firstly remind passengers of the departure time of their flights; secondly navigate passengers for various services or activities in airport; and thirdly provide location information to both operators and vendors in airport. Moreover, it may facilitate location-aided radio resources management, which is an effective way of assigning wireless resources.

In addition, supplementing an indoor location unit with the RoF network of TINA system is especially convenient. The RoF backbone provides transparent link between antenna units and central signal processor to RF signals, whose qualities decide the performance of an indoor location system. Assuming 20 metre length of cables are required to connect the antenna units with their receivers in a 20 m×20 m cell, then for a modest airport terminal size with an area of 1 $km^2$, the total length of cables required to cover the whole terminal is 50 km. If coaxial cables are used, the power

attenuation due to a 20 metre long cable alone will be around 10 dB. For optical fibres of the same length, the power attenuation is trivial, at about only 0.005 dB.

This thesis aims to design a novel active RFID indoor location system that is incorporated with TINA infrastructure, or can potentially be employed in places where RoF network is available. The TINA project does provide a valuable opportunity for the investigation of RoF based indoor location system, and the system design presented in this thesis is not limited to airport applications. In fact, the trend of broader applications of RoF is observed in recent years[7;8]. For example, in the wireless communications sector, RoF is used to link microcell and picocell systems in buildings [9]. As RoF technology being adopted by more and more manufacturers for telecommunications equipment [10;11], it can be foreseen that RoF infrastructure will be increasingly available in indoor environments. The system design presented here can be used as a basis for development of indoor location systems for these environments.

## 1.3 Contribution of the Thesis

The work presented in this thesis has made novel contributions to the field of indoor location systems in the following respects.

- A novel RoF based indoor location system has been designed (Chapter 5). The employment of a RoF backbone centralises the RF signal processing and the time measurement functionality. The system structure is consequently simplified such that the user terminals can be implemented with low-cost transmit-only RFID tags; the antenna units only deal with reception and transportation of RF signals; synchronisation among the antenna units can be achieved by simultaneous sampling in the central controller of the system.
- During the research of the proposed system, a novel and practical numerical algorithm for finding location from the time difference of arrival (TDOA) measurements has been developed. This is particularly suitable for confined indoor area situations where targets are mainly in the near field of the antenna pairs. Simulation and analysis (Chapter 4) has shown that the algorithm is able to achieve accurate location result similar to the optimum Taylor algorithm

[12]. However, the proposed algorithm is free from the difficulty of convergence that the Taylor algorithm suffers.

- Also, the proposed TDOA mapping algorithm can be used as a tool to estimate the error patterns of TDOA location results for given positions of sensors. Placement of TDOA location sensors can be designed according to specific location accuracy requirement (Chapter 6).
- A new parameter, fractional slope variation (FSV), which describes the non-linearity of a linear frequency modulated (LFM) chirp signal, is derived. It is shown that this parameter can directly relate chirp linearity with maximum detection range for non-distorted deramp processing of chirp signals (Chapter 3). It can be used to either estimate the chirp non-linearity requirement for a given detection range, or to define the distortion-free area if the chirp signal source is provided.
- Multipath propagation effects in indoor environment and their impact on the time measurement accuracy from chirp deramping is studied (Chapter 5). By analysing the multipath resultant components present at the deramped output, two convenient frequency detection strategies are used to improve the time measurement accuracy under multipath conditions. Simulation and measurement results have shown satisfying improvement from application of these simple strategies.
- A demonstration system according to the proposed design has been developed. This is, to the best of the author's knowledge, the first demonstration system of its kind. Location results from three trials have shown good agreement with the simulated error patterns (Chapter 6). More importantly, the statistics of the location results indicate that sub-metre location accuracy is achievable with the proposed system design.

## 1.4 Outline of the Thesis

The remainder of this thesis is divided into six chapters. Chapter two is a review of the technologies, applications, and system solutions in the area of indoor location sensing.

Chapter 2 provides a short overview of the indoor location applications, location technologies, and the existing indoor location systems. Different types of location methods and their implementation using various wireless technologies are also summarised. Features of the existing indoor location systems are compared in terms of their location performance, and system complexity.

Chapter 3 presents the deramp technique used to measure time delay involved in chirp signals. Signal processing models for both time of arrival (TOA) and time difference of arrival (TDOA) measurements are introduced and the limitations on measurement resolution are derived. Furthermore, the frequency non-linearity effect of chirp is studied and evaluated by a new parameter, the fractional slope variation. The non-linearity impact on the time measurement resolution of deramp technique can be estimated using this parameter.

Chapter 4 deals with the location finding algorithm using the time delay information obtained from deramping the received chirps. A one-cell indoor location system is modeled and the TDOA mapping algorithm is introduced using this example. The potential location accuracy and applicability to more complicated scenarios of this algorithm are evaluated. The performance of the proposed algorithm is compared with two classic TDOA location estimation algorithms in simulation.

Chapter 5 presents the detailed design of the TINA indoor location system. It starts with the system architecture for the entire system. The RoF technology is introduced and the RoF backbone used by the TINA demonstration system is described. The fundamental chirp generator of the RFID tags is chosen after a comparison of various chirp generation methods. A multiple access technique that is suitable for LFM chirp signals is employed and the corresponding design method is derived. Implementation of the location algorithm in LabVIEW is also described. Among the processing steps, the frequency detection strategy at the deramped signal stage is of greater concern as it decides the time measurement accuracy and thus the eventual location accuracy. The impact of multipath propagation is also clearly observed in the deramped signal. Therefore, special attention has been paid to the frequency detection strategies. Two simple and practical strategies are proposed in this Chapter. It is found that improvement in the time and range measurement can be achieved after application of these strategies.

Chapter 6 concerns the trials of the proposed system. The trial site and the demonstration system are described. Three different trials with various number of sensors located at different positions were executed. The trial results are interpreted using four different measures. The location results show good correlation with the theoretical prediction; in terms of both overall accuracy and the error spreading patterns. In general, sub-metre location accuracy was achieved in the three trials.

Chapter 7 then draws the conclusions of the work and identifies a few aspects that are worthy of further investigations.

# *Chapter 2*

## BACKGROUND OF INDOOR LOCATION SYSTEMS

Perhaps some of the earliest work on indoor location systems took place in the late 1980s in the subject of ubiquitous computing [13]. Since then, the early attention and effort has been put into military and industrial applications, while civil usage of indoor location systems is a comparatively new application occurring in the last decade. Along with the FCC's (the Federal Communications Commission) approval of the 3.1 to 10.6 GHz spectrum to ultra-wideband technology, high accuracy indoor location systems gained another wave of interest and various solutions have since been developed [14]. On the other hand, the wide use of IEEE 802.11b wireless LAN services has triggered the demand for location ability based on existing wireless systems.

This Chapter firstly introduces the concept of RF indoor location systems (Section 2.1), and some potential application scenarios (Section 2.2) of indoor location system. More importantly, the conventional location methodology and the popular wireless technologies used by existing indoor location systems are described in the following sections. A number of typical indoor location systems will also be presented and compared.

## 2.1 Indoor Location Systems

Both the names of indoor location system and indoor positioning system are used in literature to describe a system that has the ability to find the location information of its users. However, the difference between these two names is that, *location system* refers to a system that can locate the users, e.g. real-time location system (RTLS) [15], while *positioning system* provides the information for the users to compute the location of themselves, [16] e.g. Global Positioning System.

## 2.1.1 Architecture of Indoor Location Systems

Regarding the system involved in this research, the term location system is more appropriate. Figure 2-1 illustrates an architecture for the typical wireless indoor location system. Indoor location systems generally consist of the following key components: a set of wireless sensors used to sense the metrics (time, signal strength, angle of incoming signal) that contain the hints (range, direction) to the location of the targets (people or objects), the user terminals (UT) that transmit radio signal or response to the location request from the sensors, a location estimation module that collects the measured metrics and runs an algorithm to determine the location of the UT, an application program which can combine location and other useful information to provide a service to the operators and users of the system.

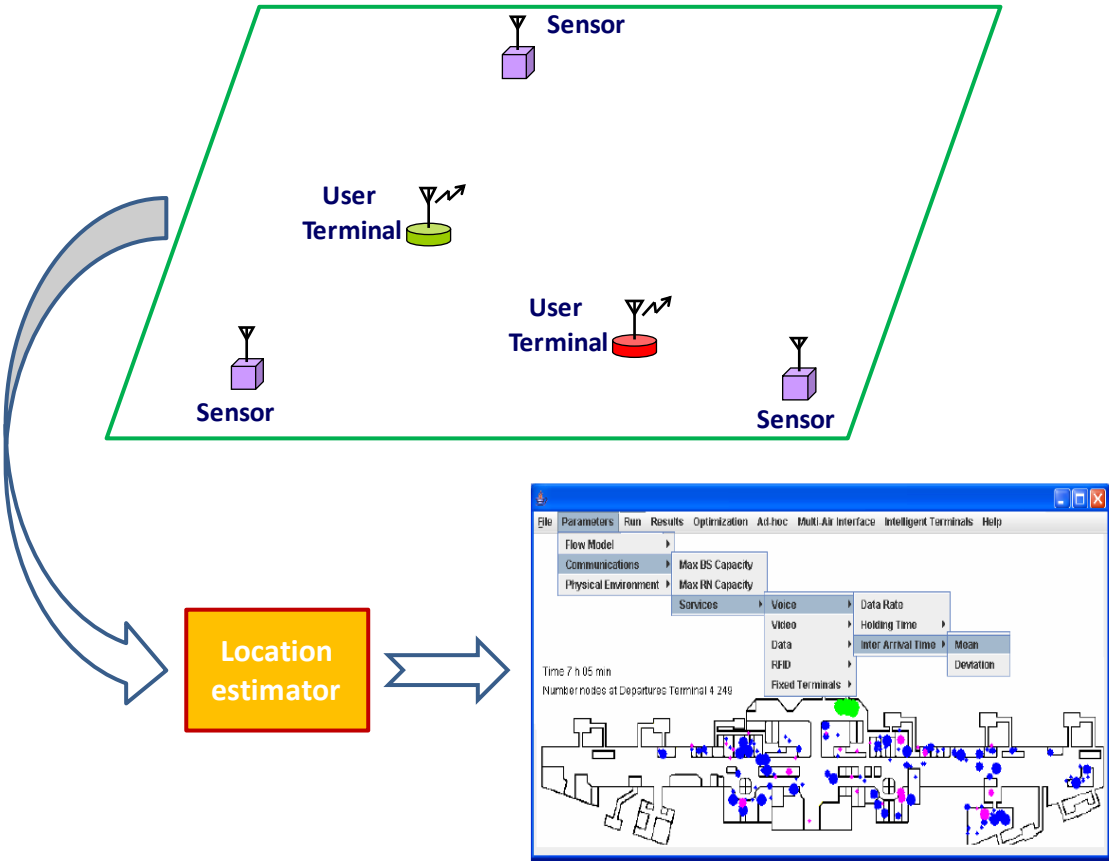


**Figure 2-1 Components of typical indoor location system**

The sensor in an indoor location system is a single module that receives, and processes the radio signal to compute the physical information needed by the following location algorithm, which will be covered by Chapter 4. Sensors can be the

wireless receivers deployed around the indoor area purely for the purpose of locating UT, or they can be part of an existing wireless infrastructure providing variety of services.

The user terminal is usually in form of a small passive or active RF device, (e.g. tags, mobiles, laptops), that can be worn by people or attached to objects of concern. Locations of the people and objects carrying UTs can be found when they are present in the area covered by the indoor location system.

The term cell is used to describe a unit of indoor area served jointly by a number of sensors who work together to find the location of UT in this cell. Size of cell varies from system to system, depending on the radio technology, transmit power, type of sensors. Different cell size and shape may co-exist in one indoor location system according to specific scenario.

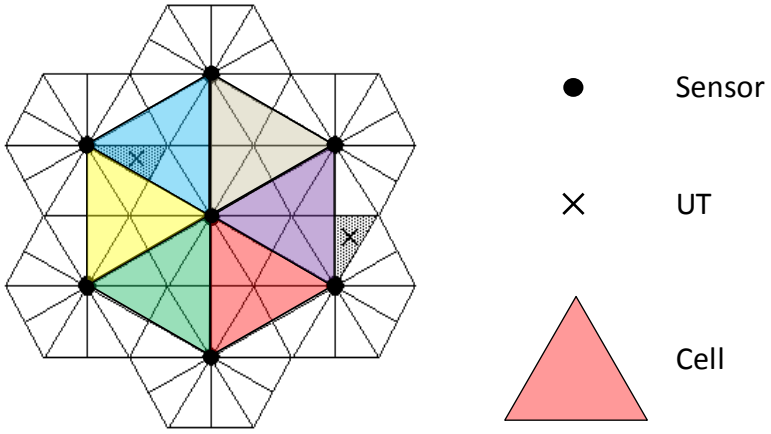


**Figure 2-2 Six indoor cells served by six different combination of three sensors**

Whereas a cell is served by a number of sensors, a sensor may be serving a few cells. Figure 2-2 illustrates a situation where there are six triangular cells, each of which is overlapped by a service area of three sensors. The sensor in the centre is serving all the six cells shown on the figure.

Since the sensors are distributed around the indoor area of concern, the total set of sensors is described as the remote site of the indoor location system. The location estimator, which may be physically located at a central control room, is defined as the central site of the indoor location system.

### 2.1.2 Types of Indoor Location System

There are two types of design approach for a wireless indoor location system. The first one is to develop a new self-contained system, including receivers and user terminals, whose sole purpose is to identify the location of the signal source. The other approach is to use an existing wireless network infrastructure and take advantage of its wireless signals to locate a target, which is probably the user of the corresponding wireless service.

The advantage of the first type of indoor location system is that the designers have full control over the physical specifications and, consequently, the quality of the location finding results, leading to higher accuracy and system performance. Systems in this category usually include the complete hardware and software relevant to the location finding tasks. Therefore, this type of systems needs to be installed specially in the area of interest, and maintenance of such systems requires specific cares too.

The advantage of the second type of indoor location system is that it avoids expensive and time-consuming deployment effort for new infrastructure and is capable of being quickly adopted by many applications. These systems, however, need to be supplemented with additional intelligent algorithms to compensate for the low accuracy of the measured metrics.

Besides the design approach, there are other ways of categorizing indoor location systems, for example, by the wireless technology employed.

As a wireless system, indoor location system must utilise a kind of wireless communication technology or protocol. Due to high penetration, WLAN is the most popular wireless technology for the indoor location systems developed over existing wireless network. Some use standard RFID technology, e.g. active UHF RFID tags and readers while more commonly people prefer specialized RFID systems using wideband technology such as UWB. Detailed discussion regarding the wireless technology options for indoor location system will be given in the Section 2.5 of this Chapter.

When discussing relative location performance, the location finding method may be used as a way to differentiate various location systems. For instance, some of the

systems may measure the signal propagation time in order to derive the range between the signal source to a sensor, a method known as time of arrival (TOA) measurement. In some cases, the power level of the received signal can be used to estimate the range. There are also systems measuring time difference of arrival (TDOA), and angle of arrival (AOA) information and the location algorithms behind these methods are variable. Systematic location performance is very much relevant to the location method adopted by a system. Consequently, we will devote a section, Section 2.3, to reviewing these different location methods.

## 2.2 Applications of Indoor Location Systems

Potential applications for the indoor location system include factory automation systems, personal advertising in shopping malls, airport security, virtual experience, consumer behaviour tracking, and asset management.

### 2.2.1 Industrial Manufacturing Management Systems

Intense competition increasingly creates the need for manufacturing companies to develop and sustain competitive advantage. Cost advantage, derived from production efficiency, is one of these advantages. Indoor location sensing can improve production efficiency through better production monitoring and controlling. Car manufacturers, for example, can apply this technology to track each step of its car manufacturing on the assembly line. What model is being built, how far along is the process and what type of mechanic is being assembled can be monitored effectively from the start. Time used at each station and possible delay in production line can then be recorded and analyzed to mitigate future inefficiencies. Luxury car manufacturers that depend considerably on customized production can apply this tracking technology to monitoring each order to ensure that orders are fulfilled in a timely manner. Besides car manufacturers, other potential customers for this indoor tracking technology include high-price-items-manufacturing related companies, such as electronic manufacturers, which operational efficiency relies on time and process management.

The WLAN based indoor location systems have been adopted by the majority of the manufacturer clients. Although WLAN is relatively inferior in terms of accuracy and precision, its lower base station costs and ability to integrate with other or pre-existing systems in factories make WLAN an outstanding choice. Although it cannot precisely locate where the item really is in the factory, it works well enough to serve operation management. An alternative to location sensing technology is the conventional tracking method that tracks items when they pass each production station along the assembly line. For mission critical applications such as manufacturing automation, higher location accuracy systems may be needed and UWB systems have found application in these situations.

### 2.2.2 Conference Site and Amusement Park Attendee Tracking

Modern industrial and academic conferences are being held everywhere in the world every day. Typically, hundreds or thousands of attendees pay a great amount of money to participate in an event which lasts for only a few days, with the hope of consulting with interested stakeholders, e.g. clients, regulation officers, vendors, and certain experts.

However, in spacious conference sites, meeting a particular person in a short social section really require a measure of luck. One might be asking around or spend a long time seeking in order to identify and meet a few of the people he wants to know.

Indoor location systems provide another option to these attendees to make their participation more worthwhile. User tags with location ability can be distributed to the attendees, and the location of these can be accessed through the information desk in the conference. The tags may contain even more information about the holders and therefore people can set specific search criteria to identify the people they might be interested in. Conference organizers may make it an optional and chargeable service to the attendees too.

Amusement park presents a similar scenario, where there are also many people spending their valuable holidays in search of memorable fun. Location-capable tags may be carried by staff and visitors. For visitors, they can use the location service to

find specific rides/attractions, and possibly track their children playing in the park. For staff, the location information of their customers may help them reunite individuals with their group, guide the attendees to certain places, and maintain security in the park.

In these applications, location accuracy of 1 to 2 m level is desired and the location targets are human beings and the scale of the indoor or outdoor area may be very large.

### 2.2.3 Personnel and Equipment Tracking in Hospital

Hospitals are also a scenario where indoor location systems may be beneficial. Big hospitals can be such busy places that everyday there may be hundreds or even thousands of visitors, seeking timely and precise diagnosis and treatment.

In some cases, many items of equipment are hard to find as they are either in use or in storage. The results are over inventory and underutilization of assets. More seriously, in emergency cases, the ability to collect adequate doctors, nurses, and medical equipments may be a life-and-death matter. However, the staff in hospital may not be confined to a single place all the time, while some important equipments may not be in place as they are usually shared by a few groups of people.

An indoor location system that is able to detect the proximity of certain personnel and track the location of portable equipment can provide valuable information to the hospital to improve the healthcare procedures, and save lives.

On the other hand, in hospitals where there are a large number of inpatients, some of whom may be advised to take walks around the hospital to assist healing, location tags may be given to these inpatients when they are away from their wards so that the nurses can track their locations in the hospital to ensure they are within a certain boundary and identify potential emergencies.

For hospital applications, room-level location accuracy is properly sufficient for most situations. Also, full coverage around the entire hospital will be essential for this application. Therefore, RFID proximity detection systems and WLAN based location

systems are two popular options as their networks are easy to deploy and maintain while the user terminals are relatively of lower cost.

### 2.2.4 Personal Advertising in Shopping Malls

Getting messages across to target customers is one of the most important marketing aims for retailers. With various offerings competing for customers' attention in a typical shopping mall, creating awareness of current promotion is the challenge. Indoor tracking systems offer a solution for stores' marketers to communicate to the right audience at the right time and the right place by tracking where exactly they are and how much time they spend on similar types of stores to assess their main interests. With targeted advertising, this technology reduces a number of irrelevant advertising messages reaching customers. Select advertising also improve consumer readiness. A customer walking to or in a sporting section, for instance, will only receive sport equipment promotions but not kitchen-ware promotions. Besides traditional advertising, advanced mobile technology offers a better alternative to indoor tracking systems.

Under GSM, each SMS text can be tailored to each individual with more precise details as senders do not only know their location but also have more demographic information about receivers.

### 2.2.5 Airport Security

Safety has become a central concern for all airport authorities around the world. Various measures have been used to ensure that airport terminals, aircrafts and passengers are safe and secure. Apart from baggage checks and passenger screening procedures, systems to track movement of passengers inside the terminals have not yet been explored. With indoor tracking technology, airport authorities can observe movement of all or suspect passengers. Together with camera systems, airport authorities can make sure that safety is within their control. In this circumstance, a sensor is attached to a boarding pass, a document that every passengers need to carry

in hand before boarding the aircraft. Once boarded, airline staffs will collect the tags, making them reusable once new set of boarding passes are issued.

### 2.2.6 Virtual World Experience

With the expansion of the Internet, video entertainment is becoming more affordable and accessible to a larger group of people. Rapid innovation in video technologies has led to growth in 3D experience in movies and games sector. Virtual experience 3D gaming is another possible application for AD tracking systems. It could facilitate game players to map their position in the 3D virtual world and make the players feel what is happening to them on the screen is real.

However, the application of tracking systems in a virtual world experience requires high precision since the system needs to be able to locate the target in a narrow range, in centimetres instead of meters. UWB technology will have an advantage in the virtual experience space, given its accuracy potential.

### 2.2.7 Consumer Behavior Tracking

Understanding customers' needs and preferences are among the basic elements that are essential to marketers. But to be more successful in a highly competitive market such as the retailing industry, marketers need to thoroughly understand their consumers' behaviors, how they evaluate one choice over another, and how they shop in real settings. Research agencies have developed several methods, such as retail measurement tracking and consumer tracking panels, to understand what consumers buy and how they buy. Retailers have also developed ways to understand their consumers through store membership programs. Examples include Tesco Club Card, Sainsbury's Nectar Card and in-store observations.

Through store membership programs, retailers gather information about buyers' demographic, socioeconomic, product choices, expense amount spend per trip. These programs, however, do not offer information on how consumers spend their time evaluating choices and how they make their journey in the stores. Even customers

may end up not purchasing any shampoo, for example, knowing that they spend considerable amount of time in this section urge marketers to promote shampoo over other categories on their next visit. Moreover, knowing their journey in the stores also helps retailers with in-store layout. Categories that receive most traffic can be relocated behind sections that receive fewer visits in order to boost off-takes of slow moving categories.

Indoor location tracking offers great value to compliment retailers' already established consumer tracking systems/studies. Tracking sensors can be tagged to carts or baskets. At the end of the shopping trip, cashiers record the cart or basket numbers and scan purchases. Information is then mapped to identify shopping pattern of this particular customer.

Having introduced a number of possible applications of indoor location systems, we shall obtain an idea of what essential concerns may be raises when employing an indoor location system. Firstly, the type of indoor location system must provide the location accuracy needed by the scenario, as otherwise the required service will not be achieved. Secondly, existing wireless networks (e.g. WLAN, GSM) may be a preferred option in case the networks are in place and the required indoor location capability is met. By taking advantage of existing networks, the users may save great amount of time and cost installing the indoor location system. Beyond these two fundamental issues, user of indoor location system may also consider other concerns regarding size of tags, throughput of system, update rate, and surely cost.

## 2.3 Location Methodology

The location methodology is taking care of how to locate a target with the physical information sensed in the measurement process. The most popular metrics used are time and range, while in a fingerprinting system the target location is found by examining the radiation pattern of a received signal. Some conventional location finding methods are summarised as below.

## 2.3.1 Time of Arrival (TOA)

In the TOA method, the propagation delay of the radio signal between a sensor and a user terminal (UT) is measured. This delay reflects the time required for a signal to travel from a transmitter to a receiver. In the usual indoor environment where wireless signal propagates at constant velocity, this propagation delay is linearly proportional to the transmission range. Therefore, multiplication of the measured time delay with the signal propagation velocity gives the distance between the corresponding sensor and UT.

In a pure TOA system, obtaining the 2-D location coordinate of a UT requires at least three sensors, as shown by the Figure 2-3. The 2-D location is determined by finding the intersection of three circles corresponding to the three TOA measurements. Determining the 3-D location of a UT therefore requires four sensors and the location of UT is considered to be the intersection of four spheres corresponding to the four TOA measurements.

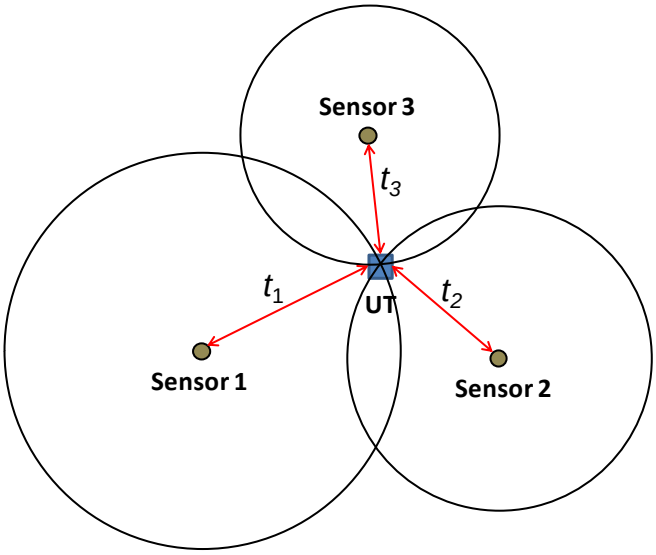


**Figure 2-3 Location finding method based on TOA/RTOF measurement**

Although the idea is simple, it comes with a cost. The TOA location method needs clock synchronisation among all the sensors and the UTs. To ensure location accuracy to one metre level, clock synchronisation of nanosecond precision is necessary, which is a high cost in terms of development time and effort.

To overcome the inherent difficulties of TOA measurements, the reflection time-of-flight can be measured instead. This is achieved by counting the time between a radio signal transmission and a received acknowledgment signal from the UT. By this means, fine clock synchronisation system might be avoided. However, the processing time of generating the acknowledgement signal must be highly predictable, which requires very stable hardware in the UT.

## 2.3.2 Time Difference of Arrival (TDOA)

Many of the existing indoor location solutions are based on a TDOA approach, which is to compute the location of a UT by measuring the time difference of arrival of a signal, transmitted from that UT, arriving at three or more sensors. Whereas TOA method records the time that a UT (tag) sends a signal to the sensors, TDOA requires that the sensors record when the signals were received. The sensors are placed at known fixed positions.

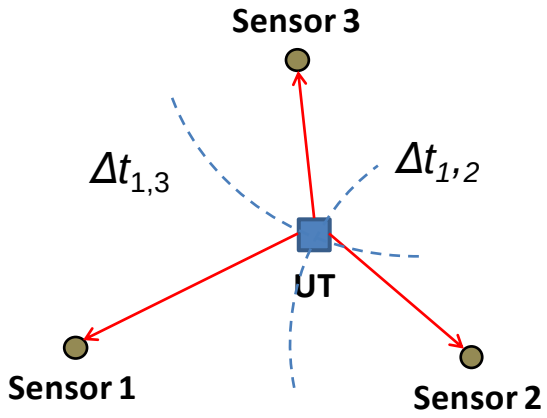


**Figure 2-4 Location finding method based on TDOA measurement**

For example, in an RFID location system, a signal emitted from an RFID tag will arrive at slightly different times at two spatially separated RFID receivers. Given the locations of the two receivers, we could find a series of tag locations that would give the same measured TDOA. The locus of possible tag locations is a hyperbola. Introducing a third receiver at a third location would provide another hyperbola. The intersection of the two hyperbola gives a curve on which the tag lies. The tag's location can be found from the 2-D point of view. If a fourth AU is introduced and placed at a plane different from the first three sensors, the 3-D position of the emitter

can be determined. Since the receivers do not need to know the absolute time at which the pulse was transmitted - only the time difference is needed, synchronisation between the tag and receivers can be ignored.

It shall be noted that, synchronisation among the receivers is still needed in order to find the time differences. Similar to the TOA case, synchronisation clock errors will cause errors in time difference measurements. Synchronizing the receivers through infrastructure is easier than synchronizing receivers with the mobile UT.

Location accuracy with the TDOA method is affected mainly by multipath, non-line-of-sight propagation, noise, and interference, which lead to inaccurate intersections of the hyperbolas.

### 2.3.3 Angle of Arrival (AOA)

In the angle of arrival approach, direction detection techniques, such as smart antennas, are used to detect the direction of a signal coming to the receiver. The sensors are placed at known positions. The location of the UT can be found by the intersection of several pairs of angle direction lines. This approach requires only two sensors for 2D positioning or three measuring units for 3D positioning. The measuring units also do not need to be synchronised.

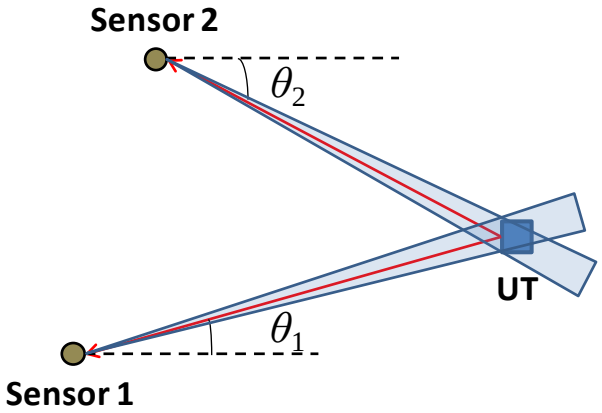


**Figure 2-5 Location finding method based on AOA measurement**

The drawback of this method is that, the accuracy of the AOA approach is limited by the directivity of the measuring antenna, whose accuracy is lower as the target moves

further away from the measuring unit. To take a measurement of angle with confidence, a complex set of antenna arrays is needed by each sensor. The angle measurement accuracy is positively correlated to the number of elements in the array. Accurate angle measurement therefore comes at the cost of a larger antenna size. In addition, angle measurement is rather sensitive to shadowing and multipath phenomena, which are common in the indoor environment.

### 2.3.4 Received Signal Strength (RSS)

The RSS location method is based on the fact that signal propagation loss is proportional to the square of the propagation path [17]. Given the transmitted and received signal power, it is possible to estimate the distance between the transmitter (e.g. a UT) and the receiver (e.g. a sensor) by applying the wireless indoor path loss model [18-20].

A practiced advantage of RSS method is convenience, in that it can be used on many existing wireless systems without modification to the existing hardware. The location system estimates the location of a UT using the computed ranges, resulted from the recorded RSS, between the UT and a few sensors. In such case, the location estimation algorithm is the same as the TOA method, although the range determination method is different.

However, in an indoor environment, multipath and shadowing make this range determination method based on pure RSS measurements not very reliable. The movement of surrounding people or vehicles in the area may result in change of the received signal strength. The disadvantage is obvious: any change to the environment may result in ambiguity in the estimated range.

Therefore, a sophisticated system usually takes both empirical measurements and signal propagation modeling into account in determining the UT location. For a cell area monitored by multiple sensors (at least three), a UT is placed at various known positions of interest in this area and the RSS from the sensors are recorded as the RF "fingerprint" of the corresponding coordinates. These measurements can be run for several times to average out the random errors, a process called training or calibration

cycle, [21] as the measurement RSS results are used to train the signal propagation model to fit the specific application environment. The diagrams presented in [21] are re-plotted below as an example of this RSS fingerprinting approach.

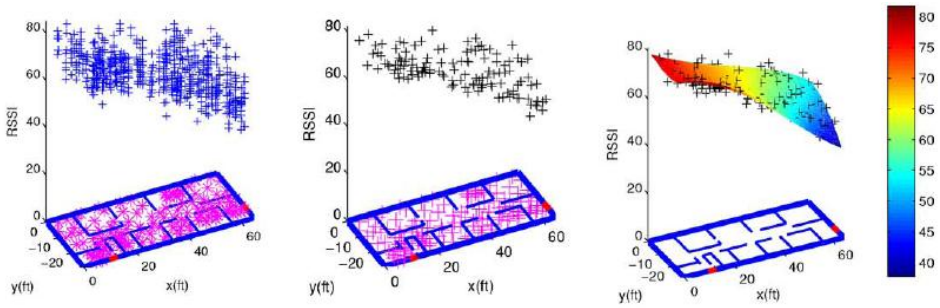


**Figure 2-6 (a) Raw RSS values recorded during the calibration cycle; (b) mean RSS values at each position of interest; (c) Fingerprint map plotted with the mean RSS values.**

From the calibration cycle, a map of fingerprints for the indoor location cell is computed using suitable indoor path loss model.[22] During real-time location measurements, the system compared the RSS observation at the sensors with the pre-stored fingerprint map in order to determine the UT locations.

The major advantage of the RSS fingerprinting method is its applicability to existing wireless infrastructures, as many of the wireless systems already have the functionality to measure RSS. Therefore, this method is widely adopted by indoor location systems based on WLAN[23], GSM, Bluetooth, ZigBee and UHF RFID[24] technologies.

However, in most cases so far, the overall location accuracy of RSS based location systems are not as good as that of the TOA or TDOA based systems. This is mainly because complexity of the indoor environment and a good widely applicable model for non-stationary environments is difficult to find. Furthermore, the received signal strength can easily be altered if someone intends to attenuate or amplify the transmitted power, which makes it a poor option for security applications.

## 2.4 Measures of Location Accuracy

When comparing a variety of location technologies or systems, definitions of measures of the location accuracy are necessary and useful. In this section, we introduce two commonly accepted measures used to describe location accuracy in literature. The measures introduced in this section will be used through this thesis in comparison of different systems, discussion of a variety of techniques, and evaluate the location performance of the proposed system.

The most apparent measures of the location accuracy is the Euclidean distance between the estimated locations, $(x_k, y_k)$, and the true location of the UT, $(x_t, y_t)$.

$$d_E(x_k, y_k) = \sqrt{(x_t - x_k)^2 + (y_t - y_k)^2} \tag{2.1}$$

Euclidean distance expressed above indicates the location error induced in a location measurement (Figure 2-7). It only counts the location error of one single measurement result.

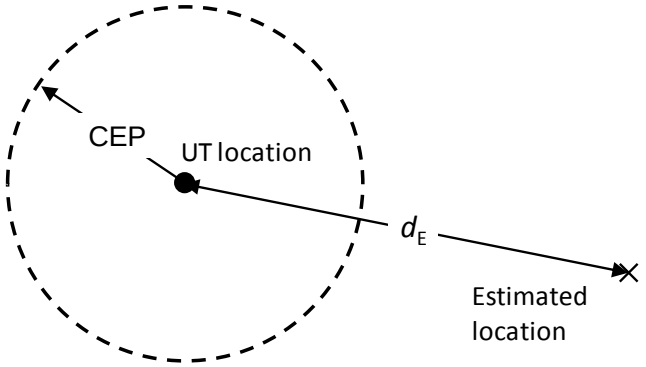


**Figure 2-7 Distance of location error and circular error probability**

To estimate the location performance of a location system, the statistics for the distance errors in a number of location estimation tasks are commonly used. An obvious parameter of this kind is the Mean Squared (MS) error defined as the mean squared value of the location error:

$$MSE = \frac{d_E^2(x_1, y_1) + d_E^2(x_2, y_2) + \cdots + d_E^2(x_n, y_n)}{n} \tag{2.2}$$

whose unit is $m^2$. While MSE reflects the location performance of a system from the statistic point of view, it is not directly describing the location accuracy in distance.

Consequently, a more commonly used parameter is the Root-Mean Squared (RMS) location error, calculated as the squared root of the MS error:

$$RMSE = \sqrt{\frac{d_E^2(x_1, y_1) + d_E^2(x_2, y_2) + \cdots + d_E^2(x_n, y_n)}{n}} \tag{2.3}$$

The RMS location error of a location system is computed from a large number of experimental results of UT location and thus it indicates the average location accuracy that can be expected from the corresponding system.

To illustrate the probability of achieving specific location accuracy, the concept of Circular Error Probability (CEP) [25] is also commonly used.

For a 2-D location system, the CEP is defined as the radius of a circle, centered at the correction position of the UT, which contains 50% of the estimated locations. If the CEP of a location system is 1 metre, it means there is 50% probability that the estimated location is within 1 metre Euclidean distance to the true position of the UT.

The concept of CEP can be extended to describe the radius of the circle which contains *xx*% of the estimated locations, noted as CEP*xx*. Therefore, the original concept of CEP is noted as $CEP_{50}$ in this thesis. The measure $CEP_{95}$ is also usually quoted in literature and system specifications to illustrate the achievable location accuracy with 95% possibility.

## 2.5 Wireless Technologies

Researchers have investigated several types of wireless technology that can be used for indoor location purposes. The popular wireless technologies used in indoor location research include radio frequency identification (RFID), ultra-wideband (UWB), mobile communications (GSM/CDMA), and wireless local area network (WLAN).

In this section, we will review some important wireless technologies employed in this field, and describe some representative systems using these technologies.

### 2.5.1 RFID

The radio frequency identification (RFID) technology uses RF communications between reader and tags for the purpose of identification and tracking [26]. RFID systems can be categorized into two types, passive and active, according to the type of tags used. Either type of RFID system comprises two basic components, RFID reader, and RFID tag. Typical frequency bands for RFID systems are: LF (125 kHz), HF (13.56 MHz), UHF (433, 868-915 MHz) and microwave frequency (2.45 GHz, 5.8 GHz).

Passive RFID tags are powered through the magnetic field generated by the RFID readers. It is called passive because it can operate without an embedded battery. A passive RFID tag contains two main parts, an antenna for receiving and transmitting RF signals, and an integrated circuit that stores and processes data. ID and relevant data information will be sent to a reader when an interrogation is received by the tag. The reader, which is usually linked to a database, is therefore able to identify the object attached by the corresponding tag. Passive RFID tags are widely used in many aspects of urban lives, include but not limited to entry control to a building, transport payment, product tracking, and inventory system. Currently the UK supermarket corporation, Marks and Spencer (M&S), is tagging around 100 million items per annum and this is forecast to increase significantly as more departments move over to the use of RFID labelling.

An active RFID tag on the other hand is an RF transceiver that has its own power source, possibly an embedded battery, and it can actively transmit the ID and other additional data if needed, or as soon as an external request is received. Its antenna may be implemented with a smaller size design and yet its radiated signal can reach a further distance, possibly of up to tens of metres. Since active RFID tag contains more sophisticated RF circuits, it is possible to implement more functions in active tags than in passive tags. In addition, active tags are able to store more data than the passive tags. Therefore, active RFID tags are usually employed in more advanced applications, e.g. manufacturing management, valuable assets management, and animal identification.

Since RFID systems can be applied in a variety of scenarios, the development trend of this technology is to incorporate sensor technology to provide more information than ID only, so that the users of RFID systems can obtain a greater amount of up-to-date information relevant to the tagged objects. For example, environment parameters such as temperature [27], pressure [28], and humidity [29] are of concern in particular applications. Also, the location of an RFID tag is valuable information to the system user.

Passive RFID based location systems usually rely on simple proximity detection and the estimated tag location is associated with the location of the corresponding reader. Since passive RFID tags have no on-board power source, their communication ranges are usually limited to around 2 m. The wide coverage of passive RFID location system requires high density of readers, which is costly and sometimes inefficient. Alternatively, passive RFID location system is able to provide pinch point tracking, in which case the location of a tag will be reported whenever it is detected passing through a pinch point served by an RFID reader. In this case full coverage over the indoor environment is unnecessary and thus the location system only needs to monitor a few places of interest.

Active RFID based location system includes two different types. Those combine standard RFID system with RSS location method, for example the LANDMARC [24] system given in the Table 2-1. The other type uses specialized RF technologies to achieve better location performance.

LANDMARC (LocAtioN iDentification based on dynaMic Active Rfid Calibration) is an approach of locating active RFID tags with commercial standardised RFID readers. The demonstration system and results are presented in [24]. While LANDMARC utilises the fingerprinting method, the novelty of LANDMARC approach is that additional reference RFID tags are placed at known positions of the indoor cell, as landmarks to the location system. The RSS patterns of the reference tag signals are use to find the relative location of user tags with respect to the reference tags. These extra fixed reference tags assist the system to achieve better location accuracy. It is obvious that the achievable location accuracy in such a system is relevant to the number of reference tags, that the higher reference tags density induces better location accuracy. In the demonstration presented in [24], one reference tag per

square metre density was used to produce the one metre $CEP_{50}$ result in a laboratory trial.

While LANDMARC uses an RSS fingerprinting technique, there is also an active RFID location system using a TDOA location method. WhereNet [30] location system is a product of the Zebra technology company that provides complete solution for indoor and outdoor real-time location of standardized active RFID tags. RFID technology is employed by WhereNet to differentiate and identify the located objects, tagged by their so-called WhereTags. Spread spectrum radio frequency beacons are sent by the WhereTags and the antennas mounted at fixed positions receive beacons from tags and forward the signals to a location processor. The location processor is therefore able to perform TDOA location estimation using the signals transmitted by the antennas. A location processor can connect with up to eight antennas via coaxial cables. The location information estimated by the location processor is saved and used by the location-based services. The WhereNet location system provides 2 to 3 m RMS location accuracy in indoor environment. By separating the identification and location functionality, WhereNet is successful in providing both compatibility with standard RFID protocols and adequate indoor location performance. The downside of WhereNet system may be the costly coaxial cable networks and the time consuming installation process.

RFID technology has been broadly accepted in many situations and the supplemented location capability to RFID system potentially opens a new area of applications of this technology. However, adding location functionality to a standard RFID system, whose RF protocol was not designed for location purpose, is an inefficient way of building an indoor location system. Therefore, specialized RF technologies are also proposed to provide better location and identification capability, for example ultra-wideband, which will be discussed in a separate section following

### 2.5.2 Ultra-Wideband

Ultra-wideband (UWB) is a radio technology that transmits ultra-short pulses (typically shorter than 1 ns) with a low duty cycle and at low energy level, for wideband communications. On the spectral domain, UWB radios have relative

bandwidths larger than 20% or absolute bandwidths of more than 500MHz. In February 2002, the Federal Communications Commission (FCC) in the United States conditionally waived unlicensed operation of the personal UWB products in the private sector [31]. This approval sparked a surge of research interests in UWB technology and particularly its applications in indoor location systems.

UWB has been demonstrated to be a good technique for indoor positioning [32] and it is able to provide perhaps the best location accuracy so far [33]. The arrival time estimation using a UWB signal is obtained by using a matched filter or a bank of correlation receivers at the receiver end. Conventional wireless systems suffer from multipath distortion which restricts the achievable location accuracy. With UWB technology, the short duration and wideband characteristic of the transmitted pulse makes it possible to provide accurate time of arrival estimates while the arriving multi-path components can be excluded due to the inherently fine temporal resolution of UWB signal. UWB systems are able to detect pulses of lower power, compared to conventional RF signals. While conventional RF signals operate on a single band, UWB system may transmit signals over multiple bands.

Several players are active in the UWB based indoor location systems. Ubisense [34] has been one of the earliest suppliers of high accuracy indoor location systems based on UWB technology. Their location accuracy can be as fine as tens of centimetres. The Ubisense tags transmit UWB beacons that can be used by a sensor pair to determine the TDOA between the two sensors. More importantly, the proprietary Ubisense sensors can also independently measure the AOA of the received UWB signal. The measured data are forwarded from these sensors via Ethernet to the Ubisense software platform. By combining the TDOA and AOA information from two sensors, the location of a user tag can be estimated through intercepting the calculated directions and TDOA curves. This innovative hybrid location method ensures the satisfying location accuracy down to 0.15 m with 95% probability (Table 2-1). Ubisense sensors are organised into cells and typically a cell is monitored by at least four cells, covering an area of 400 $m^2$ [35].

Also, another UK company, Thales, has demonstrated its indoor location system in 2008 at a fire fighters training building [36], in which demonstration sub-metre location accuracy was achieved. The Thales indoor location system also utilises UWB

technology. However, instead of sending a compressed wideband short pulse, the Thales tag transmit frequency hopped (FH) UWB signal, which is a 10~20 MHz direct sequence spread spectrum (DSSS) signal hopped over 1.25 GHz bandwidth within the 3.5 to 8 GHz band. It is able to provide the same time measurement accuracy as the pulse UWB technique given the same bandwidth covered. With the superior time measurement capability provided by its UWB signal, the Thales indoor location system is able to locate the tagged objects in hostile environment (e.g. through walls) with sub-metre location accuracy.

Besides these two examples, there are also other manufacturers are able to produce similar UWB based location systems with greater than one metre location accuracy, such as Time Domain PLUS [37]. The superior location performance of these systems is accomplished through the ultra-wideband characteristics of their radio signals. Meanwhile, these systems usually come with the highest price in the real-time indoor location area.

### 2.5.3 Mobile Communications Networks

Location information obtained through GSM or other mobile communications networks has been available to mobile users for years. The early location information provided by mobile operators were obtained using simple cell-ID technique, which is similar to the proximity detection method where the mobile user's location is associated with the location of the base station he/she is connecting to. This type of location service is available for both outdoor and indoor mobile users but the location accuracy is generally low, in the range of 50-200 m. Superior indoor positioning based on mobile communications networks is possible if the building is covered by several base stations, and the location performance depends on the density of base stations deployed.

Signal strength fingerprint techniques can be used to improve the accuracy to as fine as 2-5m. However, additional cost of the base station is required for this to work. Researchers at the Tartu University [38] had demonstrated a GSM based indoor location system using RSS fingerprinting technique. In their demonstration system, mean location accuracy of 5 metre was achieved by means of what they call the wide

signal-strength fingerprints method. It includes the six strongest GSM cells and readings of up to 29 additional GSM channels, most of which are strong enough to be detected but too weak to be used for efficient communication.

Another possible technique for location finding with mobile networks is DSSS, which is a popular technique in location finding due to its superior performance and is the spread spectrum technique employed by code division multiple access (CDMA ) systems. With this technique, the receiver determines time-of-flight information by correlation between a known Pseudo-Noise (PN) sequence and the received radio signal. The distance between the mobile user and the base station is determined from the first correlation peak. However, due to the scarcity of the available bandwidth, DSSS ranging with mobile CDMA systems may not be able to provide adequate accuracy [39;40]. Simulation analysis given in [40] shows that mean location error of 20 m is achievable with cellular CDMA systems.

### 2.5.4 Wireless Local Area Network

Wireless local area network (WLAN) is the dominant local wireless network standard worldwide. It is popular in homes and public businesses such as coffee shops and shopping malls, due to its ease of installation and reliable support for multiple accesses. The increasing number of WLAN access points in major cities attracts great interest in designing indoor location system based on existing WLAN infrastructure to reduce cost of location services.

Different location and tracing systems can be used inside WLAN for different accuracy requirements. The accuracy of typical WLAN positioning systems is approximately a few metres, with an update rate in the range of few seconds. The main advantage of this system is its compatibility with existing WLAN.

A Microsoft research group started probably the earliest experiments of locating WLAN users by means of RSS ranging [41]. Their system is named RADAR which consists of multiple access points (AP) and a laptop computer, which is tracked as the target object. The laptop is carried by an individual in the overlapping coverage area of the APs. Mean of the received signal strengths at the APs are used to compare with

a set of pre-recorded RSS fingerprints. The best match between the measured and the pre-recorded RSS sets, namely nearest neighbour in signal space, indicates the estimated location of the user target. The location demonstration given in [41] achieves location accuracy of 2.94 m with about 50% probability.

The company Ekahau provides possibly the best solution of RSS fingerprinting based indoor location system using WLAN networks [42]. Ekahau provides the complete tags and software solution, and is said to be able to operate over any brand or generation of WLAN networks to provide sub-room level location accuracy (averagely 1 m). The location method of Ekahau system is basically the RSS fingerprinting but its model can be optimised according to the indoor scenario and thus is able to provide better accuracy than the RADAR system. This is performed through a calibration process using the Ekahau software. It may take only an hour to calibrate an area of 1,111 $m^2$ [35]. However, there is no information about how often this calibration process shall be taken and sensitivity to environmental change is one of the major disadvantages of RSS based location systems.

There are also other location systems using WLAN and most of them employ RSS fingerprinting location methods (e.g. AeroScout [43]). These systems are relatively inexpensive and efficient, but there typical accuracy is between 2 to 5 m [16], in case their empirical models are validated by adequate training processes. Since RF signals deviate considerably while propagating indoors, due to multipath and reflections, stability of fingerprinting location performance is limited.

### 2.5.5 Existing systems

In the previous sub-sections, a few popular wireless technologies for indoor location systems are reviewed along with introductions to some representative systems. Table 2-1 summarises the technical specifications of these existing indoor location systems.

The wireless technologies, location methods, sensor locate range, tag radiated power, signal frequency band, and the resultant location accuracy are listed in Table 2-1. The data listed in Table 2-1 are taken from their datasheets or some relevant publications [16;35]. Among these parameters, the tag radiated power may not be a fixed figure for

these systems. Usually the tag radiated power is configurable according to specific applications. The power levels shown in Table 2-1 are the figures used in their demonstration, or the maximum power given in their datasheet. This is because the best location accuracy shown in datasheet is achieved under the best signal quality condition, which implies maximum radiated power.

The operating frequencies are also shown and in some cases the bandwidth of the RF signals are given too. The signal bandwidth is a particularly important parameter for time measurement (e.g. TOA, TDOA) based location systems as it practically defines the system's vulnerability to multipath interference.

Finally, the location accuracies of the selected systems are shown using the metrics introduced in Section 2.4. Different location systems may use different metrics to address location performance, some use RMSE and some prefer to give CEP at different probability level, making it difficult to compare the performance of various systems straight away. An empirical relation between RMSE and CEP is given by [44], which article suggests that RMSE usually lies in the region between $CEP_{63}$ and $CEP_{68}$. Also, the $CEP_{95}$ may be regarded as 1.74 times of RMSE if Gaussian distribution applies on the ranging measurements.

Among the selected systems in Table 2-1, UWB based systems surpass other systems regarding location accuracy figures. All the UWB based systems achieve sub-metre location accuracy in demonstration or according to their published materials. The WLAN based system Ekahau is also able to provide averagely one metre location accuracy which is the best in the WLAN based systems group.

Indoor location systems developed over an existing wireless system, e.g. RFID, GSM, WLAN, tends to adopt proximity detection and RSS based location methods, as these location methods can be implemented without modification to the existing wireless services. However, these methods are practically not as reliable as the time measurement methods (TOD/TDOA). On the other hand, the newly designed indoor location systems based on UWB and other RF technologies will be able to utilise more accurate location methods like TOA, AOA, TDOA, or combination of more than one kind of location method described in Section 2.3.

| | Wireless technology | Multiple Access | Location method | Combat Multipath | Location range | Tag radiated power | Frequency band[1] | Location accuracy |
|---|---|---|---|---|---|---|---|---|
| LANDMARC [24] | Active RFID | ALOHA TDMA | Fingerprinting | Proximity detection | 9 m | Not specified | 303.8 MHz | $CEP_{50}$ = 1 m |
| Zebra WhereNet [30] | Active RFID | DSSS code | TDOA | Not given | 120 m | 10 dBm | 2.4 GHz (60 MHz) | RMSE = 2~3 m<br>$CEP_{50}$ = 3 m |
| Ubisense [45] | UWB | Bluetooth | TDOA + AOA | Cross-correlation | ~50 m | -10 dBm | 5.9-7.2 GHz (750 MHz) | $CEP_{95}$ = 0.15 m<br>$CEP_{99}$ = 0.3 m |
| Time Domain PLUS [37] | UWB | ID packet | TDOA | Cross-correlation | 30 m | Not specified | 6.6 GHz | RMSE = 0.3 m |
| Thales [36] | UWB | DSSS code | TOA | Cross-correlation | 50~100 m | -10 dBm | 3.5~8 GHz (1.25 GHz) | RMSE < 1 m |
| Tartu University [38] | GSM | Mobile ID | Fingerprinting | Weighted K nearest neighbor algorithm | Not specified | Not specified | 850 MHz; 1900 MHz | RMSE = 5 m<br>$CEP_{80}$ = 10 m |
| Microsoft RADAR [23] | WLAN | Not specified | Fingerprinting | Linear-time search algorithm | 34~44 m | Not specified | 2.4 GHz | $CEP_{50}$ = 2.94 m<br>$CEP_{75}$ = 4.69 m |
| Ekahau [42] | WLAN | Carrier Sense Multiple Access | Fingerprinting | Empirical radio map | 40~60 m | 11.5 dBm | 2.4 GHz | RMSE = 1 m |
| AeroScout[43] | WLAN | WLAN messaging | RSS (indoor) TDOA (outdoor) | Empirical radio map | Up to 60 m | 19 dBm | 2.4 GHz | RMSE = 3-5 m (TDOA); 3-10 m (RSS) |

**Table 2-1 Wireless technology and location method of existing RF indoor location systems and their location performance**

[1] Figure given in the bracket is the signal bandwidth if known.

Although the indoor location systems based on existing wireless networks do not exhibit superior location performance, the features of these systems, e.g. ease of installation, relatively low cost, and broad availability of these infrastructures, indicate a large potential market that has attracted great research interests.

Generally speaking, making use of existing networks and highly accurate location performance cannot be achieved by any of these currently available systems. Operators of indoor location systems have to make their choice according to the specific applications and corresponding requirements.

However, the research presented in this thesis may suggest a different situation where both of these benefits can be achieved by a single system design. That is, in an indoor environment where RF-over-fibre (RoF) infrastructures are installed, the indoor location system can be implemented with a relatively compact design while sub-metre location accuracy is achieved.

## 2.6 Summary

The fundamental knowledge of RF indoor location systems has been summarised in this chapter. The first section describes what RF indoor location system is, and clarifies some relevant terminologies that will be used in this thesis. Section 2.2 answers the question of where will indoor location systems be needed by depicting seven potential application scenarios.

Section 2.3 to 2.5 focuses on the technical aspects of indoor location systems. There are two key technologies in an indoor location system: the wireless technology and the location method. The wireless technologies used decide what type of physical information can be obtained from the RF signals, for example range or direction. Also, correctness of the sensed information is dependent on the wireless technology chosen; for example, greater signal bandwidth leads to better time measurement accuracy.

With the same wireless technology, utilisation of different location method results in different requirements for the system design. AOA measurement requires specially designed antenna. TOA location method requires synchronisation over the entire

system. The TDOA location method waives the synchronisation between sensors and user terminals, so that only synchronisation among the sensors is needed. RSS measurement places the least requirement on system hardware but sophisticated location algorithm and reliable empirical model are needed from the software point of view, in order to produce adequate location result.

Various combinations of these techniques have been seen in the existing indoor location system designs, which are summarised in the Section 2.5. Review of these systems provides information about the potential location performance of specific location methods and wireless technologies. Analysis of their system structures suggests some fundamental issues that shall be paid attention to during new system design. It is also concluded that, superior location accuracy can only be achieved by dedicated location system such as UWB systems. The indoor location systems based on existing wireless networks usually do not exhibit comparable performance in terms of location accuracy. The information obtained from this review assists in deciding the technical route of the TINA indoor location system.

Regarding the research presented in this thesis, which is a newly designed self-contained location system, active RFID tag transmitting chirp signals and TDOA location methods are chosen. This is because, firstly, the wide band characteristic of a chirp signal provides the accurate time measurement ability desired. (Detailed analysis of the time measurement capability of chirp signal will be given in Chapter 3). Secondly, the TDOA location method is chosen as it is especially suitable for the RoF based infrastructure. The main difficulty of TDOA location method is clock synchronisation among the spatially distributed sensors. With a RoF backbone, the RF signals from the sensors are centralised at a common control site, where the RF signals can be captured and measured with a single clock signal. Given the potentially high location accuracy and suitability to RoF backbone, TDOA is regarded as the most suitable candidate for this research.

In the following Chapters, it will be shown that the TINA indoor location system builds on the existing RoF network already deployed and available, yet provides the location performance that is as good as dedicated systems.

# *Chapter 3*

## USE OF LINEAR FM CHIRP FOR TIME DIFFERENCE OF ARRIVAL MEASUREMENT

The TINA indoor location system is a self-contained design that does not rely on established wireless systems. Therefore, the radiated signals for the TINA system can be chosen and tailored according to its specific requirements. Among the wireless waveforms available to indoor location applications, the linear frequency modulated (LFM) chirp is chosen to be used in the TINA indoor location system because firstly, it is a wideband spread spectrum signal that is suitable for time measurement; secondly, spread spectrum signals are known as robust to multipath phenomena which are commonly experienced in indoor environment; also, there are a few neat techniques that can be used to generate LFM chirp signal and thus it fulfills the goal of designing the user RFID tag in a compact way.

This chapter firstly introduces the LFM chirp signal that will be used in TINA indoor location system, as well as the fundamental characteristic of this signal. The technique of detecting TOA and TDOA information with this signal is explained as well in the first section. While LFM chirp signal is suitable for time measurement, the non-linearity of its frequency variation rate, which commonly exists in chirp signal sources, may downgrade the quality of the measured results, and limit the location range when applying this technique. Therefore, in Section 2 of this chapter, a parameter is introduced, the fractional slope variation (FSV), to estimate this impact and quantify the requirement on chirp signal linearity. Introduction of FSV shall facilitate designs of LFM chirp signal in range estimation, and measure how well the actual signal sources meet the design requirements.

## 3.1 Deramping Linear Frequency Modulated Signal

The LFM signal is also known as chirp signal whose frequency linearly varies over a wide band of spectrum, either increasingly or decreasingly, with respect to time, Figure 3-1. Due to the wide band and long duration features of LFM chirp, it was adopted as one of the earliest waveforms used in radar for pulse compression. Comprehensive introduction and analysis of this signal can be found in Stimson's book [46]; Levanon [47] has derived the ambiguity function for LFM pulse signal with different weighted functions. The purpose of this section is to introduce the deramp technique that measures time delay using LFM chirp, which is a fundamental unit of an indoor location system.

A chirp signal's instantaneous frequency varies linearly with time and can be expressed as

$$f(t) = f_c + kt; \quad -T_c/2 \le t \le T_c/2 \tag{3.1}$$

where $T_c$ is the chirp duration, $f_c$ is the carrier frequency and the instantaneous frequency at time $t$=0, and $k$ is the chirp rate defined as the signal bandwidth $B$ divided by the chirp duration $T_c$:

$$k = \pm B/T_c \tag{3.2}$$

The unit of $k$ is Hz per second, or radians per second. The standing phase of the chirp signal $\theta(t)$ can be obtained by the integral of Eq. (3.1), assuming the initial phase is 0

$$\theta(t) = 2\pi \int f(t)dt = 2\pi[f_c t + (1/2)kt^2] \tag{3.3}$$

Thus, an LFM chirp signal $v(t)$ can be expressed as

$$v(t) = \cos(2\pi f_c t + \pi k t^2) \tag{3.4}$$

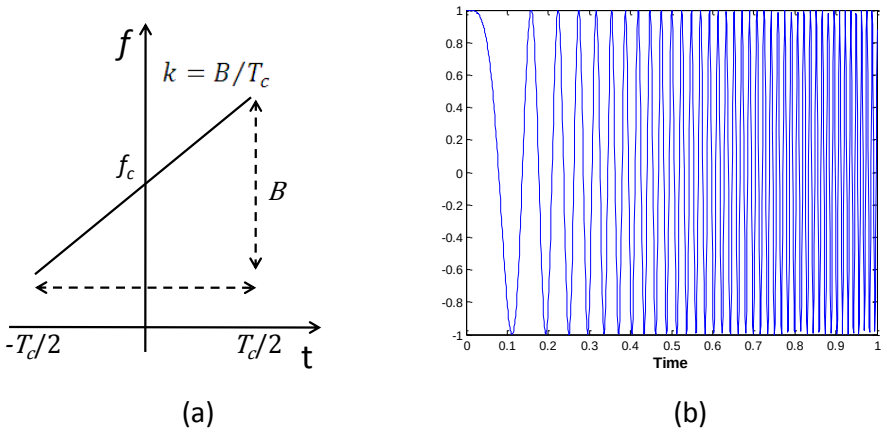


**Figure 3-1(a) Frequency vs. time relationship of a chirp signal; (b) a chirp waveform in time domain**

Due to the frequency variation characteristic of chirp signal, it is usually interpreted in a *t-f* (time-frequency) coordinate, indicating the change of frequency against time, as shown in Figure 3-1(a). In the case of LFM chirp, this characteristic is illustrated by a straight line, connecting the upper and lower bounds of the frequency band. The chirp rate *k* is represented by the slope of the line in this coordinate. A chirp signal whose frequency sweeps increasingly over time is called up-chirp, indicated by positive slope *k* in the *t-f* coordinate, while a down-chirp, whose frequency sweeps decreasingly over time, is indicated by negative slope *k*. The chirp signal presented in Figure 3-1 is example of an up-chirp.

### 3.1.1 TOA Measurement

The linear frequency modulation feature of the chirp signal is useful in time measurement in that mixing two chirp signals will convert the delay between them into a sinusoidal component in frequency domain. It is a classic approach to executing TOA measurement in FMCW radar [48] where an LFM waveform is transmitted to search for passive targets in the observation range.

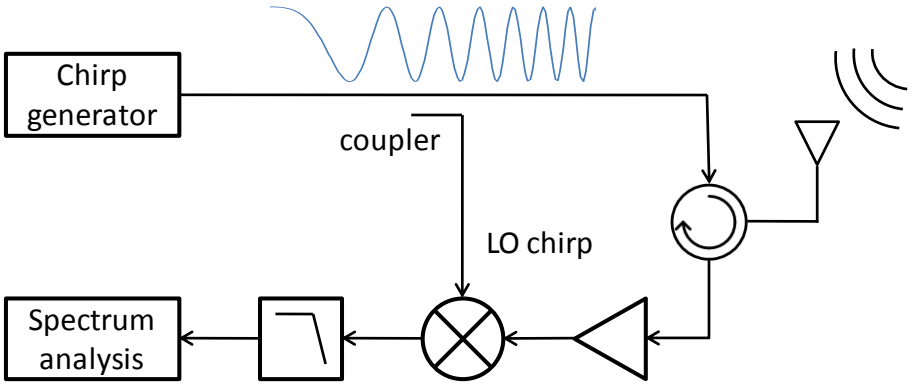


**Figure 3-2 Block diagram of FMCW radar that measures TOA by deramping**

### 3.1.1.1 TOA Measurement with LFM Chirp

A block diagram showing a simple form of such a system is given in Figure 3-2. The echo reflected from a target will consist of a replica of the transmitted LFM signal but delayed by $\tau = 2R/c$, as shown in Figure 3-3(a) where $R$ is the target range and $c$ is the propagation velocity. This echo signal $e(t)$ can be expressed by Eq. (3.5) as below

$$e(t) = A \cdot v(t-\tau) = A\cos[2\pi f_c(t-\tau) + \pi k(t-\tau)^2] \tag{3.5}$$

The received echo signal $e(t)$ is then multiplied with an LO chirp coupled from the chirp generator used for transmission. Since it is the same LFM chirp signal with obviously the identical chirp rate, the linear frequency variation features in the echo $e(t)$ will be "deramped", yielding a single tone signal whose frequency is equal to the instantaneous frequency difference between the LO chirp and the received echo, indicated by the first term of the result in Eq. (3.5). The frequency of this resultant sinusoidal signal is known as beat frequency or deramped frequency in literatures, noted as $f_d$ in both Figure 3-3 and Figure 3-4. The deramp process in this case is expressed as

$$\begin{aligned} e(t)\cdot v(t) &= A\cos[2\pi f_c(t-\tau) + \pi k(t-\tau)^2] \\ &\quad \cdot \cos(2\pi f_c t + \pi k t^2) \\ &= \frac{A}{2}\cos(2\pi k\tau t + 2\pi f_c\tau - \pi k\tau^2) \\ &\quad + \frac{A}{2}\cos(2\pi k t^2 + 4\pi f_c t - 2\pi k\tau t - 2\pi f_c\tau + \pi k\tau^2) \end{aligned} \tag{3.6}$$

The second component in the result of Eq. (3.6) is also in the form of a chirp signal, whose chirp rate is $2k$ and thus doubles the sweeping bandwidth of the original chirps.

This doubling sweeping rate chirp centres at nearly twice the frequency of the original chirp, that is $2f_c - k\tau$. Since it is of so much higher frequency than the low frequency term, it can easily be eliminated in the sampling process of the deramped signal, or by modest low-pass filter following the mixer output, Figure 3-2. The resultant high frequency chirp component is ignored because the lower frequency component has the require delay information $\tau$ already, as can be seen from the first term of the Eq. (3.6). Also, the resultant component at higher frequency band requires higher sampling rate as it is of wider band than the lower frequency component. .

By analyzing the spectrum of the deramped signal, the range information can be obtained as the deramped frequency is proportional to the corresponding return time-of-flight $\tau$ by the frequency sweeping slope *k*, as indicated by Eq. (3.7).

$$f_d = k\frac{2R}{c}$$
$$R = \frac{c \cdot f_d}{2k} = \frac{c \cdot f_d \cdot T_c}{2B} \tag{3.7}$$

where *c* is $3 \times 10^8$ m/s, which is the propagation velocity of microwave in air.

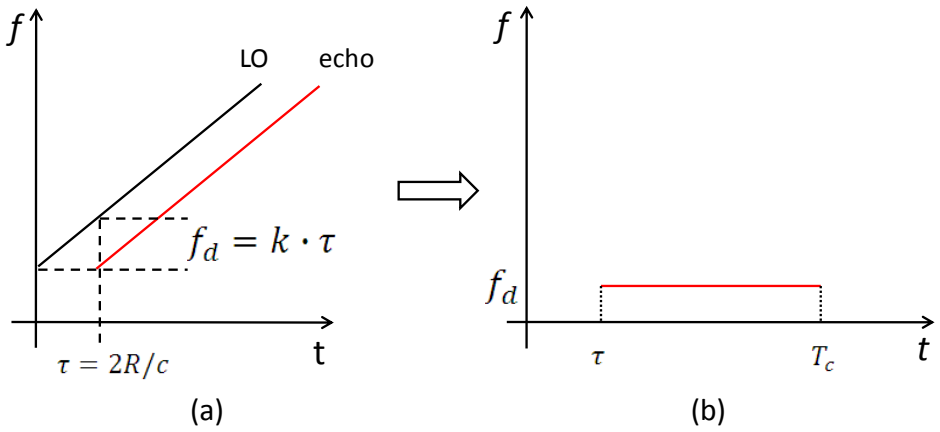


**Figure 3-3 Deramp processing with LFM chirp signal, (a) time-frequency characteristic of the LO chirp and the echo chirp; (b) constant deramped frequency over time**

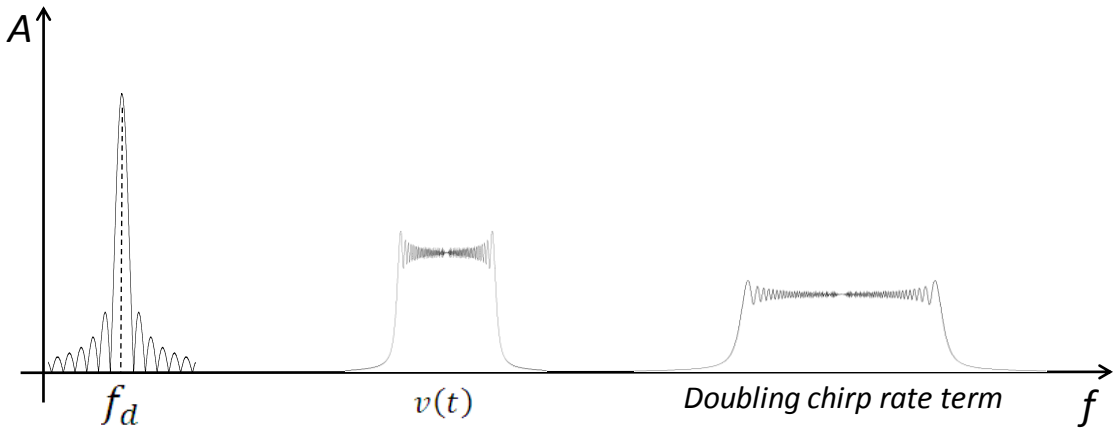


**Figure 3-4 Spectrum of deramped result, with respect to the original chirp $v(t)$**

### 3.1.1.2 Range Resolution in TOA Measurement

Due to the propagation delay $\tau$ in the echo signal, the deramped sinusoidal signal will be shortened to only $T_c - \tau$ long (Figure 3-3(b)), instead of the full duration of the original chirp signal $T_c$. To retain as much frequency resolution as possible, the designed $T_c$ is required to be much greater than the maximum delay $\tau_{max}$ the system is going to deal with, by a nominal ratio of 100 times

$$T_c > 100 \cdot \tau_{max} = 100 \cdot \frac{2R_{max}}{c} \tag{3.8}$$

Given the condition of Eq. (3.8), the spectrum analysis in Figure 3-2 will have a frequency resolution $f_{res}$ of approximately $1/T_c$, from which the well known range resolution expression may readily be deduced

$$\begin{aligned} f_{res} &= \frac{2R_{res}}{c}\frac{B}{T_c} = \frac{1}{T_c} \\ \therefore\ R_{res} &= \frac{c}{2B} \end{aligned} \tag{3.9}$$

In the subject of radar [49], the concept of resolution means the ability of a radar system to distinguish targets which are very close to each other. While targets separating beyond this resolution range can be identified in the TOA measurements, a target cannot be distinguished from another target if they are located within the range of $R_{res}$ away from each other. As interpreted by Eq. (3.9), that is because the deramped responses from the two close targets will fall into the same frequency bin, whose size is limited by the frequency resolution.

In an active RFID indoor location system, multiple active targets are identified by means of coded, modulated RF signals. Therefore, there is no such requirement to distinguish targets by only their reflected echoes. The reason we are discussing the range resolution here is that it defines the maximum errors caused by multipath in time measurement. Multipath signals will contain the same RF signals as the direct path signal but with different delay and loss, just like echoes from multiple passive targets in FMCW radar. In deramp processing of received LFM signals, they will produce similar sinusoidal components just like the direct path signal.

Let $R$ be the length of the direct path from a UT to a sensor, the multipath errors in this measurement mainly come from those multipath signals whose radiation path length is within $R + R_{res}$. Because the deramped response from a multipath beyond $R + R_{res}$ can be "distinguished" in deramp processing and thus can be abandoned in range estimation. By contrast, the deramped response resulted from a multipath with shorter length will fall into the deramped frequency bin of the direct path; consequently, it results in frequency as well as range detection errors. Therefore, $R_{res}$ is the maximum range measurement error that can be caused by multipath in an indoor location system, in that the direct path signal will not be affected by more than $R_{res}$ in range measurement. A more detailed research on the multipath signals and its specific impact on the system introduced by this thesis will be presented in the Chapter 5 of this thesis. With abundant measurement data and simulation assisted analysis, some practical detection strategies that can be used to eliminate multipath impact will be given too.

### 3.1.2 TDOA Measurement

While LFM chirp can be used for return time-of-flight measurement, or TOA measurement, it can also be used to determine the TDOA information between two chirp signals arriving at two spatially separated sensors. This can be done by also deramping the incoming chirps separately with an LO chirp of identical chirp rate *k*, which is equivalent to the match filtering process. The frequency difference between the two deramped frequencies is then proportional to their TDOA. This technique is

similar to the TOA measurement method introduced in the previous section, and their difference will be summarised as below.

### 3.1.2.1 TDOA Measurement with LFM Chirp

To clarify the technique of using LFM signal for TDOA measurement, a simplest example is discussed. Consider there is a pair of sensors measuring the TDOA between their incoming signals from a UT, which transmits an LFM chirp of duration $T_c$ and swept-frequency over bandwidth $B$.

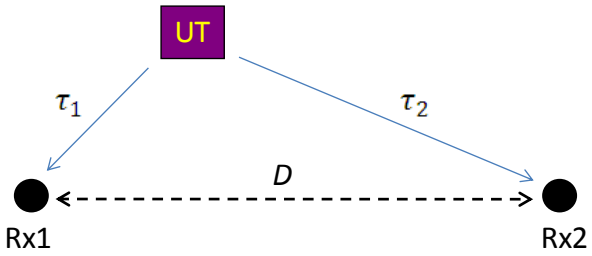


**Figure 3-5 Time-of-flight for signal transmitted from a UT to a pair of sensors**

The transmitted signal from the UT is also LFM chirp waveform which has been defined in Eq. (3.4). As illustrated in Figure 3-5, this signal arrives at a known pair of sensors, Rx1 and Rx2, with different time delays, $\tau_1$ and $\tau_2$, dependant on the corresponding transmission paths between the tag and the two sensors. Due to the difference in transmission path lengths, the two received signals $r_1(t)$ and $r_2(t)$ are also attenuated to different extents, which are noted by $A_1$ and $A_2$ in Eq. (3.10).

$$\begin{aligned} r_1(t) &= A_1 \cos[2\pi f_c(t-\tau_1) + \pi k(t-\tau_1)^2] \\ r_2(t) &= A_2 \cos[2\pi f_c(t-\tau_2) + \pi k(t-\tau_2)^2] \end{aligned} \tag{3.10}$$

Similar to the echo signal in the TOA case, the time-of-flight information are retained in the received signals as in Eq. (3.10). If the transmission time $\tau_T$ is given, the delay information, $\tau_1$ and $\tau_2$, can be directly determined. For a location system, this usually requires fine synchronisation between the sensors and the UT, and thus adds up complexity to the system. In case where the UT is not synchronised with the sensors, there will be no way to find out when the signal was transmitted. Therefore, $\tau_1$ and $\tau_2$ cannot be found directly, but alternatively, the TDOA $\Delta\tau$ as below can be found and this can also be used to locate the UT.

$$\Delta\tau = \tau_2 - \tau_1 \tag{3.11}$$

To find this time difference caused by the difference in transmission paths (Figure 3-5), the received signals $r_1(t)$ and $r_2(t)$ are firstly deramped with a replica of the LFM chirp $v(t-\tau_{LO})$ generated or saved digitally at the sensors.

$$\begin{aligned} d_1(t) &= r_1(t)\cdot v(t-\tau_{LO}) \\ d_2(t) &= r_2(t)\cdot v(t-\tau_{LO}) \end{aligned} \tag{3.12}$$

This can be considered as performing two independent deramping processes, as illustrated by Figure 3-2, one in each of the two sensors. By introducing Eq. (3.12), it is assumed that the sensors are synchronised. Therefore, the time $\tau_{LO}$, when the LO chirp starts, is known to the system, and usually can be controlled by the system. Similar to (3.6), each of the equations in (3.12) will yield a lower frequency term and a higher frequency term but the higher frequency term will be rejected by the low-pass filters in the sensors. Thus, the actual deramped outputs at the two sensors are noted by

$$\begin{aligned} d_1(t) = \frac{1}{2}A_1\cos\,[&2\pi k(\tau_1-\tau_{LO})t + \pi k(\tau_{LO}^2-\tau_1^2) \\ &+ 2\pi f_c(\tau_1-\tau_{LO})] \\ d_2(t) = \frac{1}{2}A_2\cos\,[&2\pi k(\tau_2-\tau_{LO})t + \pi k(\tau_{LO}^2-\tau_2^2) \\ &+ 2\pi f_c(\tau_2-\tau_{LO})] \end{aligned} \tag{3.13}$$

Both $d_1(t)$ and $d_2(t)$ are sinusoidal signals whose frequencies are proportional to the relative time delay between incoming chirps and the LO chirp, correspondingly $\tau_1 - \tau_{LO}$ and $\tau_2 - \tau_{LO}$. By examining the frequency of $d_1(t)$ and $d_2(t)$, the time difference can be found from the distinction in their frequencies(Figure 3-6).

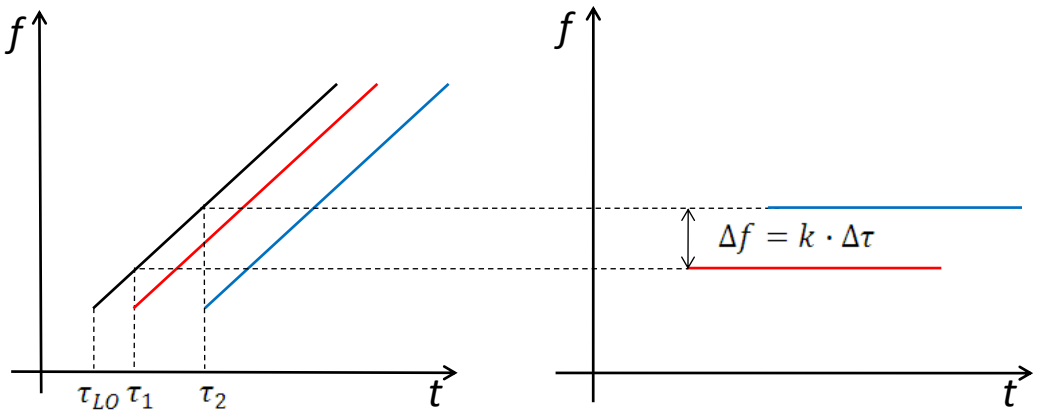


**Figure 3-6 Finding time difference from deramped frequency difference**

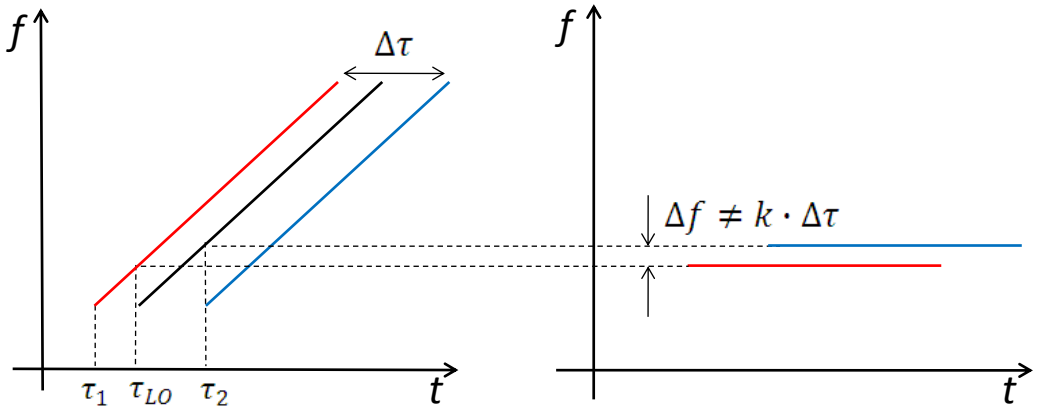


**Figure 3-7 Ambiguous measurement of frequency difference between the arrival signals**

$$\Delta f_d = f_{d2} - f_{d1} = k(\tau_2 - \tau_{LO} - \tau_1 + \tau_{LO}) = k \cdot \Delta\tau \tag{3.14}$$

The measurement of this frequency difference therefore allows for a very straightforward calculation of TDOA and hence the range difference causing it, as follows

$$\delta R = R_2 - R_1 = c \cdot \Delta\tau \tag{3.15}$$

$$\delta R = c\frac{\Delta f_d \cdot T_c}{B} \tag{3.16}$$

where $R_1$ and $R_2$ are the distance from the UT to sensor 1 and 2 respectively, $\Delta\tau$ and $\Delta f_d$ are the time difference and deramped frequency difference obtained in a TDOA measurement.

A condition for successful measurement of $\Delta f_d$ is that the LO chirp signal must not be activated in between the arrival time of the two received chirps $r_1(t)$ and $r_2(t)$. As shown by Figure 3-7, in this case, the one of the two received signals is leading while the other is lagging with respect to the LO chirp. The resultant frequency difference that does not indicate the actual time difference $(\tau_2 - \tau_1)$ between the two arrival signals (Figure 3-7) but an error time delay $(\tau_2 + \tau_1 - 2\tau_{LO})$. The difficulty of doing so in TDOA system is that the sensors and the UTs are not synchronised, and thus the signal transmitted time $\tau_T$ is unknown to the sensors. Hence a technique to examine if a chirp signal is received is needed to trigger the LO chirp at the appropriate time. The technique used in the TINA demonstrator to resolve this problem will be introduced and discussed in Section 5.5.2 of Chapter 5.

#### 3.1.2.2 Range resolution in TDOA measurement

The range resolution in this case will be half the resolution obtained in TOA measurement, as given by Eq. (3.17). This is because the deramp processing performed in either sensor, Eq. (3.13), is used to measure one-way relative time-of-flight information, $\tau_1 - \tau_{LO}$ and $\tau_2 - \tau_{LO}$, instead of return time-of-flight in the TOA measurement.

$$R'_{res} = \frac{c}{B} \tag{3.17}$$

The requirement on the chirp duration, Eq. (3.8), is also applied. The LFM chirp duration $T_c$ must be much longer than the maximum relative time-of-flight $\tau_{max}$, so that the spectrum analysis resolution $f_{res}$ will be approximately $1/T_c$. The range resolution $R'_{res}$ again defines the maximum error caused by multipath interference in the indoor location estimation using chirp deramping for TDOA measurement.

In this section, the use of LFM chirp signal in TOA and TDOA measurement is discussed, which are the fundamental measurements for a target location estimation

process. Compared to TOA, TDOA measurement is an indirect way of location estimation, finding relative time delay instead of direct measurement of range. The advantage of TDOA measurement is that it bypasses the synchronisation requirement between active targets and the sensors, but requires relatively more complicated calculation for the target location, which will be discussed in the Chapter 4. Another trade-off is lower resolution, as shown in Eq. (3.17) and Eq. (3.9). In the following section we will continue the discussion on a common concern when using LFM chirp signal, namely the linearity of chirp signal and its effect on the FFT analysis.

## 3.2 Determination of Sweep Linearity Requirements

The chirp linearity is clearly a key issue in determining the achievable performance and may constrain the range resolution and other aspects of system performance. A number of researchers have investigated this issue. Meta et al [50] have developed a novel processing solution to correct such nonlinearities based on a residual-video-phase (RVP) correction technique; Wang [51] has investigated the impact of quantization errors, spurs, and frequency nonlinearities in linear FMCW waveforms on the quality of SAR images; Piper [52] has analysed the effect of sinusoidal nonlinearities on the range resolution of linear FMCW radar. These papers tend to consider specific radar source nonlinearities in some detail, and then accurately characterize and maybe compensate for them. This may offer very good results in terms of system performance improvement, but lacks the means to quickly and readily estimate the necessary linearity specification of the LFM chirp signal and the likely performance of a given ranging system based on LFM chirp deramping. Therefore, a research has been made on this issue and the method of determining this requirement for FMCW radar has been accepted for publication in [53]. A similar analysis is rewritten in the following sections, which are tailored to the TDOA ranging system that we are discussing.

### 3.2.1 Fractional Slope Variation

The upper graph of Figure 3-8 illustrates a somewhat exaggerated non-linear chirp characteristic, of sweep bandwidth *B* and pulse duration $T_c$, showing frequency versus time relative to an ideal linear characteristic, the peak deviation from the linear case (dotted line) being denoted by $\Delta f$. The slope of the chirp characteristic, *f'*, is also indicated in the lower graph of Figure 3-8 and would of course be constant in the ideal case; instead it shows a steady and progressive reduction during the course of the pulse, which is typical of a free-running voltage-controlled oscillator, the total slope variation being $\Delta f'$.

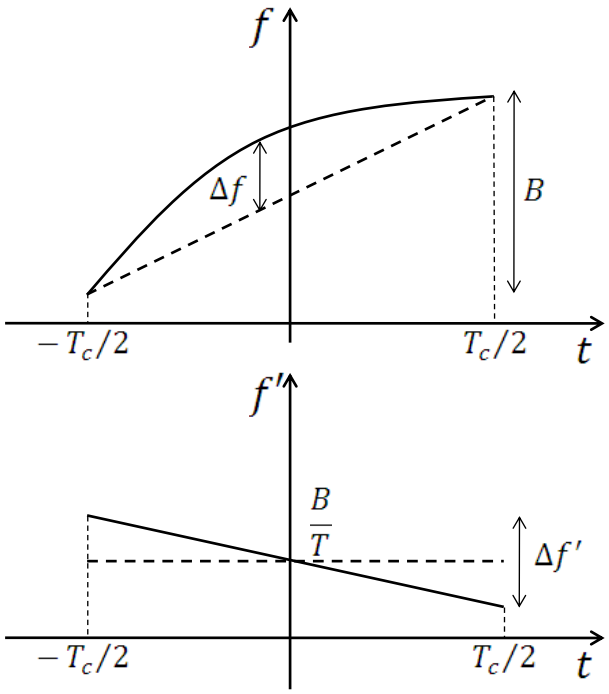


**Figure 3-8 Illustration of FM sweep (chirp) characteristic nonlinearity of chirp signal (upper), and the according frequency slope changes against time (lower)**

To offer a simple, practical and novel means of estimating the impact of chirp nonlinearity, we introduced a new parameter, the *fractional slope variation* (FSV), which may easily be obtained if the linear FM sweep tuning characteristic is given. This is defined as the ratio of maximum frequency slope variation, $\Delta f'$, to the mean frequency slope $\overline{f'}$, which is equivalent to the linear frequency modulated slope $k = B/T_c$.

$$FSV = \frac{\Delta f'}{\bar{f}'} = \frac{\Delta f'}{k} = \frac{\Delta f' T_c}{B} \tag{3.18}$$

The *FSV* can be used to analytically describe the time-frequency characteristic of the nonlinear chirp waveform, evaluate the nonlinearity level, and define the relationship between nonlinearity and its impact on range resolution. Firstly, the frequency slope function of LFM chirp can be found from the lower graph of Figure 3-8, as rewritten in Eq. (3.19).

$$\begin{aligned} f' = \frac{df}{dt} &= k - \frac{\Delta f'}{T_c} t \\ &= k - \frac{FSV \cdot k}{T_c} t \end{aligned} \tag{3.19}$$

The analytic function for the time-frequency characteristic of the nonlinear chirp waveform is obtained from integration of Eq. (3.19).

$$\begin{aligned} f(t) &= \int k - \frac{FSV \cdot k}{T_c} t \, dt \\ &= kt - \frac{FSV \cdot k}{2T_c} t^2 + f_m \end{aligned} \tag{3.20}$$

where the constant resulted from integration is $f_m$, the instantaneous frequency in the middle of the chirp duration:

$$f_m = f_c + \frac{FSV}{8} kT \tag{3.21}$$

Figure 3-9 shows the results of using Eq. (3.20) to illustrate a group of chirps with various FSV values, among which the FSV=0 case indicates the ideal linear version of the chirp that has the same bandwidth *B* and duration $T_c$.

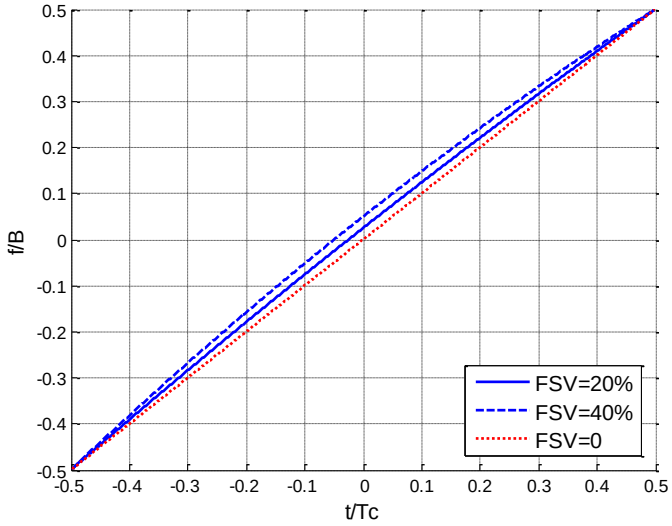


**Figure 3-9 Time frequency characteristics for nonlinear up-chirps with FSV=20%, 40%, and their linear version**

## 3.2.2 Sweep Linearity Requirement

If deramp processing is performed with a nonlinear chirp, the deramped frequency is given simply by the product of the chirp slope and associated time delay $\tau$, which is given by

$$f_d(t) = f(t) - f(t-\tau) = \tau \frac{df}{dt}(t) \tag{3.22}$$

The assumption of the time delay, $\tau$, being small in comparison to the pulse duration is also applied, which is the normal mode of operation of a ranging system using LFM chirp. For a perfectly linear chirp, the FM sweep rate *df/dt* has a constant value of $k=B/T_c$ and the result in Eq. (3.22) reduces to $k\tau$. However, if there is significant chirp nonlinearity then the deramped frequency will be time-variant over the pulse duration, as indicated by Eq. (3.22), and spread over a range of values, $\Delta f_d$, as follows, in which Eq. (3.18) is used to eliminate $\Delta f'$,

$$\Delta f_d = \tau \cdot \Delta f' = FSV \cdot k\tau \tag{3.23}$$

If the chirp nonlinearity is sufficient to cause a deramped frequency variation of the order of the reciprocal of the pulse duration, $1/T_c$, then a significant degradation in range resolution and/or range sidelobes might be expected. Considering a deramped

frequency expansion of $a/\ T_c$ (Hz), an upper limit on the nonlinearity coefficient $a$ may be established for which this degradation is just tolerable, with the following expression for the associated required fractional slope variation

$$FSV \cdot k\tau = \frac{a}{T_c};\ hence\ FSV = \frac{a}{k\tau \cdot T_c} \tag{3.24}$$

The time delay found in deramp processing have different physical meaning in TOA and TDOA measurement.

In a system measuring TOA, the time delay $\tau$ is given by twice the measurement range $R$. By replacing $kT_c$ with bandwidth $B$, and substituting Eq. (3.9) into Eq. (3.24), the relationship between FSV and the measurement range $R$ is obtained:

$$FSV = \frac{ac}{2RB} = \frac{aR_{res}}{R} \tag{3.25}$$

where $R_{res}$ is the range resolution given in Eq. (3.9).

This result has direct practical value in determining the required chirp linearity for a given system specification, indicating that the linearity requirement becomes progressively more stringent with increasing range.

In a system measuring TDOA, the time delay $\tau$ under measurement is the time difference between two received signals, and thus the maximum value of $\tau$ is given by the physical distance between the two receivers $D$, Figure 3-5. By substituting Eq. (3.17) into Eq. (3.24), the relation between FSV and the receivers' separation distance $D$ is obtained:

$$FSV = \frac{aR'_{res}}{2D} \tag{3.26}$$

Since linearity requirement is more stringent for longer range detection, fulfillment of Eq. (3.26) ensures adequate linearity for any possible TDOA values between the two receivers. This can be used to estimate the required chirp linearity which is constrained by the receivers' distance.

### 3.2.3 Evaluating Ranging Resolution using FSV

It now remains to establish a sensible value for $a$. To a first approximation, the chirp nonlinearity can be represented by a linear change in slope *f'*, (Figure 3-4) over the pulse duration, Eq. (3.19), with a resulting deramp signal instantaneous angular frequency of the form

$$\begin{aligned}\omega_d(t) &= 2\pi\tau\frac{df}{dt}\\ &= 2\pi\tau\left(k-\frac{FSV\cdot k}{T_c}t\right)\\ &= 2\pi k\tau - 2\pi\frac{a}{T_c^2}t\end{aligned} \tag{3.27}$$

Eq. (3.24) is used to replace FSV in order to interpret $\omega_d$ with $a$. This yields an expression for the deramped signal phase containing a square-law nonlinearity component:

$$\phi_d(t) = 2\pi k\tau t - \pi a(t/T_c)^2;\ for -\frac{T_c}{2}\le t\le\frac{T_c}{2} \tag{3.28}$$

Thus the impact of such nonlinearity on the range resolution can be predicted by considering the Fourier transform of the deramped signal based on this square-law phase variation:

$$F_d(\omega) = \mathcal{F}[\exp(j\pi a t^2/T_c^2)] \tag{3.29}$$

Figure 3-10 shows the results of such a process normalized in terms of a peak amplitude of 0 dB for a perfectly linear chirp and a normalized range axis of $R/\Delta R$, where $\Delta R$ is the range resolution, equal to $c/2B$ for TOA measurement, and $c/B$ for TDOA measurement. Referring to Figure 3-10(a), with no pulse weighting and perfect sweep linearity the point-target response is a sinc function, with a -3 dB width of $0.885\Delta R$. The range resolution is seen to steadily degrade as the level of nonlinearity is increased, to $0.889\Delta R$, $0.94\Delta R$, and $1.05\Delta R$, for $a$=1, 2, and 3, respectively. Whilst the degradation in range resolution is quite modest there is a significant deterioration in the range sidelobe profile, which essentially disappears for $a$=3. There is also a significant reduction in signal level, and hence sensitivity, of 1.0 dB for $a$=2, and 2.2 dB for $a$=3.

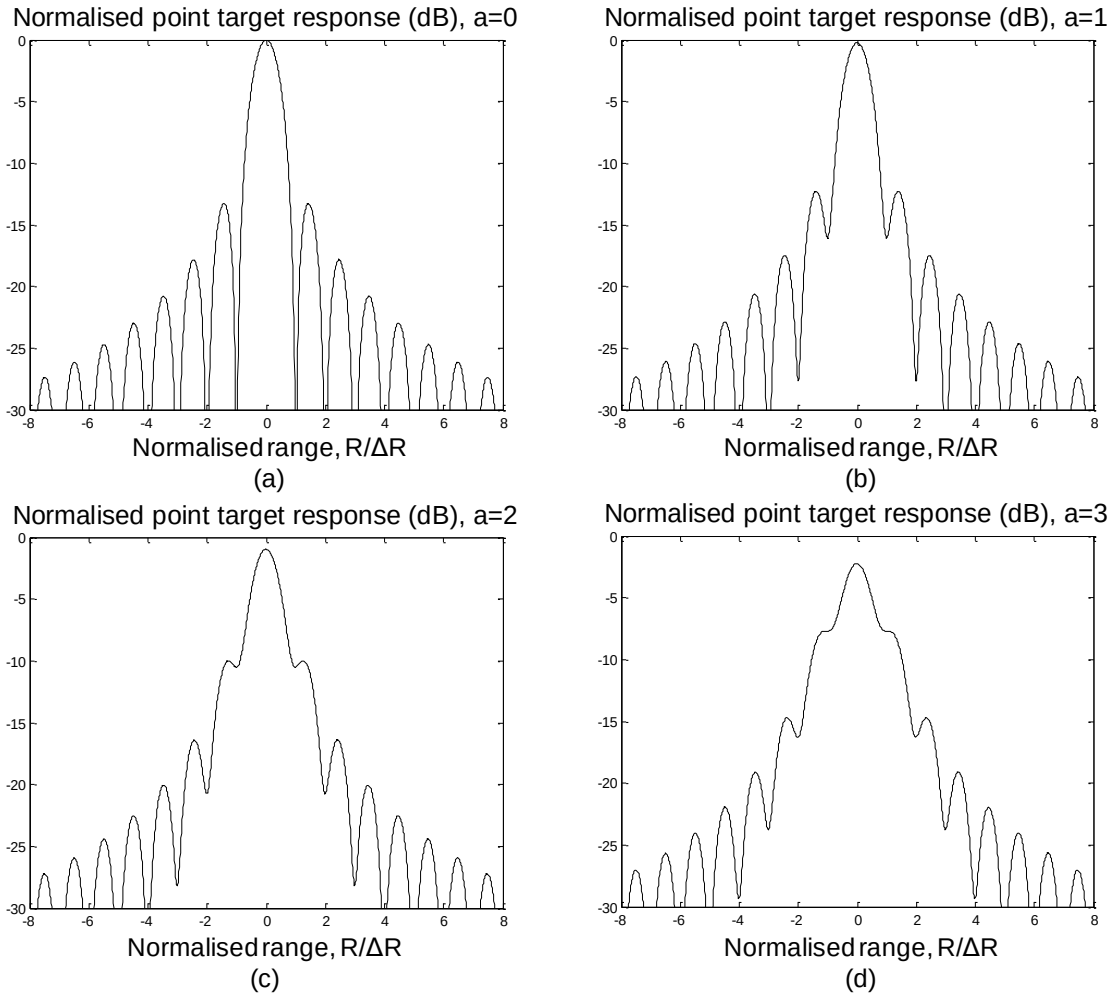


**Figure 3-10 Effect of chirp sweep nonlinearity on point-target response, uniform shaping; (a) *a*=0, (b) *a*=1, (c) *a*=2, (d) *a*=3, where the nonlinearity coefficient *a=FSV·ΔR/R*.**

Figure 3-11 shows the corresponding results for a cosine-weighted pulse. With perfect linearity, Figure 3-11(a), the point-target response exhibits the ideal -23 dB range sidelobe level and 1.18$\Delta R$ -3 dB mainlobe width associated with cosine pulse weighting. The range resolution gradually degrades with increasing nonlinearity to 1.20$\Delta R$, 1.24$\Delta R$, and 1.34$\Delta R$, for $a$=1, 2, and 3, respectively. Similarly, the sidelobe structure deteriorates with increasing nonlinearity, becoming almost indistinct for $a$=3. The sensitivity decreases by 0.50 dB for $a$=2 and 1.0 dB for $a$=3.

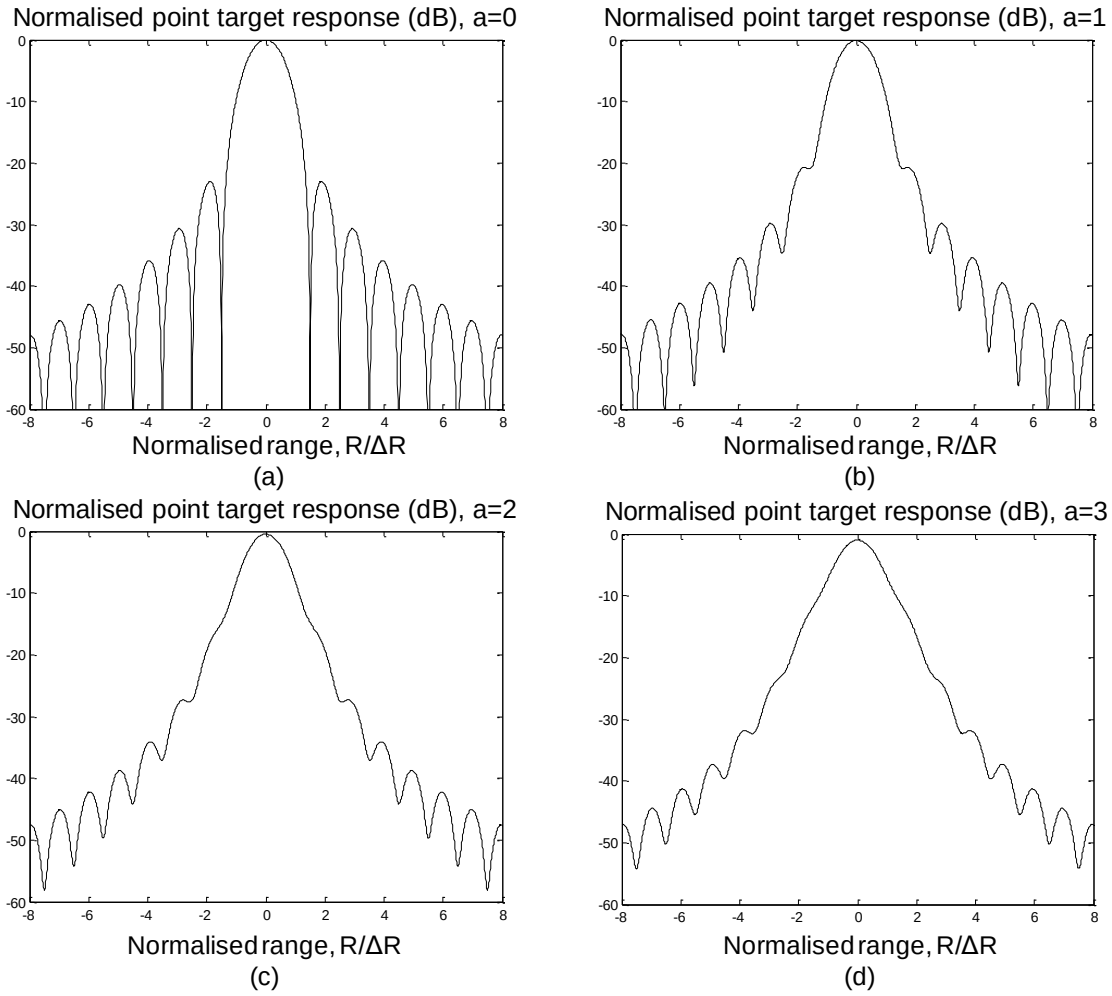


**Figure 3-11 Effect of chirp sweep linearity on point-target response, cosine pulse shaping; (a) *a*=0, (b) *a*=1, (c) *a*=2, (d) *a*=3.**

Finally, Figure 3-12 shows the results for a raised-cosine-weighted pulse. With perfect linearity, Figure 3-12, the point-target response exhibits the ideal -31 dB range sidelobe level and 1.44$\Delta R$ -3 dB mainlobe width associated with raised-cosine weighting. The range resolution now degrades even more gradually with increasing nonlinearity to 1.44$\Delta R$, 1.48$\Delta R$, and 1.68$\Delta R$, for $a$=1, 2, and 4, respectively. The sidelobe structure deteriorates, becoming indistinct for $a$=2 and the sensitivity decreases by 0.25 dB for $a$=2 and 1.0 dB for $a$=4. Further results expressing the broadening of the point-target response due to nonlinearity, to specified levels, are summarised in Table 3-1 to Table 3-3, which may be a valuable input to the design process to determine the tolerable source nonlinearity for a given range resolution requirement.

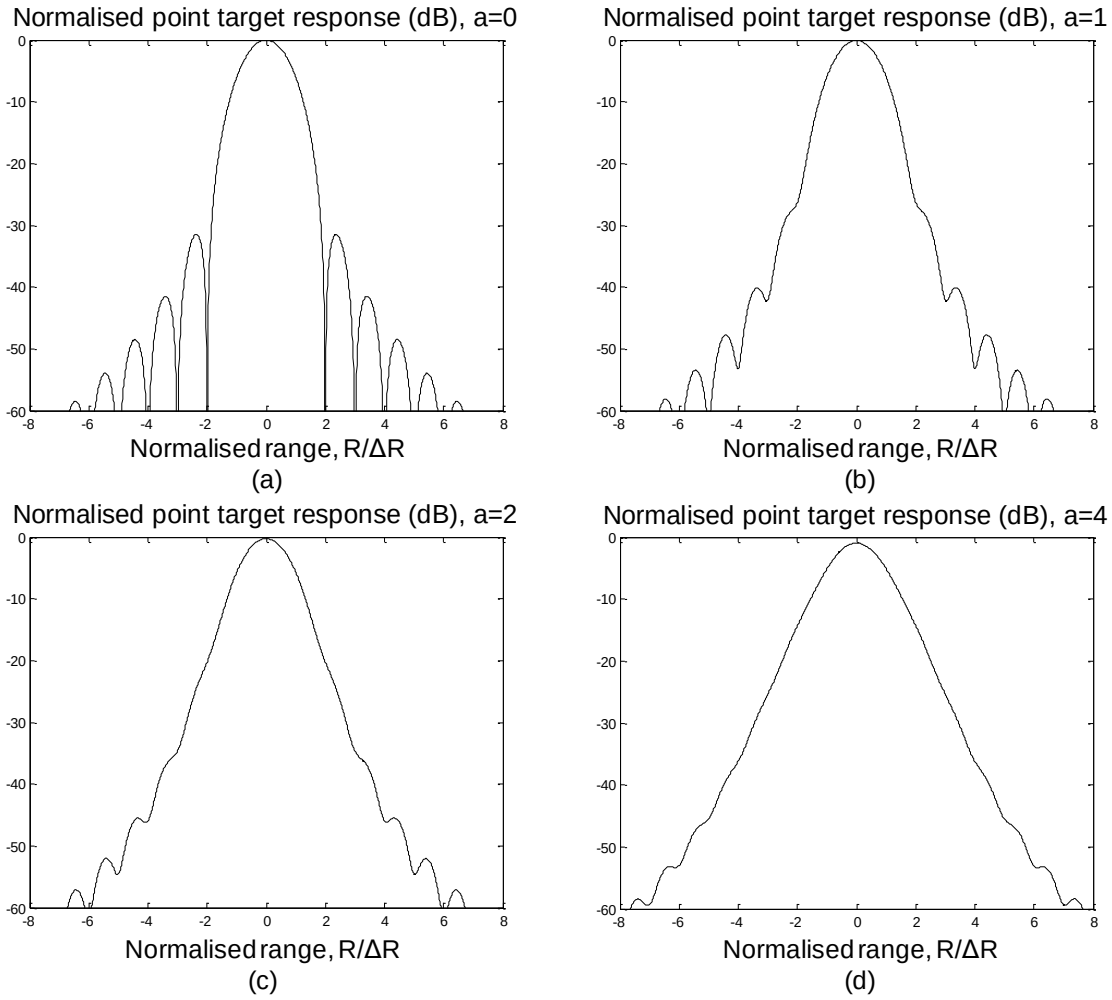


**Figure 3-12 Effect of chirp sweep nonlinearity on point-target response, raised-cosine pulse shaping; (a) *a*=0, (b) *a*=1, (c) *a*=2, (d) *a*=3.**

| | **Range resolution (×$\Delta R$) to specified levels** | | | |
|---|---|---|---|---|
| *a* | -3 dB | -10 dB | -20 dB | -30 dB |
| 0 | 0.88 | 1.5 | 1.84 | 1.96 |
| 1 | 0.889 | 1.54 | 3.68 | 5.86 |
| 2 | 0.94 | 1.76 | 3.86 | 7.82 |
| 3 | 1.05 | 3.06 | 5.6 | 9.78 |
| 4 | 2.62 | 3.24 | 5.88 | 9.9 |

**Table 3-1 Range resolution versus nonlinearity coefficient, from uniform pulse shaping**

| | **Range resolution (×$\Delta R$) to specified levels** | | | |
|---|---|---|---|---|
| *a* | -3 dB | -10 dB | -20 dB | -40 dB |
| 0 | 1.18 | 2.06 | 2.64 | 2.98 |
| 1 | 1.2 | 2.12 | 2.92 | 6.82 |
| 2 | 1.24 | 2.26 | 4.14 | 8.68 |
| 3 | 1.34 | 2.62 | 4.54 | 10.46 |
| 4 | 1.56 | 3.12 | 5.36 | 10.68 |

**Table 3-2 Range resolution versus nonlinearity coefficient, from cosine pulse shaping**

| | **Range resolution (×$\Delta R$) to specified levels** | | | |
|---|---|---|---|---|
| *a* | -3 dB | -10 dB | -20 dB | -30 dB |
| 0 | 1.44 | 3.32 | 3.92 | 4.02 |
| 1 | 1.44 | 3.46 | 5.82 | 9.92 |
| 2 | 1.48 | 4.00 | 7.34 | 11.84 |
| 3 | 1.56 | 4.58 | 7.88 | 13.66 |
| 4 | 1.68 | 5.06 | 9.02 | 15.34 |

**Table 3-3 Range resolution versus nonlinearity coefficient, from raised-cosine pulse shaping**

These results indicate that the range resolution, as measured by the -3 dB width, is not particularly sensitive to nonlinearity, although there is a much more pronounced sensitivity when measured to the -20 dB point. It is evident that shaped pulses can offer a slightly reduced vulnerability to source nonlinearity, no doubt because of the inherently reduced range resolution associated with such pulse shapings. There is clearly no absolute cutoff on the acceptable degree of nonlinearity, but taking a 1 dB sensitivity reduction criterion would define a maximum limit on $a$ of 2, 3, and 4, for uniform, cosine, and raised-cosine weightings, respectively, with (Table 3-1 to Table 3-3) a corresponding 52-110% increase in the point-target response mainlobe width measured to the -20 dB point. These values for $a$ can be used to sensibly inform the result of Eq. (3.25) and Eq. (3.26) so as to give a simple, practical means of estimating the source linearity specification over a range of system requirements.

For example, let us consider an indoor location system measuring TDOA information between receivers; therefore Eq. (3.26) is applied. Say the chirp sweeping bandwidth is 83.5 MHz, and the receivers are separated in 28 m distance. The range resolution from TDOA measurement is thus 3.6 m. With $a$=1 and $a$=2, the according requirements on FSV value of the chirp signal with uniform pulse shaping are:

$$when\ a = 1, FSV = \frac{1 \cdot 3.6}{2 \cdot 28} \times 100\% = 6.4\% \tag{3.30}$$

$$when\ a = 2, FSV = \frac{2 \cdot 3.6}{2 \cdot 28} \times 100\% = 12.8\%$$

The results from Eq. (3.30) can be used as a guidance to select different approaches of generating the LFM chirp signal for the assumed system specifications. Alternatively, if the signal source is given, and the FSV value is known, one can find the nonlinearity coefficient *a* from Eq. (3.25) and Eq. (3.26) in order to estimate the potential degradation of range resolution when measuring time delay (Table 3-1 to Table 3-3).

### 3.2.4 Relation of Fractional Slope Variation to Linearity

Referring to Figure 3-8, which depicts a non-linear chirp characteristic of instantaneous frequency *f*, and its derivative, *f'*, the linearity definition based on the *fractional slope variation* is rewritten as

$$FSV = \frac{\Delta f'}{\bar{f}'} = \frac{\Delta f' T_c}{B} \tag{3.31}$$

In contrast, the standard definition of linearity [54;55] in common use relates to the ratio of peak deviation from linear to total range, as follows

$$linearity = \frac{\Delta f}{B} \tag{3.32}$$

where $\Delta f$ is the maximum excursion of the characteristic from linear. Clearly, these two definitions are quite different, though they may in fact be related. To a first approximation, which is actually very reasonable in many cases, the slope of the frequency sweep characteristic in Figure 3-8 varies linearly with time during the course of the radar pulse around a mean value equal to the ratio of the sweep bandwidth, *B*, and the pulse duration, $T_c$. The slope of the characteristic may therefore be written as

$$f' = \frac{B}{T_c} - \mu t;\ for - \frac{T_c}{2} \le t \le \frac{T_c}{2} \tag{3.33}$$

where $\mu$ is the derivative of the frequency slope $f'$. Thus, from Eq. (3.31), the fractional slope variation can be expressed as

$$FSV = \frac{\Delta f'}{\bar{f}'} = \frac{\mu T_c^2}{B} \tag{3.34}$$

By integrating Eq. (3.33), the instantaneous frequency may be expressed as

$$f = \frac{B}{T_c} t - \frac{\mu t^2}{2} + constant;\ for - \frac{T_c}{2} \leq t \leq \frac{T_c}{2} \tag{3.35}$$

where the $Bt/T_c$ term represents the linear and the $\mu t^2/2$ term the nonlinear component of the characteristic, exhibiting a square-law behavior. The maximum deviation of the sweep from linear is thus given by the value of $\mu t^2/2$ at the $t=T_c/2$, as follows

$$\Delta f = \frac{\mu t^2}{8} \tag{3.36}$$

and so the linearity, as defined by the Eq. (3.32), is given by

$$linearity = \frac{\mu t^2}{8B} = \frac{FSV}{8} \tag{3.37}$$

This demonstrates a factor-of-eight relationship between the fractional slope variation and the linearity so that the result of Eq. (3.26), specifying the degree of linearity required for acceptable TDOA measurement performance, may be rewritten as

$$linearity \approx \frac{FSV}{8} = \frac{aR'_{res}}{16D} \tag{3.38}$$

where the '≈' sign alludes to the assumption of approximately linear sweep slope variation over the duration of the pulse. This simple result is valuable to estimate the linearity requirements.

## 3.2.5 Non-Linearity of Typical Voltage-Controlled Oscillator

Figure 3-13 (a) shows the measured tuning characteristic of the Hittite HMC386LP4 voltage-controlled oscillator (VCO), which is evidently highly non-linear and tunes over the range 2.12 GHz to 2.57 GHz. The slope of this characteristic is shown in Figure 3-13 (b) and decreases almost monotonically from approximately 150 MHz/V at lower frequencies to 30 MHz/V at higher frequencies. If this device is to be used in

the 2.4 GHz ISM band (2.4 GHz to 2.485 GHz), then a narrower tuning voltage range of 4.2 V to 6.6 V is required and the region of interest of the characteristic is now replotted in Figure 3-14.

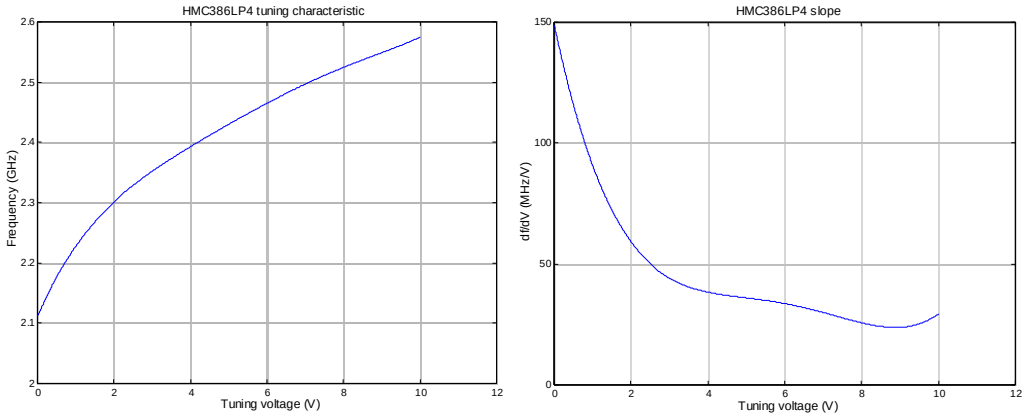


(a) (b)

**Figure 3-13 (a) Measured tuning characteristic of the HMC386LP4 voltage-controlled oscillator; (b) Measured slope of the HMC386LP4 voltage-controlled oscillator.**

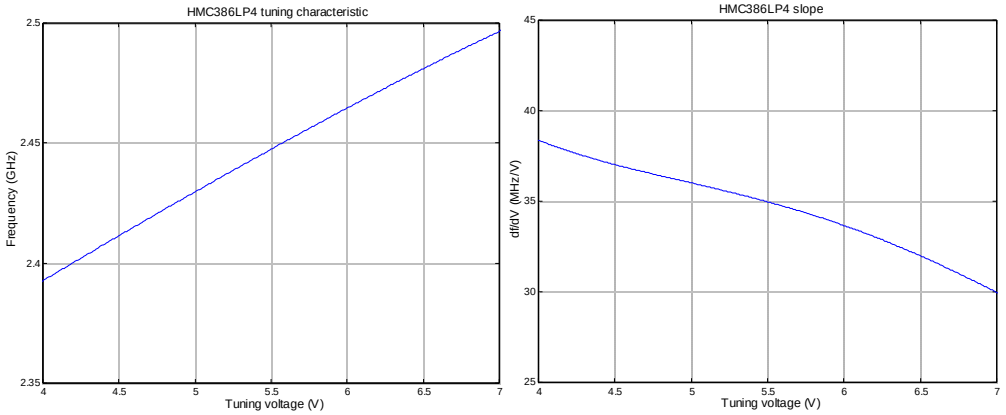


(a) (b)

**Figure 3-14 (a) Measured slope of the HMC386LP4 voltage-controlled oscillator; (b) Measured slope of the HMC386LP4 voltage-controlled oscillator, over the 2.4 to 2.485 GHz range.**

Whilst the tuning characteristic looks, superficially, to be rather more linear, its slope (Figure 3-14 (b)) still varies over a significant range, from 37.8 MHz/V to 31.6 MHz/V, thus betraying the FM sweep linearity of this VCO. It is, of course, this variation in slope that sets the performance limit of an LFM chirp-based TDOA ranging system using this device which may be readily predicted from Eq. (3.26) with the measured FSV value of this device, of 0.179, or 17.9%. Taking $a$ = 2 and a range resolution commensurate with 83.5 MHz sweep bandwidth of 3.6 m, Eq. (3.26)

indicates the maximum operating range due to source nonlinearity is some 20.1 m. This very low figure is no surprise in view of the high degree of nonlinearity of this VCO.

In order to use the *linearity* parameter of the same device to accurately estimate operating range, the source VCO characteristic must fulfil the assumption that its slope varies linearly over the desired tuning range of the device. Figure 3-14 (b) would suggest that this assumption is not perfectly valid, though it may still be used with reasonable accuracy. In order to measure the VCO *linearity*, the peak deviation from the linear trend must be determined. Figure 3-15 shows the deviation of the tuning characteristic from a linear fit between 2.4 GHz and 2.485 GHz. It exhibits a characteristic that is evidently a good approximation to the square-law, in spite of the very poor linearity of this particular source, which is again consistent with expectations, Eq. (3.36). From Figure 3-15, the maximum deviation from linear is 1.78 MHz and the FM sweep range is 83.5 MHz thus giving a *linearity* of 0.0213. The maximum operating range based on this figure, from Eq. (3.38), is now 21.1 m. This compares to the 20.1 m figure that was calculated directly from the *FSV* figure showing agreement to within 5% and thus vindicating the approach.

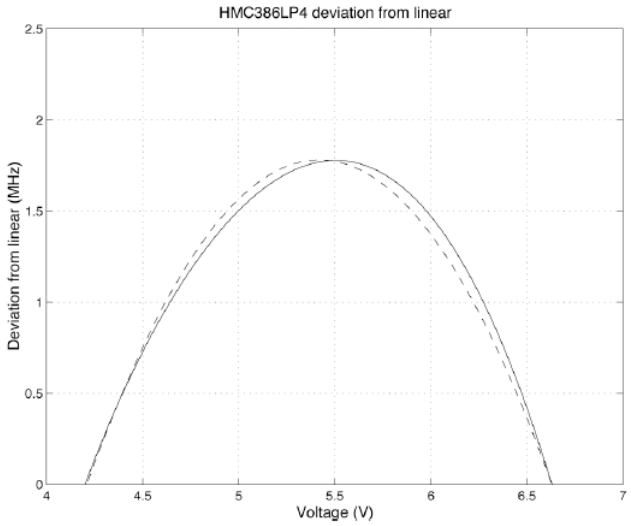


**Figure 3-15 Measured deviation from linear of the HMC386LP4 voltage-controlloed oscillator, over the 2.4 to 2.4835 GHz range (solid line), showing a good approximation to the postulated square-law (parabolic) error variation (dashed line)**

The analysis above suggests that such simple VCO based chirp signal is likely to produce distorted deramped component if the required operating range is beyond

roughly 20 m. In case of a greater operating range than this distance, a chirp signal source of better linearity shall be used. For example, the direct digital synthesizer (DDS) is believed to be able to generate highly linear (better than 0.01% linearity) chirp signal [56] due to its precise digital operation. Therefore, the TINA tag used in the proposed demonstration system uses DDS as its signal source.

## 3.3 Summary

In this chapter, the deramping technique that finds the time delay information of chirp signal was introduced. Signal model of chirp signal and corresponding deramping process were presented with examples describing the TOA measurement and the TDOA measurement cases. The resultant range resolution in both TOA and TDOA measurements were derived. This will be useful in the multipath mitigation study in that the respective range resolution defines the maximum error that could be caused by multipath, which will be covered in the Section 5.6 of Chapter 5.

The second section then showcased a straightforward means of estimating the FM sweep linearity required in a ranging system based on LFM chirp signal generated from a free-running voltage-controlled oscillator source which is increasingly commonplace in low cost systems. By assuming that, typically in these sources, the FM sweep nonlinearity takes the form of a uniformly decreasing or increasing tuning slope over the duration of the pulse, a very simple result is obtained to determine the required linearity, in terms of the *fractional slope variation*.

This result is then qualified by considering the effect on point target response, for a variety of pulse shaping functions, yielding a set of expressions applicable to uniform, cosine and raised-cosine weightings where it is found that tapered pulses are more resistant to such sweep nonlinearities. These results were then expressed in terms of the standard *linearity* definition, which is shown to be typically related to the *fractional slope variation* by a factor of eight.

Experimental measurements from a particularly non-linear commercial voltage-controlled oscillator were next presented to validate these results, in which agreement to within 5% is obtained.

# *Chapter 4*

## MULTILATERATION LOCATION ESTIMATION

In Chapter 3, we have introduced the time-of-arrival (TOA) and time-difference-of-arrival (TDOA) ranging technique using LFM chirp signals. In the TINA indoor location system, the TDOA method is chosen because it simplifies the communication between the active tags and the sensors, in the way that it requires only one way communication from the active tag to the sensor without the synchronisation between all the tags and the sensors [57]. This is desirable for an indoor location system where multiple sensors are used in every single indoor cell covered by the system, where the synchronisation between all the user tags and the sensors therein can be a tricky job.

In this chapter, we will first introduce the approach of locating the signal source from the TDOA information obtained, a method referred to as multilateration in the literature. More importantly, a simple and flexible computer algorithm for multilateration will be proposed in Section 4.2. This algorithm has been implemented in the TINA indoor location system to perform location estimation using TDOA.

The location accuracy related to this approach is investigated in Section 4.3, and it is found that deployment of the sensors in the indoor environment will affect the location finding performance. The concept of sensitive region is introduced to explain the location sensitivity spreading. The conclusions addressed in this section will assist the analysis of the real measurement data presented in Chapter 6.

## 4.1 Multilateration Process

Multilateration is a process for estimating the location of a user terminal by measuring the TDOAs of its transmitted radio or acoustic signal received at a number of spatially separated sensors. Multilateration has been employed in radar and sonar applications [58], microphones localisation [59] and recently indoor location systems [16].

The concept of multilateration is simple. Consider there is a pair of spatially separated sensors that measure the TDOA from a user terminal (UT). A signal transmitted from the UT will arrive at the two sensors at slightly different times, where this TDOA is due to the difference between distances from the user to the sensors. By measuring the arrival time difference (i.e. TDOA) of the transmitted signal between these two fixed but spatially separated receiving sensors, a hyperbola can be obtained to represent all the possible locations of the transmitter in a 2-D plane, calculated from this particular TDOA value alone. With an additional receiving sensor, a second TDOA value can be measured between this third sensor and one of the previous two sensors. A second hyperbola can also be obtained. The intersection of the two hyperbolae is therefore the estimated location of the transmitter. That is to say, in order to perform 2-D location finding of the user transmitter, a minimum of three receiving sensors are needed.

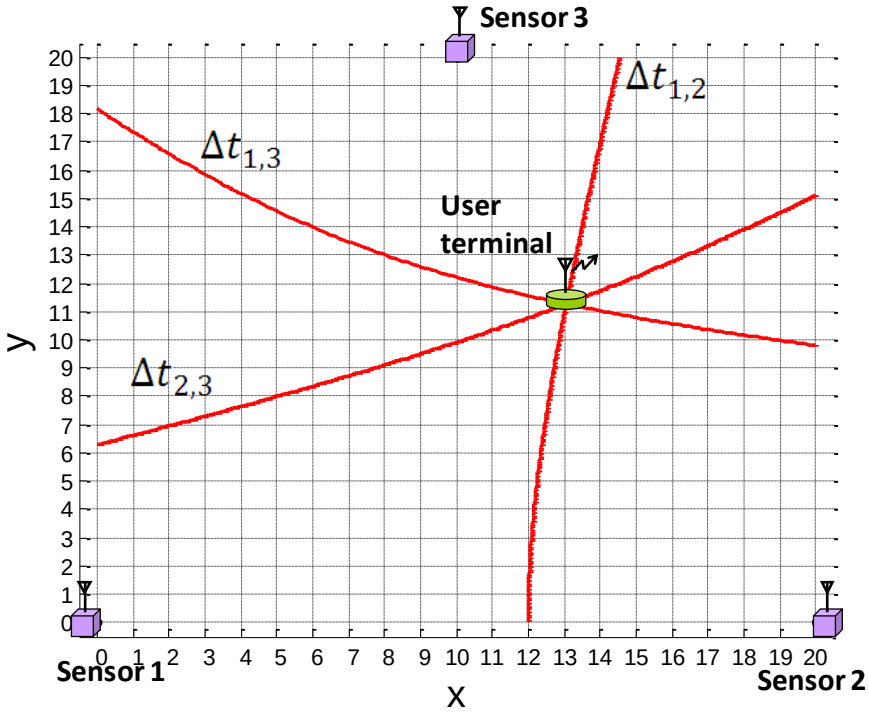


**Figure 4-1 A three-sensor location system measuring UT location from the TDOA parabolic curves**

The detailed process of multilateration can be explained with a simple example of a three-sensor location system using TDOA measurements shown in Figure 4-1. The goal of the system is to estimate the 2-D location of an active UT by analyzing the measured TDOA information obtained from the received signal of the sensors.

Note the transmission time between a UT and the $n_{th}$ sensor as $t_n$, and the TDOA between the $n_{\text{th}}$ and the $m_{\text{th}}$ sensor as $\Delta t_{n,m}$, which is defined by

$$\Delta t_{n,m} = t_n - t_m \tag{4.1}$$

In the example of Figure 4-1, three TDOAs $\Delta t_{1,2}$, $\Delta t_{1,3}$, and $\Delta t_{2,3}$ are measured by the system. The relationship between the UT location and the measured TDOA can be expressed in form of a nonlinear equation. Since one TDOA measurement, between a pair of sensors, results in a $\Delta t_{n,m}$ value, three nonlinear equations are found from the measurements of $\Delta t_{1,2}$, $\Delta t_{1,3}$, and $\Delta t_{2,3}$, as in Eq. (4.2).

$$\begin{aligned}
\Delta t_{1,2} &= \frac{1}{c}\left(\sqrt{(x_t - x_1)^2 + (y_t - y_1)^2} - \sqrt{(x_t - x_2)^2 + (y_t - y_2)^2}\right) \\
\Delta t_{1,3} &= \frac{1}{c}\left(\sqrt{(x_t - x_1)^2 + (y_t - y_1)^2} - \sqrt{(x_t - x_3)^2 + (y_t - y_3)^2}\right) \\
\Delta t_{2,3} &= \frac{1}{c}\left(\sqrt{(x_t - x_2)^2 + (y_t - y_2)^2} - \sqrt{(x_t - x_3)^2 + (y_t - y_3)^2}\right),
\end{aligned} \tag{4.2}$$

where $c$ is the speed of light, $(x_t, y_t)$ is the coordinates of the UT location, while $(x_n, y_n)$ and $(x_m, y_m)$ are the known coordinates for the $n_{\text{th}}$ and the $m_{\text{th}}$ sensor respectively.

Each one of the nonlinear equations in Eq. (4.2) is a locus representing all the possible locations of the UT, which is a one half of a two-sheeted hyperboloid in a 2-D plane view. Therefore, the three TDOAs produce three hyperbolas, as indicated by the three red lines in Figure 4-1. If the TDOAs are measured correctly with line-of-sight reception of signal at all of the three sensors, the three hyperbolas shall intersect at one single point, which is the estimated location of the user terminal.

In some cases, introducing more than three sensors to the indoor area of interest is beneficial. Theoretically, minimum two of the hyperbolas are required to perform 2-D location finding, as the third hyperbola is supposed to come across the same intersection point between the other two curves. However, in the presence of noise, multipath, and non-line-of-sight (NLOS) propagation, the three intersection points resulting from measurement of three TDOAs may not overlap with each other, and thus ambiguity of estimated location occur. Further information is needed to determine which of the three coordinates stand for the location of the UT. Useful

information for resolving this ambiguity can be angle-of-arrival (AOA) information in hybrid TDOA/AOA system [60] or received-signal-strength (RSS) in other cases. Also, in a pure TDOA system, redundant sensors can be placed at different positions in order to provide extra groups of intersection points, and the location where most of the intersection points overlap is the estimated location. The number of redundant sensors depends on the level of TDOA measurement errors and the requirement on the location estimation accuracy.

Regardless of the number of sensors employed in a location system, the principle of multilateration location finding is to solve the UT location coordinate from two TDOAs obtained. Solving this problem has attracted many interests in the past decades, and a practical algorithm has been developed and implemented during the TINA project, which will be presented in the following section.

## 4.2 A Numerical Algorithm for Multilateration

Finding the intersection of two hyperbolae has been proven to be computationally difficult [61]. Analytical methods often produce multiple false locations and further knowledge and constraints are needed to determine the correct location [62;63]. The iterative Taylor series based technique [12] has been used in tackling the multilateration problem. However, this technique is computationally intensive, the success of which depends strongly on how close the initial guesses are to the real solutions or the convergence to local minima can occur. Closed-form methods achieving optimum performance with relatively small computation load are available [64;65] but they are difficult to implement without knowing the statistics of the TDOA, which in turn depend on the particular environment.

### 4.2.1 TDOA Mapping

In this section, we present a conceptually simple, non-iterative algorithm for location estimation based on multilateration. The algorithm sets out to determine the unique location of the user terminal by comparing the measured, real-time TDOA values at

fixed sensor locations with the ideal, pre-calculated TDOA set with the best matched coordinates producing the smallest error interpreted as the estimated UT location.

The proposed algorithm will again be illustrated using the simple three-sensor scenario. Suppose that a transmitting user terminal is located somewhere within the 20 m-by-20 m indoor area and the three receiving sensors are located at fixed coordinates (0 m, 0 m), (20 m, 0 m) and (10 m, 20 m) as shown in Figure 4-1.

In the algorithm, the indoor area is uniformly divided into and represented as an *N*-by-*N* grid with a total of $N^2$ grid points in a 2-D plane. The number *N* is chosen based on the precision requirement and larger *N* values result in higher precision. In Figure 4-1, the 20 m-by-20 m area is represented as a 21-points-by-21-points grid by choosing *N*=21, where the grid points are the interceptions of the dotted grid lines.

Before actual measurements are taken, the algorithm calculates a set of TDOA numbers between every pair of sensors at all the grid points that define the entire indoor area. The TDOA between sensors *n* and *m* for a signal originating from the grid point with coordinates $(X, Y)$ is given by

$$TD_{n,m}(X,Y) = \frac{1}{c}\left(\sqrt{(X-x_n)^2 + (Y-y_n)^2} - \sqrt{(X-x_m)^2 + (Y-y_m)^2}\right), \quad (4.3)$$

where, $(x_n, y_n)$ and $(x_m, y_m)$ are the coordinates of sensors *n* and *m*, respectively. Eq. (4.3) represents the ideal TDOA calculation and assumes perfect line-of-sight reception of the signal originating from $(X, Y)$ by the sensors without noise or interference present. The above calculations are performed for each of the $N^2$ grid points by substituting the corresponding coordinates $(X, Y)$ into the equations above. With three sensors, the algorithm thus calculates $TD_{1,2}(X,Y)$, $TD_{1,3}(X,Y)$, and $TD_{2,3}(X,Y)$, and the results form three 2-D matrices containing the pre-calculated TDOA corresponding to *X* and *Y*. The matrix of pre-calculated TDOA can then be illustrated by a wireframe mesh with colour determined by the values of $TD_{n,m}$, Figure 4-2.

To combine the three matrices into one, a 2-D matrix of 3-D vectors $\boldsymbol{p}_{X,Y}$ is defined as

$$\boldsymbol{p}_{X,Y} = TD_{1,2}(X,Y)\boldsymbol{i} + TD_{1,3}(X,Y)\boldsymbol{j} + TD_{2,3}(X,Y)\boldsymbol{k} \tag{4.4}$$

which can be regarded as the ideal, pre-calculated TDOA map for the indoor area concerned.

One TDOA map is generated only once and then stored for use in all future location calculations, provided the sensor locations remain unchanged.

When measurements start, the location system detects and returns the actual, real-time TDOAs $\Delta t_{1,2}$, $\Delta t_{1,3}$, and $\Delta t_{2,3}$ between the three corresponding sensor pairs due to a user terminal signal coming from an unknown location. After each measurement, a vector is formed according to

$$\boldsymbol{m} = \Delta t_{1,2}\boldsymbol{i} + \Delta t_{1,3}\boldsymbol{j} + \Delta t_{2,3}\boldsymbol{k} \tag{4.5}$$

By calculating the distance of this vector from each of the $N^2$ vector elements in the pre-calculated TDOA map matrix $\boldsymbol{p}_{X,Y}$, the desired user terminal location must be the coordinates used for calculating the element that produces the shortest distance. An error matrix for the $N$=21 three-sensor location system example is introduced as

$$\boldsymbol{e} = \begin{bmatrix} |\boldsymbol{p}_{0,0} - \boldsymbol{m}| & \cdots & |\boldsymbol{p}_{0,20} - \boldsymbol{m}| \\ |\boldsymbol{p}_{1,0} - \boldsymbol{m}| & \cdots & |\boldsymbol{p}_{1,20} - \boldsymbol{m}| \\ \vdots & \vdots & \vdots \\ |\boldsymbol{p}_{20,0} - \boldsymbol{m}| & \cdots & |\boldsymbol{p}_{20,20} - \boldsymbol{m}| \end{bmatrix}, \tag{4.6}$$

where each element of $\boldsymbol{e}$ is the modulus of the corresponding distance vector and represents the root-square time difference between the measured and the pre-calculated TDOA vectors at the coordinates concerned. The coordinates that produce the smallest element in $\boldsymbol{e}$ is thus the estimated location of the UT. As an example, a UT is seen to be situated at coordinates (13 m, 11 m) in Figure 4-1. The corresponding error matrix $\boldsymbol{e}$ plotted in Figure 4-3 therefore has a minimum at the same coordinates which are duly selected as the correct location of the user terminal.

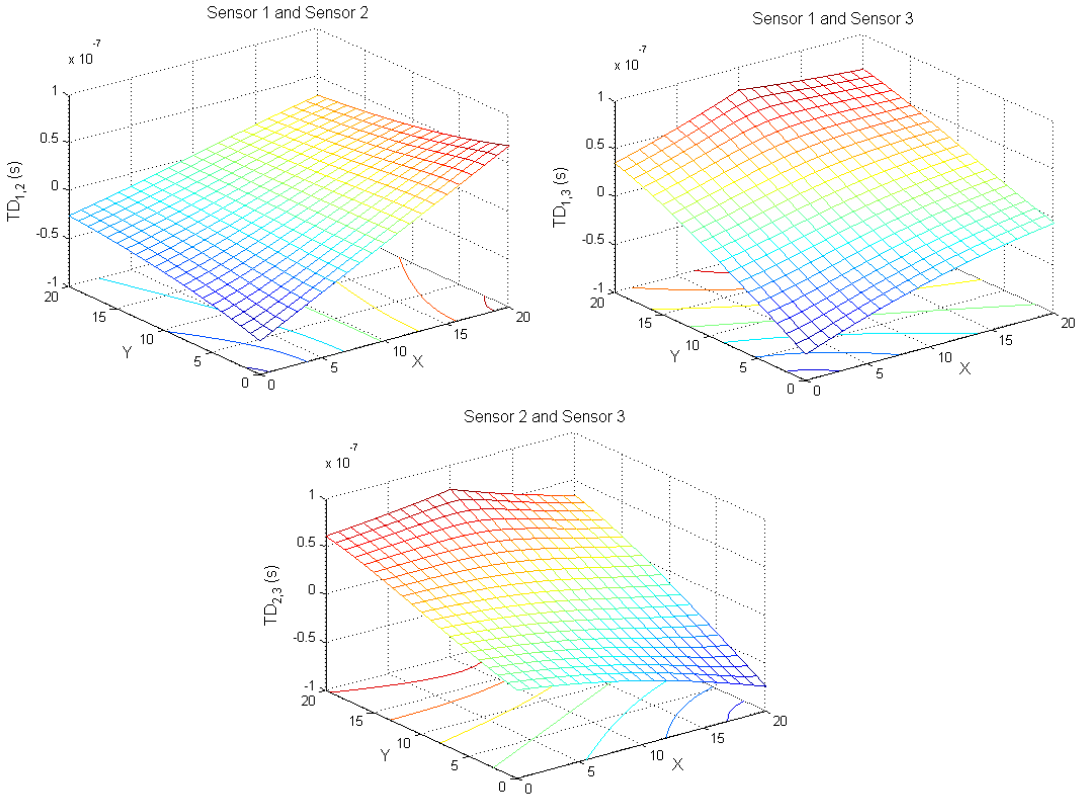


**Figure 4-2 Mesh plots of the 2-D matrices of pre-calculated TDOA, *N*=21**

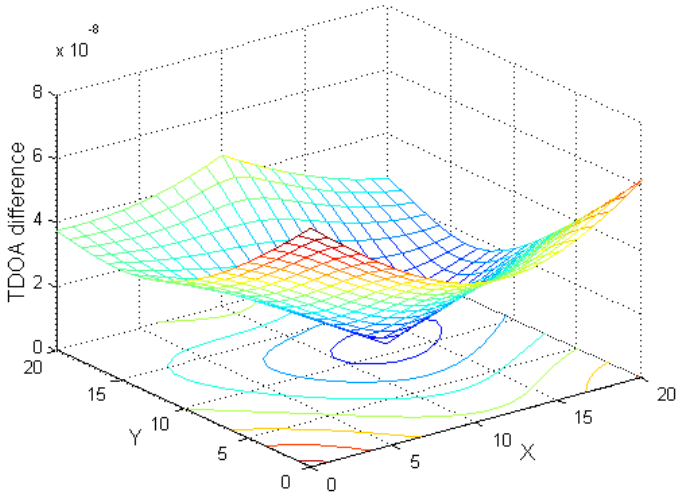


**Figure 4-3 TDOA difference by location coordinates, *N*=21**

## 4.2.2 Location Estimation Errors

The previous UT location example has proved that in a noise-free environment, the TDOA mapping algorithm shall produce accurate location estimation result, with

errors only caused by the discrete divisions of the grid points in the TDOA map. The first step of the proposed TDOA mapping algorithm divides the area of interest into a grid of $N_x$ $N_y$ points. In the case where a UT is in the middle between two grid points, the division error caused by the algorithm is the maximum, which is defined by:

$$d = \frac{\sqrt{\Delta X^2 + \Delta Y^2}}{2}, \tag{4.7}$$

where $\Delta X$ and $\Delta Y$ are the length of divisions along the x-axis and the y-axis of the TDOA map. They are equal to the width $w$ and length $l$ of the indoor area divided by the number of divisions $N_x$-1 and $N_y$-1 used to generate the TDOA map. Thus, $\Delta X$ and $\Delta Y$ is given by

$$\Delta X = \frac{w}{N_x - 1};\ \Delta Y = \frac{l}{N_y - 1} \tag{4.8}$$

It is obvious that a larger $N$ value tends to cause a smaller division error $d$. But increasing $N$ will increase the computation complexity of the TDOA mapping process as there are more grid points to search in the TDOA map. It will be shown that, to achieve adequate location accuracy with the TDOA mapping method, the $N$ value is not necessarily the larger the better. On the contrary, the division error becomes insignificant when the TDOA measurement error $\tau$ due to noise or interference is dominant and the division error is not comparable.

Let us recall the example given in Figure 4-1, the area of interest in this case has equal width and length, $X$=$Y$=20 m. If an identical number of points $N = N_x = N_y$ are used to divide the x and y axis, the division error caused by the TDOA mapping algorithm against the $N$ values is given in Table 4-1. The equivalent time errors $\tau$ (listed besides the division errors $d$) is the time needed by a wireless signal in the air to propagate a distance $d$. That is to say, this is the equivalent errors in TDOA measurement but caused by the division errors in the TDOA mapping process.

A Monte Carlo simulation of the Figure 4-1 scenario, where the TDOA mapping method is employed to estimate UT location, is used to find out at what value of $N$ the division error becomes an insignificant error source to the eventual location results.

| $N$ | $d$ (m) | $\tau$ (ns) |
|---|---|---|
| 100 | 0.14 | 0.47 |
| 50 | 0.29 | 0.97 |
| 20 | 0.74 | 2.5 |
| 10 | 1.57 | 5.2 |

**Table 4-1 Division errors and their equivalent time errors in TDOA measurement**

In the simulations, the $N$ value is set to be 100, 50, 20, and 10. A virtual UT is placed at the (0, 0) position in all cases because this point is always in the middle between the nearby grid points, and thus induces the maximum division errors. In each of the simulated target location tasks, time errors $\tau_e$, following a Gaussian distribution of standard deviation $\sigma$, are added to the three TDOA measurements, imitating the errors in reality. Ten thousand location tasks are simulated for every $N$-$\sigma$ settings, and the RMS errors of the estimated location results are calculated and shown in Figure 4-4.

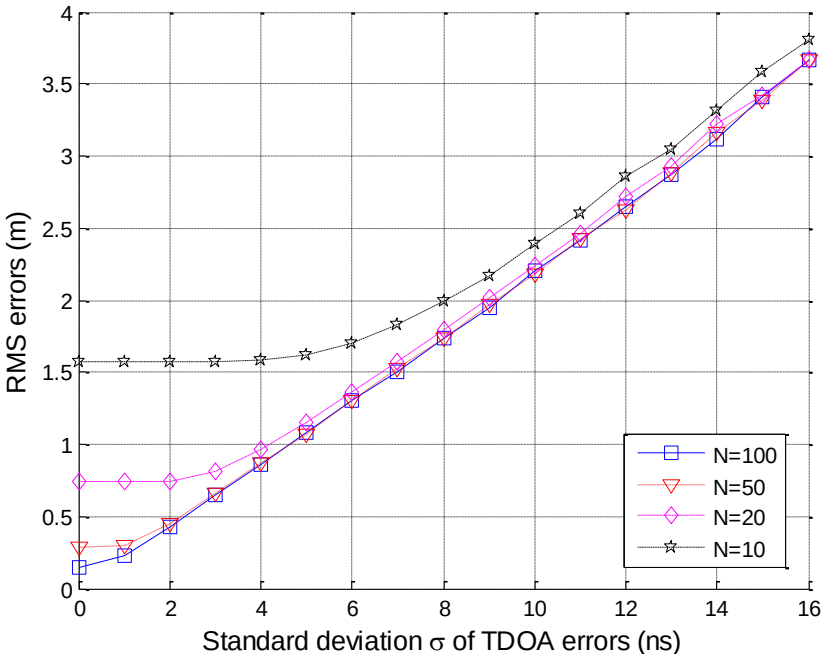


**Figure 4-4 RMS location estimation errors vs. standard deviation of time error in TDOA measurements**

It can be seen from Figure 4-4 that, when zero TDOA error applies, the division error is the only error source and thus the statistical RMS location errors for the $N$=100, 50, 20, and 10 cases are 0.14 m, 0.29 m, 0.74 m, and 1.57 m respectively, identical to the $d$ values listed in Table 4-1.

It is also shown that, the resultant location errors grow as the TDOA measurement error increases. When the TDOA error $\sigma$ is larger than about 10 ns, the RMS location errors for the four cases become very close to each other. It suggests that, when the $\sigma$ value is greater than 10 ns, the location estimation accuracy does not improve very much even if the *N* value increases from 10 to 100. This is the situation when division error caused by the TDOA algorithm is insignificant, and thus the location error is mainly caused by the TDOA measurement errors, which is dependent on the location system specifications, e.g. signal bandwidth, sensor positions, SNR, and time measurement resolution.

The condition for division errors being insignificant is relative to the *N* values, and a general guideline is that if the TDOA error $\sigma$ is larger than twice the equivalent time error $\tau$ listed in Table 4-1, there will be no substantial location accuracy improvement obtained from increasing *N*. These thresholds $\sigma$ are 1.94 ns, 5.0 ns, and 10.4 ns for *N*=50, 20, and 10 cases accordingly. It can be proved by the Figure 4-4 that, from $\sigma >$ 2 ns, the RMS error curve of *N*=50 case starts to merge with the curve generated from the *N*=100 case. This indicates that increasing *N* from 50 to 100 does not produce more accurate location result in case the TDOA error $\sigma$ is greater than 2 ns. If the TDOA error is greater than 5 ns, the RMS errors given by an *N*=20 TDOA map will be similar to that given by *N*= 50 or *N*=100 TDOA map, and thus it is not necessary to use more than 20 divisions.

In practice, since the systematic time measurement resolution $t_{res}$ is usually known by the system designer, the *N* value can thus be chosen so that its division error will not induce an equivalent time measurement error $\tau$ that is larger than half of the system resolution $t_{res}$, that is

$$\tau = d/c \leq t_{res}/2 \tag{4.9}$$

## 4.2.3 Potential Extension of the Algorithm

The previous section has introduced the proposed algorithm for location estimation based on TDOA measurements, using a three-sensor 2-D location finding example. It

should be noted that this algorithm can be adapted to various scenarios after some simple alteration. For example, the shape of the indoor area concerned can be freely defined, the sensors can be arbitrarily placed therein, and it can work for a scheme based on any number of sensors.

Firstly, the number of grid points along *x*-axis $N_x$, and *y*-axis $N_y$, of the TDOA map can be set to be unequal, depending on the indoor geometry and the step size preferred. It also does not matter where the sensors are placed in the indoor area as long as that their positions $(x_i, y_i)$ are measured with adequate precision and is not changed after installation. If all these information are specified in the generation of the TDOA map, the algorithm can naturally work according to the given settings.

Also, the proposed algorithm can be extended to accommodate more than three sensors by introducing additional dimensions into the TDOA vector. In a 2-D location system, redundant sensors are employed in some applications to enhance robustness to NLOS propagations [57]. Note that when the number of sensors employed in a location system is *M*, there are *L=M(M-1)/2* combinations of distinct sensor pairs. In a practical system, not all of the L combinations are taken into account in a location estimation task as optimization technique is usually used to select the sensor pairs with better signal qualities.

However, even if all the possible combinations are used, the TDOA map in such case is a matrix of no more than *L*-dimension vectors, and thus the estimated location is found by searching for the minimum modulus of the *L*-dimension distance vectors. In a computing system supporting linear algebra, the computer time required to calculate *L*-dimension modulus is insensitive to the dimension of vectors.

| No. of sensors, *M* | No. of distinct sensor pairs, *L* | CPU time (μs) |
|---|---|---|
| 3 | 3 | 4.63 |
| 4 | 6 | 4.67 |
| 5 | 10 | 4.67 |
| 6 | 15 | 4.75 |
| 7 | 21 | 4.79 |
| 8 | 28 | 4.78 |

**Table 4-2 Average CPU elapsed time for the modulus calculation of *L*-dimension vectors, from 1000 experiments in Matlab**

An experiment in Matlab has shown that, the average CPU time taken to calculate $L$-dimension vector modulus varies less than 2%, for $L$ ranges from 3 to 28, as given in the Table 4-2. Therefore the algorithm can be easily extended to applications with more than three sensors without downgrading the location estimation speed very much, given adequate computer memory. The algorithm can of course be implemented in software based on an ordinary PC. Also, with rapid advances of technology, FPGA-based hardware supporting linear algebra calculation is readily feasible too [66;67], and is a possible solution for developing a stand-alone location system.

Last but not least, the proposed algorithm can be used for 3-D location finding as well. The method is representing the indoor space as a 3-D grid of $N_x$-by-$N_y$-by-$N_z$ points. Therefore, the TDOA map is also set to be a 3-D matrix of maximum $L$-dimension vectors. Similar distance vector as Eq. (4.6) can be formed by subtracting the measured TDOAs from the 3-D TDOA map.

### 4.2.4 Comparison with Existing Algorithms

The proposed TDOA mapping algorithm is compared with two current algorithms, the Taylor-series method [12] and Chan's method [65], through simulation of a four-sensor indoor location system with the sensors placed at the four corners of a 20m-by-20 m room as in Figure 4-1.

The iterative Taylor-series method was proposed by Foy over 30 years ago [12] and is still a popular method for solving the location finding problem. This algorithm first linearizes the non-linear TDOA equations, e.g. Eq. (4.2), through Taylor-series expansion. The iteration process then starts with an initial guess for the UT location, and adjusts the location estimate at each iteration by determining the local linear least-square (LS) solution. The Taylor-series method is known as an algorithm that achieves optimum performance [65;68] when the iteration process converge. However, this technique is computationally intensive, and its success depends strongly on the proximity of the initial guesses to the true positions; otherwise convergence may not occur or it may converge to local minima.

By contrast, Chan's method [65] is a non-iterative algorithm to the multilateration problem and is also a popular technique in radar and microphone array applications. In this algorithm, one of the TDOA measurement sensors is assigned as the reference node, and the measured TDOA are referenced to the signal received at this reference node. It solves the UT location using the range from the UT to the reference node as an intermediate variable, and the UT location is found through two-stage LS methods. This method is attractive because it provides a closed-form solution to the non-linear TDOA equations. When the TDOA estimation errors are small, this method is an approximation to the maximum likelihood (ML) estimator. Chan has shown that when the UT location is at the far field of the sensor array, the results from this algorithm is able to attain the Cramer-Rao Lower Bound (CRLB) for TDOA measurement errors up to 0.03 ns. However, the far field assumption in the first stage LS method [65] may induce considerable errors when the UT is actually located in the near field of the sensors array.

Simulation results have shown that the proposed TDOA mapping method is able to achieve similar accuracy as the Taylor method, but without the initialization and convergence problems usually associated with the Taylor method. The location results of the new method are more accurate than the Chan's method in near field and large TDOA error cases, and thus it is especially suitable for wireless indoor location systems where the UT location is usually within the near field of the sensors array.

In the simulations, two different cases are modelled for performance comparison of the three methods.

- In the first case, random TDOA measurement errors with Gaussian distribution are added to the measured TDOA sets. The mean of the TDOA errors is zero while the standard deviation of the errors is $\sigma$, rangeingfrom 0.1 ns to 5 ns.
- In the second case, both the aforementioned random TDOA errors and a further additive error, caused by NLOS in the channel of the reference node, are included. In the simulation, NLOS error with mean additive range of 2 m and standard deviation of 1 m is used.

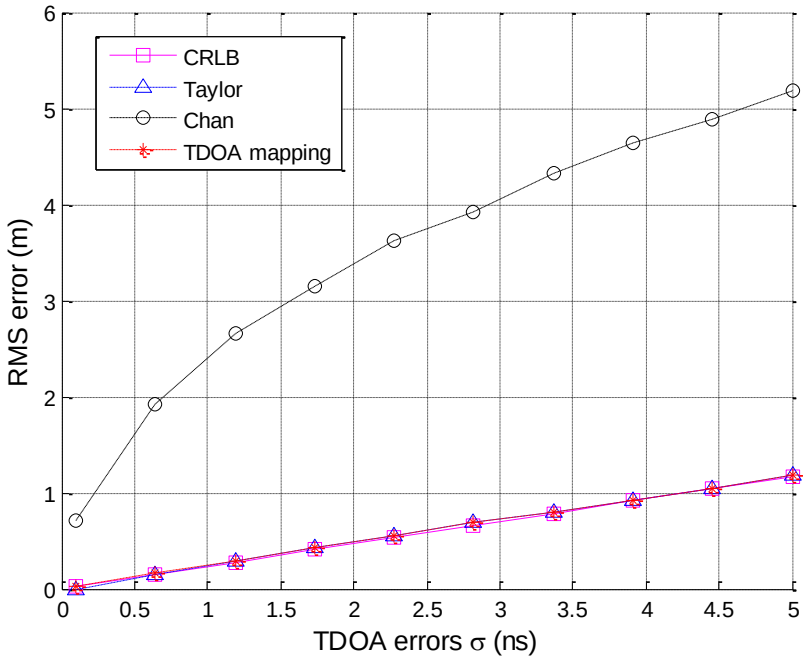


**Figure 4-5 Simulation results comparing the RMS location error induced in the Taylor method, Chan's method, the proposed TDOA mapping method and the CRLB.**

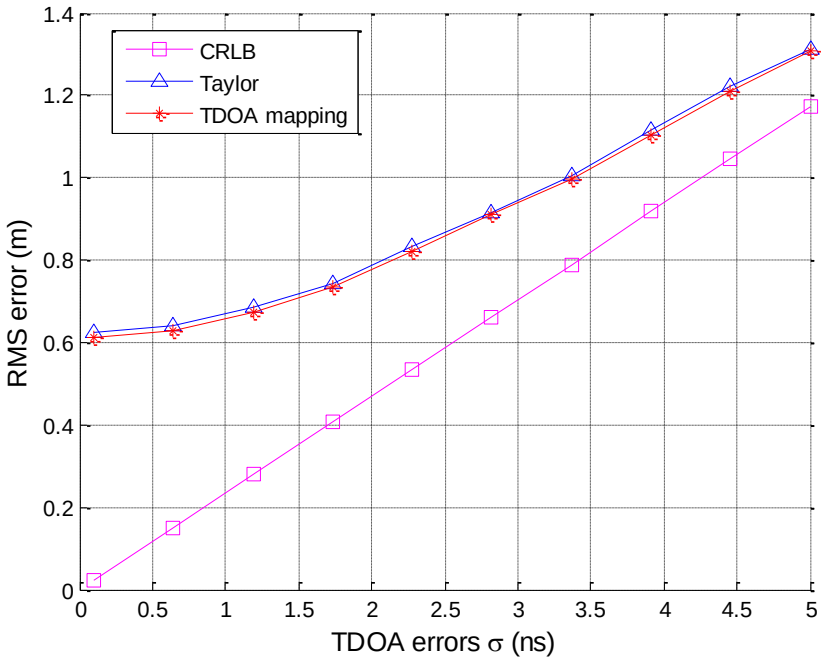


**Figure 4-6 Simulation results comparing the RMS location error induced in the Taylor method, the TDOA mapping method and the CRLB, in presence of NLOS errors.**

The RMS location estimation errors induced by the three different methods are recorded against different standard deviation value, σ, of the added TDOA errors. The RMS location errors are then compared with the CRLB, which is the theoretical limit

for the location accuracy in the presence of Gaussian TDOA measurement errors. The derivation of the CRLB in case of Gaussian TDOA errors can be found in [65;69;70]. The equation given by Chan [65] on the mean square location errors is used in our simulations.

The UT positions are generated randomly in ten thousand runs and the output statistics of the algorithms as well as the according CRLB from the first case are plotted in Figure 4-5, while the results from the second case are plotted in Figure 4-6. The initial guess for the Taylor method has been set to a random location within 1 m distance to the true location. As for the proposed TDOA mapping algorithm, the number of grid points has been set to $N$=201.

In the first case, where only the Gaussian TDOA errors are considered, the proposed TDOA mapping method performs equally well as the Taylor method (Figure 4-5) and outperforms Chan's method. This is because placing sensors at the four corners ensures that the UT positions are always in the near field of the sensors array and thus the approximations made in the first stage of Chan's method produces large errors in the location results in such a confined indoor scenario. The location results from the Taylor method and the TDOA mapping method are shown to attain the theoretical CRLB limit. That is to say, both methods are able to obtain maximum location accuracy if independent and identically distributed TDOA errors occur applies on the measured TDOA sets. In case this assumption is not valid, the RMS location errors can be larger than the predicted level shown in Figure 4-5. Also, the RMS errors along $x$-axis and $y$-axis might deviate, depending on the TDOA error distributions. As a result, the estimated locations may be biased with respect to the true location. These phenomena are witnessed in the trial results that will be presented in the Chapter 6.

In the second case, results from Chan's method are producing errors between 3 and 5 m, and thus for clarification purpose they are not displayed in the Figure 4-6. The NLOS effect is included in this simulation case. The TDOA mapping method achieves slightly better accuracy than the conventional Taylor method, Figure 4-6. In wireless indoor location application, NLOS is a common issue as it can occur even when the UT signal is partially blocked by a person or an object. One effect of NLOS is additional range in the transmission path of the received RF signal. Since both the Taylor method and Chan's method use one of the sensors as a reference node, NLOS

in the corresponding channel therefore increases the overall RMS error level, as can be seen by comparing the Figure 4-5 and the Figure 4-6. On the other hand, the proposed TDOA mapping method, which takes into account the full TDOA sets between every sensor pair, is relatively less sensitive to NLOS errors and induces 3.5% smaller RMS error in comparison to the Taylor method in the small TDOA error region.

| | Taylor | Chan | TDOA mapping |
|---|---|---|---|
| Iteration | Yes | No | No |
| Explicit result | Depends on convergence of the algorithm | Yes, but in some cases prior information may be needed | Always |
| Computation load | Low to high, depending on cell area | Low | Medium |
| Advantage | Optimum location performance | Suitable for far field location scenario | Optimum explicit result is given |
| Disadvantage | A good initial guess may not be available in practice and thus convergence does not always occur. | Approximation made in the algorithm induces significant errors in near field location cases. | Not suitable for far field location finding<br>Update of TDOA map is required if sensor placements are changed |

**Table 4-3 Comparison of the three TDOA location algorithms discussed**

The proposed TDOA mapping algorithm is shown to achieve slightly improved location accuracy over the Taylor method, and more importantly it is immune to the initialization and convergence problems that could cause unsolved results in the Taylor method. The proposed TDOA mapping algorithm thus guarantees an explicit result with good accuracy.

### 4.2.5 Discussion

We have presented a novel and practical TDOA location algorithm that resolves target location $(x_t, y_t)$ from the measured TDOA information. The performance has been evaluated through a three-sensor example, proving that accurate and single location result can be obtained using this algorithm.

The potential errors induced from the algorithm have also been analyzed. The result is a simple equation that can be used to determine the number of grid points value *N*, in order to best balance the speed of the algorithm and the associated location errors. Methods for extending the algorithm to broader cases are given as well, showing that the proposed algorithm is highly adaptable to various scenarios, which is desirable by the indoor location applications.

The simulation results and comparison with the Taylor and Chan's methods in Section 4.2.4 considering input TDOA errors further demonstrate the reliable location estimation achieved by the TDOA mapping algorithm. A summary of this comparison is given by the Table 4-3. The proposed approach is particularly suitable for real-time wireless indoor location applications where sensors are deployed in a crowded indoor area, such as airports and conference venues. This is because in these applications, the system sensors are usually fixed in locations for long-term usage and the proposed algorithm can re-use the same TDOA maps which do not need to be re-calculated unless the sensor arrangement is changed. The proposed TDOA mapping algorithm has been employed in our previously reported experimental demonstration of an indoor location system [71].

## 4.3 Deployment of TDOA Measurement Sensors

The TDOA mapping algorithm for calculating target location from TDOAs measurement is proposed in the previous section. A TDOA map representing the indoor area is generated with equally spaced discrete grid points. When the space between the grid points is sufficiently small, the error due to discretization is insignificant (as discussed in Section 4.2.3). Therefore, the main error source is from TDOA measurements. This section starts from an illustration of the TDOA contour lines for a pair of sensors. It will be shown in this section that error in TDOA measurement may induce different location errors, depending on the position of the target and the geometric arrangement of the sensors.

### 4.3.1 Contours for Range Difference of Arrival

The TDOA contour lines are a group of hyperbolic curves, each of which associates with a TDOA value. These TDOA contour lines are defined in the Eq. (4.10) with $\Delta t$ varies from zero to *D/c*, where *D* is the distance between the two sensors and *c* is the propagation velocity.

$$\frac{1}{c}\left(\sqrt{(x-x_1)^2+(y-y_1)^2}-\sqrt{(x-x_2)^2+(y-y_2)^2}\right)=\Delta t \tag{4.10}$$

A given $\Delta t$ is due to a specific range difference from a UT to the sensors. In this section, the TDOA is in lieu of its linearly related parameter, the range difference of arrival (RDOA). Figure 4-7 (a) illustrates a group of TDOA contour lines labeled by their corresponding RDOAs $\Delta r$ , which is defined as

$$\Delta r = c \cdot \Delta t \tag{4.11}$$

In Figure 4-7 (a), the sensor Rx2 is located at (10, 0), and the sensor Rx1 is at (-10, 0), while the origin is chosen to be the middle point of the baseline connecting Rx1 and Rx2.

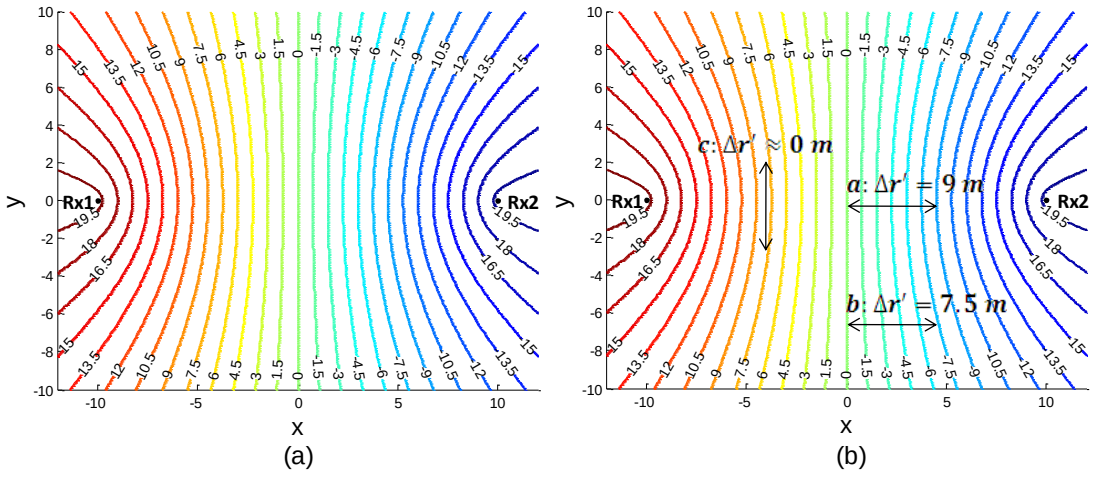


**Figure 4-7 Contour lines of range difference $R_2 - R_1$ (a); change in range difference $\Delta r$ due to physical movement of the same distance (b)**

The *x-y* coordinate represents a 2-D plane where the sensors are monitoring. On this 2-D plane, the color-coded hyperbolic curves are the RDOA contours. Each of these curves is associated with a range difference. The range difference on each curve is constant. That is, when a UT moves along a RDOA contour, the range difference to

the sensor pair does not change. Hence, the TDOAs between Rx2 and Rx1 also remains the same during the movement. However, the range difference $\Delta r$ changes as well as TDOA when a UT moves across different RDOA contours.

The change in $\Delta r$ is noted as $\Delta r'$ in Figure 4-7 (b). $\Delta r'$ depends on the direction of UT movement, and the location of UT.

Any physical movement of the UT on the 2-D plane of interest can be represented as combination of the parallel and orthogonal movements. The parallel movement describes movement along a parallel direction with respect to the baseline of the sensors (*x*-axis direction in Figure 4-7). In like manner, movement along an orthogonal direction to the Rx1-Rx2 baseline (*y*-axis direction in Figure 4-7) is called orthogonal movement.

( In Figure 4-7, the arrow headed lines *a, b,* and *c* represent UT movements with the same distance: *a*, *b* are parallel movement; *c* is orthogonal movement. The $\Delta r'$ resulted from these movements are 9 m, 0 m, and 7.5 m respectively. They clearly are not identical.

A perceptual impression is that, the movement of UT along the parallel direction induces larger $\Delta r'$ (illustrated by the arrows *a* and *c* in Figure 4-7 (b)). Since the range difference resulted from vertical movements can be rather small, which may impede the system's ability to measure vertical movements. Therefore, to increase the sensitivity to vertical movement, additional sensors may be employed as long as they are not placed not in line with Rx2 and Rx1.

The arrow headed lines *a* and *b* show parallel UT movements at different vertical coordinates *y*. Although movement *a* and *b* have the same distance, the range difference variations $\Delta r'$ induced are different. In fact, range difference (9 m) from movement *a* is larger than that (7.5 m) resulted from movement *b*. This is because the RDOA are not straight lines that are orthogonal to the *x*-axis, but hyperbolic curves. Even though a and b movements both start from the same hyperbolic curve, they end at different hyperbolic curve and result in different changes in the range difference. In general, the change in range difference resulted from the parallel movement of a UT is negatively proportional to the absolute value of *y* coordinate of the corresponding UT.

In other words, sensor pair Rx1 and Rx2 observes smaller $\Delta r'$ due to parallel movements occurred at outer position (larger absolute value of *y*), compared to that induced from parallel movements at inner position (smaller absolute value of *y*).

The change in the range difference resulting from the orthogonal and parallel movements can be expressed analytically by the partial derivatives of Eq. (4.10) with respect to *y* and *x*, as shown by the Eq. (4.12) and Eq. (4.13), respectively.

$$\begin{aligned}\frac{\partial \Delta r}{\partial y} = \frac{c \cdot \partial \Delta t}{\partial y} &= y \cdot \left(\frac{1}{r_2} - \frac{1}{r_1}\right) - \left(\frac{y_2}{r_2} - \frac{y_1}{r_1}\right) \\ &= y \cdot \left(\frac{1}{r_2} - \frac{1}{r_1}\right)\end{aligned} \tag{4.12}$$

$$\begin{aligned}\frac{\partial \Delta r}{\partial x} = \frac{c \cdot \partial \Delta t}{\partial x} &= x \cdot \left(\frac{1}{r_2} - \frac{1}{r_1}\right) - \left(\frac{x_2}{r_2} - \frac{x_1}{r_1}\right) \\ &= x \cdot \left(\frac{1}{r_2} - \frac{1}{r_1}\right) - x_2 \left(\frac{1}{r_2} + \frac{1}{r_1}\right)\end{aligned} \tag{4.13}$$

where $(x_1, y_1)$and $(x_2, y_2)$ are the coordinates of the two sensors, and the relations $x_2 = -x_1$, $y_2 = y_1$ apply. $r_2$ and $r_1$ are the distances between the UT and the two sensors, defined by:

$$r_1 = \sqrt{(x - x_1)^2 + \left(y - y_1\right)^2} \tag{4.14}$$

$$r_2 = \sqrt{(x - x_2)^2 + \left(y - y_2\right)^2} \tag{4.15}$$

It is clear that the parallel movement produces more significant changes in range difference because of the presence of the second component in the result of Eq. (4.13), while in Eq. (4.12) the corresponding component is cancelled due to difference of the two *y* coordinates being zeros ($y_2 - y_1 = 0$). Since the orthogonal movement shall be measured with additional sensors, it is only the parallel movement (Eq. (4.13)) that is of interest to the analysis in the following part.

### 4.3.2 RDOA Detection Sensitivity

As discussed above, measured TDOA/RDOA varies due to physical movement of the UT under monitor. According to the TDOA measurement technique presented in the Chapter 3, a small change of RDOA could be difficult to detect if the physical movement causing it is comparable or smaller than the resolution given by Eq. (3.17).

It is also mentioned above that RDOA variation depends not only on the actual distance of the UT movement, but also on the position and direction of the movement. Therefore, the region where UT movement induces similarly large change of RDOA is regarded as sensitive region to physical UT movement. In this section, this sensitive region for a pair of sensors is studied.

An RDOA detection sensitivity parameter is defined as the ratio of the change in RDOA and parallel movement distance, as below.

$$S = \frac{\Delta r'}{\Delta x} \tag{4.16}$$

Obviously this parameter is the same as the partial derivative of Eq. (4.10) against *x*, and therefore can be expressed by Eq. (4.13).

In the region where the sensitivity parameter is 1, a $\Delta x$ parallel movement shall cause same amount of change in RDOA $\Delta r'$. This is the boundary between "sensitive" and "insensitive" indoor regions. If the *S* parameter is less than 1, a parallel UT movement for 1 metre will induce less than 1 metre change in RDOA. Thus the equivalent TDOA measurement is regarded as less susceptible to the physical movement it is trying to sense. On the other hand, in the region where *S* parameter is greater than 1, the RDOA measurement is sensitive because a parallel UT movement of 1 metre will result in greater than 1 metre change in RDOA.

The sensitivity parameter defined above has another practical meaning. It can be used to illustrate robustness of the sensor pair to TDOA measurement errors. In practice, TDOA measurements suffer from errors due to multipath, NLOS and interference. For a non-moving UT, these errors result in RDOA measurement errors, as well as errors in the resultant estimated location of the UT.

The location measurement error in this case is related to the RDOA measurement error by the factor of the *S* parameter. Considers a RDOA measurement error of $\Delta r_e$, the resultant estimated location error in *x* direction is given by

$$\Delta x_e = \frac{\Delta r_e}{S} \tag{4.17}$$

It can be seen that, in the sensitive region where *S*>1, the location error $\Delta x_e$ will be smaller than the corresponding RDOA error $\Delta r_e$. On the other hand, the RDOA error will be "amplified" by 1/*S* and result in a location error $\Delta x_e$ that is greater than $\Delta r_e$.

Therefore, if a UT is at the sensitive region of a sensor pairs, where *S*>1, the UT location estimation is more robust to errors in RDOA measurement, when compared to measuring a UT located at the *S*<1 region.

Figure 4-8 shows the contour lines of sensitivity parameter *S*, calculated from a pair of sensors, Rx2 at (10, 0), and sensor Rx1 at (-10, 0).

It can be seen that, the maximum value of the sensitivity parameter is 2. This maximum sensitive region is the baseline of the sensor pairs. Along this line, one metre of UT movement causes two metre change in RDOA. On the other hand, two metre of RDOA error induces only one metre error in estimated UT location along this line. In between the two *S*=1.9 curves is the area where $1.9\Delta x \leq \Delta r' \leq 2\Delta x$, which is the next high sensitive area.

In Figure 4-8, the entire oval shape area enclosed by the *S*=1 contours is the sensitive region defined by the criteria set above, where the parallel movement causes at least the same amount of variation in RDOA. It is suggested that the placement of indoor location sensors shall expand the sensitive region as large as possible. In other words, it is preferred that the placement of sensors can provide large enough sensitive region (*S*>1) to cover the entire indoor area under monitor.

To obtain an idea about the relative size of the sensitive region, two examples are shown in Figure 4-9. The two diagrams here are plotted in an *x*-*y* coordinate which is normalized to *D*, the separation distance between the two sensors.

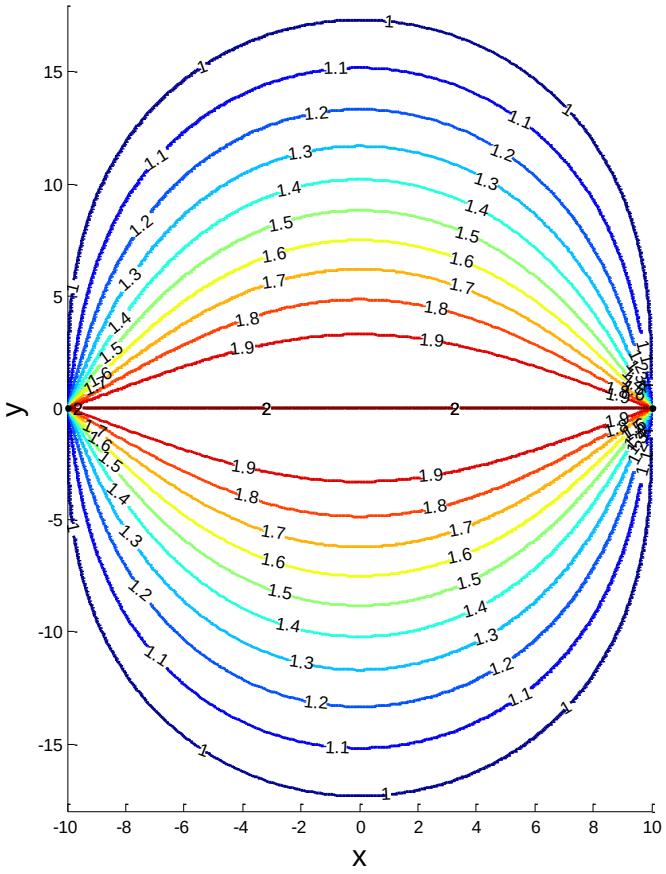


**Figure 4-8 Contours of RDOA detection sensitivity parameter; sensitive region (*S*>1) for sensor pair Rx2 at (10, 0), and sensor Rx1 at (-10, 0)**

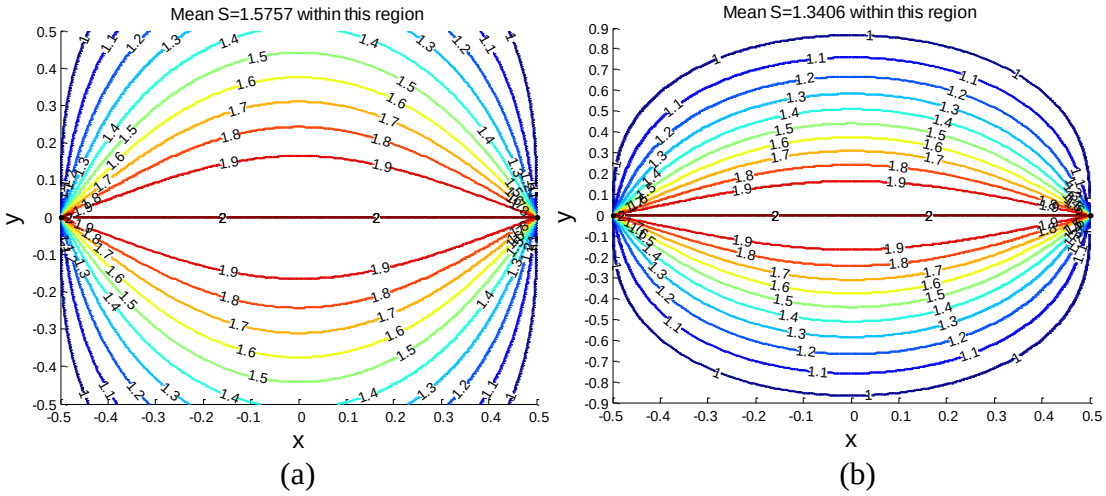


**Figure 4-9 Sensitive region in normalized scale. *x* and *y* labels are normalized to *D*, the distance between the two sensors. (a) *D*-by-*D* area where average sensitivity parameter is 1.5757; (b) *D*-by-1.8*D* area where average sensitivity parameter is 1.3406.**

Figure 4-9 (a) shows a case where the sensor pair are placed at the two ends of the middle line in the $D \times D$ area. In this diagram, the mean sensitivity parameter value is about 1.58, ensuring good range difference measurement sensitivity. If the sensors are used to monitor a longer district, with normalized length of $1.8 \times D$, Figure 4-9 (b), the average sensitivity parameter will be reduced to 1.34. This has included the full sensitive region where $S$ is not smaller than one.

This section has discussed the relations between positions of sensors and the corresponding RDOA measurement sensitivity to UT movement. RDOA contours for one pair of sensors are used in the discussion as a sensor pair, which is the fundamental unit of a TDOA location system. However, in practice there will usually be more than three sensors in a single cell. Consider that there are three sensors and thus three distinct sensor pairs. The overall sensitive region will be the area overlapped by the sensitive regions corresponding to the three sensor pairs. This overall sensitive region may not be exactly the same shape or size as the location cell. A trial presented in the Chapter 6 will use this simple technique to predict the sensitive region for a three-sensor indoor location system setting.

By introducing the sensitivity parameter, it is shown that the size of sensitive region is directly related to the distance between the sensors. Further separation between the two sensors enlarges the sensitive region, and results in higher average sensitivity to UT movements in the area of interest.

To minimize the impact of TDOA measurement errors, the orthogonal detection range for a pair of sensors shall not exceed 0.9 times the distance between the sensors (Figure 4-9 (b)). It is also suggested that keeping the orthogonal detection range to be $0.5 \times D$ (Figure 4-9 (a)) will provide much better overall performance (mean $S$=1.58). It shall also be noted that this conclusion is based on the condition that the received signal power at the two sensors are large enough to be detected. If this is the case, for a given indoor area, the placement of sensors shall try to utilise the longest distance in the area, e.g. diagonal of a rectangular area.

## 4.4 Summary

The theoretical model of locating a signal source by means of TDOA measurement is reviewed at the beginning of this chapter. While a number of algorithms exist in literature for this application, a novel algorithm designed for indoor location finding is proposed in the second section of this chapter. After comparison with two classic algorithms, it is found that the new algorithm is able to produce explicit location result with maximum accuracy. This algorithm can be easily implemented in computer software or by DSP that supports linear algebra calculations.

In the third section, we have defined the sensitive region for a pair of TDOA measurement sensors, and made the suggestion that further separated sensors are likely to provide reliable range measurement result. This is because further separation between the sensors result in larger sensitive region or better sensitivity for a given range.

In practice, there will be at least three sensors deployed to perform 2-D location finding and in some cases redundant sensors will be introduced to allow over-determined target locating. Therefore, the location error spreading patterns are the combined effect of all the sensors deployed. For a given error level in TDOA measurement, the theoretical location error of a TDOA location system varies from position to position and is relevant to the placement of all the sensors. This effect will be further discussed along with the real measurement data that will be presented in the Chapter 6.

# *Chapter 5*

## DEVELOPMENT OF A PROTOTYPE INDOOR LOCATION SYSTEM

The overall goal of this research is to design and develop an indoor location system based on RFID tags for use in conjunction with a high-speed RoF network, assuming an airport terminal building environment. In this chapter, the world's first experimental demonstrator of such a real-time indoor location system is presented.

This system is based on multilateration that determines the tag location by measuring the TDOA of the tag transmitted signals at different location sensors. The use of an optical fibre backbone not only allows the remote deployment of the sensors, but also removes the need to synchronise sensors with special signaling. Instead, accurate TDOA measurement is performed through centralised signal processing. In particular, the received tag signals are sent back from the sensors over fibre to a central hub where they can be digitised by a single DAQ device.

The design of this prototype system is presented in this Chapter in the following order. Section 5.1 describes the system architecture by its functional blocks and the corresponding hardware implementations. Section 5.2 introduces the fundamentals of the RoF technology and the hardware facility employed by the prototype system. Section 5.3 deals with the RFID tag design, focusing on the chirp signal generator. The identification and multiple access functionalities of the RFID tags are given in the Section 5.4. Section 5.5 presents implementation of the RF receiver and the location estimator, from the hardware to the signal processing model. As a particularly important part in the location estimation, the frequency detection strategy is studied in the Section 5.6. It will be shown that the carefully designed strategies are able to mitigate the multipath impacts on TDOA measurement.

## 5.1 System Architecture

In this section, the system architecture for the TINA indoor location system is introduced. It is written as a base for the following sections of this chapter where individual units of the system are explained.

Due to the employment of RoF backbone, the indoor location system structure and communications are simplified in terms of the following points.

Firstly, the signal processing required in the remote sensors is simplified to signal reception and transportation only, as most signal processing functions are undertaken at a central site. In an indoor location system, the number of sensors grows rapidly as the size of the indoor area increases. Therefore, this centralised processing feature saves a great number of hardware and processing loads that should be originally carried by every remote sensor of the system.

Secondly, in a RoF based system, there is no need to worry about synchronisation error and its impact on TDOA measurement. For the conventional indoor location system where the TDOA values measured are in the order of only a few nanoseconds, asynchronous sampling will directly affect the accuracy of TDOA measurement. In TINA indoor location system, synchronisation between sensors is essentially achieved by having centralised RF and digital signal processing units. There is no need to send a global clock signal to every sensor at the remote end; instead they are synchronised by simply sharing the reference signal at the central site.

In the following, the TINA indoor location system is illustrated by a functional block diagram. The signal processing involved is discussed with the corresponding unit. This gives a general idea about what processes are required in the measurement of the target location. After explaining the functional blocks of the system, the actual specifications of the TINA indoor location system are given in the following subsection, in order to provide an overall view of the hardware implementations employed to record the data presented in Chapter 6.

## 5.1.1 Functional Blocks

Similar to the conventional real-time location system, the TINA indoor location system consists of user tags, RF sensors, and the core computational unit performing location estimation algorithms. One distinct feature of the TINA indoor location system is the employment of optical links, and the resulting simplified system structure. Figure 5-1 shows the basic functional blocks of the TINA indoor location system, as well as the signal interfaces between these blocks.

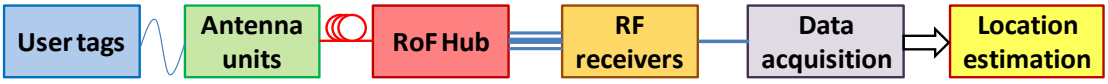


**Figure 5-1 Functional blocks and their interfaces of the TINA indoor location system**

*User tags*

The TINA user tags are in the form of an RF module, that generates and amplifies the radio signal (which can be used for both location estimation and user identification), as well as the antenna that radiate these RF signals. They are termed active tags or active targets because on-board batteries are included to power the RF module, in contrast to passive tags which have no on-board batteries. The signals are radiated away and received by the sensor antennas through wireless propagation (Figure 5-1). It is the signal propagation time that provides us clue to the location of the corresponding user tag. The design of the RF signal has been presented in Chapter 3, while the actual implementation of these tags is given in the Section 5.3 of this chapter. In Section 5.4, a novel technique of identifying target using differential LFM slopes is proposed, along with the theoretical analysis of this technique and simulation results.

*Antenna Units*

The location sensor of the TINA indoor location system is a simple antenna unit. The antenna unit (AU), the optical fibres, and the hub constitute the backbone RoF network of the TINA indoor location system. A number of antenna units are deployed at known positions of the cell of interest, and are used to collect radio signal from the user tags in the corresponding cell. An antenna unit consists of an antenna that works in the same frequency band as the tag's radiated signal, and the components that

convert signal between optical and electrical formats. When an RF signal is received by an AU, it transmits signals through the optical fibre link (Figure 5-1) to the RoF hub, where the optical signal is first converted back to electrical format and then routed to the analogue output connecting the respective RF receiver. The length of fibre link can be from a few metres to hundreds of metres, depending on the physical distance between the AUs and the RoF hub. It does not matter that different AUs are connected to the RoF hub through different length, because the fibre loss is insignificant and the time delay is calibrated accurately afterward. For an indoor location system targeting at 1 metre accuracy, fibre link differences of less than 0.1 m are considered to be acceptable and calibration to this level of precision will be adequate. Section 5.2 introduces the background and fundamental knowledge of this RoF technique and the actual RoF system used in the TINA project.

*RF receivers*

The signals output from a RoF hub are analogue electrical signals, in the same frequency band as the radiated signal from a user tag. They are then transported through RF cables to the RF receivers. In the RF receivers, the received signals from a number of AUs can be down-converted by the same LO signal to an intermediate frequency (IF) band, so that the signals fall into the analogue bandwidth of the DAQ input. The electrical link between the RF receivers and the DAQ device shall have flat, low-loss frequency response over the frequency band of the IF output from the RF receivers.

*Data acquisition*

The IF outputs from the RF receivers must be sampled simultaneously by the DAQ device. This can be a high speed multi-channel DAQ card performing simultaneous sampling or a few separated DAQs synchronised by sharing the same sampling clock. The sampling rate shall fulfil the Nyquist sampling criterion, which is at least doubling the bandwidth of the signal of concern.

*Location estimation*

The digitized samples are then transported through a digital bus to a digital signal processor that carries out the location estimation algorithm, details of which are

explained in the Section 5.5. The processor can be implemented by means of circuit arrays of FPGA, ASIC, programmed with the required algorithm. In this processor, the digitised RF signals are deramped with a pre-recorded digital copy of the LFM chirp radiated by the user tags. The LFM chirp deramping technique and its performance in indoor location system have been discussed in Chapter 3. The deramped beat frequencies can be detected by simply applying FFT on the digitally deramped signal. However, to select direct path information from the deramped output, special detection strategies must be used, and an introduction to these strategies is given in the Section 5.6 of this chapter. The time information can be derived from the frequencies detected in the previous step according to Chapter 3. The location mapping algorithm introduced in Chapter 4 is then used to estimate the location of the signal source. The estimated locations of the user tags can then be displayed in real-time by a computer or other user interface.

So far every step of a location finding cycle of the TINA indoor location system has been introduced, in the order of the functional blocks diagram in Figure 5-1. Details of designing such a system and some practical concerns are to be discussed in the following sections.

## 5.1.2 Demonstration System

Table 5-1 lists the basic technical parameters of the TINA demonstration system. It operates in the 2.4 GHz ISM band (2400 MHz to 2483.5 MHz) [72;73].

| Parameter | Description |
|---|---|
| Frequency | 2.4GHz ISM band |
| Bandwidth | 83.5MHz |
| Antenna units | Receive-only AU |
| Tag type | Transmit-only active tag |
| Modulation scheme | Linear frequency modulation |
| Chirp pulse | 10 μs short-chirp followed by an 80 μs long chirp |
| Max. reading range | 28 meters |
| Tag radiation power | 5 dBm |

**Table 5-1 Specifications for the TINA indoor location demonstrator**

The designed cell size for the TINA system is a square of 20 m×20 m area, which defines a typical indoor area unit under consideration. Assuming that the AUs are placed at the corners of the square cell, the diagonal length of the cell will be $28\,m$, which is the furthest distance between AUs.

Figure 5-2 shows an example of the overall hardware implementation of the TINA indoor location system demonstrator. Three AUs were employed in this example. They are setup to monitor one cell area in the indoor environment.

The RFID tags used in the TINA demonstrator radiate a continuous LFM chirp signal that is modulated as a 10 μs short-chirp followed by an 80 μs long-chirp. They both sweep over the 2400-2483.5 MHz band, which defines the TDOA range resolution of about 3.6 m. The output power from a tag is around 5 dBm, 15 dB lower than the power limit for the 2.4 GHz WLAN, according to ETSI regulation.

The tag signals received by the AUs were transported back to the RoF central hub via three 40 m long single mode fibres. The three received tag signals at the outputs of the hub were down-converted from the original 2400–2483.5 MHz band to the 10–93.5 MHz band. This down-conversion allowed the received tag signals to be captured directly with a real-time oscilloscope for subsequent data processing.

The real-time oscilloscope used in the TINA demonstrator is the Tektronix TDS5104B oscilloscope. The input sensitivity of this instrument is 1 mV/div, with 8 bits digitization resolution. Therefore, it is able to deal with a signal input as low as –71 dBm. The three received signals Rx 1, Rx 2, and Rx 3, outputs from the RoF hub, are digitised by the real-time oscilloscope (Figure 5-2). These data are then recorded through a GPIB interface by a LabView programme running on a laptop computer (Figure 5-2).

In each measurement, the three frequency down-converted tag signals, Rx1, Rx2, and Rx3, were sampled for 200 μs at 250 MSp/s by the real-time oscilloscope, which acts as a high-speed ADC. The sampled data were processed in real-time in the LabVIEW programme. They need to be deramped with a reference chirp stored in the oscilloscope, as introduced in Chapter 3.

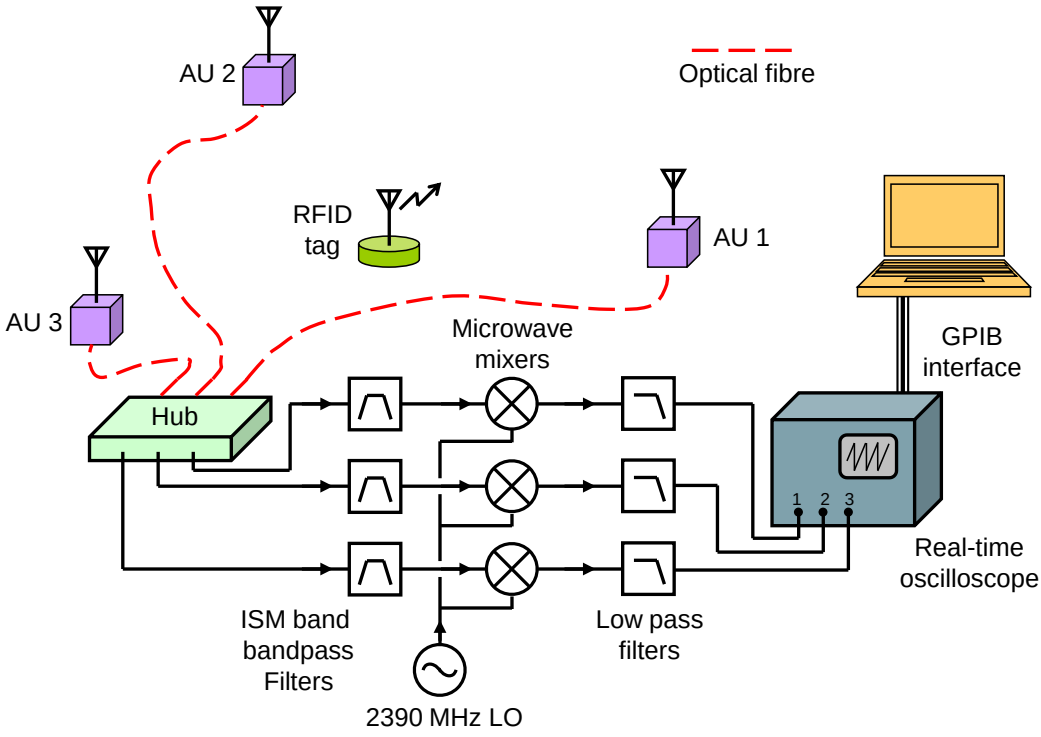


**Figure 5-2 Schematic of the hardware implementation of the TINA indoor location system**

The estimation of the location of the RFID tag in a 2-D plane is based on the measurements of the TDOA of the tag signals at three different AUs situated at known coordinates. Because the tag output frequency varies linearly with time, the instantaneous frequency "seen" at each AU will vary linearly with time as well. However, between any two AUs there is a constant frequency difference which is proportional to the TDOA of the tag signals at the two AUs concerned. This frequency difference is found by deramping the incoming signals with the locally stored reference chirp. This process produces the TDOA information required to find the signal source location. In current specification, the location estimation algorithm only performs deramping between the 80 μs long-chirp part of the received signal and the 80 μs long-chirp part of the pre-recorded reference chirp.

By measuring this frequency difference between two or more pairs of AUs, the corresponding TDOA information found can be used to determine the tag location by multilateration, as introduced in Chapter 4. This is performed in the LabView, and a real-time display has been developed to show the estimated location on a map representing the monitored cell. The estimated location data can be saved for post-processing such as statistical analysis.

## 5.2 RoF Backbone

First proposed in the mid-1960s by Professor Charles Kuen Kao, Nobel Laureate in Physics 2009, optical fibre has been widely used as the backbone for telecommunications, and has transformed the way we communicate with each other. Compared to conventional coaxial cables, the first advantage of optical fibre is low transmission loss. A standard single mode fibre typically has an optical transmission loss of about 0.2 dB/km at a wavelength of 1550 nm, while a good quality coaxial cable operating at a frequency of 1 GHz typically shows an attenuation of 0.5 dB/m. Additionally, the utilisation of Wavelength Division Multiplexing (WDM) greatly enlarges the data transmission capacity of a single fibre and makes it an ideal choice for long-haul, and high-capacity data transmission. For short distance applications, optical fibre is also an important medium in constructing networks since it has the capacity to carry more data than any electrical cable, at lower cost. Furthermore, optical transmission is immune to electrical interference, such as cross-talk between cables, and pickup of environmental noise. The research on optical communications has never stopped and now it has come to the stage of transporting radio signals over fibre [74].

RoF (RoF), or RF-over-Fibre, refers to transmission of radio signals in their respective radio frequency bands over fibre medium. This is different from the traditional optical transmission systems that carry purely digital data with occupied modulation bandwidths extending from a few MHz to the highest data rate (> 10 GHz). With the emerging 4$^{th}$ generation wireless communication standard known as the Long Term Evolution (LTE)[2], and the increasing demand for ubiquitous and reliable mobile reception in both indoors and outdoors, RoF is going to play a more important role in wireless mobile communications.

Conventionally, provision of wireless coverage inside buildings relies on the penetration of RF signals from base stations outside of the buildings. However, this is an indirect way of providing cellular services to within the buildings, tunnels, and basements. It is highly unreliable without radiating a lot more radiation power rather than supplying the wireless services directly inside the buildings, which will originally require installation of both antennas and base stations inside the buildings.

[2] http://www.3gpp.org/LTE

Equipped with RoF technology, the wireless systems can provide services to the in-building users through an optical network, with remote antennas deployed where these services are required. In some modern commercial office buildings, these optical fibre infrastructures have already been in place for carrying Ethernet traffic. The same optical fibre infrastructure can also be used to carry wireless services by means of the RoF technique. In this case, different wireless signals can share the same optic network without deploying dedicated facilities for each service provider. Many key telecommunications equipment manufacturers, including Alcatel-Lucent, Ericsson, Huawei, Nokia-Siemens, and ZTE, have adopted RoF in their BBU+RRU (Baseband Unit, and Remote RF Unit) solutions [75;76] to extend the existing radio coverage and capacity.

The trend of broader applications of RoF technology thus provides a new opportunity for novel implementation of real-time location system (RTLS) in indoor environments. In this section, some basic introduction to RoF technique will be presented. Further information of the RoF solutions that was used in the TINA project will be shown as well with measured data.

### 5.2.1 Fundamentals of RoF

Figure 5-3 shows a simplified RoF link where a number of wireless systems, mobile communication, WLAN, and wireless indoor location systems, share the same optical fibre to their antennas. The key components of a RoF system are the remote antenna units (AUs), the optical fibre link, and a central hub. Thanks to the low attenuation in optical fibre, the AUs can be set to the remote locations only where the wireless coverage is required or needs to be improved, while they are connected through fibre to the central hub that serves a few wireless base stations. In this case, the AU function can be simplified to just radio signal radiation, reception, as well as electrical-optical conversion. Thus it is easy to install and maintain.

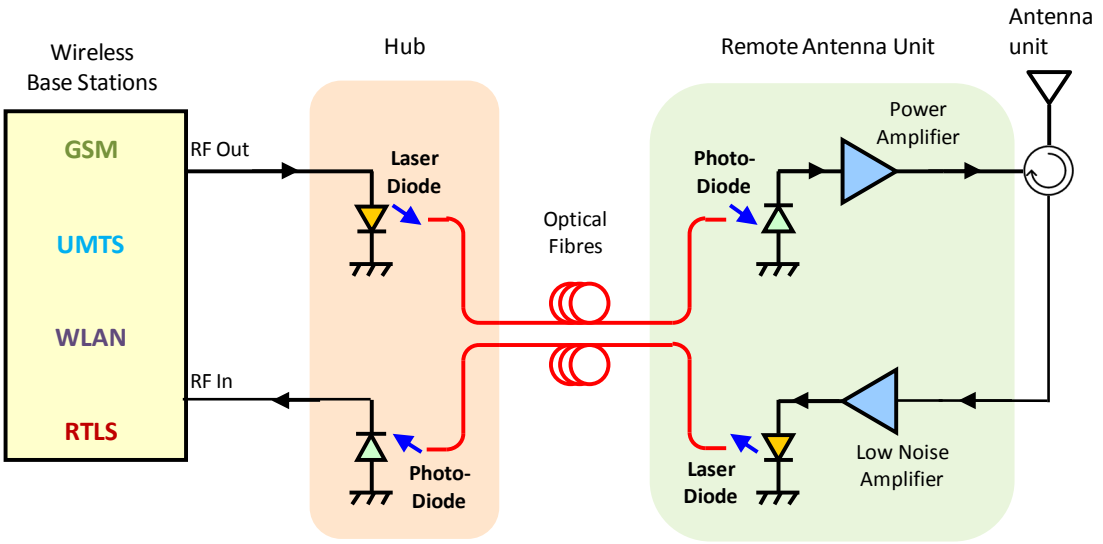


**Figure 5-3 System diagram for a simplified RoF backbone network**

The photo-diode converts optical signals to electrical, while the laser diode converts the electrical signals to optical signal by means of intensity modulation, Figure 5-3.

Different wireless services, including mobile communication and RF location system signals, usually use different bands of the radio spectrum. Therefore, they can be combined together for transmission, and split up at the central hub by using simple frequency selective filters.

In the case of transmission, the radio frequency (RF) signal output from the base stations are transported to the RoF hub where the RF signals are combined and used to directly modulates a laser diode, with a typical emission wavelength of around 1300 nm. This process is performed by superimposing the RF signal onto the laser bias current. It is the simplest technique to modulate the intensity of a laser optical output. The intensity modulated optical signal is now carrying the RF signal and is to be delivered to the designated remote antenna unit through fibre connection. At the remote site, the photo-diode embedded in the AUs detects the intensity of the optical signal, and then generate respective electrical signals for further amplification before being radiated. The processes for received signals are similar but in opposite order to the transmission procedure. The received signal is firstly amplified to adequate level in order to modulate the optical output from the laser diode. After transmission over fibre, the incoming optical signal is photo-detected and then fed to the base stations connected with the central hub.

In practice, a single RoF hub is able to communicate with a few remote AUs through their respective fibre links. Therefore, only one hub is needed to serve a few sectors, or floors in a building, depending on its designed number of channels.

The fibre link used in a RoF system usually is the single mode optical fibre, because multi-mode optical fibres (MMFs) suffer from modal dispersion, limiting their bandwidth-distance products to between 500 MHz.km and 1 GHz.km at 1300 nm wavelength. For a wireless system operating at 2.4 GHz, this constrain means the length of fibre link shall not exceed about 400 metres. However, since most fibres installed in buildings are MMF, there are some situation where additional hardware is used to down-convert the radio signal to an intermediate frequency (IF) which is selected to be within the -3 dB bandwidth of the MMF. By contrast, a RoF system with dedicated single mode fibre does not require this additional processing, and thus is able to provide simpler but reliable solution.

Typical commercial RoF products have a 6 GHz upper limit on the radio frequency due to the small direct modulation bandwidth of commercially available semiconductor laser diodes. This limit is high enough to carry most established commercial radio services for civilian and public use. However, a RoF system with higher operating frequency can be implemented by introducing an additional component, e.g. Mach–Zehnder, to the laser diode. Alternatively, utilisation of more advanced photonic devices, e.g. Asymmetric Fabry-Perot Modulator (AFPM) [77], is another means of implementing RoF system for higher frequency wireless services.

### 5.2.2 RoF Link used in TINA

The RoF facility, including AUs and RoF hub, used in the development of TINA project has been kindly provided by a project partner, Zinwave[3], who is one of the main providers of RoF solutions. The basic technical specifications for the system used in TINA are shown in Table 5-2.

[3] http://www.zinwave.com/solutions.php

| | |
|---|---|
| Up-link Gain: | 30 dB |
| No. of channels per hub: | 4 |
| RF bandwidth: | 400 MHz to 2600 MHz |
| Optical wavelength: | 1300 nm |

**Table 5-2 Specifications for the RoF system used for TINA**

This model of RoF hub supports up to four duplex channels and thus can be used to communicate with four AUs at the remote end, and four wireless receivers at the central site. These can be four sensors of indoor location system whose antennas are deployed at four corners of one cell and their RF receivers are placed at the central site, enabling an indoor location demonstrator with up to four sensors. Although the RoF hub supports duplex communications, only the up-link channels will be used in the TINA indoor location system, while the down-link channels are left unused.

The radio signal of the TINA indoor location system operates at the 2.4 GHz ISM band, which is from 2400 MHz to 2483.5 MHz [72;73], well within the RF bandwidth of the RoF infrastructure (Table 5-2). This allows the tag signal to fully utilise the 83.5 MHz bandwidth for linear frequency modulation. The radio signals received by the AUs are then converted to optical signals with 1300 nm wavelength.

Both single-mode and multi-mode fibres are supported by the Zinwave RoF system. The multi-mode fibre is of lower cost and is easy to align in terms of its interfaces to other equipments. However, due to its smaller distance-bandwidth product and modal dispersion explained in the previous section, it is not suitable for very long distance applications, for example in large airport terminal. The single mode fibre on the other hand is free from modal dispersion. But due to its small diameter size, in the micro metre range, it requires very precise alignment and better interfaces.

The fibre links used in the TINA indoor location system are single mode fibres of 40 metre length, in order to suit different geometry shape of indoor area. The cable loss caused by these fibre links will be insignificant when compared with the propagation path loss.

## 5.3 RFID Tag Design

As proposed in Chapter 3, the TINA RFID tag shall be able to transmit an LFM chirp signal in order to facilitate the location finding process. The chirp signal has been commonly used in sonar and radar systems [46;49;78], as well as application in spread spectrum communications. A chirp is a signal in which the instantaneous frequency increases, namely up-chirp, or decreases, down-chirp, over a frequency band within a period of time. It is therefore a wideband signal with inherent spread spectrum characteristic to cope with multipath and noise.

As an academic research project, TINA is allowed to use the free-of-charge 2.4GHz ISM band, where up to 83.5MHz bandwidth is available. Therefore, the fundamental hardware design requirement is to build such a signal generator that is able to produce an LFM chirp signal over the 2.4 GHz ISM band.

Conventional chirp generation techniques can be categorized into two groups, analogue and the digital solutions. Analogue solutions include an active method based on voltage-controlled oscillator (VCO) and a passive method based on specially designed surface acoustic wave (SAW) devices. Digital solutions have recently been widely used as well. Chirp generation based on a direct digital synthesizer (DDS) technique is one of the typical digital techniques that are known to be good at generating frequency varying signals.

In this section, we are going to briefly introduce these chirp signal generator solutions and explain in detail about the active RFID tag design developed for TINA especially.

### 5.3.1 VCO-based chirp generator

The most straight-forward solution is a VCO-based chirp generator. VCO is an oscillation source whose frequency is controlled by the tuning voltage input to the device. Output from a linearly tuned VCO is therefore a linearly frequency modulated chirp. Figure 5-4 shows a block diagram of an ordinary VCO-based chirp generator. It consists of two main parts, the ramp tuning voltage generator, and the VCO. The ramp generator may produce sawtooth or triangle wave, depending on the signal design

requirement. The frequency converter in Figure 5-4 is optional, depending on whether there is a need to convert the VCO output signal to a different frequency band.

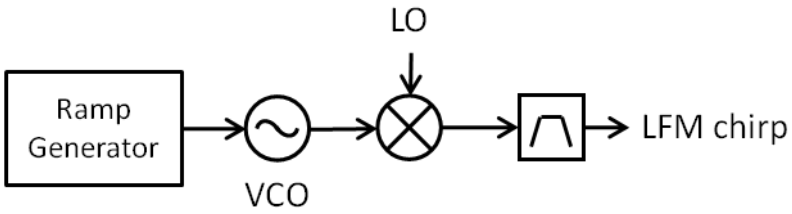


**Figure 5-4 VCO based LFM chirp generator**

Simplicity in hardware implementation is the main advantage of this solution. However, it should be noted that large modulation bandwidth, who defines the tuning speed of a VCO, is essential for a VCO to be used in chirp generation. The modulation bandwidth of a VCO are generally determined by the internal filter capacitor on the tuning input port and the tuning drive impedance that is being used externally to the VCO. On the other hand, the difficulty of employing this method in a chirp system is that linearity of VCO is usually not as good as the following DDL and DDS generators. The linearity of a typical RF VCO is about 2-3%[4]. Also, VCO output stability with temperature variation is another practical issue.

## 5.3.2 SAW-DDL-based chirp generator

The use of a SAW device is also a conventional method for chirp generation. Specifically, it is SAW dispersive delay line (DDL) that is able to generate and compress a chirp, because it provides the frequency dependent delay characteristic. The advantage of SAW technology is that the signal delay from input to output can be designed arbitrarily. If a SAW-DDL is programmed to have signal delay vary linearly with frequency over operating bandwidth of an input signal, it can be used to generate LFM chirp. When such a component is excited by a wideband pulse input, the output signal will become a chirp signal with longer time period over the same bandwidth of the original pulse. That is to say, the impulse response of such a SAW-DDL, usually referred as "expander", is exactly an LFM chirp. The other SAW-DDL used in the

[4] http://www.hittite.com/products/view.html/view/HMC385LP4

receive channel is called “compressor”, Figure 5-5. A SAW-DDL compressor on the other hand packs the expanded chirp signal back to its original impulse waveform.

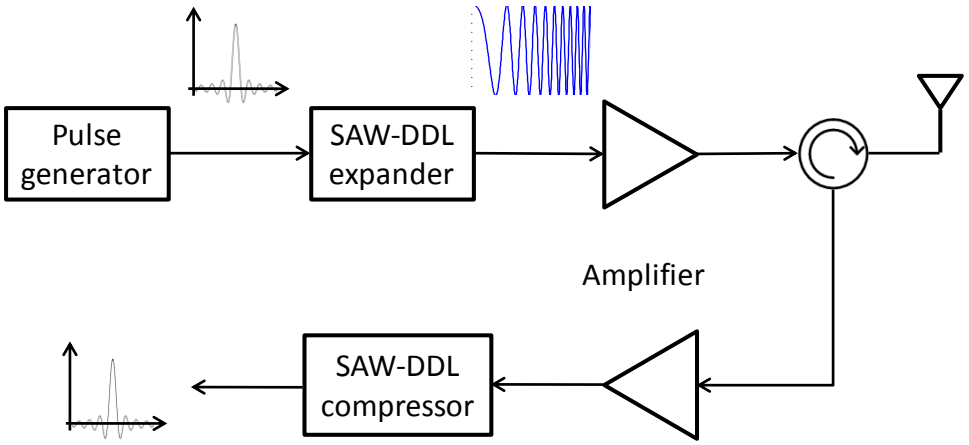


**Figure 5-5 SAW DDL chirp generation and pulse compression system**

Usually SAW-DDLs are manufactured in pairs, one acting as the pulse expander and the other acting as a compressor. Since the SAW-DDL expander and compressor are designed together, they are naturally matched filter to each other. This chirp generation process is using the inherent characteristic of SAW-DDL. Due to its easy-to-use and reliable characteristics, SAW-DDL is a good option to be employed in a system product. However, this technology requires customized design for every chirp generator, a different device will need to be manufactured for a different time-bandwidth product specifications. Therefore, it leaves no tuning flexibility to the users and is not suitable for an experimental system.

### 5.3.3 DDS-Based Chirp Generator

Another possible solution is based on a DDS, which is a technique that can digitally produce a waveform and convert the digital signals to RF waveform with an internal DAC. Modern DDS is developed to generate complex waveform, including linear FM chirp.

Designing RF waveform with a DDS is easy and flexible. Considering the sampling theory in reverse order, a DDS source produces digital samples of a sine wave by means of a phase accumulator and sine lookup table; these digital samples are

converted to analogue waveforms via a DAC followed by a filter. The number of digital bits in the process determines the ultimate resolution of the output waveform.

If a second accumulator is added in front of the first accumulator, the phase generator becomes a double accumulator, or a double integrator, which has a parabolic output. The first accumulator is called frequency accumulator, as it counts the clock signal $t$ to increase or decrease the output frequency bits linearly, noting as $F = kt$. The frequency bits output from the first stage accumulator is then use as input by the second stage phase accumulator, which accumulates the frequency bits and thus act as an integrator, producing $\phi = kt^2/2$. In the analog domain, this translates to sin $(kt^2/2)$, which is an LFM chirp signal.

Figure 5-6 is a block diagram of the essential parts in a DDS chirp generator. A DDS chirp source generates accurate and repeatable chirps, and its linearity is limited by its discrete frequency steps only, which is minimal compared to other methods. However, the low-pass filter that follows the DDS may have a dispersive delay characteristics that can affect the chirp linearity [79]. Main source of noise in this sort of DSP technique is the quantization noise in the DAC. Another restriction of this DDS method in chirp generation is the clock speed, which determines the processing bandwidth of a DDS. The bandwidth of a DDS must cover the chirp bandwidth needed. The latest DDS chip manufactured by Analog Devices[5] is able to produce up to 400 MHz analog output with 1 GSp/s clock rate.

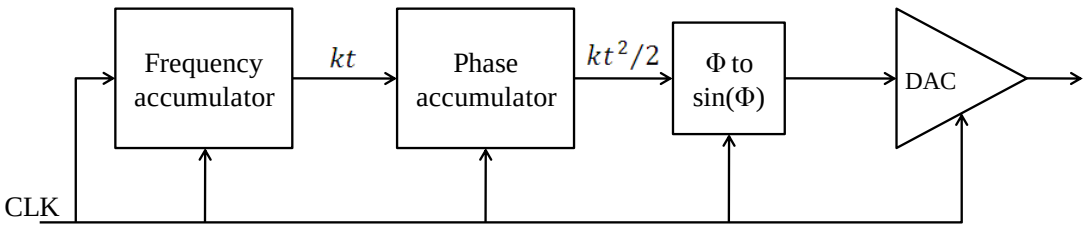


**Figure 5-6 Block diagram of the fundamental components in a DDS chirp generator**

In the subsections above we have reviewed three well-known chirp generation techniques and their advantages and disadvantages in terms of chirp generation. The

[5] http://www.analog.com/en/rfif-components/direct-digital-synthesis-dds/products/index.html

actual chirp generator design developed for TINA system will be given in the next subsection.

## 5.3.4 TINA RFID Tag

The RFID tag used in the TINA demonstration system is a type of transmit-only tag. The transmit-only tag is simpler compared with transceiver tags in a number of areas: structure, circuit, and protocol. All these simplify tag implementation and therefore reduce the potential cost of the entire system.

The portable transmit-only active RFID tag used in the demonstration system was constructed around an Analog Devices DDS evaluation board, using the AD9910 DDS chip. The highest sample rate supported by this device is 1 GSp/s, which limits the maximum analogue signal frequency to 500 MHz, according to the Nyquist criterion. However, the actual DDS output signal frequency is not recommended to go beyond 80% of Nyquist criterion, making a practical upper limit of 400 MHz, if the 1 GSp/s clock rate is used.

By means of the techniques described in Subsection 5.3.3, the AD9910 chip can easily be programmed to generate an LFM chirp signal at any frequency from DC to 400 MHz. However, to meet the TINA signal frequency band requirement of 2.4 GHz, there needs to be a way to somehow move the DDS output signal to the desired radiation band.

### 5.3.4.1 Schemes Generating 2.4 GHz Chirp using DDS

The most obvious approach is to up-convert the DDS output by mixing it with a higher frequency LO to produce a signal sideband at the 2.4 GHz ISM band. The chirp signal is thus up-converted to the band desired and can be filtered out with a simple band-pass filter (BPF). In such a scheme, the frequency of the LO signal must be highly stable and thus will usually be implemented by a phase lock loop (PLL).

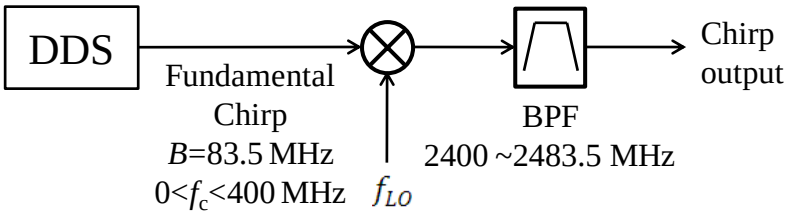


**Figure 5-7 DDS up-converter scheme for generating 2.4 GHz LFM chirp**

A more advanced method is to construct a DDS driven PLL circuit. PLL is known as a circuit whose output phase is related to the phase of the input reference signal. The output frequency of a PLL is fed through an *N* divider to its phase detector input, in order to produce a negative feedback to the VCO tuning voltage so that the output frequency is steadily locked to the input reference signal frequency, by the ratio of *N*. In the DDS-PLL scheme (Figure 5-8), the DDS generated signal is taken as the reference signal to the PLL. Therefore, the VCO output frequency is *N* times the reference DDS frequency. If the DDS signal is a chirp, the VCO output will be a chirp signal as well but with *N* times the centre frequency and the sweep bandwidth. By correctly setting the divider ratio *N* and the DDS generated chirp, the PLL output can be designed to perform a wideband chirp in the desired 2.4 GHz band.

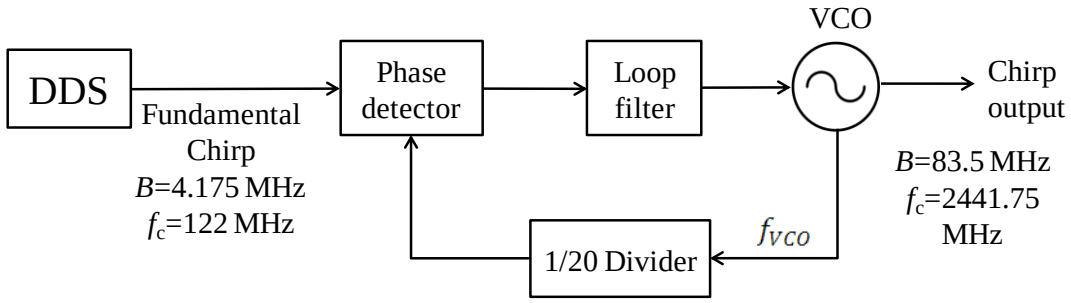


**Figure 5-8 DDS driven PLL scheme for generating 2.4 GHz LFM chirp**

For example, Figure 5-8 shows the block diagram of a DDS driven PLL circuit with *N*=20. If the DDS is programmed to generate a 4.175 MHz chirp at 122 MHz, the VCO output signal will then be a chirp signal sweeping over 83.5 MHz (=20×4.175 MHz) bandwidth with centre frequency at 2441.75 MHz (≈20×122 MHz), which is the chirp signal desired.

Compared to the up-conversion method, the DDS-PLL scheme directly uses DDS chirp signal to drive a PLL circuit to produce the required chirp output, and thus

avoids using the RF mixer as well as the BPF at the last stage of the Figure 5-7 design. It not only avoids the power attenuation at the RF mixer but also is free from the potential non-linear phase characteristics of a BPF. Consequently, it is a superior design over the simple up-converter method.

#### 5.3.4.2 Super-Nyquist Operation of DDS

Both of the schemes described above require an additional PLL stage, which makes the design not compact enough for an RFID tag. Therefore, a different method called super-Nyquist operation is utilised instead to construct the TINA RFID tag. This scheme will still require the BPF and possibly an additional amplifier but does not require the PLL.

As introduced above, DDS device generates an output analogue signal from a digital stream input by means of a DAC triggered by a sampling clock. Besides the fundamental signal generated from the DAC, it also produces spectral images that extend well beyond the frequency of the sampling clock. Some of these images, although considerably suppressed due to the sinc shape frequency response of a DAC, may be useful for special applications. By correctly setting the DDS system clock rate and the fundamental output signal band, it is possible to produce an image at a higher frequency band. Super-Nyquist operation is to select the image that is at the frequency desired and reject the unwanted images along with the fundamental, and thus enable generation of very high frequency signal from a DDS with much lower clock rate. The frequency of images can be computed by the following equations.

$$\begin{aligned} odd\ numer\ image, f_{2N-1} &= N \cdot f_{clk} - f_0, \qquad N \in \{1,2,3,\cdots\} \\ even\ number\ image, f_{2N} &= N \cdot f_{clk} + f_{0,} \qquad N \in \{1,2,3,\cdots\} \end{aligned} \tag{5.1}$$

Figure 5-9 illustrates the spectrum of a DDS output, with fundamental signal and its images up to the fifth one. It shows that a pair of images always appears beside the multiple frequency of the system clock rate. A simple BPF can be used to filter out the unwanted images and output the signal in the required band.

Since the desired image is to be selected by a BPF, attention must be paid to the frequency gap between the neighbouring images. For example, it is possible that an even number image is so close to its next higher odd number image that the desired

one is very difficult to be selected without a filter of sharp roll-off rate. This suggests the first rule for implementing the super-Nyquist operation method, which is to prevent the neighbouring images from being too close to each other.

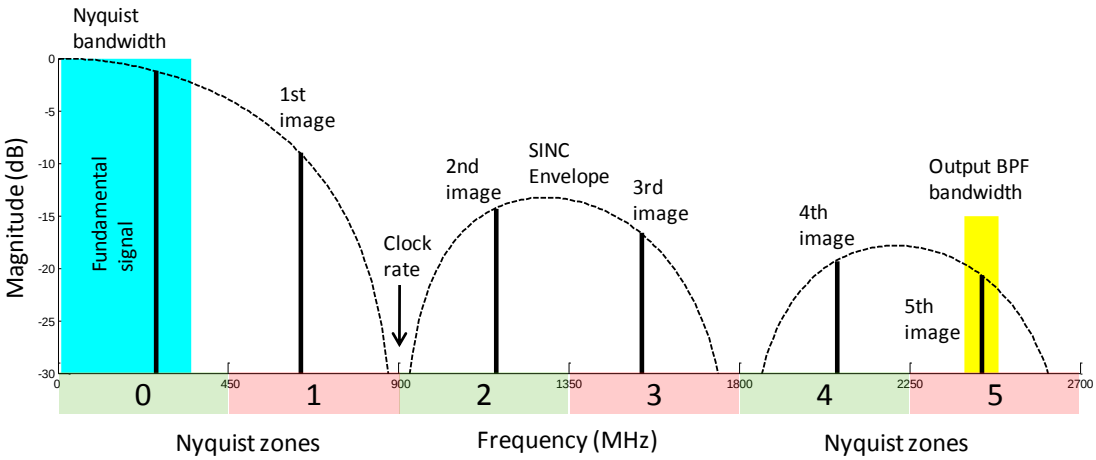


**Figure 5-9 Spectrum showing Super-Nyquist images from DDS**

The second rule is a lower order image is preferred over a higher order one. It can be seen from Figure 5-9 that an image at higher order is attenuated further than those at lower orders, due to the sinc envelope effect. This is the trade-off for obtaining higher frequency signal output with a relatively low sampling clock rate.

To fulfil both these design rules for super-Nyquist operation, a higher sampling clock rate is favoured. A higher sampling clock will firstly produce a broader band gap between the multiple frequencies of the sampling rate, and thus leave larger gap for filtering (first rule). Also, a higher sampling clock is more likely to enable an image signal at the required frequency with lower order (second rule).

### 5.3.4.3 Profile of TINA RFID Tag

According to the specifications of the AD9910 chip, the lower limit on the sampling clock rate is 420 MHz and it can be tuned up to 1000 MHz at 25 MHz step, which is defined by the crystal provided by the evaluation board. As discussed above, a higher sampling clock rate is favoured by super-Nyquist operation. The Nyquist zones from fundamental to the $5^{th}$ image have been calculated for a sampling clock rate ranging from 875 MHz to 1000 MHz, results are listed in Table 5-3.

| | Nyquist zones (MHz) | | | | | |
|---|---|---|---|---|---|---|
| **Clock** | 0 | 1 | 2 | 3 | 4 | 5 |
| 1000 MSp/s | DC~400 | 600~1000 | 1000~1400 | 1600~2000 | 2000~ 2400 | 2600~ 3000 |
| 975 MSp/s | DC~390 | 585~975 | 975~1365 | 1560~1950 | 1950~ 2340 | 2535~ 2925 |
| 950 MSp/s | DC~380 | 570~950 | 950~1330 | 1520~1900 | 1900~ 2280 | 2470~ 2850 |
| 925 MSp/s | DC~370 | 555~925 | 925~1295 | 1480~1850 | 1850~ 2220 | 2405~ 2775 |
| 900 MSp/s | DC~360 | 540~900 | 900~1260 | 1440~1800 | 1800~ 2160 | **2340~ 2700** |
| 875 MSp/s | DC~350 | 525~875 | 875~1225 | 1400~1750 | 1750~ 2100 | **2275~ 2625** |

**Table 5-3 Nyquist zones according to various sampling clock rates**

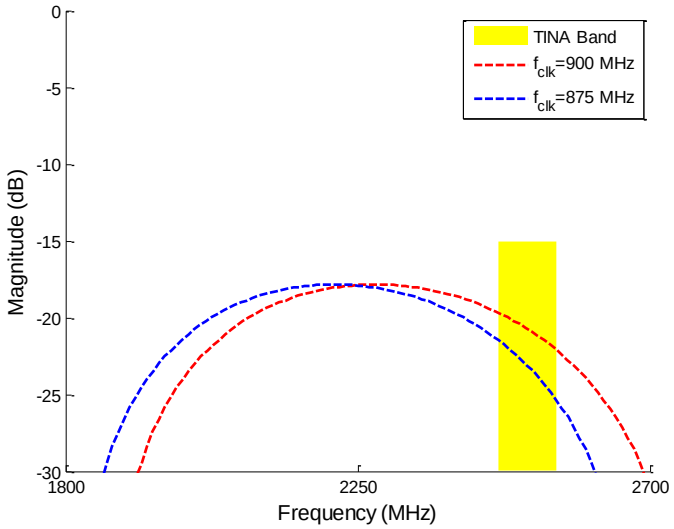


**Figure 5-10 Comparison of frequency responses when clocked by 900 MSp/s and 875 MSp/s**

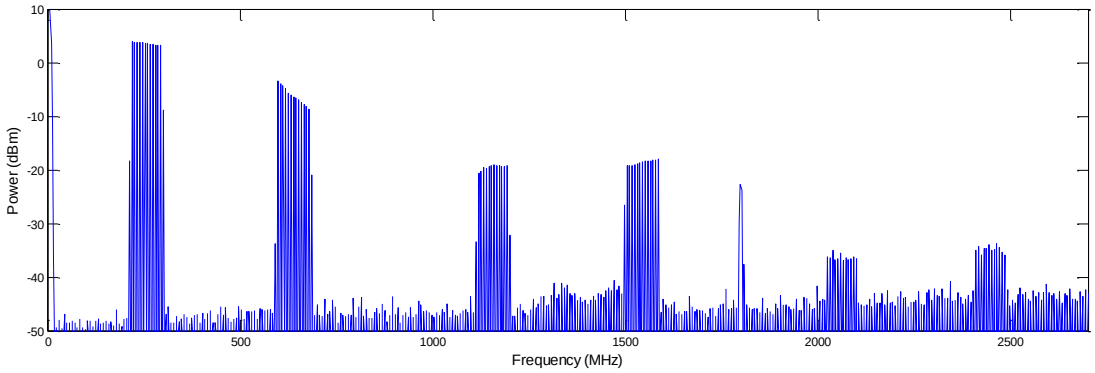


**Figure 5-11 Spectrum analyzer plot of the DDS output signal, displaying DC to 2700 MHz power spectrum, with resolution bandwidth set as 3 MHz**

The desired LFM band for TINA transmission is from 2400 MHz to 2483.5 MHz. Due to the 1 GHz upper limit of the sampling clock to the AD9910 chip, this band cannot be achieved at any Nyquist zones lower than the 5$^{th}$, as given by Table 5-3.

The only two Nyquist zones that fully cover the TINA frequency band are the 5$^{th}$ Nyquist zones resulting from 900 MHz and 875 MHz clock rates.

A sampling clock rate of 900 MHz was eventually chosen because the suppression level over the TINA frequency band is less than that resulted from an 875 MHz clock rate, as indicated by the comparison shown in Figure 5-10.

Consequently, the AD9910 DDS was programmed to produce continuously an 83.5 MHz wide linear FM chirp signal from 216.5 MHz to 300 MHz. With a 900 MHz system clock, the fifth-order image of the fundamental chirp resulting from the super-Nyquist operation of the DDS therefore coincided with the 2400 MHz to 2483.5 MHz ISM band. The power spectrum of the unfiltered DDS output signal is firstly examined by a spectrum analyzer, as shown in Figure 5-11. The 5$^{th}$ image is seen to be present in the expected ISM band, with typically 38 dB lower power than the fundamental signal, agreeing with the -20 dB magnitude suppression estimated from the sinc envelope (Figure 5-10).

This image was extracted by BPF and used as the RFID tag signal. The tag signal was further amplified to around 5 dBm, measured at the output SMA port to which a monopole antenna was attached. Therefore, the LFM chirp generation scheme utilised in the TINA RFID tag can be summarised by the diagram of Figure 5-12.

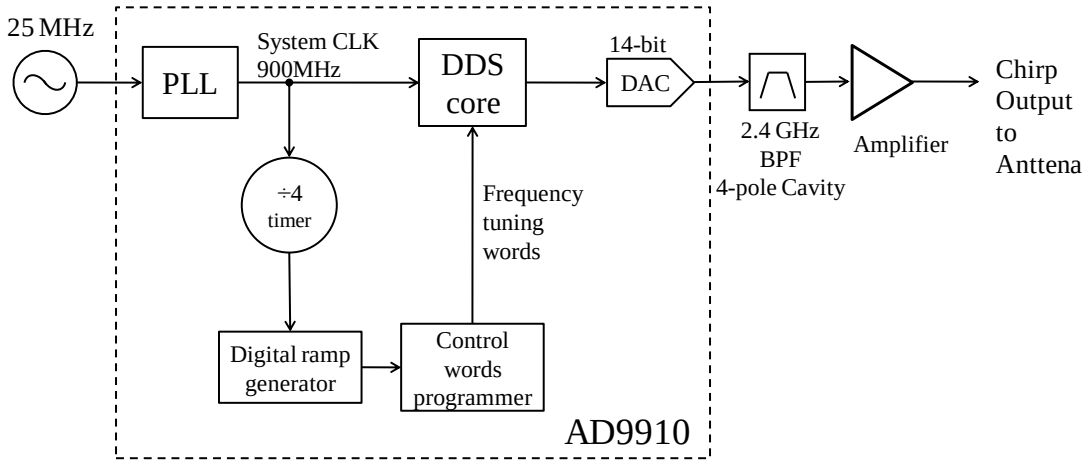


**Figure 5-12 Super-Nyquist DDS scheme for generating 2.4 GHz LFM chirp**

It shall also be noted that, in addition to the attenuation distortion caused by super-Nyquist operation, the frequency sweeping feature of a chirp signal is inversely

related to the fundamental signal if an odd number image is used. For example, in the TINA tag, the $5^{th}$ image is used to produce the 2.4 GHz signal desired. In this case, an up-chirp (increasing frequency) at the fundamental band is inverted to be a down-chirp (decreasing frequency) at its $5^{th}$ image. This effect is important as it will be shown that the technique allowing multiple user access employed in TINA is utilizing different sweeping rates for different users, which will be introduced in the following section.

## 5.4 Multiple Access Using Sweeping Slope Differentiation

Since LFM chirp is chosen as the modulation technique in the TINA indoor location system, it will be beneficial if multiple access capability can also be implemented using chirp signals.

Chirp signals with differential modulation slopes have been used to represent binary data in communication system and Winkler [80] started the early research in this topic. Cook [81] has also proposed the use of a chirp signal set hopping different modulation slopes and different bandwidth for multi-user applications, in which positive slope is related with symbol +1 and negative slope stands for -1.

In this section, a multiple access scheme that differentiates different users by their frequency sweeping slopes is proposed and its inter-user interference is analyzed so that a multiple access scheme can be designed according to specific system requirement.

### 5.4.1 Frequency Sweeping Slope Differentiation

The sweeping slope differentiation scheme identifies multiple transmitters in an LFM chirp system by intentionally assigning chirp signals with different frequency sweeping slopes to different transmitters in the system.

An LFM chirp with duration $T_c$ and bandwidth $B$ can be defined by the following equation:

$$v(t) = \cos(2\pi f_o t + \pi k t^2)\,;\ 0 \le t \le T_c \tag{5.2}$$

where $f_o$ is the starting frequency of the LFM chirp, and $k$ is its sweeping slope, which is equal to $B/T_c$ for an up-chirp, and $-B/T_c$ for a down-chirp.

We firstly consider a basic situation where there are two tags transmitting LFM chirp. Each of the tags is assigned a unique frequency sweeping slope, noted as $k_1$, and $k_2$. Their transmitted chirps can be modelled as:

$$\begin{aligned} s_1(t) &= \cos(2\pi f_1 t + \pi k_1 t^2)\,;\ 0 \le t \le T_c \\ s_2(t) &= \cos(2\pi f_2 t + \pi k_2 t^2)\,;\ 0 \le t \le T_c \end{aligned} \tag{5.3}$$

The locations of the tags are unknown and their distance to a receiver may be different, resulting in different propagation delays, noted as $\tau_1$ and $\tau_2$. At the receiver, the received signal $r(t)$ contains two attenuated and delayed versions of the transmitted chirps as shown by Eq. (5.3):

$$r(t) = A_1 \cdot s_1(t - \tau_1) + A_2 \cdot s_2(t - \tau_2) \tag{5.4}$$

In the receiver of this system, deramp process is applied to the received signal $r(t)$. Since there are two unique sweeping slopes $k$ in this system, there will be accordingly two channels of matched filters in the receiver to cope with signals from the two user tags. Firstly, the deramp outputs from one of the users are considered. Figure 5-13 shows the process of deramping received signal from only UT1 in the two deramp channels.

In Figure 5-13, the matched filters are implemented by multiplication with two locally generated chirp references following sweeping slope $k_1$, and $k_2$. Details of this deramping technique can be found in the Section 3.1 of Chapter 3.

In terms of channel 1, the received UT1 signal is matched to the chirp reference (with identical frequency sweeping slope) and thus the frequency sweeping ramp of the received signal will be deramped. The deramp output shall contain a single tone signal whose frequency is proportional to the time difference between the received chirp and the reference chirp.

The mixer output is usually low-pass-filtered to eliminate the high frequency components from multiplication. Deramping a received chirp with matched sweeping slope can be modelled as:

$$A_1 \cdot s_1(t-\tau_1) \cdot s_1(t) = A_1 \cdot \cos(2\pi k_1 \tau_1 t - \pi k_1 \tau_1^2 + 2\pi f_1 \tau_1) \tag{5.5}$$

It can be seen that the output is a single tone signal whose frequency is $k_1\tau_1$.

On the other hand, the received UT1 signal is mismatched to the reference chirp of channel 2. Therefore, at the output from the channel 2, a wideband noise-like component is seen in the corresponding spectrum (Figure 5-13).

In fact, the received signal shall contain both replica of $s_1(t)$ and $s_2(t)$, as defined by the Eq. (5.4). In this case, the outputs from both deramp channels will include a single tone component resulted from the matched chirp signal input surrounding by a spread spectrum component resulted from the mismatched chirp signal input.

As derived in the Eq. (5.5), the matched deramp output will be a sinusoidal signal. If a mismatched chirp input is also present at the input to the deramp processor, there would be another output component interfering with the matched deramp output. The interference from a mismatched chirp input will be maximum in case the input mismatched chirp happens to be aligned with the input matched chirp in time, for example the case shown by Figure 5-14. Without loss of generality, it is assumed $f_1 = f_2$ in the Figure 5-14.

Taken the channel 2 of Figure 5-13 as an example, in this case, local chirp reference $s_2(t)$ (whose sweeping slope is different from the received chirp) is sweeping at the rate of $k_2$. The deramp output in this case will be a new spread spectrum chirp whose energy is distributed over a wider bandwidth. This resultant signal is:

$$\begin{aligned} &A_1 \cdot s_1(t-\tau_1) \cdot s_2(t) \\ &= A_1 \cdot \cos(2\pi(f_2 - f_1 + k_1\tau_1)t - \pi(k_1 - k_2)t^2 - \pi k_1 \tau_1^2 \\ &\qquad + 2\pi f_1 \tau_1) \end{aligned} \tag{5.6}$$

As can be seen from the Eq. (5.6), the deramp output in a mismatched case is also a spread spectrum chirp signal, with the starting frequency at $f_2 - f_1 + k_1\tau_1$ and the

frequency sweeping slope of $k_1 - k_2$. The bandwidth of the mismatched deramped signal $\Delta B$ is equal to $(k_1 - k_2)T_c$, whose value depends on the signs of $k_1$, and $k_2$:

$$\Delta B = (k_1 - k_2)T_c = \begin{cases} |B_1 - B_2| & if\ k_1 k_2 > 0 \\ |B_1 + B_2| & if\ k_1 k_2 < 0 \end{cases} \tag{5.7}$$

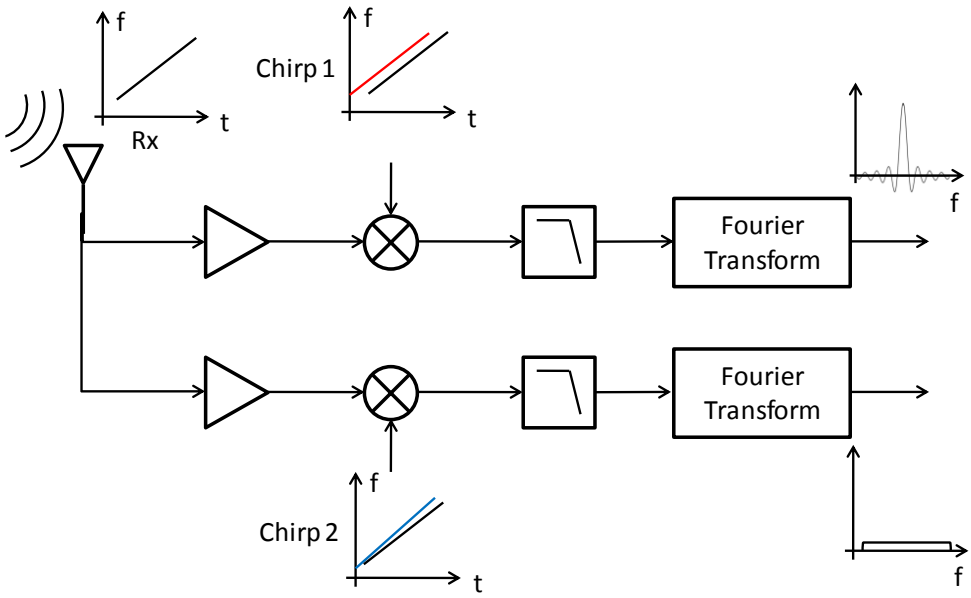


**Figure 5-13 Block diagram the receiver with two channels of deramp processing**

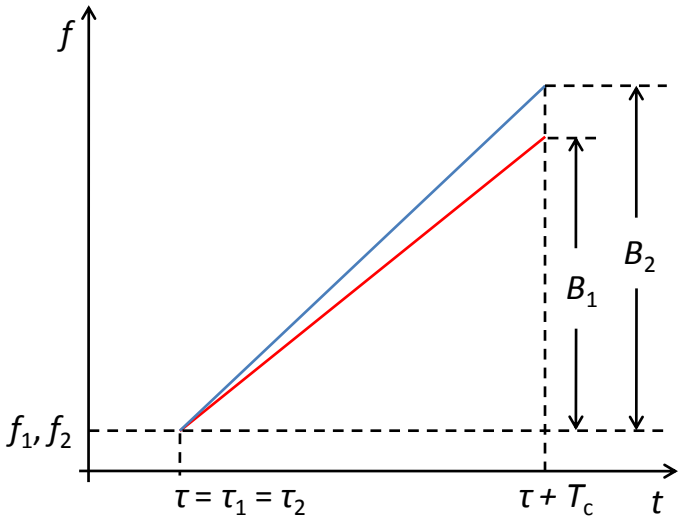


**Figure 5-14 Two input chirps aligned in time**

If the power of the spread spectrum component is much lower than that of the single tone component, the mismatched interference to the matched deramp output can be regarded as insignificant and the time delay information of the matched chirp signal

may still be determined without errors. The next subsection discusses this inter-users interference and derives an equation to estimate its level.

## 5.4.2 Inter-users Suppression Level

As explained above, in case that the received signal is of the same frequency sweeping slope as the reference chirp, a single tone sinc component (Eq. (5.5)) will be found in the spectrum of the deramp output. However, in case that there is a difference in the slope rates between the received signal and the reference chirp, a noise-like component will be found (Eq. (5.6)) as the energy of deramped result will be spread across a wider band $\Delta B$ which is given by Eq. (5.7). Figure 5-15 shows the simulated power spectral density for both matched and mismatched deramp outputs.

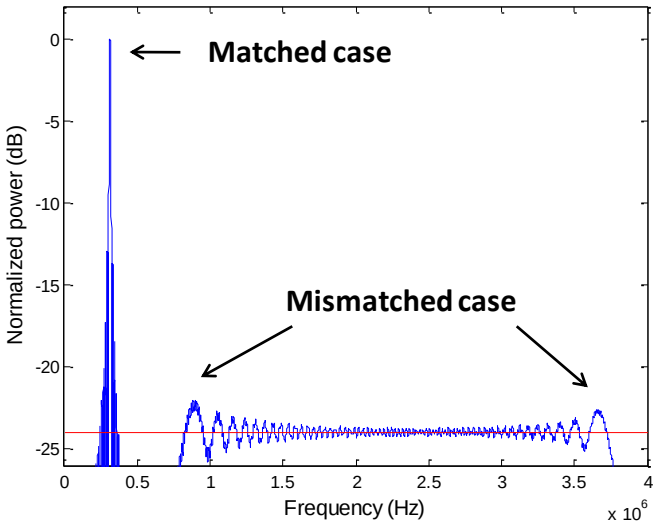


**Figure 5-15 Power spectral density for a matched deramp component and a mismatched deramp component**

The suppression level in such case is defined by the power of the mismatched deramp component $P_c$ measured within a given bandwidth divided by peak power of the matched deramp component $P_s$ measured within the same given bandwidth:

$$G_d = \frac{P_c}{P_s} \tag{5.8}$$

To design a system using sweeping slope differentiation for multiple access, it is necessary to estimate the inter-users interference at the stage of deramp output.

It is assumed that in a deramp channel (Figure 5-13), the matched deramp output and the mismatched deramp output are of the same power, $\boldsymbol{P}$.

Since the matched deramp output is a single tone sinc function, most of its power is concentrated at its centre frequency, producing a peak $P_s = \boldsymbol{P}$ in the power spectrum. On the other hand, power of the mismatched deramp output is distributed over a wider bandwidth $\Delta B$, producing a much lower power level in the spectrum. The average power level of this component can be estimated by the total power $\boldsymbol{P}$ divided by the number of frequency samples it is sweeping across, $N_f$, which is given by:

$$N_f = \Delta B / f_{res} \tag{5.9}$$

where $f_{res}$ is the frequency resolution for the FFT analysis, which is the reciprocal of the length of time samples used [82]. In this case, the length of time samples is the time duration of the input chirp signal $T_c$.

$$f_{res} = 1/T_c \tag{5.10}$$

Therefore, the average power level of the mismatched deramp component $P_c$ can be found by

$$\begin{aligned} P_c &= \frac{P}{N_f} \\ &= \frac{P}{\Delta B \cdot T_c} \end{aligned} \tag{5.11}$$

Substituting Eq. (5.11) into Eq. (5.8) gives the equation estimating the inter-user suppression level:

$$G_d = 10 \cdot \log\left(\frac{1}{\Delta B \cdot T_c}\right) \tag{5.12}$$

For example, in the case shown by Figure 5-15, the spread spectrum bandwidth $\Delta B$ is 3 MHz and the input chirp duration $T_c$ is 80 μs; thus the logarithmic suppression level $G_d$ shall be -23.8 dB, as indicated by the red line in Figure 5-15.

For given chirp duration $T_c$, the estimated inter-user suppression levels against mismatched spread spectrum bandwidth $\Delta B$ from 0.1 MHz to 8 MHz are illustrated by Figure 5-16. As can be seen, the inter-user suppression level reaches over -20 dB difference if more than 1 to 2 MHz mismatched spread spectrum bandwidth applies. However, this inter-user suppression level does not go down as fast for spread spectrum bandwidth that is larger than 2MHz.

It shall also be noted that, the suppression levels estimated using Eq. (5.12) is the worst case that could happen in the deramp processor. This is because derivation of Eq. (5.6) is based on the assumption that the input chirps are aligned in time. This is usually not the case in a practical ranging system for location applications, as the user tags are usually at unknown and different positions in the indoor environment. The arrival times of their transmitted chirps are likely to be different while this difference will be sufficient to break the coherent deramping and produce a much smaller inter-user interference than that is estimated using Eq. (5.12).

By this means, a concise and easy to implement multiple access scheme for chirp based ranging systems can be designed. The drawback of this scheme is relatively low capacity, due to limited spectrum resource and the resolution requirement on chirp duration (refer to Eq. (3.8) in Chapter 3). Consider the 83.5 MHz bandwidth available in the 2.4 GHz ISM band, it is possible to assign distinct sweeping slope to multiple users by simply adjusting the chirp duration to provide minimum 2 MHz band difference between different users. If both up and down chirps are used and the chirp duration ranges from 72 μs to 80 μs, a possible multiple user scheme containing ten different chirps for ten users can be designed. The ten distinct frequency modulation slopes are illustrated by Figure 5-17.

To ensure identical time measurement resolution (Section 3.1) for all users, the ten distinct chirps are of the same 83.5 MHz bandwidth but are configured to sweep for various lengths. The minimum inter-user suppression level is -22 dB, between a 78 μs chirp and an 80 μs chirp, both of which sweeps in the same direction.

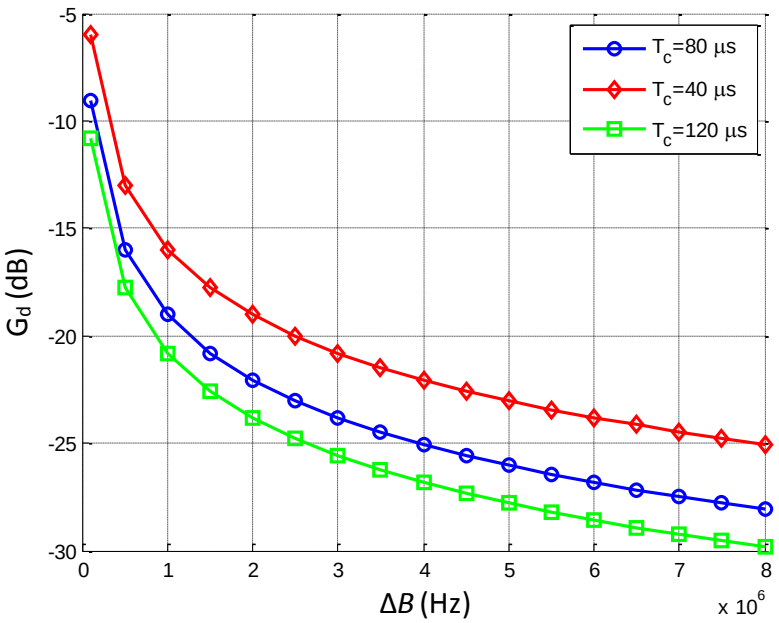


**Figure 5-16 Inter-user suppression level vs. spread spectrum bandwidth**

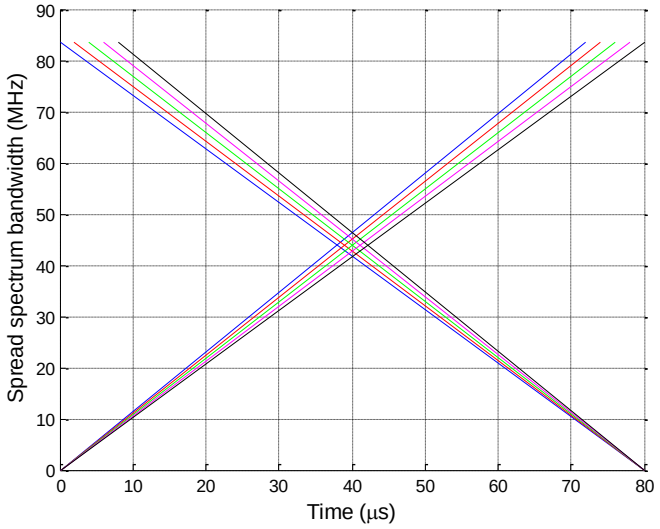


**Figure 5-17 Frequency sweeping characteristics for 10 distinct chirps of various durations**

The largest inter-user suppression occurred between an 80 μs up-chirp and an 80 μs down-chirp. Even if two of such incoming chirps are aligned in time when they are received by a deramp processor, there will be effectively -41 dB suppression gain between their deramped outputs, providing adequate separation between different users. These are also the two chirps assigned to the two TINA tags in the demonstration presented in Chapter 6.

As a standalone multiple access scheme, capacity of ten users is obviously not enough for most indoor location applications. However, this scheme may be integrated with other multiple access technology to enlarge the system capacity by several times. For example, this sweeping slope differentiation scheme has the potential to be combined with ALOHA TDMA [83;84] to enlarge the multiple access capacity for a few times, depending on how many distinct sweeping slopes are assigned.

The neatness of this sweeping slope differentiation technique is that sufficient inter-user suppression level can be achieved without synchronisation between transmitters and the receivers. This feature is especially useful for a TDOA location system where user tags are located at unknown positions and are not synchronised to the network.

## 5.5 Central Receiver and Location Estimation Program

The location estimation accuracy relies on proper measurement of the TDOA information based on the RF chirp signals received. The procedure includes down-converting the signals to a lower frequency band, detect appearance of incoming chirps, select the chirp signal for deramping, and applying appropriate frequency detection strategies. All of these processing are executed in the central site of the system, by the RF receivers, and a laptop equipped with the LabView platform.

### 5.5.1 Central Receiver and Data Acquisition

The received tag signals at the AUs are transported to the central RoF hub via 40 m long single mode fibres, and converted back to analogue signals, Figure 5-2. The received tag signals at the outputs of the hub were down-converted from the original 2400–2483.5 MHz band to the 10–93.5 MHz band. This down-conversion allowed the three tag signals to be digitised directly with a real-time oscilloscope for subsequent data processing. It should be noted that other moderate signal acquisition devices can equally be used in place of a real-time oscilloscope. The oscilloscope is employed in the TINA demonstration system for its convenient interface with the laptop.

In each measurement and location estimation, the frequency down-converted tag signals are sampled for 200 μs at 250 MSp/s by the real-time oscilloscope. The 200 μs sampling time is chosen because this is greater than twice the duration of the chirp. Since the duration of the chirp signal transmitted by a TINA user tag is 90 μs, sampling for 200 μs ensures acquisition of at least one complete chirp replica needed by the location estimation algorithm. The sampled data are processed in real-time in the LabView on a laptop.

## 5.5.2 LabView Program for TDOA and Location Estimation

In the TINA indoor location demonstrator, the digitized received signals are deramped in a virtual instrument program on the LabView platform. This program finds the required TDOA, and performs the location estimation algorithm. Since the trial results and figures used in the following sections are produced from this program, it is necessary to provide an overview of this program and explain the essential steps required when using it to estimate the location of the tags.

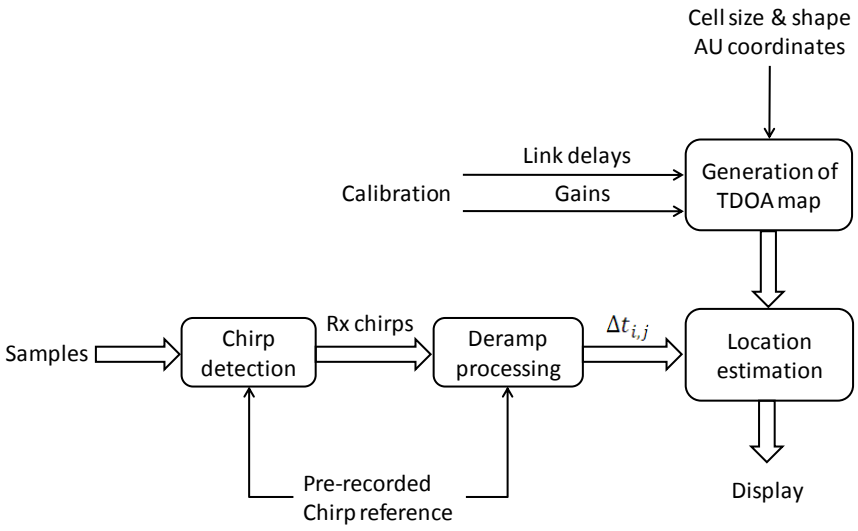


**Figure 5-18 Block diagrams of the LabView program performing TDOA detection and location estimation**

Figure 5-18 shows a block diagram of the respective signal processing steps in the LabView program. They will be explained in the order of execution steps in a trial below.

*Pre-recording chirp reference*

Before the system can be used for locating the tags, some preliminary work shall be taken to assist the LabView program. The first one is recording the LFM chirp signals that will be used by the chirp detection and deramp processing step.

In this step, the user tag generated chirp signal is directly input to the receiver, to imitate a perfectly received chirp signal. It is then digitized and saved by the real-time oscilloscope (Figure 5-2). Therefore, this reference chirp, recorded for also 200 μs at a sampling rate of 250 MSp/s, contains at least one continuous occurrence of the 80 μs long-chirp part of the tag signal. It is regarded as the "perfect" chirp free from environmental noise, multipath, and interference. This recorded "perfect" chirp copy is noted as the chirp reference, as it will be called by the chirp detection and deramp processing unit of the LabView program to be used as the LO chirp in the TDOA measurements (Chapter 3).

*Calibration of imbalanced gains and delays*

In a real system, even if the fibre links and amplifiers used in all the input channels are of the same kinds, there might still be small differences in terms of fibre length (link delays) and the amplifier gain, which will introduce errors to the TDOA measurements and thus the location estimation result. Therefore, the next preliminary work required is calibration through a closed-loop measurement, which finds the delays of all the fibre links connecting remote AUs and the central hub, as well as the amplification gains applied onto the RoF channels.

The delay and gain information by channels are obtained from the calibration step and used as input to the TDOA map generation step, Figure 5-18. So that when the TDOA map is initialized, the practical imbalances in delays and gains (caused by optical transportation, signal conversion, and amplification) are taken into account.

*Measurement of indoor geometry*

It is also required that the geometry information of the indoor cell area (e.g. room size and shape) and the relative coordinates of AUs deployed in this cell are measured. These figures construct the second group of input to the TDOA map generation step.

*Generation of TDOA map*

When all the information required by the TDOA map generation step are found, they are used in a pre-measurement program to generate the specific TDOA map of the current indoor cell, Figure 5-18. The approach of initiating the TDOA map has been introduced in Chapter 4. This TDOA map is used in real-time tag location estimation, which estimates the tag location by comparing the TDOA information measured from deramp processing step with the TDOA map corresponding to the indoor area under monitor.

*Chirp detection*

The required inputs to the deramp processing step are the received chirp replicas at every AU. However, the captured data is a 200 μs long signal which contains more than one complete chirp replica. To ensure that the received chirps are correctly found, the recorded 200 μs samples are firstly correlated with the chirp reference to detect if the required chirp signal has been received. If there are three receive channels, there will be three 200 μs received signals. Thus, cross-correlations between the previously recorded chirp reference and all the three received signals are performed. The timestamp of the strongest correlation peak of the three cross-correlations is then used to extract the chirp replicas. At this point, only the 80 μs long-chirp sections of each tag signal and the reference chirp were retained for further processing while the remaining sections of the waveforms, including the 10 μs short-chirp sections, were discarded.

A small time offset of 0.479 μs (≈ 80 μs / 83.5 MHz × 500 kHz) was also added mathematically to all the three retained tag signal waveforms so that subsequent de-ramp frequencies would appear at around 500 kHz instead of 0 Hz. This offset acts as a guard margin preventing the deramped components fall into the negative frequency domain.

*Deramp processing*

The purpose of deramping is to find the frequency difference between a pair of incoming chirps, as it is proportional to the time difference between the two chirps by

their chirp sweeping rate *k*. A straightforward way to find the frequency difference is to mix the tag signals received by two of the AUs in a RF mixer followed by measurement with a spectrum analyser. However, in indoor environments, such a technique is very susceptible to multipath effects. This is because the measured frequency differences can be due to mixing between any combination of the line-of-sight (LOS) and non-line-of-sight (NLOS) components contained in the received signals. It is therefore impossible to select only the frequency difference between the two line-of-sight signals required for the correct location estimation.

Alternatively, the selected 80 μs long-chirps from all channels are actually deramped with the 80 μs long-chirp reference by mathematically multiplying them together.

The reason why deramping with a local chirp reference can help combat multipath effects is that although each received tag signal still contains both the LOS and NLOS components, mixing or deramping between the reference chirp and the LOS component always produces a signal peak at a lower frequency than those between the reference chirp and other indirect components. This is because the line-of-sight path between the tag and an AU is always the shortest possible and thus the deramp signal frequency is also the lowest. Therefore, it avoids production of random deramped frequencies which can go down to DC. This feature has been used to define a practical detection strategy alleviating multipath, details of which will be covered in the Section 5.6 of this chapter.

After deramping, an FFT was performed on the 80 μs de-ramped signals in order to find the corresponding frequencies, and hence the time differences with respect to the local chirp reference. Since the FFT window was 80 μs, set by the long-chirp duration according to TINA specifications, the FFT frequency resolution is therefore $1/T_c$=12.5 kHz, corresponding to a spatial resolution of 3.6 m (= 12.5 kHz × 80 μs / 83.5 MHz × c). When detecting the deramped frequency by FFT, only discrete frequency values with 12.5 kHz step will be produced. Therefore, the deramped signal needs to be zero padded before performing the FFT in order to detect the continuous value of the deramped frequency, avoiding errors in case the deramped frequency falls in between two frequency bins. In the TINA demonstration system, the number of samples contained in the 80 μs period is 20,000 (=250 MSp/s × 80μs). Therefore, the

deramped signals are zero-padded to a total number of $2^{17}$ points in order to obtain the fine frequency step required.

The key steps involved in TDOA measurment, starting from chirp detection to inter-channel time differences calculation, can be summarised and illustrated by the Figure 5-19.

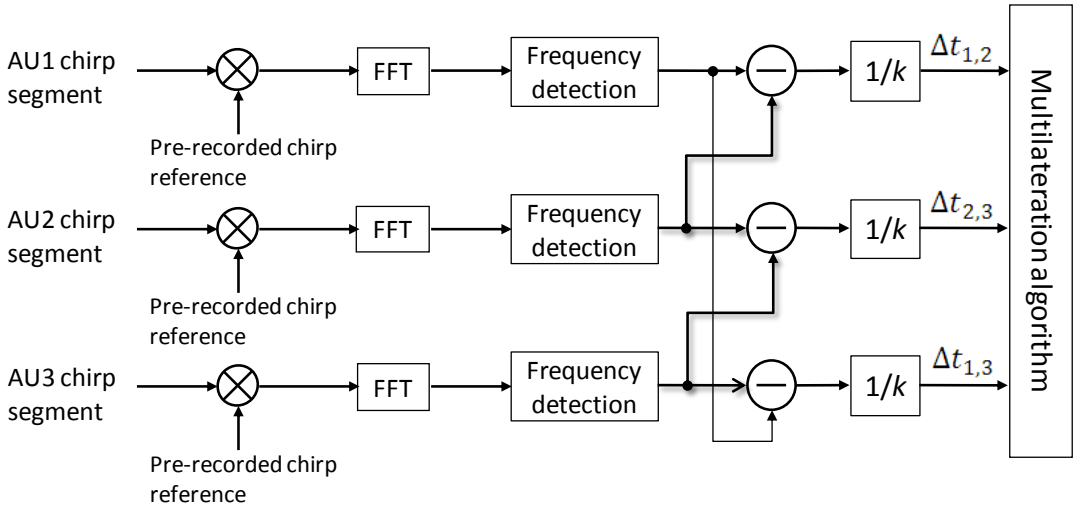


**Figure 5-19 Key signal processing steps in TDOA detection**

*Location estimation*

The TDOAs measured in the deramp processing step are then used by the location estimation module, which utilises the TDOA map generated in the pre-measurement steps to find location of the user tags through multilateration algorithm introduced in Chapter 4.

In order to find the tag location using TDOAs of received signals, minimum of three AUs per indoor location cell are needed, the signal processing in which case has been shown by Figure 5-19. However, in some situations, more than three AUs are deployed to monitor a single cell. Redundant AUs can be used to improve the location performance, due to the following reasons.

Firstly, depending on the propagation range of a tag to the AUs, the signal to noise ratio (SNR) of the received signals may vary from one to another AU channel. If redundant AUs are introduced, the received signals with higher SNR can be selected

while the signals with the lowest SNR will be ignored. In this case the variance of measured TDOAs can be controlled to minimum.

Secondly, in a crowded indoor environment, the wireless propagation path from an RFID tag to the AUs may be blocked by people or objects. In this NLOS propagation case, location found using the TDOA method may include considerable errors. However, by deploying more than three AUs at different positions, the possibility of having LOS propagation in at least three received channels is increased.

To sum up, received signals from redundant AUs can be used to improve quality of the measured TDOAs, and reduce the possibility of error location result due to NLOS. To achieve these benefits, one or more AU channels shall be dismissed in the location estimation process. In the location estimation algorithm of the TINA demonstrator, the AU channels with the lowest received signal power will be dismissed. This is a simple but practical criterion because lower received signals usually imply further propagation or occurrence of NLOS, provided that the signals are transmitted from an identical source.

In case more than three AUs are available, there will be $M(M-1)/2$ combinations of distinct AU pairs, where $M$ is the total number of AUs. Deramp processing in such a system produces $M(M-1)/2$ TDOAs that can be used for location finding. From this full TDOA set, only those TDOAs derived from channels with good signal qualities are used.

For instance, in the TINA indoor location system, if there are four AUs deployed, the full TDOA set comes with six measured TDOAs. The location estimation algorithm then follows these steps:

1. The AU channel with the lowest received signal power is ignored;
2. Only the three TDOAs irrelevant to this AU channel are used for location estimation;
3. TDOA map corresponding to the three remaining AUs is called to match the measured TDOAs with the pre-calculated map;
4. Location coordinate with the smallest TDOA difference is chosen as the estimated tag location.

Therefore, the estimated tag locations are computed from the best available received signals only.

Regarding location measurements with multiple tags, location estimation is performed for every tag whose transmitted signal appears at three or more AU channels of the system. The resultant location coordinates of multiple tags are displayed in real-time by the LabView interface.

It should be noted that, although a LavView program in a laptop is used to estimate the tag location in the demonstration system, the same function can be executed by an FPGA array that is programmed to run the same algorithms stated in this section, which will allow production of a standalone indoor location system.

### 5.5.3 Discussion

To sum up, the technical details regarding the signal processing beyond fibre transportation have been clarified in this section. The demonstration system of TINA therefore is able to find the user tags location by executing all the functionality introduced from Section 5.1 to Section 5.5. However, an important issue we do need to cover is that practical location finding may be affected by noise, interference from other systems, and multipath. Among them, multipath is the most significant and long-term error source that an indoor location system has to cope with. During the research of TINA, a few simple but practical techniques have been found and implemented to mitigate the impacts of multipath on the location estimation results. Experimental data have demonstrated these techniques and they will be covered in the next section.

## 5.6 Mitigating Impacts of Multipath

Multipath propagation has been a common issue and a main source of errors for many wireless systems. A variety of techniques have been devised to mitigate the impacts of multipath and maintain reliable communication through wireless channel, e.g. diversity reception[85], channel equalization[86-88], and spread spectrum

techniques[89;90]. The LFM chirp employed in TINA is also a kind of spread spectrum anti-multipath technique that is robust to multipath propagation, in the way that multipath components can be differentiated from their direct path. However, to improve the location performance of TINA system, it is necessary to understand the multipath impacts on the location results of TINA indoor location system, so that its impacts can be minimized.

In Chapter 3 we have presented the signal model of LFM chirp and the deramp technique used to retrieve time delay information from such a signal. In the TINA location system, the user tag radiates LFM chirp waveform, and it is received by the antenna unit (AU) through wireless propagation. A practical issue that has not been discussed in Chapter 3 is that the received signal is not just a delayed version of the chirp waveform transmitted by the user tag, but actually a summation of chirps delayed and attenuated in different wireless propagation paths. This is because of the existence of more than one possible transmission path. The radiated signal can reach the AU through both the LOS path and the NLOS paths, which are due to reflections off the surrounding objects, walls, ceiling, and floor. Therefore, the received signal can be modeled as

$$r(t) = \sum_{m=0}^{L-1} A_m \, v(t - \tau_m) + n(t) \tag{5.13}$$

where $v(t)$ is the transmit chirp, as defined by Eq. (5.2), $L$ is the number of echo received, including direct path and multipath signals, $v(t - \tau_m)$ is the *m*th path with delay $\tau_m$, $A_m$ is the amplitude of the *m*th path, *n(t)* represents total noise and interference (from other systems) that is added to the received signal. This multipath phenomenon is well known in wireless propagation. The impacts of multipath propagation in the system performance are dependent on the type of wireless system and the signal processing approaches involved. In an indoor location system, it is the errors in time or range detection that are of concern to the system designers and users.

In a TDOA ranging system using LFM chirps, the direct impact induced by multipath is errors in TDOA, and thus range difference measurement. In a fundamental two-channel TDOA measurement, the relationships between the deramp frequency

difference $\Delta f_d$, and the corresponding TDOA $\Delta\tau$ or the equivalent RDOA $\Delta r$ are re-written in Eq. (5.14), where *k* is the frequency sweeping slope, *c* is the speed of light.

$$\Delta\tau = \frac{\Delta f_d}{k}$$
$$\Delta R = c\frac{\Delta f_d}{k} \tag{5.14}$$

It can be seen that the estimated range difference is directly related to the deramped frequency difference detected from the two receive channels. Therefore, any errors in the deramped frequency detection in either channel will affect the resultant TDOA measurement, and thus the eventual estimated location.

Let us consider two examples of TDOA measurement between two receive channels, the first example is free from multipath interference (Figure 5-20) and the second example contains multipath component in the second receive channel (Figure 5-21). In the situation depicted in Figure 5-20, the deramped frequencies at both channels can be perfectly detected, giving $f_1 = 80$ kHz and $f_2 = 50$ kHz. The resultant deramped frequency difference $\Delta f_d$ is thus 30 kHz, indicating 28 ns TDOA or 8.6 m RDOA, assuming *k* =1.04 MHz/μs.

The two examples above explain the impact of multipath on TDOA measurements. In the second example, the Channel 2 deramp signal is distorted by a multipath component, resulting in incorrect detection of the deramped frequency in Channel 2. In the Figure 5-21 case, a multipath signal arrives at AU2 together with the direct path signal, the consequence is $f_2$ being shifted to 56 kHz from 50 kHz. The resultant deramped frequency difference $\Delta f_d$ is reduced to 24 kHz, instead of 30 kHz, due to the interference of the multipath. In this case, the frequency measurement error is 6 kHz, equivalent to approximately 5 ns error in TDOA or 1.5 m error in RDOA, if *k* =1.04 MHz/μs.

In the following sections, we will firstly analyze some real measurement results affected by multipath propagation, and then two detection strategies are proposed to be applied to the frequency detection process in order to reduce the errors brought by multipath. It will be shown that by employing these strategies, the TDOA

measurement accuracy is better than only relying on the inherent robustness that the LFM chirp signal offers.

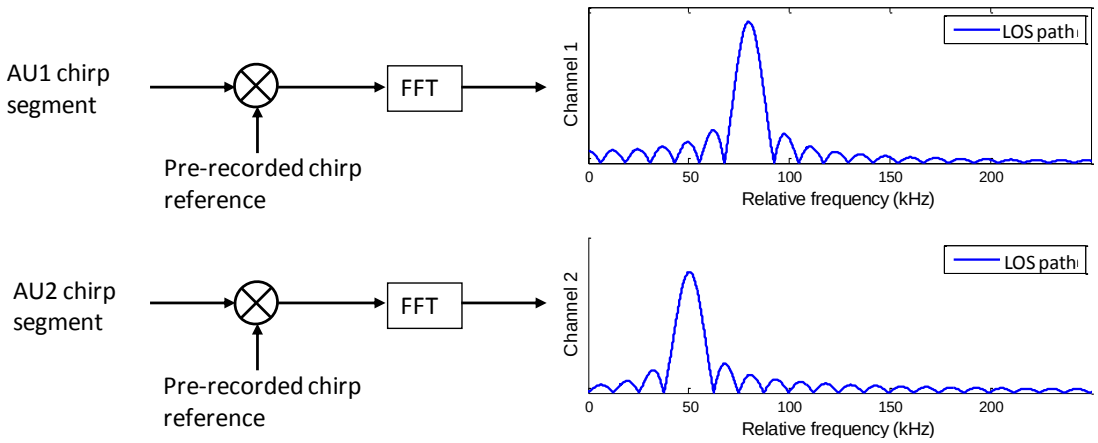


**Figure 5-20 Multipath-free TDOA measurement between a pair of receive channels**

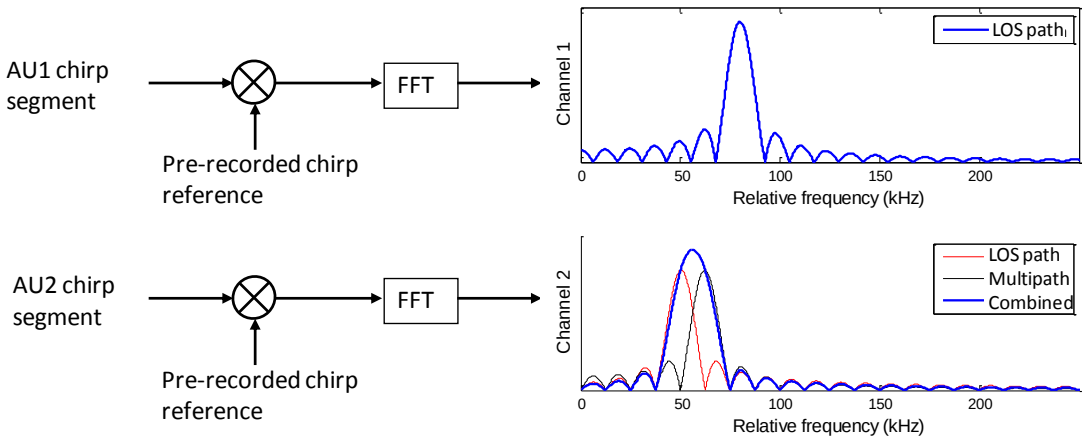


**Figure 5-21 TDOA measurement between a pair of receive channels, when multipath appears at Channel 2**

## 5.6.1 Earliest Tone Detection

In the TINA system, location estimation is performed by using the TDOA information from all the receive channels, whose accuracy relies on the beat frequency detection process after deramping (as referred to Section 5.5). As introduced in Chapter 3, the TDOA information between a pair of receive channels is determined by the difference between the deramped beat frequencies (Eq. 3.14) produced at the two channels. Ideally, if there is only one direct path signal received, the deramped beat frequency generated from the receive signal can be determined by the frequency value

correspond to the peak in spectrum. However, if multipath propagation occurs, there will be multi-tones generated in deramping. Mistaking a multipath component as the direct path component introduces error to the TDOA estimation and thus the final location results.

The example of Figure 5-21 has shown that the presence of a multipath tone in the deramped spectrum is likely to distort the deramped response of the LOS path signal by shifting the peak position. Before introducing the techniques used to mitigate multipath impact in the TINA system, we are going to continue using the multipath model given in the Eq. (5.13).

At a typical receive channel, the received signal $r(t)$ includes the chirp signal that are transmitted by a tag to the receive AU through the LOS path, and a number of chirp echo that are received through reflections, as modelled by the Eq. (5.13). Since any of the received chirp replica $\sum_{m=0}^{L-1} v(t-\tau_m)$ has the same frequency modulation characteristic as the transmit LFM chirp signal $v(t)$, deramping the received signal $r(t)$ with LO chirp reference $v(t-\tau_{LO})$ (Chapter 3) will produce $L$ beat frequencies and thus $L$ components can be seen in the spectrum, among them only one component is generated from the direct path transmission and contains the delay information that is required. The deramped results from Eq. (5.13) can be expressed by Eq. (5.15).

$$d(t) = \frac{1}{2}\sum_{m=0}^{L-1} A_m \cos[2\pi f_m t + \theta_m] + \sigma_n(t) \tag{5.15}$$

$\sigma_n(t)$ is the noise term; $\theta_m$ is a phase term dependent on transmission delay $\tau_m$; and $f_m$ is the deramped beat frequency for each of the $m$ received chirp replica and is directly proportional to the transmission delay by the factor of chirp sweeping rate $k$, as shown in Eq. (5.16).

$$f_m = k(\tau_m - \tau_{LO}) \tag{5.16}$$

Since multipath propagation may involve single or multiple reflections, the transmission path length of any multipath signal will always be longer than the LOS path, and thus will induce longer delay than the delay corresponding to the LOS path. Note the transmission delay of LOS path as $\tau_0$ and the resultant beat frequency as $f_0$, we have

$$\begin{aligned} &\tau_0 < \tau_1, \tau_2, \cdots \tau_{L-1} \\ \therefore\ &f_0 < f_1, f_2, \cdots f_{L-1} \end{aligned} \tag{5.17}$$

This simple fact inspires the first frequency detection strategy; which is, from all the beat frequency components, only the earliest tone (of the lowest frequency) is chosen and regarded as the beat frequency generated by the LOS path. This strategy significantly reduces the chance of mistaking the result of an NLOS path as that of the LOS path. In case the LOS path exists, this detection strategy will directly output the desired beat frequency $f_0$, which is needed by the TDOA measurement of the two receive channels. With the LOS path induced beat frequencies at both receive channels, the time differences required for determining the tag location can be obtained by Eq. (3.14).

Let us now consider an example of the frequency detection process using real measurement results. Figure 5-22 is a snapshot of the LabView produced FFT results, taken in a measurement with the three-AU TINA demonstrator deployed in a laboratory. The three diagrams show the spectra of the deramped signals from the three AU channels. Each of them contains both LOS component and multipath components. It shows three different kinds of deramped results affected by multipath propagation in three different ways.

The three AU channels are named as Channel 1, Channel 2, and Channel 3 in the diagram. The task of this frequency detection step is to find the deramped beat frequency corresponding to the LOS path at the three channels, noted as $f_{1,0}$, $f_{2,0}$, and $f_{3,0}$ respectively. So that the inter-channels TDOA information $\Delta\tau_{1,2}$, $\Delta\tau_{2,3}$, and $\Delta\tau_{1,3}$ can be found from the differences between the LOS beat frequencies, $f_{2,0} - f_{1,0}$, $f_{3,0} - f_{2,0}$, and $f_{3,0} - f_{1,0}$, multiplied with the chirp frequency modulation rate *k*. The multipath components at the three channels are also noted by the channel number followed by the multipath number, such as $f_{1,1}$, $f_{1,2}$, $\cdots f_{1,L-1}$ for Channel 1, $f_{2,1}$, $f_{2,2}$, $\cdots f_{2,L-1}$ for Channel 2, and $f_{3,1}$, $f_{3,2}$, $\cdots f_{3,L-1}$ for Channel 3.

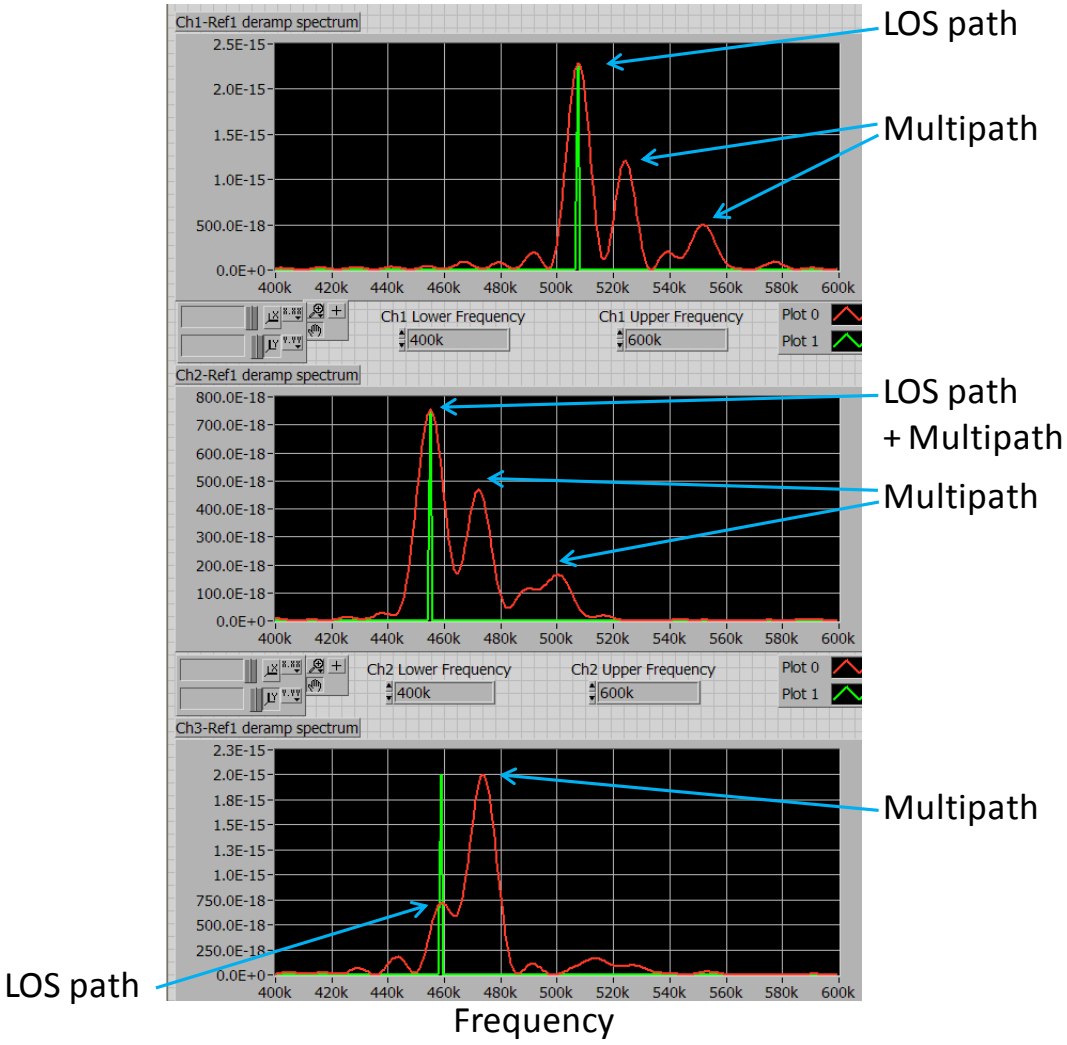


**Figure 5-22 LabView graphic interface showing the FFT spectra of the deramped signals**

For the upper diagram (Channel 1), there are three clearly separated frequency components, indicating the LOS path and two multipath signals. The differences between their deramped frequency, $f_{1,1} - f_{1,0}$, and $f_{1,2} - f_{1,1}$, are greater than the frequency resolution, 12.5 kHz; which means the difference between their path lengths are greater than the systematic range resolution $\boldsymbol{R}$. Since deramped frequency is directly proportional to the length of path, the earliest tone (at the lowest frequency) among the three tones, must be caused by a chirp radiation through the least path length. Thus it is more likely to be resulted from the direct path signal, or at least its propagation path is the closest to the direct path length. With adequate *SNR* level, the earliest tone is selected and the beat frequency value (about 510 kHz in Figure 5-22) corresponding to this component is chosen.

The middle diagram (Channel 2) of Figure 5-22 is a similar but different example compared to the Channel 1 case. The earliest deramped tone in the Channel 2 appears at about 455 kHz in the spectrum, while there are at least two significant multipath tones at around 470 kHz and 500 kHz. However, the -3 dB width of the earliest tone in the spectrum of Channel 2 is slightly larger than the one seen in the spectrum of Channel 1, which implies that it is very likely this component is a combination of the LOS path, at $f_{2,0}$, and a very close multipath component, at $f_{2,1}$, where $f_{2,1} - f_{2,0} < 12.5\ kHz$. Since the difference between the frequencies of these two tones is so small, they can hardly be distinguished from each other in the spectrum. Let the beat frequency of this combined component as $f'_{2,0}$. If the earliest tone detection strategy is applied, the output beat frequency of this step will be $f'_{2,0}$. Although $f'_{2,0}$ is not the beat frequency resulted from the LOS path, the error it induces, $f'_{2,0} - f_{2,0}$, is still the smallest compared to those resulted from the other maxima $f_{2,2}$ and $f_{2,3}$ in the spectrum. Therefore, in other words, the earliest tone detection strategy produces the closest result in this case.

Usually the LOS signal is stronger than the received multipath signals. Therefore, the simple earliest tone detection strategy is to select the LOS component out from the received signal. However, the assumption, that the LOS signal is larger than multipath signal, is not always true and therefore an alteration to the detection strategy is needed when dealing with cases like the Channel 3 in the Figure 5-22. This is a special case where the power of the earliest tone is smaller than a later tone. This will happen if there is obstacle in the way of the LOS path, blocking or attenuating the LOS signal. In this situation, the beat frequency of the earliest tone is not the accurate LOS beat frequency but again is the closest. Another possibility is that there is more than one multipath signal combined to produce the same beat frequency. These multipaths are of very similar length, and the received signals thus are nearly in-phase with each other. It means that their deramped signals are enforcing each other and producing a tone that is stronger than the one produced by a single multipath signal, or by even the LOS signal.

Since LOS signal can be smaller than the multipath tone, it is necessary to set a threshold for the minimum peak power of a tone to be regarded as a deramp component. In the TINA indoor system, this threshold has been set to be 30% of the

global peak power in the deramped spectrum, which is the case shown in the lower diagram of Figure 5-22. This percentage is an empirical value that has been tested in a few indoor areas and demonstrated to be producing stable results. By this means, the earliest peak at the 460 kHz will be chosen as the frequency detection result in the case of the Channel 3 in Figure 5-22.

After analyzing these examples from real measurements, the earliest tone detection strategy can be summarised as below.

Firstly, the frequency component with the peak power is found from the deramped spectrum. Secondly, according to this peak power, set a threshold for the earlier peak search. A good practice is setting this threshold to be 30% of the global peak power. The algorithm then searches for the lowest frequency component whose power level is higher than the threshold.

The reason why this technique can help lessen multipath effects is that although each received tag signal still contains both the LOS and NLOS components, mixing or de-ramping between the reference chirp $v(t-\tau_{LO})$ and the LOS signal $v(t-\tau_0)$ always produces a signal peak at a lower frequency than those between the reference chirp $v(t-\tau_{LO})$ and other indirect components $\sum_{m=1}^{L-1} v(t-\tau_m)$. This is because the LOS path between the tag and an AU is always the shortest possible and thus the deramp signal frequency is also the lowest. As a result, the frequency differences required for determining the tag location can be obtained from the lowest deramped signal frequency, thus significantly alleviating the effects of multipath.

## 5.6.2 Half-peak Detection

The earliest tone detection strategy has been shown to be capable of rejecting the multipath tones whose transmission paths are considerably longer than the LOS path. However, it is difficult for this simple strategy to distinguish the LOS component from nearby multipath components. For example, the middle diagram of Figure 5-22 shows such a situation where the length difference between a multipath and the LOS path is less than the range resolution. Detecting the LOS path in such cases is the topic of this section.

Many researchers have investigated the advantage of employing chirp signal in indoor wireless communications because of its robustness to multipath interference[91]. It had been widely discussed that multipath replica of the transmitted chirp signal can be identified and thus ignored in the receiver; either by correlation technique in time domain, or by deramp processing. Typically this advantage was achieved because multipath replica would yield a pulse response (correlation process) or beat frequency (deramp process) that is different from the result of the LOS path signal. The performance of this technique itself depends on the bandwidth of the chirp signal which sets the limit on the minimum range difference that can be resolved between a multipath and the corresponding LOS path component. If the path length difference between a multipath and the corresponding LOS path is shorter than the systematic range resolution, the multipath component cannot be clearly differentiated as it will fall into the same frequency bin of the LOS component. Existing literatures have also derived supper-resolution methods to resolve direct path component from the received signal [92-95]. These algorithms can resolve multiple received signals contained in the spectrum but the processing involved is rather computationally intensive and thus not suitable for real-time system. Alternatively, it will be shown in this section that by applying another uncomplicated detection strategy, the TDOA information can be determined with better accuracy even when close multipath components appear, and thus the problem is greatly relieved.

#### 5.6.2.1 Detection Error by Peak Search

Firstly, let us consider a simulated example comparing two different types of multipath interferences and their impacts on the frequency detection. This example will show that why the ordinary frequency detection strategy by signal peak will result in significant errors in a multipath environment. It will also be shown that the close multipath component interferes the TDOA and RDOA measurement much more than the multipaths that are out of the frequency bin of the LOS component.

Since we will be discussing the propagation path difference between LOS path and multipath in the following analysis, the frequency axis in the spectrum will be shown in its equivalent range axis. They are related in the way that, as indicated in Eq. (5.14), the RDOA is linearly proportional to the deramp frequency difference $\Delta f_d$.

Therefore, showing the spectrum in range axis can directly reflect the difference in propagation distance between a LOS path and a corresponding multipath.

The concept of range resolution has been introduced in Chapter 3 and it can be calculated using Eq. (3.17) for a TDOA ranging system, which is the range detection technique employed in this research. According to the TINA system specifications, the range resolution (equivalent to the 12.5 kHz frequency resolution) is 3.6 metres. In other words, this is the minimum propagation range difference required to successfully distinguish two paths from a range spectrum.

A simulation example is presented in Figure 5-23. Figure 5-23 (a) is a 2-D plane view of an indoor area, with a receive AU placed at the bottom right corner, and a user tag located around the top left corner of the indoor area. There are three transmission paths from the user tag to the receive AU, noted as LOS path, NLOS path 1, and NLOS path 2. Signal transmission through these paths results in three replicas of the transmitted chirp signal at the AU. Therefore, there are also three components that can be seen from the range profile in Figure 5-23 (b), drawn in red, black, and green for the LOS path, NLOS path 1, and NLOS path 2 respectively. But the resultant deramp response from the received signal is a combination of all of the three components, which is shown by the blue curve in the Figure 5-23 (b). The LOS component has been intentionally located at 10 m in the range spectrum for display convenience. The range axis is showing the relative range to the local chirp reference in the receiver, instead of real distance from the user tag to the receiver (as can be seen in Figure 5-20 and Figure 5-21).

From the range spectrum shown in Figure 5-23 (b), it can be seen that the NLOS path 2 is not affecting the LOS path at all in terms of peak detection, as its path length is 13 m longer than the LOS path, beyond the 3.6 m minimum requirement by the system specification. Severe multipath interference comes from the NLOS path 1, whose path length is exactly 3.6 m longer than the LOS path. Since the deramp component of NLOS path 1 falls within the range bin of the LOS component, they jointly produce one large sinc component, shown by the blue curve between the red and the black ones in Figure 5-23 (b). The impact of multipath in this case is that the peak of the LOS component (red) is shifted by the NLOS component (black).

If the peak detection strategy is applied in this case, the peak of the combined component (blue) will be chosen and the corresponding relative range detected from it will be 11.75 m. Therefore, the measurement error in range detection is 1.75 m, indicated by the Figure 5-24 (a). This error obviously will limit the eventual location estimation accuracy of the system.

However, we may find another fact from Figure 5-23 (b) that, although the peak of the LOS component has been shifted due to the existence of multipath, earlier (lower frequency) null point and half-peak point of the LOS component are not distorted as much as the peak point does. Clearly, the first left null points of the combined (in blue) and the LOS (in red) component nearly overlap, while the half-peak point is shifted to a small extent. This is because of the rolling-off sinc characteristics: the power of the NLOS path 1 becomes much smaller at the half-peak and the null point to the left of LOS peak.

This observation inspires the second frequency detection strategy, which is determining the deramp frequencies between a pair of receive channels by their lower-frequency half-peak points, instead of their peaks, in order to avoid the error caused by the ordinary peak detection. It shall be noted that, the first lower-frequency null point is not chosen as the reference point because it can be easily distorted by noise. On the other hand half-peak point technique is not as much affected by noise provided adequate *SNR* is achieved.

The performance of this detection strategy can be witnessed in a simulated example shown in Figure 5-24. As can be seen, the error from peak detection is 1.75 m for the simulated example. However, if the proposed half-peak detection strategy is applied, the detection error will be reduced by 60% to 0.7 m, which leads to a significant improvement in the location estimation.

This detection strategy will work for TDOA ranging system using LFM chirp deramping. In such system, it is the frequency difference between two channels that matters, rather than the exact frequency at either channel. Therefore, even if the algorithm is not detecting the exact deramp frequency at either channel, the relative frequency difference can still be found by applying the same half-peak detection strategy on both channels.

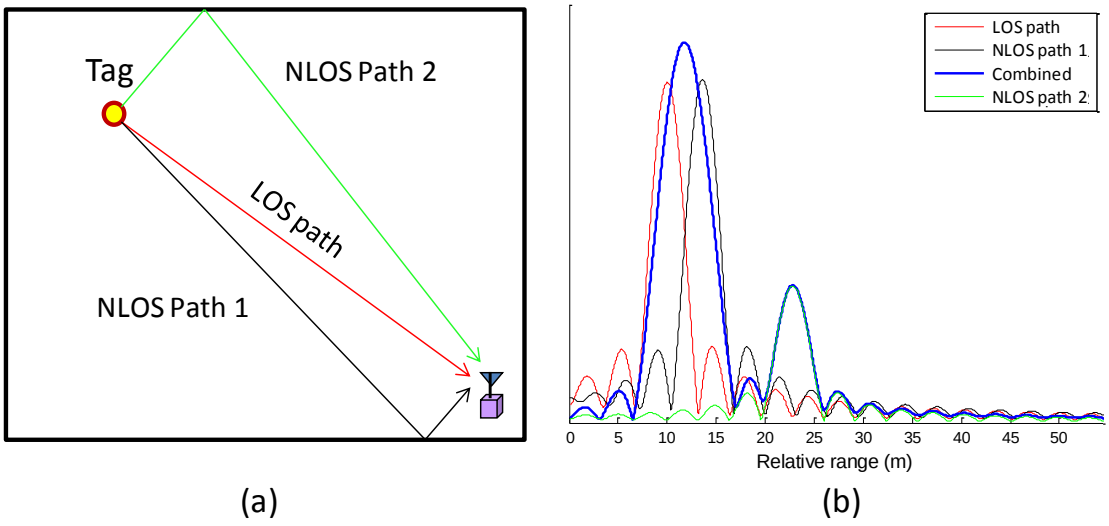


**Figure 5-23 Example of the multipath impact on the deramp processing result, (a) a LOS path and a LOS path, (b) the respective deramp output in form of range spectrum with the relative range axis**

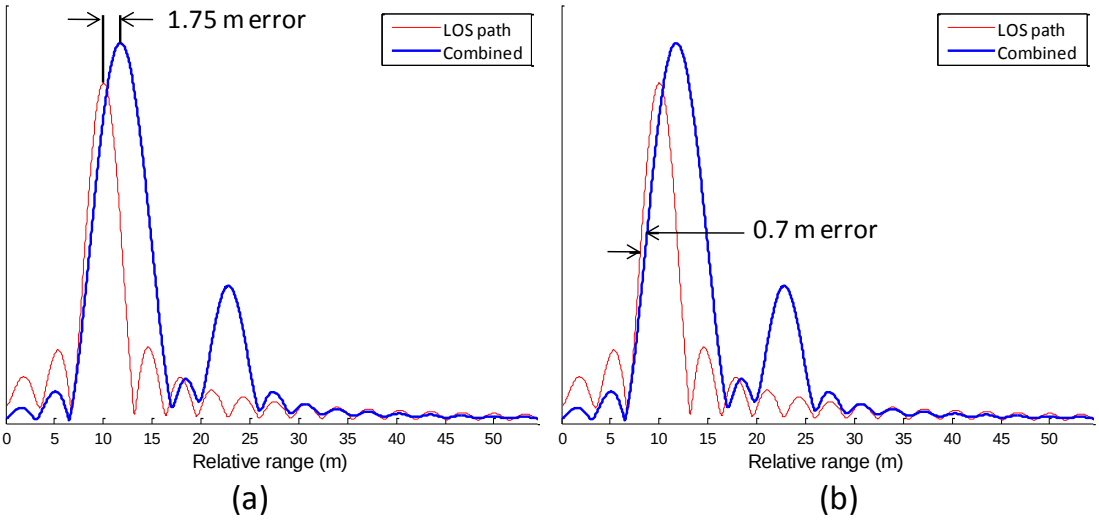


**Figure 5-24 Comparing errors by (a) peak detection and (b) half-peak detection**

The performance of this strategy relies on a few conditions. Firstly, the number of zero-padding used in the FFT process must be kept identical for both receive channels under TDOA measurement. Secondly, the window function, if applicable, applied onto the chirp signal must be identical for both receive channels. Thirdly, duration of the LFM chirp must be the same as well for both channels. These conditions are usually the case in a real system, as the received chirp signals at different channels must originate from a single user tag, which will not be sending two different signals

at the same time. Also, the receiver structures and signal processing are usually the same for different channels as well.

### 5.6.2.2 Monte-Carlo Simulation for detection strategies comparison

To evaluate the performance of the proposed half-peak detection strategy, a Monte-Carlo simulation has been set up to simulate the situations that multipath components fall near the range bin of the LOS path. An LOS path is intentionally set up to appear at the 10 m range, and one or a few multipath components are added to the LOS signal too. There are two variables of the multipath signal that are changed in the experiments. The first one is the additive range of the multipath, with respect to the direct path. It represents the physical propagation path difference between a multipath and the LOS path, Figure 5-23 (a). The other variable is the power of the multipath, which can be smaller or larger than the power of the LOS path, Figure 5-25. In the simulation, they are generated using uniform distribution covering the range of interest in this research.

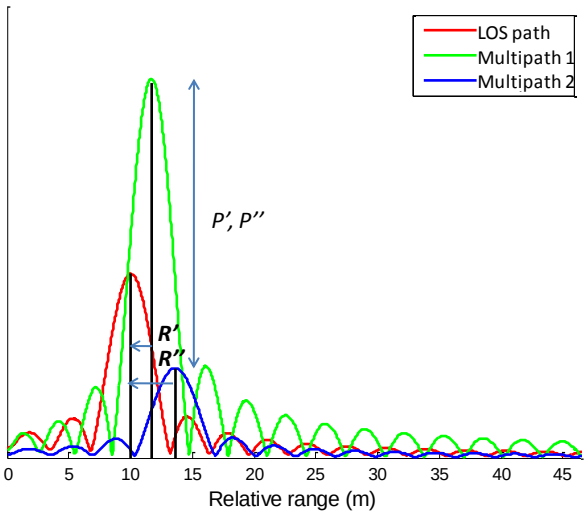


**Figure 5-25 Variables range setting in the Monte-Carlo simulation**

Since we are only interested in the multipath that are close to the LOS path, the additive range $R'$ is set to be within the [0, $R_{res}$] region, which is [0, 3.6] metre for TINA indoor location system according to the specifications. Also, multipath of very small power are not in the interest of this part neither, as the impact of multipath with small power is limited and will not interfere the range detection very much. The power of the simulated multipath $P'$ is set to have a lower bound at half of the LOS power $P_D$, while the upper bound is varying according to the purpose of the cases.

The earliest tone detection strategy introduced in Section 5.6.1 is also employed in the simulation, for consistency with the actual system. Both detection techniques, by the peak point and the half-peak point of the earliest tone, are used in the simulation and their measurement errors are recorded for comparison. In each of the following cases, the simulation has been run for ten thousand times with the two random variables, additive range $R'$ and multipath power $P'$, regenerated in every simulation experiment.

The purpose of this Monte-Carlo analysis is to compare the range detection performance between the conventional peak detection strategy, and the proposed half-peak detection strategy. Statistical results are calculated to find how likely that an improvement in range detection is achieved by applying the half-peak detection strategy, as well as how much improvement is likely to be achieved.

There are in total eight cases simulated for different multipath interferences. They can be categorized into two groups. In the first four cases, the propagation distance of the multipath signals have been set to be very close to the LOS path, where additive range is from 0 to 1 metre. The second group is the last four cases, where the additive range has been set to be uniformly distributed from 1 metre to 3.6 metre. This group is simulating the worst multipath impacts that the range detection error may go up to a few metres.

Parameter settings for the first four cases of the Monte-Carlo simulation are listed in the Table 5-5. Case 1 and 3 are simulating the situation that there is only one multipath appearing in the range bin of the LOS path. Their difference is that the power of multipath tone in Case 3 is ranging from half of the LOS power to twice the LOS power, larger than in Case 1, Table 5-5. Case 3 is in fact simulating the situation shown by Channel 3 of Figure 5-22. On the other hand, Case 2 and 4 are simulating severer multipath distortion where there are three multipaths in the range bin of the LOS path. The additive range and power of the three multipaths are generated randomly and independently every time the experiment is run. Similar situations are simulated by the second group, Case 5 to Case 8, whose detailed settings are shown in Table 5-6.

Statistical results from the eight cases are summarised by seven parameters listed in Table 5-7 and Table 5-8. The meanings of these parameters are also given in Table 5-4.

| Parameter | Symbol | Meaning |
|---|---|---|
| Probability of improvement | $P_{Im}$ | The percentages of cases that range detection errors induced by half-peak detection are smaller than the errors induced by peak-detection. |
| Max. improvement | $G_M$ | The largest error reduction in relative range detection due to applying half-peak detection strategy. |
| Average improvement | $G_A$ | The average error reduction in relative range detection due to applying half-peak detection strategy, calculated from the $P_{Im}$ cases. |
| Average degradation | $G_D$ | The average error increment in relative range detection due to applying half-peak detection strategy, calculated from the $1 - P_{Im}$ cases. |
| Improvement expectation | $G_E$ | Equal to $G_A \cdot P_{Im} + G_D \cdot (1 - P_{Im})$, the mathematical expectation of the overall improvement of applying half-peak detection strategy. It shall also be equal to $\Delta R_P - \Delta R_H$. |
| Error from peak detection | $\Delta R_P$ | Range detection error in case peak detection strategy applies. |
| Error from half-peak detection | $\Delta R_H$ | Range detection error in case that half-peak detection strategy applies. |

**Table 5-4 Meanings of the statistic results**

| | DLOS path | Number of multipath | Additive range with respect to DLOS path | Normalized power to $P_D$ |
|---|---|---|---|---|
| Case 1 | 10 m | 1 | $R' \in [0, 1]\ m$ | $P' \in [0.5, 2]$ |
| Case 2 | 10 m | 3 | $R', R'', R''' \in [0, 1]\ m$ | $P', P'', P''' \in [0.5, 2]$ |
| Case 3 | 10 m | 1 | $R' \in [0, 1]\ m$ | $P' \in [2, 4]$ |
| Case 4 | 10 m | 3 | $R', R'', R''' \in [0, 1]\ m$ | $P', P'', P''' \in [2, 4]$ |

**Table 5-5 Multipath simulation settings for Case 1 to Case 4**

| | DLOS path | Number of multipath | Additive range with respect to DLOS path | Normalized power to $P_D$ |
|---|---|---|---|---|
| Case 5 | 10 m | 1 | $R' \in [1, 3.6]\ m$ | $P' \in [0.5, 2]$ |
| Case 6 | 10 m | 3 | $R', R'', R''' \in [1, 3.6]\ m$ | $P', P'', P''' \in [0.5, 2]$ |
| Case 7 | 10 m | 1 | $R' \in [1, 3.6]\ m$ | $P' \in [2, 4]$ |
| Case 8 | 10 m | 3 | $R', R'', R''' \in [1, 3.6]\ m$ | $P', P'', P''' \in [2, 4]$ |

**Table 5-6 Multipath simulation settings for Case 5 to Case 8**

| | Probability of improvement $P_{Im}$ | Max. improvement $G_M$ | Average improvement $G_A$ | Average degradation $G_D$ | Improvement expectation $G_E$ | Error from peak detection $\Delta R_P$ Mean | Std. | Error from half-peak detection $\Delta R_H$ Mean | Std. |
|---|---|---|---|---|---|---|---|---|---|
| Case 1 | 45.20% | 1.26 m | 0.12 m | 0.06 m | 0.02 m | 0.41 m | 0.48m | 0.39 m | 0.42 m |
| Case 2 | 48.30% | 0.90 m | 0.08 m | 0.06 m | 0.01 m | 0.49 m | 0.40 m | 0.48 m | 0.39 m |
| Case 3 | 38.20% | 0.27 m | 0.04 m | 0.06 m | -0.02 m | 0.49 m | 0.41 m | 0.51 m | 0.42 m |
| Case 4 | 44.10% | 1.61 m | 0.08 m | 0.05 m | 0.00 m | 0.52 m | 0.35 m | 0.52 m | 0.34 m |

**Table 5-7 Statistics records from multipath simulation Case 1 to Case 4**

| | Probability of improvement $P_{Im}$ | Max. improvement $G_M$ | Average improvement $G_A$ | Average degradation $G_D$ | Improvement expectation $G_E$ | Error from peak detection $\Delta R_P$ Mean | Std. | Error from half-peak detection $\Delta R_H$ Mean | Std. |
|---|---|---|---|---|---|---|---|---|---|
| Case 5 | 91.66 % | 2.85 m | 0.37 m | 0.09 m | 0.34 m | 1.00 m | 0.64 m | 0.66 m | 0.43 m |
| Case 6 | 79.10 % | 2.77 m | 0.28 m | 0.10 m | 0.21 m | 1.45 m | 0.88 m | 1.24 m | 0.87 m |
| Case 7 | 92.67 % | 2.08 m | 0.29 m | 0.08 m | 0.26 m | 1.54 m | 0.72 m | 1.28 m | 0.64 m |
| Case 8 | 70.06 % | 2.59 m | 0.23 m | 0.08 m | 0.13 m | 1.80 m | 0.90 m | 1.67 m | 0.92 m |

**Table 5-8 Statistic results from multipath simulation Case 5 to Case 8**

The results above show that the proposed half-peak detection strategy provides apparent improvement in the second group of simulation while its performance is similar to the peak detection strategy in the first group of simulation.

For those situations assumed in the first group, the proposed strategy induces similar range detection error as compared to peak detection strategy. The probability of achieving improvement is less than 50% in any case of the first group while the improvement expectation is insignificant. However, these results do not necessarily mean that the half-peak detection strategy fails. This is actually due to the fact that the multipaths in these cases are so close to the LOS path that their deramped responses nearly overlap with each other. There is not much difference between the two detection strategies under comparison as they are similarly good. It can be seen that, the multipath impacts on Case 1 to 4 are relatively small, and thus the mean range detection errors from either strategy are limited to below 0.5 m level, which is evidenced by the $\Delta R_P$ and $\Delta R_H$ results in Table 5-7, and an example shown in Figure 5-26 (a). This range detection error level is fairly acceptable to the 1 m requirement defined by TINA specifications.

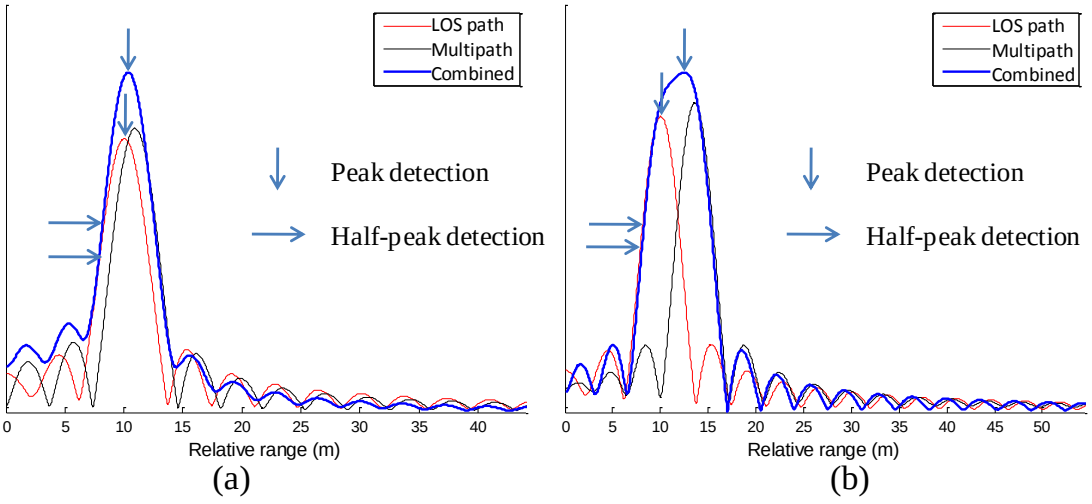


**Figure 5-26 Examples of (a) Multipath tone falls into the [0, 1] m region; (b) Multipath tone falls into the [1, 3.6] m region**

More importantly, the half-peak detection strategy does perform superiorly to the peak detection strategy in case that the multipath tones are of additive range between 1 m and 3.6 m, which is also the worst case of multipath impacts that could occur in the deramped processing.

It is shown that, when there is only one multipath signal (Case 5 and Case 7), the probability of achieving improvement in range detection is high, over 90%. Taking Case 5 as an example, the average improvement $G_A$ from the 91.66% of the 10,000 cases is 0.37 m. Half-peak detection strategy induces larger range detection error than the peak detection strategy in the other 8.34% of the experiments. But the degradation figure $G_D = 0.09$ m is a few times smaller than the $G_A = 0.37$ m. That is to say, general performance improvement is achieved from the proposed half-peak detection strategy, for a reasonable price of small amount of range error increment for a low probability.

On average, the half-peak detection strategy is likely to achieve about 30 cm range error reduction, with $G_E = 0.34$ m in Case 5 and $G_E = 0.26$ m in Case 7. Therefore, the 1.00 m mean range error $\Delta R_P$ from Case 5 can be reduced to 0.68 m if half-peak detection strategy is employed. Similar error reduction is seen in Case 7 where the mean range error is reduced to 1.28 m from 1.54 m.

The result of Case 5 is better than that of Case 7, because the multipath power for Case 5 is set to be smaller than that of Case 7. The maximum range error reduction obtained from Case 5 is 2.83 m, also higher than the 2.03 m figure obtained from Case 7. This maximum range error reduction is achieved in case when the additive range of multipath is comparable to the system range resolution $R_{res}$. An example of such a situation is illustrated in Figure 5-26 (b), where the error due to peak detection is obviously much larger than the error due to half-peak detection.

Besides the power of multipath signals, the number of multipaths added to the received signal can also affect the range detection performance. As defined in Table 5-6, Case 6 and Case 8 are reproducing multipath signal with much greater power than the LOS path signal. Firstly, the probabilities of achieving improvement in these cases decrease to 79.10% for Case 6 and 70.06% for case 8 (Table 5-8), although this figure is over 90% for Case 5 and Case 7. While improvement is still achievable in over two thirds of the experiments simulated, the mathematical expectation of the range error reduction is lessen, becoming 0.21 m for Case 6 and 0.13 m only for Case 8. This is for the cases when a number of high power multipaths appear in the received signals. The half-peak detection strategy in these cases reduces the detected range error for Case 6 and Case 8 by 15% and 7%, respectively. In the worst case,

Case 8, the mean range error from half-peak detection is 1.68 m, equivalent to 5.6 ns error in TDOA measurement.

Summarily, from the simulations presented above we found that the proposed half-peak detection strategy is superior to the ordinary peak detection strategy, regarding the range errors and equivalent time measurement errors resulted from these strategies. If the half-peak detection strategy is employed in the frequency detection step after deramp process (Figure 5-21), the resultant range errors are likely to be reduced.

A limitation to the simulation given above is that there is a lack of information about the exact distribution of additive range and multipath power in the real indoor environment. Actually, their exact distribution must vary from places to places. Therefore, we assumed uniform distribution in the simulation in order to obtain a general conclusion from the analysis. Conclusion of this analysis was also evidenced from a few on-site experiments, where a variety of multipath types were observed. Some real measurement data are going to be shown in the following subsection as a support to the analysis presented.

## 5.6.3 Multipath Impacts on Frequency Detection

In this part we will go through three different examples of multipath impacts observed from real measurements. These examples cover the typical types of multipath impacts and thus are shown here as a support to the simulation of multipath above. The on-site trial results are shown together with their respective reproduction copy, which have been modeled from a Matlab program simulating the LFM chirp propagation and deramping. By this means we are able to reproduce the received signals that cause these effects.

### 5.6.3.1 Wider Width Component

The first example shows the deramped spectrum of a receive AU channel, which has experienced severe multipath interference, Figure 5-27 (a). There are at least four replicas of chirp signals received by the AU and thus four apparent deramped components can be seen from the spectrum. The width of the component at around

500 kHz is wider than the other components, possibly due to a multipath close to the LOS path. Simulation model has reproduced a similar deramped spectrum from a LOS path followed by four multipaths, while the closest multipath falls at only 8 kHz higher frequency than the LOS path, Figure 5-27 (b). The reproduction result demonstrates that the most common type of multipath effect, which is enforcing the LOS component to produce a component with widening width.

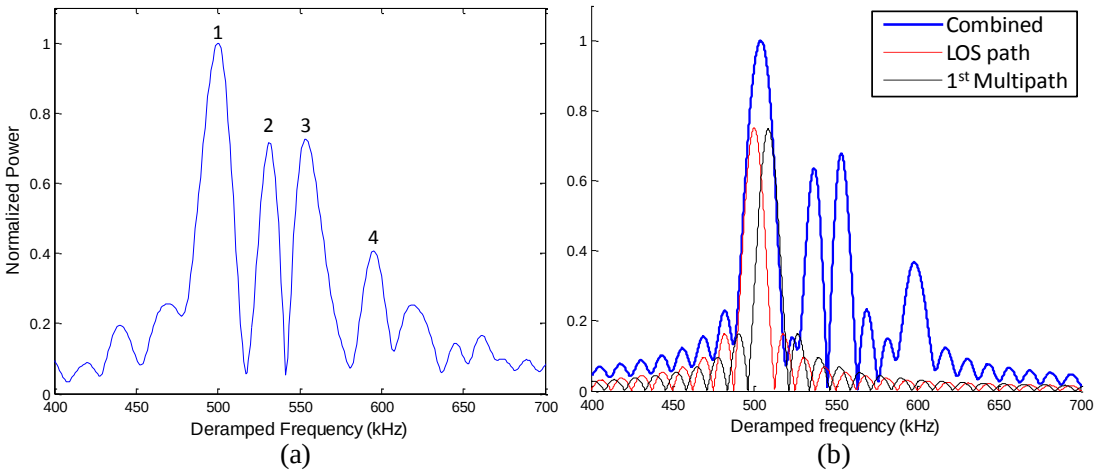


**Figure 5-27 Example of widening width caused by multipath effect. (a) The deramped spectrum from experimental data; (b) the reproduced spectrum from modeling, showing the possible multipath profile**

### 5.6.1.2 Flattened Peak

The second type of multipath impact is also frequently seen in experiments. Figure 5-28 (a) shows a flattened peak at about 460 kHz to 480 kHz, which is obviously a combination of at least two received chirp signals with offset delay between them. Rather than enforcing the LOS path, the multipath signal in this case may be of a special phase difference against the LOS path such that they are not added coherently to produce an enlarged single tone. The reproduction spectrum has indicated a possible combination of LOS path and multipath, indicated by the red and black curves respectively, in Figure 5-28 (b). Another phenomenon that can be observed from this example is that there are many more multipath present this measurement and their power can be larger than the LOS path.

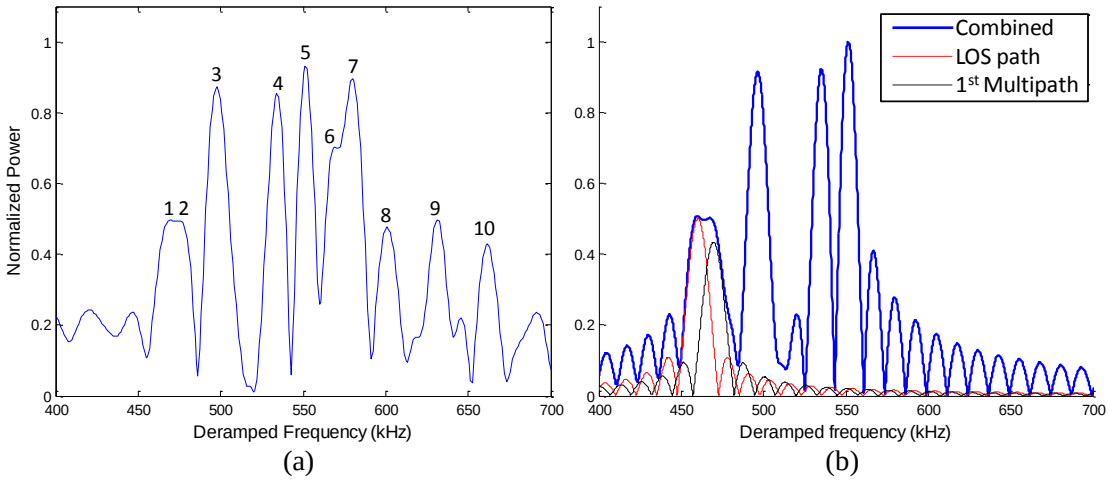


**Figure 5-28 Example of flatten peak caused by multipath effects. (a) The deramped spectrum from experimental data; (b) the reproduced spectrum from modeling, showing the possible multipath profile**

### 5.6.1.3 Double Peaks

The third example looks like two components joining each other at the lower half of them, making a wide frequency component with two peaks. There are also a few multipaths present in the spectrum of Figure 5-29 (a), with various frequency differences to the LOS path. Reproduction of the possible LOS path and multipath shown in Figure 5-29(b) has suggested that this effect may occur when the two paths are weakening each other. Original peaks of the two tones are shifted to their outer directions.

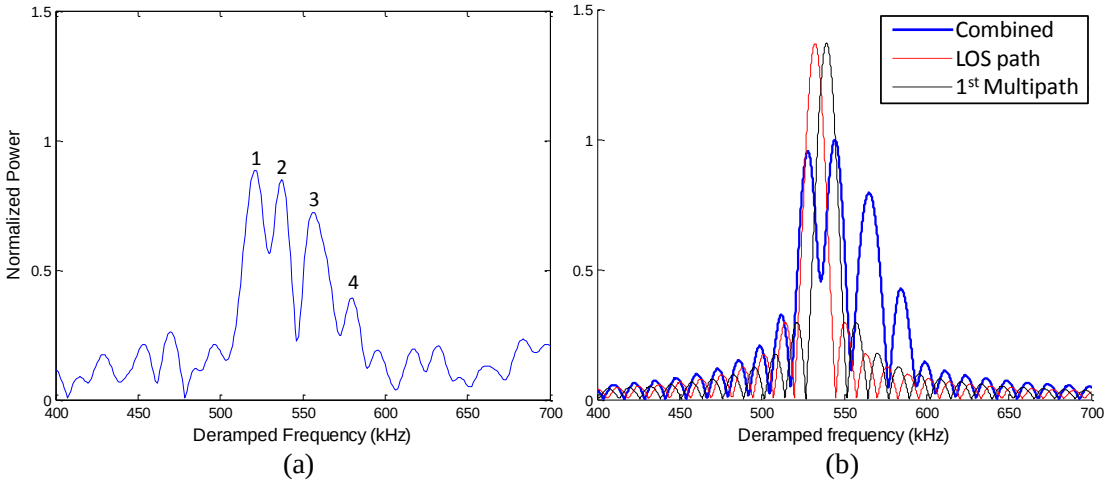


**Figure 5-29 Example of double peaks caused by multipath effects. (a) The deramped spectrum from experimental data; (b) the reproduced spectrum from modeling, showing the possible multipath profile**

From these three examples, we can see that the two observation made in the detection strategy analysis are sensible. They are, firstly, the earliest tone over threshold is closer to the LOS path, and secondly the lower-frequency rolling-off part of the LOS component is less influenced by the multipath close to it. If the two detection strategies are applied on the three examples, the frequency, and thus range detection accuracy is likely to be improved.

### 5.6.4 Location Performance in the Presence of Multipath

The performance of the proposed frequency detection strategies were also witnessed in real indoor location experiment. In this section, the estimated location results from conventional peak detection strategy are compared with the results derived from algorithm using the two proposed detection strategies. The data are recorded in an indoor location experiment using four sensors deployed in an indoor area, where the user tag is placed at the position (3.3 m, 7.8 m), in a 15.6 m-by-6.6 m room. Multipath propagation effects similar to the examples shown in the Section 5.6.3 were observed during the experiment.

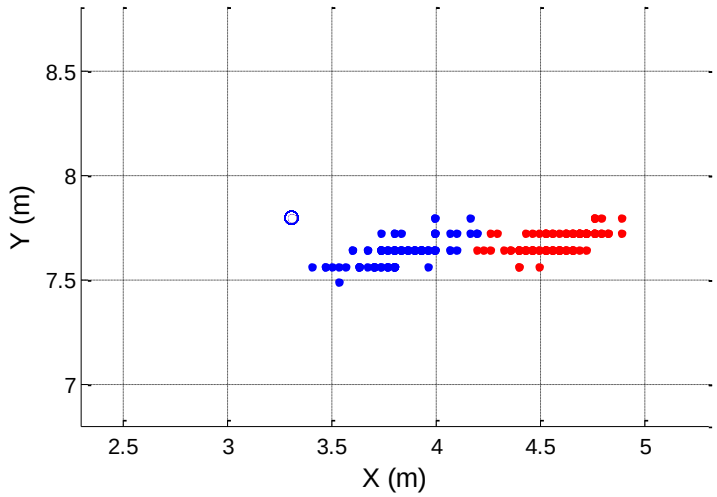


**Figure 5-30 Estimated locations using simple peak detection (red), and proposed strategies (blue)**

In Figure 5-30, the true location of the user tag is marked as the blue circle. The estimated locations from an algorithm using simple peak detection strategy are plotted as red dots while the corresponding results using the proposed earliest half-peak detection strategy are plotted as the blue dots. It can be seen from the Figure 5-30 that

the location accuracy is improved by using the proposed strategies, as the blue dots are nearly always closer to the true location, in comparison to the red dots. The statistic results shown in the Table 5-9 also agree with this judgment. Table 5-9 shows that the standard deviation of the detected TDOAs derived with the proposed strategy is only 0.68 ns, which is 0.74 ns smaller than the simple peak detection method, implying that the measured TDOAs are relatively less diverse. According to the analysis given in Chapter 4, smaller variation of measured TDOAs is likely to induce improved location accuracy, which is the direct cause of improved location accuracy in this example.

| | STD* of measured TDOA (ns) | RMS location error (m) |
|---|---|---|
| Simple peak detection | 1.42 | 1.26 |
| Earliest half-peak detection | 0.68 | 0.56 |

**Table 5-9 Comparison of the location accuracy for different frequency detection strategies**

* Standard deviation

The spreading patterns of the estimated locations for the two groups are similar in terms of their shapes and the extents of their spreading. This phenomenon implies that the TDOA measurement errors caused by noise or other unbiased error source would not be mitigated significantly by using the proposed strategies.

However, it can also be seen that both groups of locations are biased (Figure 5-30), with their mean locations diverse from the true location. The biased effect is mainly due to the impact of multipath. Since the multipath signal always arrive later than the direct signal, the multipath affected TDOA is a biased estimator, resulting in biased location results. The improved location accuracy observed from Figure 5-30 is clearly obtained by mitigating the multipath induced errors.

It has now been shown how the proposed earliest half-peak detection strategy could improve the TDOA measurement accuracy, through simulation analysis in Section 5.6.2, and the analysis of real deramped results in Section 5.6.3. The improvement in the location accuracy is also revealed in Section 5.6.4 by a comparison of the real location results, derived from the two different frequency detection strategies.

## 5.7 Summary

This chapter has introduced the design of TINA indoor location system from the overview to the individual functional block. The system architecture has been shown compact but flexible, and is suitable for lots of applications. The employment of RoF network facilitates the simple protocol between remote user tags and the central location estimator. Therefore, the hardware design can be implemented with fairly straightforward technologies. For example, the super-Nyquist scheme of the DDS-based chirp generator is a promising method for a compact active RFID tag. The location estimator design also has the potential to be built over a mixed signal hardware system, including RF receivers and digital signal processors.

Additionally, the ability of this system in combating multipath effects has been demonstrated. Besides its intrinsic robustness to multipath propagations, two detection strategies have been proposed through investigation of the multipath impacts on the specific TDOA deramping technology. These detection strategies have been verified by analysis, real measurement data and also supported by intuitive reasoning. The earliest tone detection strategy deals with selecting the LOS component from many received components, while the half-peak detection strategy is able to reduce the errors caused by closer multipath. These two strategies therefore increase the location estimation accuracy and retain higher stability.

# *Chapter 6*

## FIELD TRIAL RESULTS AND ANALYSIS

This chapter presents an overview of the field trials carried out to examine the location performance of the proposed indoor location system described in Chapter 5. Detailed settings of the measurement platform and installation of the indoor location system are depicted in the first section. Three different sensor placement schemes were implemented for locating multiple tags in the chosen indoor environment. Statistics of the estimated locations are summarised to show the overall performance of the proposed location system. By using the location estimation algorithm (Chapter 4) and the multipath mitigation techniques (Chapter 5) employed, RMS location accuracy of better than 1 m level was achieved during the three trials. Comprehensive analysis and discussion of the trial results are given in the Section 6.3 to 6.6.

## 6.1 Field Trials Venue and Location System Settings

The trials were conducted in a café on the ground floor of a modern building with glass windows and steel structure, as shown in Figure 6-1. The entire area of the café is 18 m in length and 8 m in width, and the floor is covered with 60 cm by 60 cm square tiles. A slightly smaller inner area of 15.6 m by 6.6 m, which corresponds to 26 tiles by 11 tiles, was marked out for the experiments within which the locations of the tag were to be determined. The AUs were fixed in position at the corners or along the perimeters of this cell; the indoor area wherein the target location tasks were executed. The bottom left corner of the cell shown in Figure 6-1 was assigned the coordinates (0 m, 0 m) defined as the origin, and all locations of the tag were determined and displayed relative to this point.

The rear of the room was used as the central site of the location system, in which the instruments from the RoF hub to the laptop (Figure 5-2) were gathered. The UT locations are estimated by the TDOA mapping algorithm, and the results were

displayed in the LabView interface, which was projected to the back wall of the room, Figure 6-2.

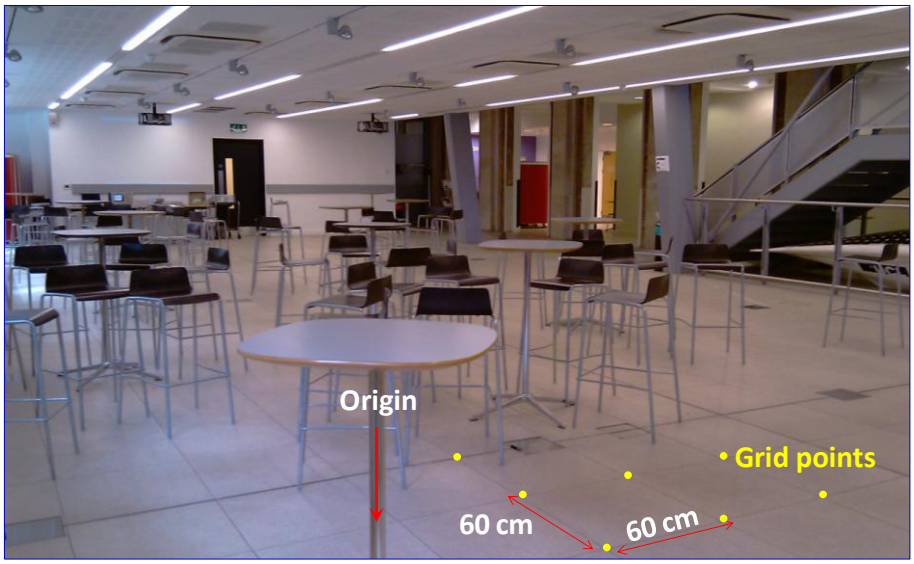


**Figure 6-1 Photo of the indoor environment used to examine the indoor location system**

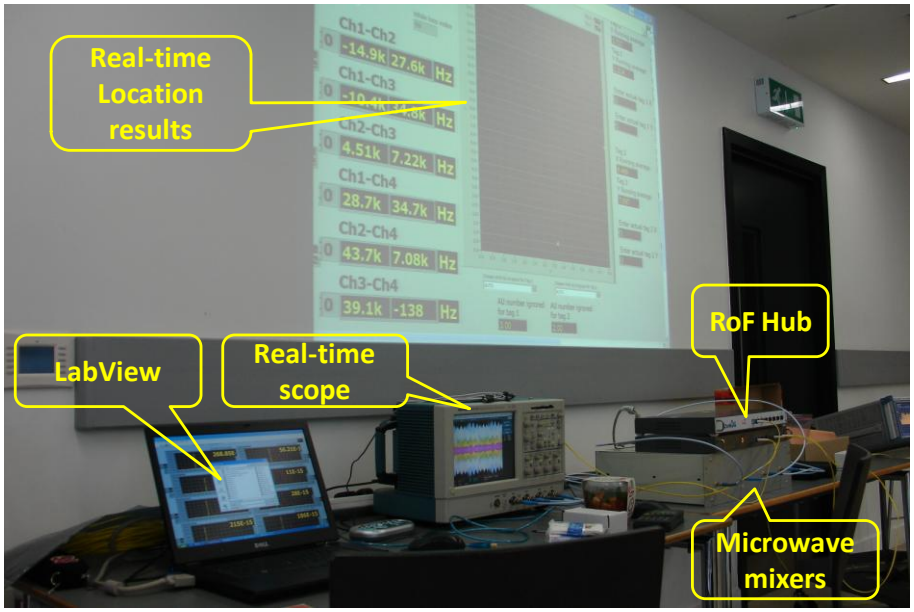


**Figure 6-2 Central site of the indoor location system**

As introduced in Section 5.5.2, the imbalanced delays and gains corresponding to the fibre channels need to be calibrated in a closed-loop experiment before placing the AUs. In the closed loop experiment (Figure 6-3), the UT generated chirp signal was directly fed into the inputs to the four AUs connecting to the RoF hub. The

imbalanced delays and gains between RoF channels were measured and recorded at the TDOA measurement step in the LabView program (Section 5.5.2).

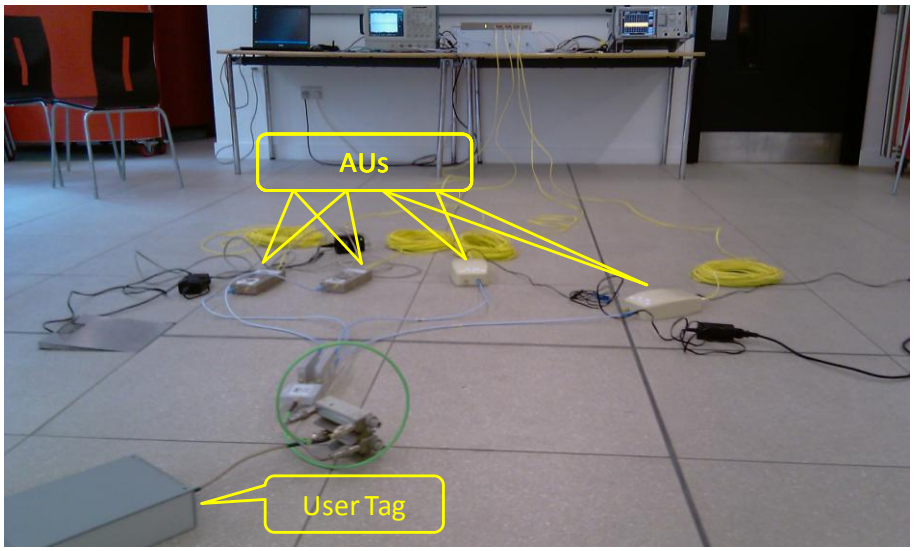


**Figure 6-3 Closed-loop experiment measuring RoF channel delays and gains**

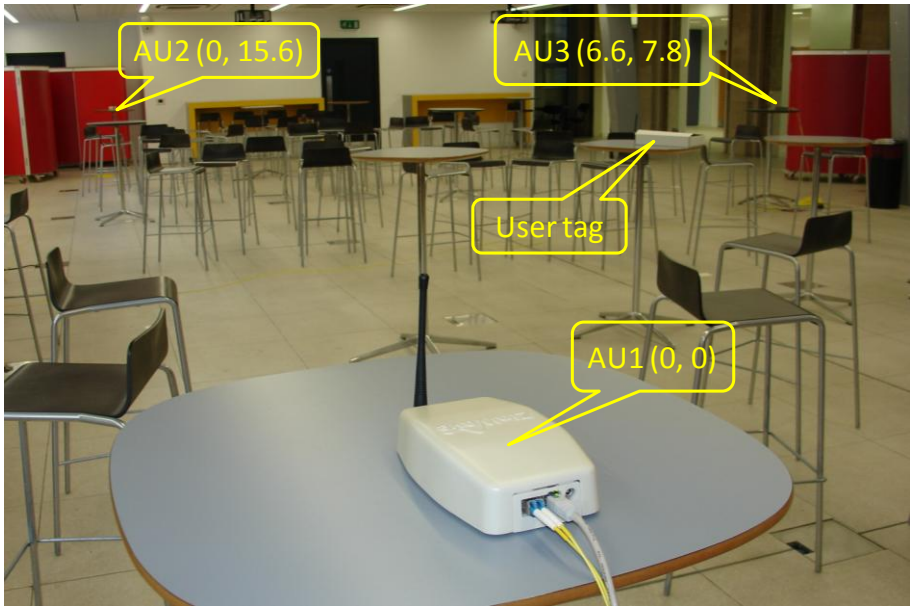


**Figure 6-4 AUs placement for three-sensor case**

After the calibration step, the AUs were set up at their positions according to the sensor placement schemes. The 40-metre fibres used in the trial are long enough to remotely deploy the AUs to any position in the 15.6 m by 6.6 m cell. During the trials, three sensor placement schemes were conducted, one is a three-sensor scheme and the others are four-sensor schemes. The arrangements for the AU coordinates are:

- Scheme 1, three sensors: AU1 (0 m, 0 m), AU2 (0 m, 15.6 m), and AU3 (6.6 m, 7.8 m).

- Scheme 2, four sensors placed along perimeters: AU1 (0 m, 7.8 m), AU2 (6.6 m, 7.8 m), AU3 (3.3 m, 15.6 m), and AU4 (3.3 m, 0 m).

- Scheme 3, four sensors placed at corners: AU1 (0 m, 0 m), AU2 (0 m, 15.6 m), AU3 (6.6 m, 15.6 m), and AU4 (6.6 m, 0 m).

Figure 6-4 shows the three-sensor placement scheme, where the three AUs were situated at positions (0 m, 0 m), (0 m, 15.6 m) and (6.6 m, 7.8 m), respectively, and were placed on tables at a height of 1.1 m.

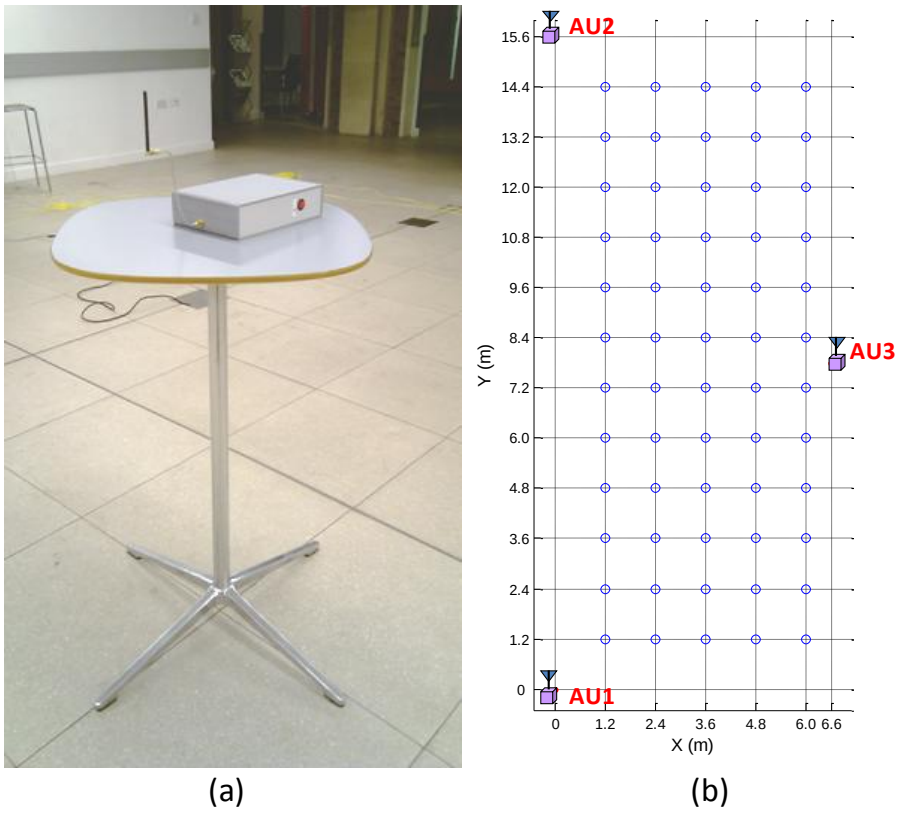


**Figure 6-5 (a) user tag placed on a table at one of the 60 test coordinates; (b) three-sensor placement example and the test points (blue circles)**

For every sensor placement scheme, a total of 60 different coordinates (marked by the blue circles in Figure 6-5(b)) within the grid of the cell were selected for location measurements. The separation between two adjacent test points is 1.2 m, equivalent to the length of two tiles on the floor. At each selected coordinate, the tag was placed on

a table at the same height as the ones on which the AUs (Figure 6-5(a)) are placed, and multiple measurements for the locations of the tag were computed by the location system. The location tasks, including deramped frequencies measurement and location estimation process, are presented through a LabView user interface as shown in Figure 6-6.

We have introduced the venue for the field trials at the beginning of this section, and explained the arrangements of the central site as well as the sensor placement schemes that were implemented in the trials. The user tags were placed at a number of known test points and corresponding location results were recorded for analysis using a statistical method. Choice of the test points has been given in Figure 6-5. The user tag and AUs were always placed at the intersection points between the tiles on the floor of the venue, in order to ensure that the coordinates of them were accurate, with relatively small displacement errors that are insignificant to the location performance measurements.


**Figure 6-6 LabView interface showing the inter-channel frequency differences, and estimated location results**

It should also be noted that a number of obstacles such as chairs and tables remained within the measurement cell in the venue during the trials, as can be seen from the Figure 6-1. There was also a WLAN access point operating in the same ISM band near the venue during the measurements. The data traffic to and from the WLAN access point was picked up by the TINA AUs and was clearly visible on the real-time

oscilloscope as sudden bursts of signals. The detected WLAN signal amplitude could be more than three times as large as the TINA tag signal. However, the WLAN signal should not interfere with our location system provided that the signals from the TINA RFID tags are properly sampled. This is because the WLAN signal is not correlated with the reference chirp. The deramped product between the WLAN signal and the reference chirp therefore only produces broadband noise-like signals rather than a strong signal peak in the band of interest in the location algorithm. To further demonstrate the ability for the two systems to co-exist, we were able to stream live video from the Internet via the laptop WLAN connection when the location system was running.

In the following sections, the trial results for the three sensor placement schemes will be presented. A statistical summary of the location results are to be given with discussion and analysis. The trial results will be analyzed using a few different methods that shall be covered in the next section. From these trials, firstly, the location capability of the proposed indoor location system is demonstrated and examined; secondly, the ability to locate multiple RFID tags simultaneously is demonstrated; thirdly, the theoretical and practical differences among different sensor placement schemes are studied. In addition, the theoretical model and tools introduced in this thesis will be applied to the analysis of the results, showing how these tools may help researchers predict the performance of a specific installation scheme of an indoor location system.

## 6.2 Interpretation of Trial Results

In the trials of the TINA indoor location system, the active RFID tag was placed at a number of known locations (test points) for location estimation, and the estimated results were recorded for the corresponding locations. The performance of the system is evaluated by the result statistics for these records, which are interpreted using the following methods:

1. 2-D plot of the estimated locations along with the corresponding true locations;

2. Root-mean-square (RMS) location error and standard deviation of the estimated locations (as defined in Chapter 2);

3. The 50% and 95% circular error probability (CEP) of the estimated locations (as defined in Chapter 2);

4. RMS location error against the standard deviation of the measured TDOA results (refer to Chapter 4).

In a 2-D plot of the results, the estimated locations are plotted as dots in one of the following colours: red, blue, green, cyan, magenta, yellow, and black. The true location is marked by a circle using the same colour as the corresponding estimated locations. The location errors and the variation of the estimated locations are visualized in such a diagram. The variation pattern can be compared with the simulated error spreading pattern predicted from the TDOA mapping algorithm (Chapter 4), obtained by finding the TDOA contour for a specific TDOA (as referred to Eq. (4.6) and Figure 4-3). Figure 6-7 shows an example of these diagrams using simulated results for a tag located at (2.4 m, 2.4 m) coordinate. The respective error spreading pattern given in Figure 6-7(b) is a distorted oval shape. The closed oval shape pattern indicates an area where the estimated location may appear if the time error occurs in the TDOA measurements is 3.3 ns (equivalent to 1 m range error).

Figure 6-7 (a) shows the estimated locations from 100 rounds of simulation, where the standard deviation of TDOA error has been set to 3.3 ns. It can be seen that the variation of the estimated locations given in Figure 6-7 (a) follows a similar pattern as the 3.3 ns TDOA contour shown in Figure 6-7 (b). This is what to be expected if the location algorithm works properly.

Besides this 2-D display of the estimated locations, the RMS error and CEP of location results are also computed. For comparison convenience, the RMS and CEP are presented just beside their corresponding true location on also a 2-D map of the cell, Figure 6-8.

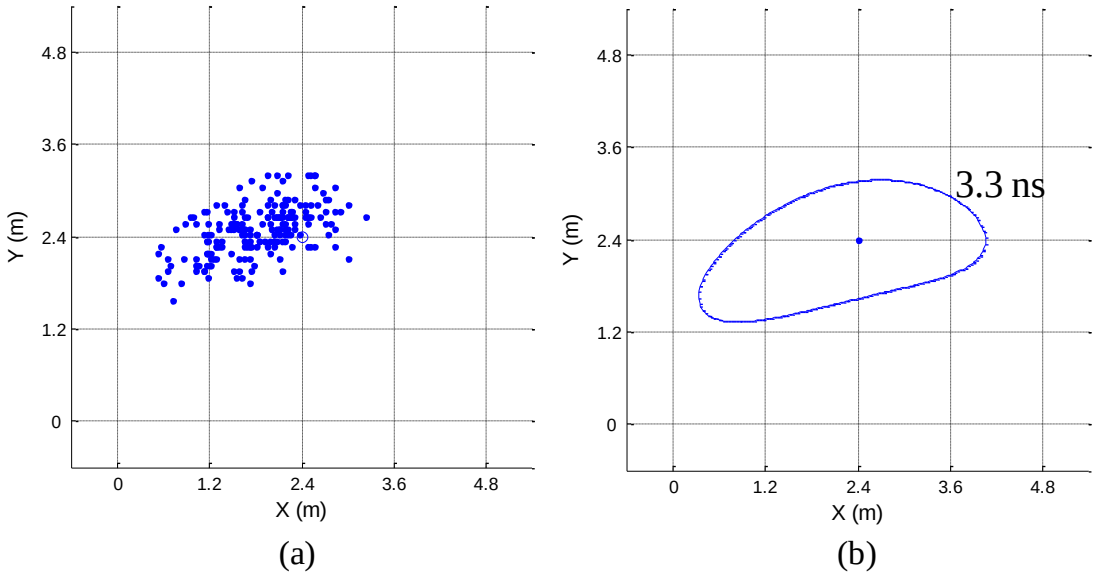


**Figure 6-7 (a) 2-D plot of estimated locations and true location, and (b) simulated error spreading pattern by setting TDOA difference to 3.3 ns.**

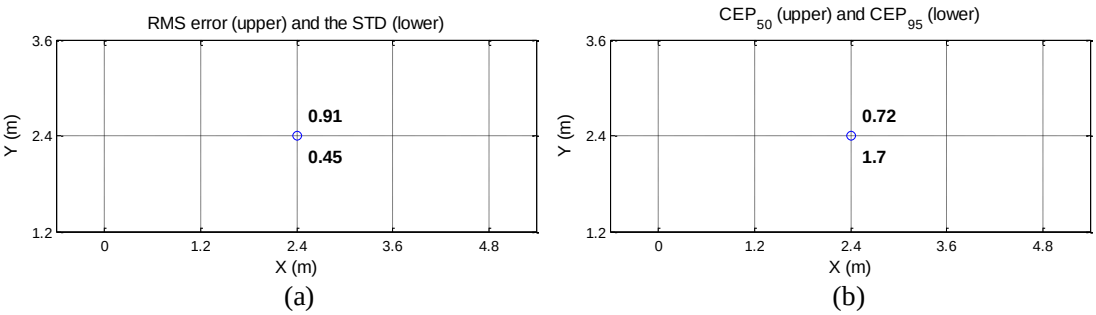


**Figure 6-8 (a) RMS error and the standard deviation of the estimated locations; (b) 50% and 95% CEP**

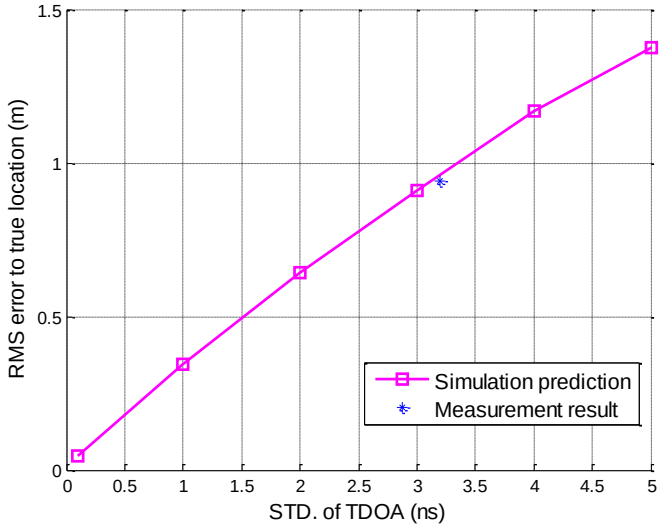


**Figure 6-9 Comparison of the location results with respect to the theoretical prediction**

During the trials, full sets of the measured TDOAs that led to the location results were also recorded. The variation level of the time measurements can be depicted by the standard deviation of the measured TDOAs. According to Section 4.2.4, standard deviation of the TDOAs directly decides the theoretical limit on the RMS location accuracy. Therefore, in the diagram plotting the RMS location error against the associated standard deviation of the measured TDOAs, e.g. Figure 6-9, the theoretical location accuracy predicted by simulation using TDOA mapping algorithm is also given. It can be used to analyze how do the experimental results, plotted as a star marker in the Figure 6-9, agree or disagree with the theoretical estimates, and thus help us to understand the location performance of the system.

In the following sections, the trial results will be presented and analyzed using these four different methods. The 2-D plot of estimated locations shows the error spreading pattern along with the correct location in an intuitive way. The location performance is then evaluated quantitatively with the RMS location error and the CEP parameters. While the RMS location error is an estimate of the true systematic location accuracy, the CEP indicates the probability for achieving specific location accuracy. Further analysis is then made by comparing the experimental RMS location error with a theoretical prediction, obtained from a TDOA mapping simulation using the corresponding sensor placement scheme. This analysis then helps us to understand what might have been the cause of a particular location spreading pattern.

## 6.3 Trial 1: 3-AU Scheme

In the first trial, three sensors are placed along the perimeters of the indoor cell, two at the corners and one at the middle of the other perimeter, which has been shown as an example in Figure 6-4 and Figure 6-5(b). Three sensors are the minimum number required to allow TDOA location finding. The sensor in the TINA location system is in the form of a remote antenna unit (AU). Therefore, the 3-AU scheme employed in the first trial represents the basic configuration of the indoor location system based on TDOA measurements.

Fundamental specifications of the trial are listed in the Table 6-1. Only one RFID tag was used in this trial and was placed sequentially at the 60 test positions shown by Figure 6-5.

There are three sensor pairs in this case, the AU1-2, AU1-3, and AU2-3. According to the analysis given in the Section 4.3, better location accuracy shall be obtained in the sensitive regions of these sensor pairs. The 15.6 m by 6.6 m indoor cell is fully covered by the sensitive area of the sensor pair AU1-2.

| Specifications | Descriptions |
|---|---|
| Coordinates of sensors | AU1 (0 m, 0 m), AU2 (0 m, 15.6 m), and AU3 (6.6 m, 7.8 m) |
| Number of measurement location points chosen | 60 |
| Number of user tag | 1 |
| Number of measurements per location | 30 |

**Table 6-1 Trial 1: Specifications for the 3-AU trial**

However, the sensitive area of the pair AU1-3 and AU2-3 does not cover the whole indoor cell. The overlapped sensitive regions from the three sensor pairs are a triangle shown in the middle of the Figure 6-10. The upper and lower polygon areas are overlapped sensitive regions for two sensor pairs only, and thus the achievable location accuracy within this region is not as good as that in the middle triangle.

This prediction can then be demonstrated by the trial results shown in the Figure 6-11. For every position chosen as an experimental point, the respective estimated locations vary due to the presence of noise, multipath, and other interference. In general, the shapes of variation of the location results (Figure 6-11(a)) are similar to the error spreading patterns (Figure 6-11(b)) simulated from the TDOA mapping method, where the TDOA difference is set to be 3.3 ns.

Consider those location results from the overlapped sensitive region for all three sensor pairs. The trial results show that, when the RFID tag is placed within this red triangle region indicated by Figure 6-10, the variation of estimated locations is smaller. This is because, in the overlapped sensitive region, certain amount of time measurement error will induce lesser location error, as discussed in the Section 4.3. This phenomenon can also be observed from the simulated error spreading pattern given in the Figure 6-11(b).

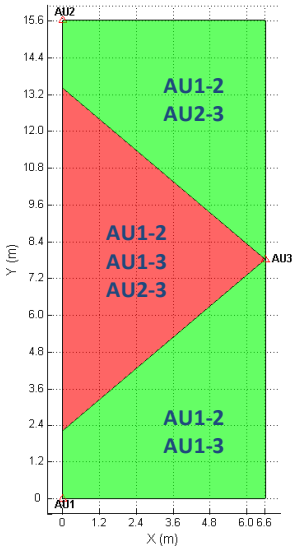


**Figure 6-10 Trial 1: Overlapped sensitive regions for the 3-AU scheme**

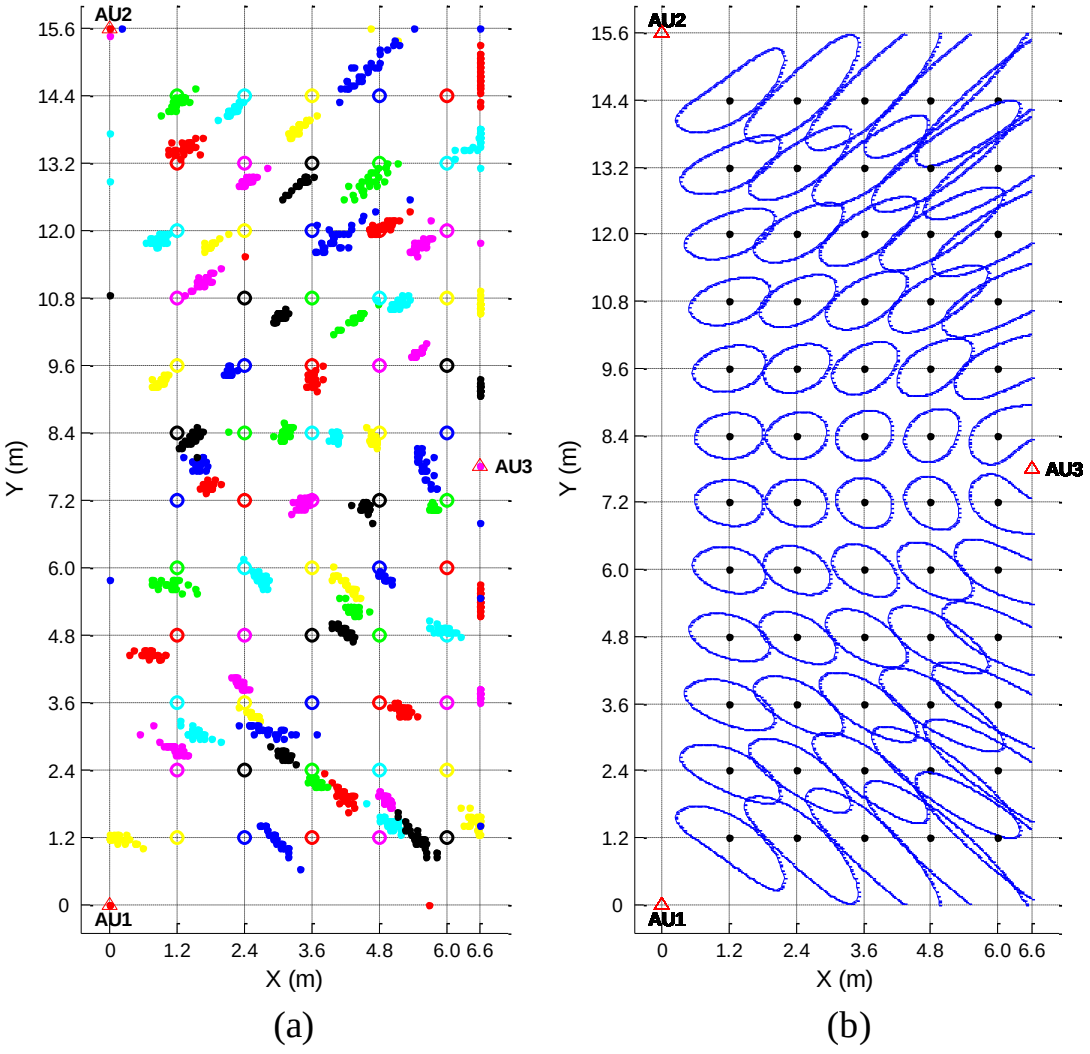


**Figure 6-11 Trial 1: (a) 2-D plot of estimated locations, and (b) simulated error spreading pattern by setting TDOA difference to 3.3 ns.**

Regarding the two green polygon regions that are overlapped by two sensor pairs only, the estimated locations obtained from these regions exhibit slash-shape variations. The slash directions are identical to the error spreading patterns (Figure 6-11(b)).

Another interesting observation is that most of the estimated locations experience a bias with respect to their true locations. Take a typical measurement point (1.2 m, 1.2 m) from Figure 6-11(a) as an example, the variation of estimated locations is around a mean position different from the true position, whereas the mean estimated coordinate is roughly 1 m to the left of the true position.

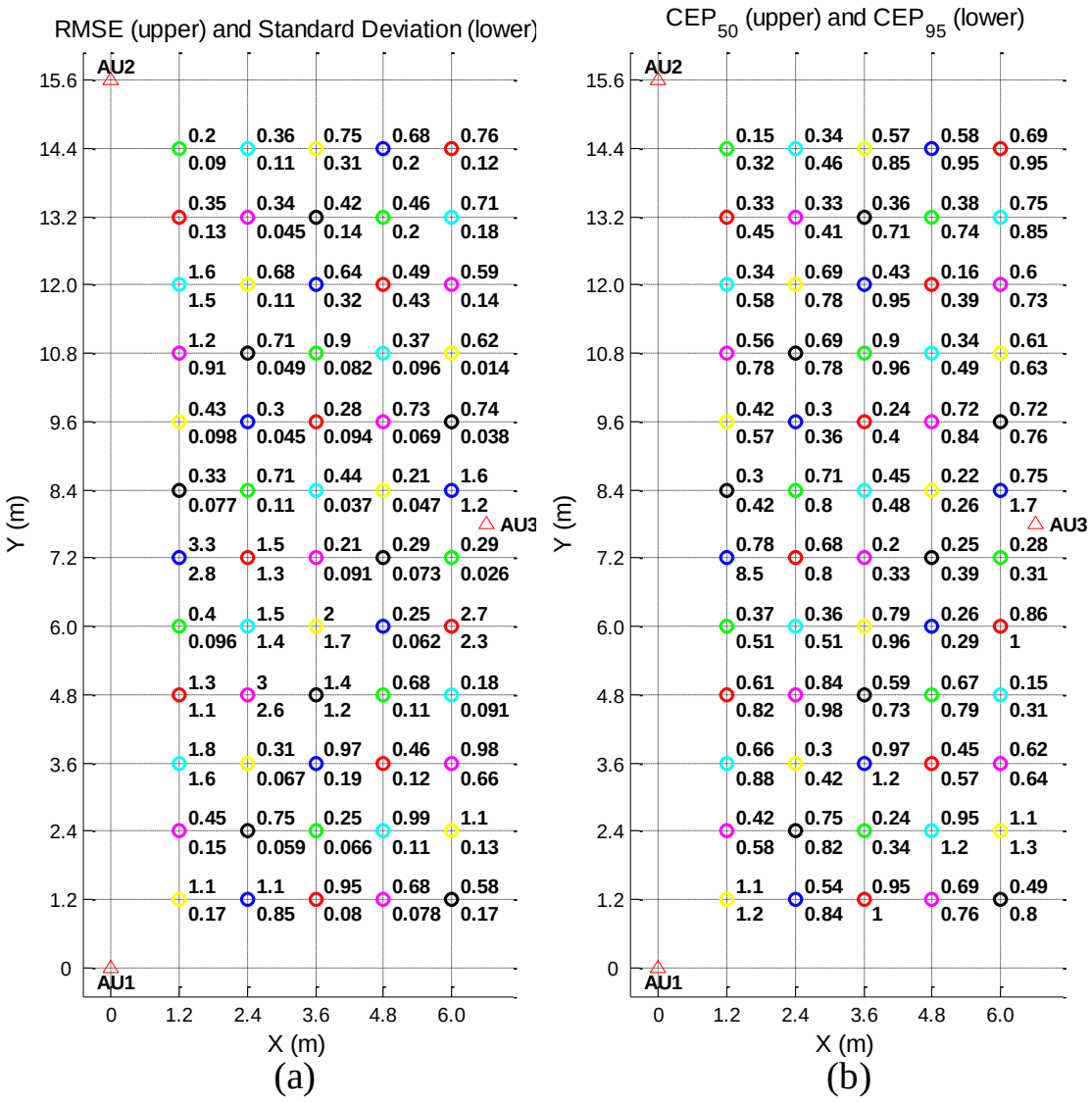


**Figure 6-12 Trial 1: (a) RMS error and the corresponding standard deviation; (b) $CEP_{50}$ and $CEP_{95}$ for the estimated locations.**

This diverse estimated mean and true position effect is observed at most of the test points. The cause of this effect is unresolved multipath interference, which occurred in one or more of the wireless channels. As discussed in Chapter 5, the multipath interference is likely to be reduced but cannot be fully removed from the TDOA measurements. The impact of multipath on location measurements is a long-term stable additive range, which is the cause of the biased location means seen in the Figure 6-11(a).

The overall location performance is then quantified by the RMS location error and the CEP values shown on the diagrams in Figure 6-12. To illustrate the overall location performance of the system in this scenario, the average levels of RMS location error, 50% CEP, and 95% CEP are computed and listed in Table 6-2.

The average RMS location error in this scenario is 0.84 m, reflecting the overall location accuracy of the TINA indoor location system with this sensor placement scheme. Also, at 52 out of the 60 measurement points, the $CEP_{95}$ is not larger than 1 m, which means that there is 95% probability of achieving below-one-metre RMS location accuracy at most of the measurement points.

| Parameters | Values |
|---|---|
| RMS error | 0.84 m |
| $CEP_{50}$ | 0.54 m |
| $CEP_{95}$ | 0.84 m |

**Table 6-2 Trial 1: Average location performance**

Besides the overall performance, attention shall also be paid to those positions where the recorded RMS location errors are large.

Among the total 60 measurement positions, there are four positions where the achieved RMS location error is greater than 2 m. Their RMS errors and corresponding coordinates are {3.3 m, (1.2 m, 7.2 m)}, {3 m, (2.4 m, 4.8 m)}, {2.7 m, (6.0 m, 6.0 m)}, and {2 m, (3.6 m, 6.0 m)}. The estimated locations obtained from these positions are re-plotted along with the corresponding RMS error in Figure 6-13.

It can be seen from Figure 6-13 that, although the RMS errors from these positions are greater than 2 m, most of the estimated locations determined by the algorithm are actually within 1 m range to their true locations. The reason for the large RMS errors

can be found near the corner of the room, as indicated by the orange arrows. It can be seen that a few dots representing the estimated locations from these experiments are present at various corners of the indoor cell. This type of burst error estimations was observed occasionally during the trial and is believed due to the interference from other wireless system, possibly WLAN.

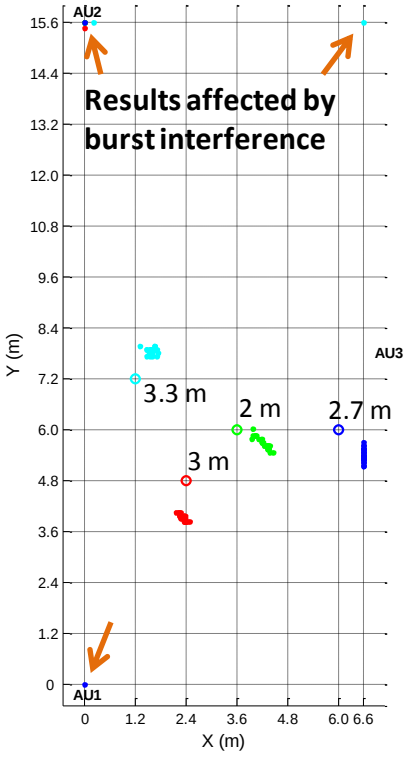


**Figure 6-13 Trial 1: Estimated locations from the large RMS error experiments**

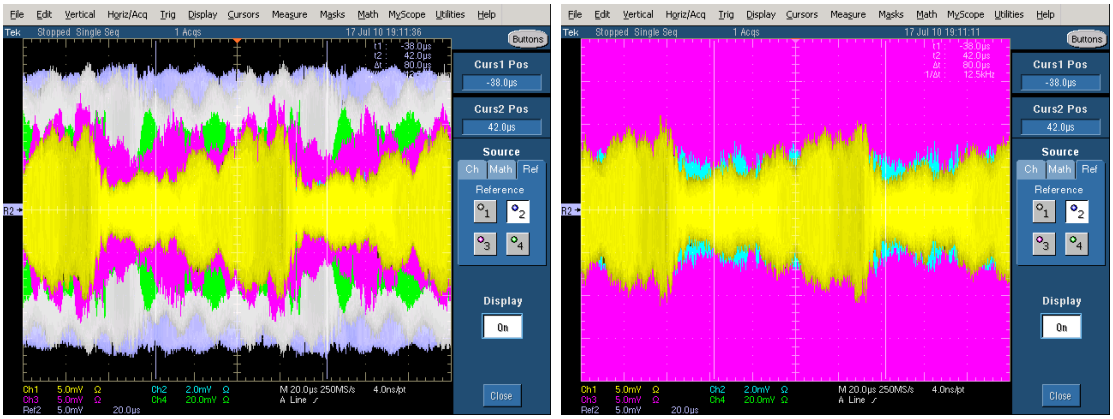


**Figure 6-14 Time domain signals captured in oscilloscope showing the normal chirp signals received (left) and the presence of interference signal in the AU3 channel (right).**

These interference effects are shown by two screen captures of the time domain signals from the oscilloscope, Figure 6-14. The diagram on the left illustrates normal

received chirps in time domain. The diagram on the right shows the case when a much larger burst signal is present in the AU3 channel. The magnitude of this signal is so large that the signal from AU3 cannot be fully displayed on the oscilloscope screen, where the y-axis division is set to be 5 mV per division.

The burst signals in this case saturate the analog-to-digital conversion (ADC) process and thus the samples captured no longer represent the actual signal received. This is due to the fact that the ADC input dynamic range is set to be fixed for fully utilizing the ADC quantization levels for the ordinary chirp signals, or in other words due to the setting of the demonstration rather than the system design.

Therefore, the location results related to this effect shall be removed from the analysis, and the key parameters illustrating the overall performance of the location system are re-calculated and listed in the Table 6-3. The revised RMS errors and CEP values are also re-plotted in the Figure 6-15, where the location errors inferred from the four positions as in Figure 6-13 have been corrected to reflect the actual achievable location performance.

| Parameters | Values |
|---|---|
| RMS error | 0.57 m |
| $CEP_{50}$ | 0.54 m |
| $CEP_{95}$ | 0.74 m |

**Table 6-3 Trial 1: Revised average location performance**

The 60 RMS location errors from Figure 6-15 are also plotted against their corresponding TDOA deviation levels, represented by the standard deviation of the measured TDOAs, as shown in Figure 6-16. A series of simulation results calculated for different TDOA deviation levels are also given in this diagram, indicated by the magenta curve in Figure 6-16.

From the trial results it can be seen that the measured TDOAs vary with roughly 0.2 ns to 0.9 ns standard deviation. If measurements of the TDOAs are unbiased, the resultant RMS location error shall be between 0.1 m to 0.4 m, as predicted by the simulated curve. However, the trial results show that the actual RMS location error ranges from roughly 0.2 m to 1.1 m, which obviously violates the simulation prediction. These results indicate that the TDOA measurements contain stable biased error, which explains the fact that the mean estimated locations are not exactly their

true locations, shown by the Figure 6-11. The cause of this deviation is unresolved multipath error, because the estimated locations differ from the true location and the deviation is fairly stable for a given position.

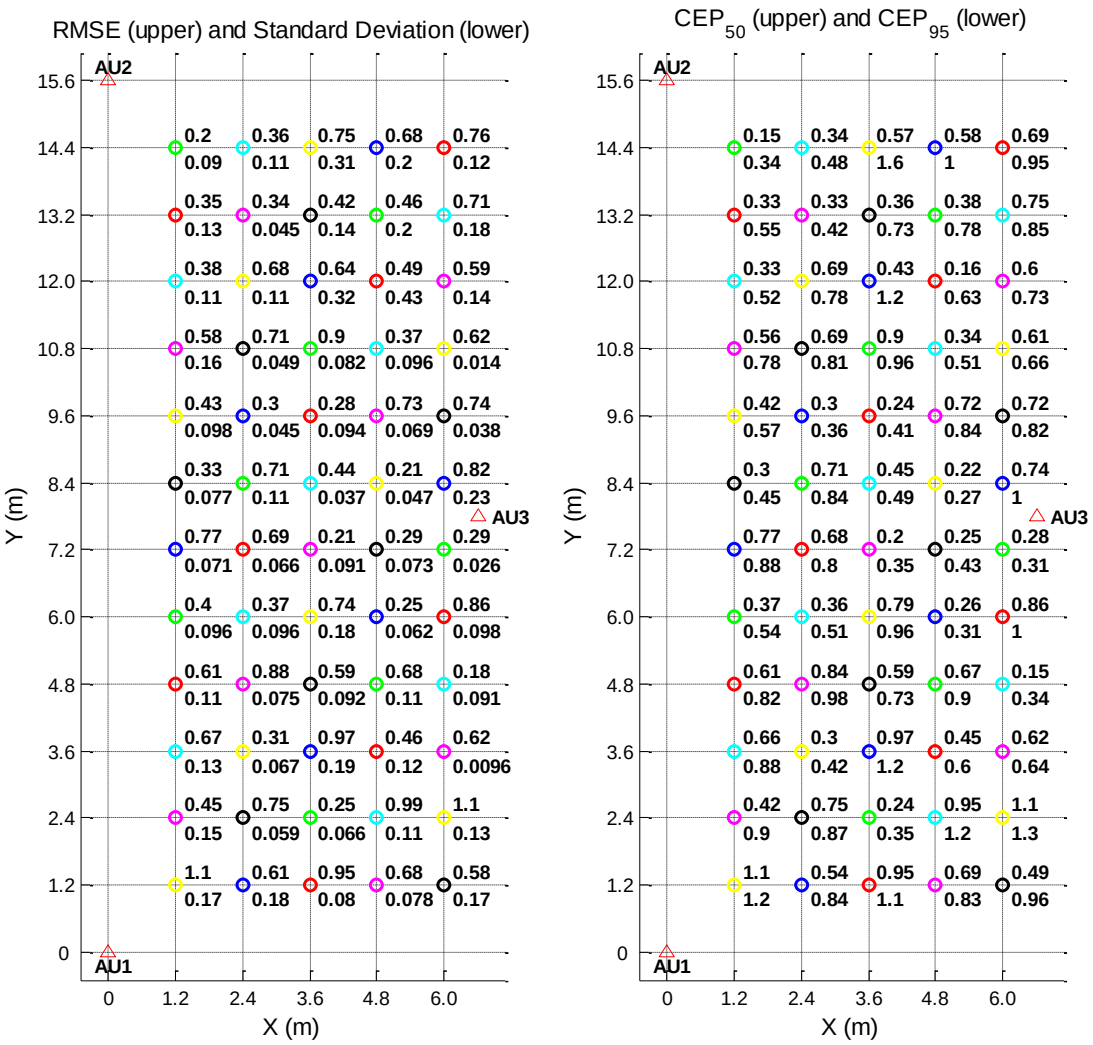


**Figure 6-15 Trial 1: (a) revised RMS error and the corresponding standard deviation; (b) revised $CEP_{50}$ and $CEP_{95}$ for the estimated locations.**

From the variation of the RMS errors in Figure 6-16, it is found that the "hidden" TDOA errors are at the range of 0.6 ns to 3.5 ns, which indicates 0.2 m to 1 m additive distance error caused by unresolved multipath impacts. This multipath error scope agrees with the multipath simulation results using half-peak frequency detection strategy, as given in the Table 5-8.

Although the exact multipath errors in each experiment cannot be removed at this stage, the additive distance error caused by multipath can be ignored by recalculating

the RMS location errors with respect to their mean estimated location, instead of the true location. By this means, the long-term biased error caused by multipath is taken away and the RMS location errors shall be dependent mainly on the TDOA errors caused by noised.

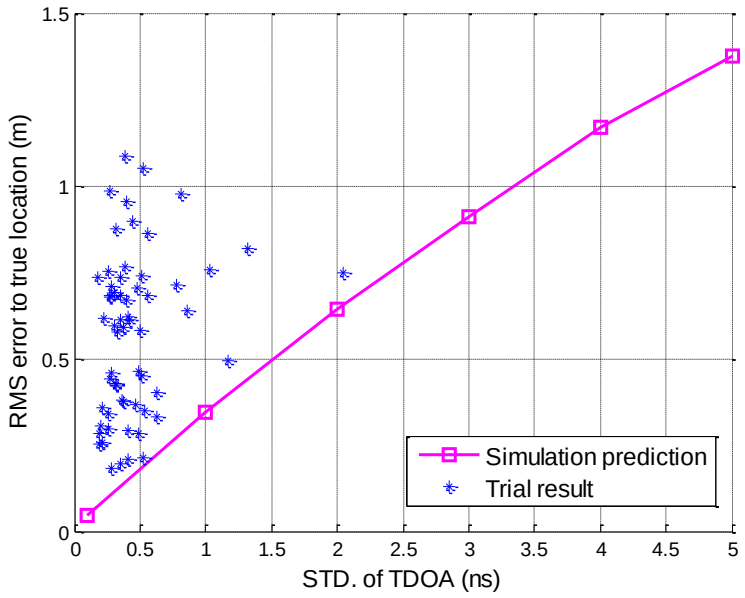


**Figure 6-16 Trial 1: RMS error with respect to true location vs. TDOA errors**

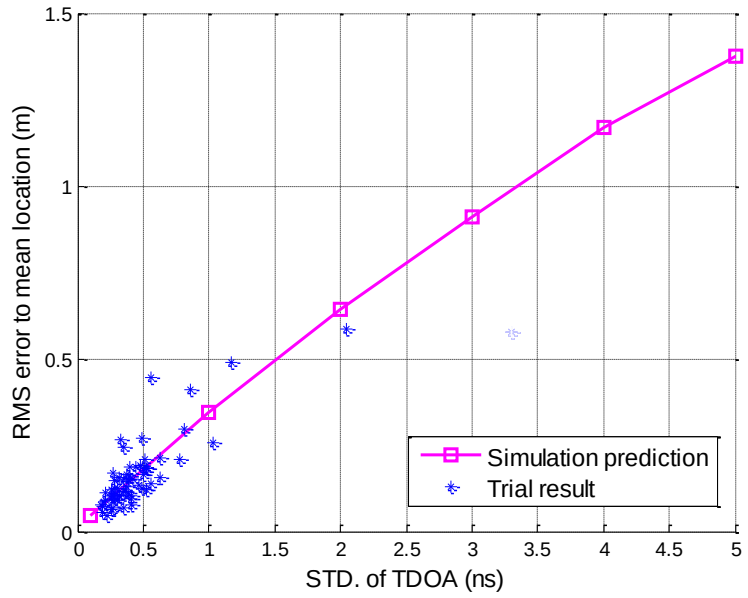


**Figure 6-17 Trial 1: RMS error with respect to mean location vs. TDOA errors**

The associated results are re-plotted and compared with the simulation prediction again in Figure 6-17. It can be seen that, the RMS location errors with respect to the mean estimated location are aligned with the simulation prediction fairly well. The

first point it tells is that the biased location offset is the reason of the violation between the trial results and simulated curve in the Figure 6-16. This diagram also reflects that the RMS errors caused by random TDOA errors are in agreement with the simulation prediction, validating the integrity of the TDOA mapping algorithms employed by the TINA indoor location system.

This section has firstly shown that the tag locations determined by the TINA system vary in a very similar way as the simulated spreading pattern. The relatively small variation of estimated locations in the highly sensitive region is also observed from the 2-D plot of the results. Subsequently, the overall location performance of the system is summarised by the statistical records of the trial results, demonstrating below-one-metre location accuracy which was required by the design objective. Some practical error sources are also observed and analyzed in this section. The RMS error against TDOA error diagram (Figure 6-17) from another aspect supports the hypothesis that the biased location error is due to the presence of multipath.

## 6.4 Trial 2: 4-AU Perimeter Placement Scheme

The second trial was a four-sensor scheme, with the four AUs placed at the middle points of the four perimeters of the indoor cell. Half of the 60 test points were chosen as the measurement locations in this trial. Two RFID tags were used in this trial, with one transmitting 80 μs down-chirp (Tag 1), and the other transmitting 80 μs up-chirp (Tag 2). The two RFID tags were placed at two different locations at the same time for demonstrating the user identification and location estimation functionality of the system. In each experiment, a hundred of location estimation measurements were executed. The Figure 6-18 shows the positions of the AUs and the 30 measurement points chosen in this trial, while the specifications of this trial are summarised in Table 6-4. As explained in Section 5.5.2, in the TINA indoor location system, the 4-AU scheme provides useful redundancy. To improve measurement accuracy and robustness, the AU channel with the smallest received signal power is ignored. Only the remaining three AU channels with higher signal power are chosen in the corresponding experiment to perform location estimation.

| Specifications | Descriptions |
|---|---|
| Coordinates of sensors | AU1 (0 m, 7.8 m), AU2 (6.6 m, 7.8 m), AU3 (3.3 m, 15.6 m), and AU4 (3.3 m, 0 m) |
| Number of measurement location points chosen | 30 |
| Number of user tags | 2 |
| Number of measurements per location | 100 |

**Table 6-4 Trial 2: Specifications for the 4-AU perimeters placement scheme**

The received signal power is inversely proportional to the square of the propagation path length from the source to the receiver. Consider the sensor placement scheme shown in Figure 6-18, this is a rectangular shape area whose length is more than double the width. In this case, a tag in the upper half of the area will more likely to be located by using the AU1, AU2, and AU3, as the received signal power of AU4 shall be the smallest if the RFID tag is at the upper half of the cell. Likewise, a tag in the lower half of the room will usually be located by using AU1, AU2, and AU4.

This placement scheme effectively divides the room into two smaller cells, either of which is monitored by three sensors. The benefit of having a smaller cell area is that the average signal propagation path length is reduced, and therefore the average received signal power at the three sensors is likely to be higher. For TDOA ranging systems, the resultant advantage is the reduced TDOA variations.

The blue circles in Figure 6-18 indicate the test points used for Tag 1, and the red circles indicate the test points for Tag 2. In the first experiment, Tag 1 was placed at position (1.2 m, 1.2 m), while the Tag 2 was placed at an upper right position (6 m, 13.2 m) of the room. For every following experiment, they were moved one step forward to the next positions indicated by the arrows besides the test points in the Figure 6-18. During the trial, the distance between the two tags varied from over 10 m to 2.4 m.

The trial results firstly show that, the two tags could be identified properly in all experiments, and their locations were estimated without causing interference to each other. Estimated locations from all the experiments for both tags are shown in Figure 6-19 (a), along with the corresponding simulated error spreading patterns (Figure 6-19 (b)), where the results in the upper half of the room are computed using AU1-2-3, and the results for the lower half are computed from AU1-2-4.

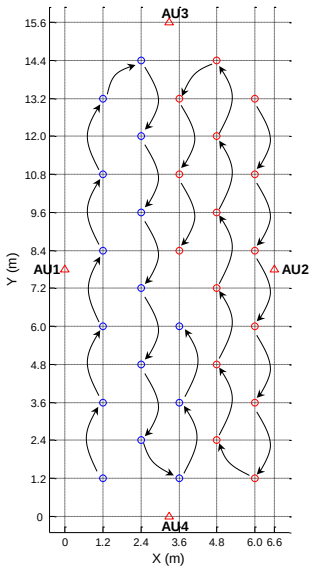


**Figure 6-18 Trial 2: 4-AU perimeter placements and the test points**

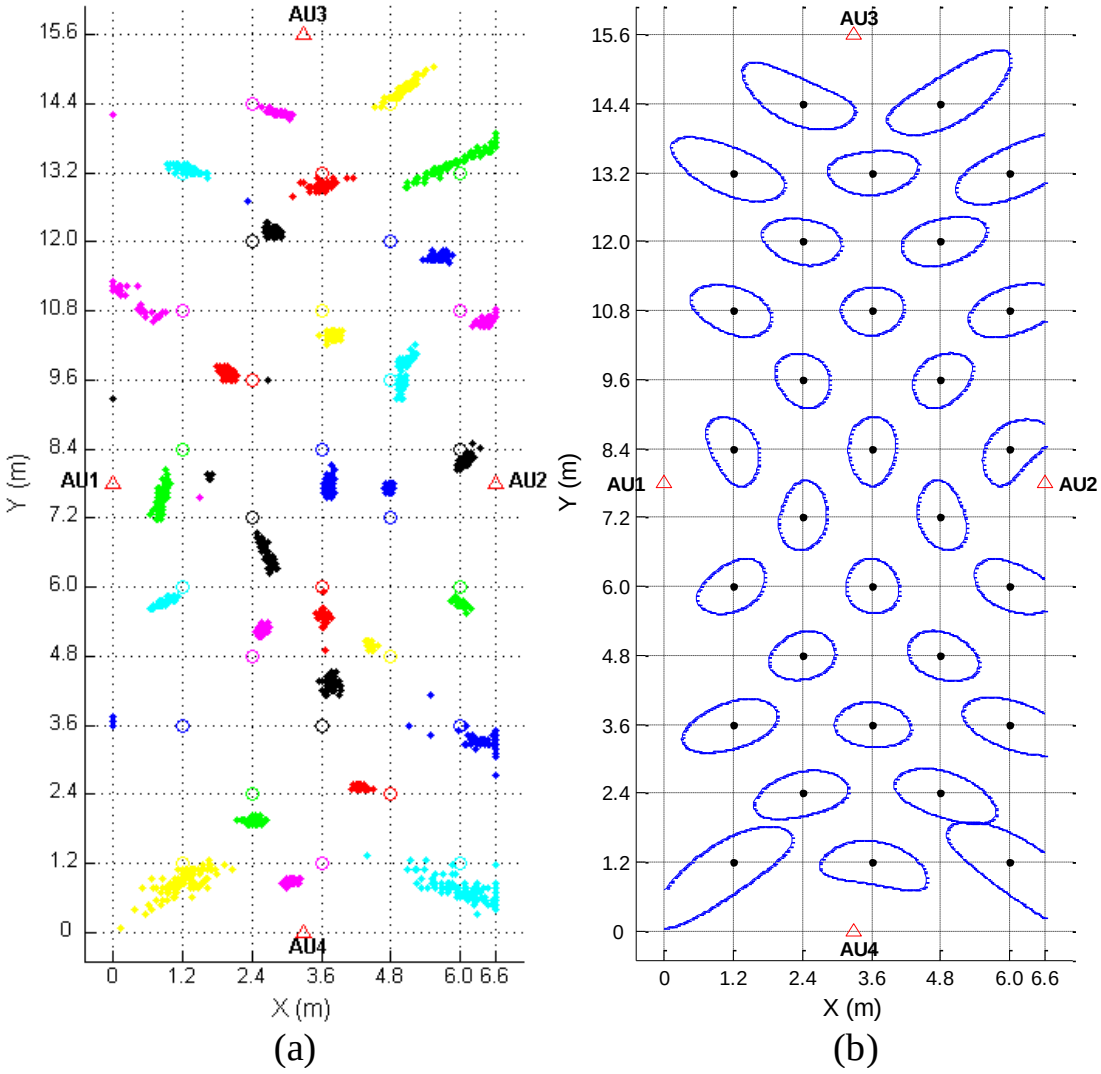


**Figure 6-19 Trial 2: (a) 2-D plot of estimated locations, and (b) simulated error spreading pattern using AU1-2-3 for upper half and AU1-2-4 for lower half, by setting TDOA difference to 3.3 ns.**

The variations of estimated locations show good alignment with the simulated patterns in a few ways. Firstly, for positions outside the AU triangles Δ123 and Δ124, the estimated locations vary in the form of a slash or backslash, as predicted from Figure 6-19 (b). In addition, for the positions in the middle of the room ($y$=7.2 m or 8.4 m), variations of estimated locations along $y$-axis are larger than that along the $x$-axis. In contrast, at the positions inside the triangles Δ123 and Δ124, variations along x-axis and y-axis are similar, e.g. results at positions (2.4 m, 4.8 m), (3.6 m, 3.6 m), (4.8 m, 4.8 m), and (2.4 m, 9.6 m), (3.6 m, 10.8 m), (4.8 m, 9.6 m).

To quantify these observations, the RMS location errors and their respective standard deviations are given in the Figure 6-20 (a), where burst error induced results have been removed from calculations. While most of the results show similar location errors, relatively small location deviations are found around the centre of the room, where a few points have shown standard deviations of 0.1 m levels. Standard deviations of worse than 0.2 m level are found at the positions (6 m, 13.2 m), (6 m, 3.6 m), (6 m, 1.2 m), (2.4 m, 7.2 m), and (1.2 m, 1.2 m). Four of these positions are outside of the AU triangles, where relatively large standard deviation agrees with expectation.

Regarding point (2.4 m, 7.2 m), the reason for the 0.25 m standard deviation can be found from the 2-D plot of Figure 6-19 (a). It can be seen that, the estimated locations (indicated by black dots) consist of two biased groups, one to the bottom right and the other to the upper left. This is because the tag was located at the boundary between the two AU combinations, AU1-2-3 and AU1-2-4. In this case, the received power at AU3 and AU4 were similar. Thus, the location algorithm occasionally chose AU1-2-3 or AU1-2-4 to locate this target. While this mechanism exaggerates the standard deviation in this experiment, the resultant 0.74 m RMS location error is still at the acceptable range. From the CEP diagram (Figure 6-20 (b)), it can also be seen that 95% of the results induce lower than 0.99 m errors.

The overall location performance is evaluated by the average RMS location error and the average circular error probability (CEP) of all 30 groups of measurement results, as summarised in the Table 6-5.

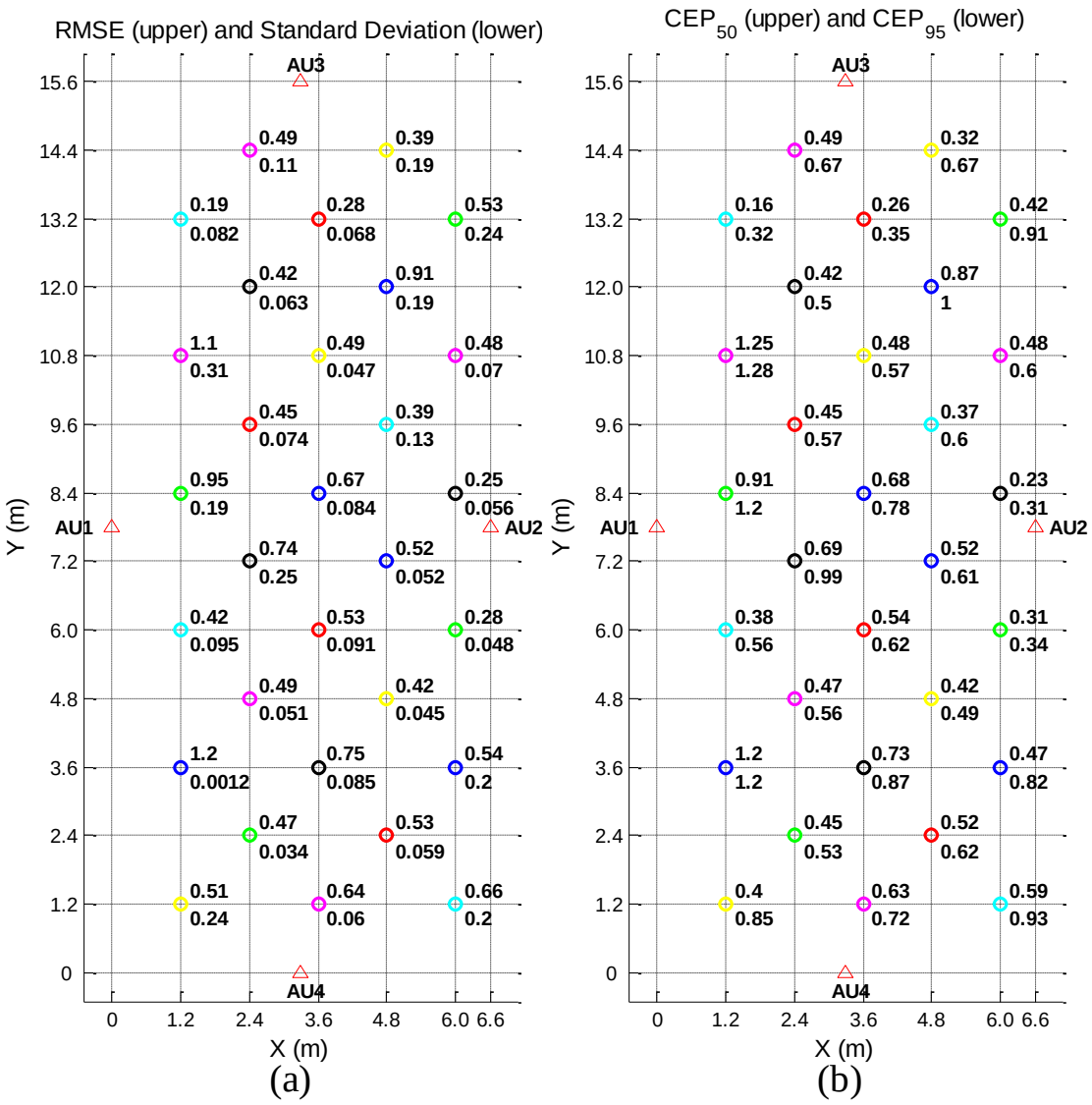


**Figure 6-20 Trial 2: (a) RMS error and the corresponding standard deviation; (b) $CEP_{50}$ and $CEP_{95}$ for the estimated locations.**

| Parameters | Values |
|---|---|
| RMS error | 0.56 m |
| $CEP_{50}$ | 0.54 m |
| $CEP_{95}$ | 0.70 m |

**Table 6-5 Trial 2: Average location performance.**

The average results demonstrate that the TINA indoor location system in this trial shows on average 0.56 m location accuracy, while there is 95% probability that the estimation locations are found within 0.7 m range to the true locations.

Since the RMS location errors shown above are calculated with respect to the true location of the tag in a multipath environment, violation of the location results from

the simulation predicted performance curve can be observed from Figure 6-21. In Figure 6-21, the simulation prediction curve is obtained by calculating the average RMS error from a ten-thousand round Monte-Carlo simulation using the TDOA mapping method with varying TDOA errors. Violation levels of the trial results from the simulation curve indicate that the multipath induced TDOA error involved in the measurements is between 0.8 ns and 4 ns, corresponding to 0.24 m to 1.2 m additive ranges.

If the biases are removed, giving the RMS location error with respect to the mathematic expectations, the trial results will show much better alignment with the simulation prediction, as shown by Figure 6-22.

Besides the well-aligned trial results, there are also a few results showing large violation from the simulation prediction, as indicated by the four marks with greater than 0.4 m RMS errors in Figure 6-22. They are results from the positions (6 m, 13.2 m), (6 m, 1.2 m), (2.4 m, 7.2 m), and (1.2 m, 1.2 m). As analyzed previously, three of these positions are outside of the AU triangles, and thus are likely to produce worse than average performance. Whereas, the position (2.4 m, 7.2 m) has been monitored by different AU combinations (Figure 6-19 (a)), and thus the mean location is in between the two groups of results.

From Figure 6-22, it can also be seen that most of the TDOA error deviations from both tags are at lower than 0.5 ns level, lower than that obtained in the Trial 1 (Figure 6-17) as well as that obtained in the Trial 3 (to be shown in Figure 6-27). This is attributed to the sensor placement scheme, which effectively divides the room into two smaller location cells, as introduced previously in this section. The reduced cell size also leads to reduced average range from tag to AUs, which improves the received signal quality and the TDOA measurement stability.

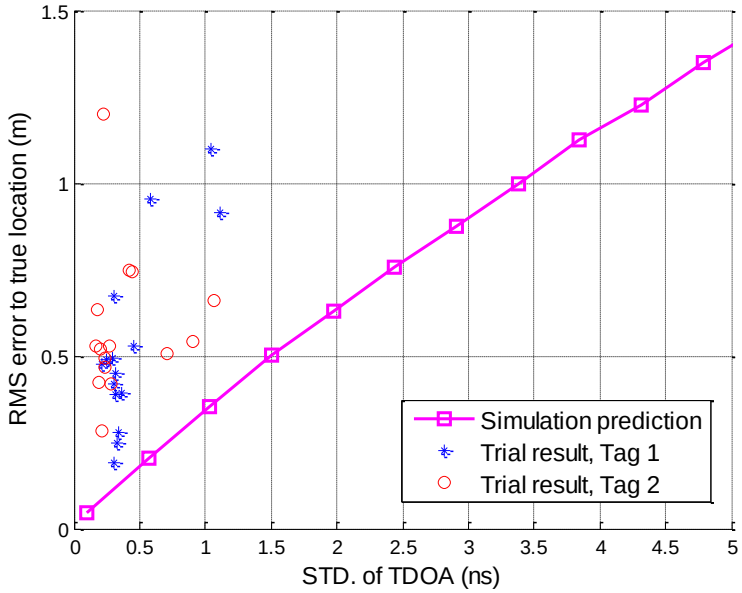


**Figure 6-21 Trial 2: RMS error with respect to true location vs. TDOA errors.**

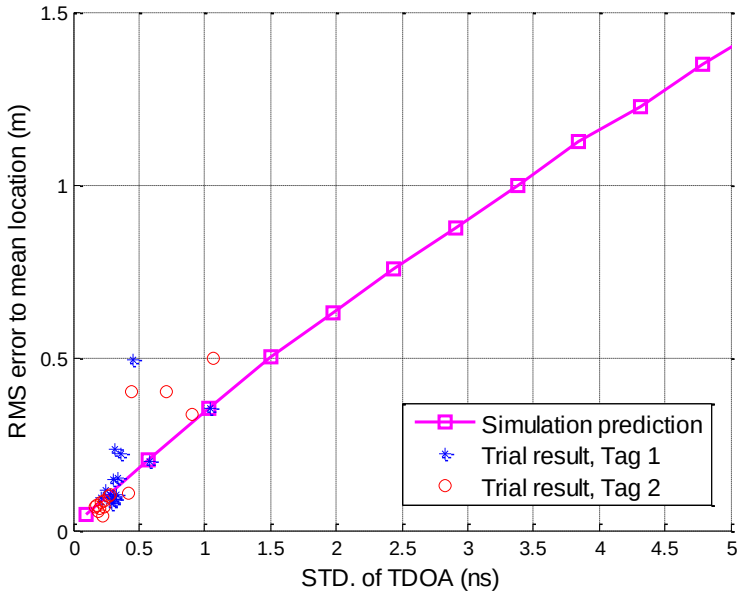


**Figure 6-22 Trial 2: RMS error with respect to mean location vs. TDOA errors.**

In this section, a 4-AU perimeter placement scheme has been introduced and the trial results are interpreted in the same way as the previous section. The feature of this scheme is reduced effective cell size, providing some benefits. Firstly, higher received signal power can be expected, as the average transmission path from the source to the receivers is reduced. Secondly, in a crowded indoor area, smaller cell size implies that the possibility of experiencing non-line-of-sight propagation is reduced. This scheme ensures better location performance in the centre area of the room, which has also

been demonstrated from the trial results. In the next section, another 4-AU scheme will be introduced, which provides better location performance at the front and rear areas of the indoor cell.

## 6.5 Trial 3: 4-AU Corner Placement Scheme

When considering installation of an indoor location system in a rectangular room such as the one chosen in these trials, the most straightforward idea one would think of will be placing the four sensors at the four corners of the room. The benefit of this scheme is that it fully utilises the furthest range available in this geometry, which is the diagonal of the rectangle. In this case, the indoor area shall be well covered by the sensitive region of the sensor pairs. The third trial of the TINA indoor location system employed this sensor placement scheme. The parameters of this trial are summarised in the Table 6-6. It will be proved by trial data that this sensor placement scheme does lead to better overall location performance, when compared to the previous two schemes.

| Specifications | Descriptions |
|---|---|
| Coordinates of sensors | AU1 (0 m, 0 m), AU2 (0 m, 15.6 m), AU3 (6.6 m, 15.6 m), and AU4 (6.6 m, 0 m) |
| Number of measurement location points chosen | 60 |
| Number of user tags | 2 |
| Number of measurements per location | 100 |

**Table 6-6 Trial 3: Specifications for the 4-AU corners placement scheme**

In this trial, the two RFID prototype tags were also used in each experiment. They were placed at two different groups of 30 test points, as indicated by Figure 6-23, where the blue circles mark the positions for Tag 1 and the red circles mark positions for Tag 2. In the first experiment, Tag 1 was placed at the bottom left position (1.2 m, 1.2 m), while Tag 2 was placed at the upper right position (6 m, 14.4 m). The positions of the two tags were again adjusted in every experiment as specified by the arrows shown on Figure 6-23, where the blue arrows represent movement of Tag 1 and red arrows represent movement of Tag 2. During the trial of 30 experiments, the distance between Tag 1 and Tag 2 varied from over 10 m to a minimum of 1.2 m.

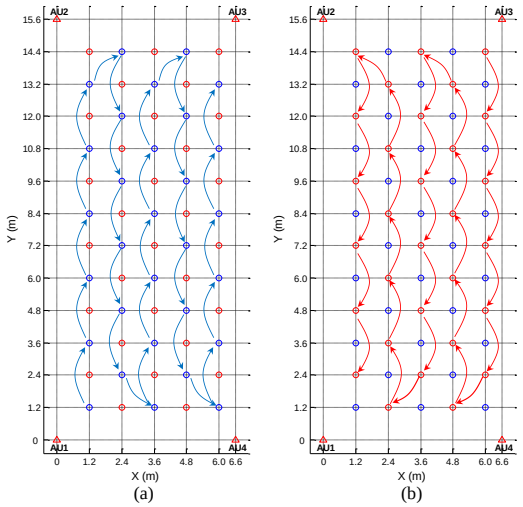


**Figure 6-23 Trial 3: 4-AU corners placements and the test points for Tag 1 (blue) and Tag 2 (red); (a) movement of Tag 1, (b) movement of Tag 2.**

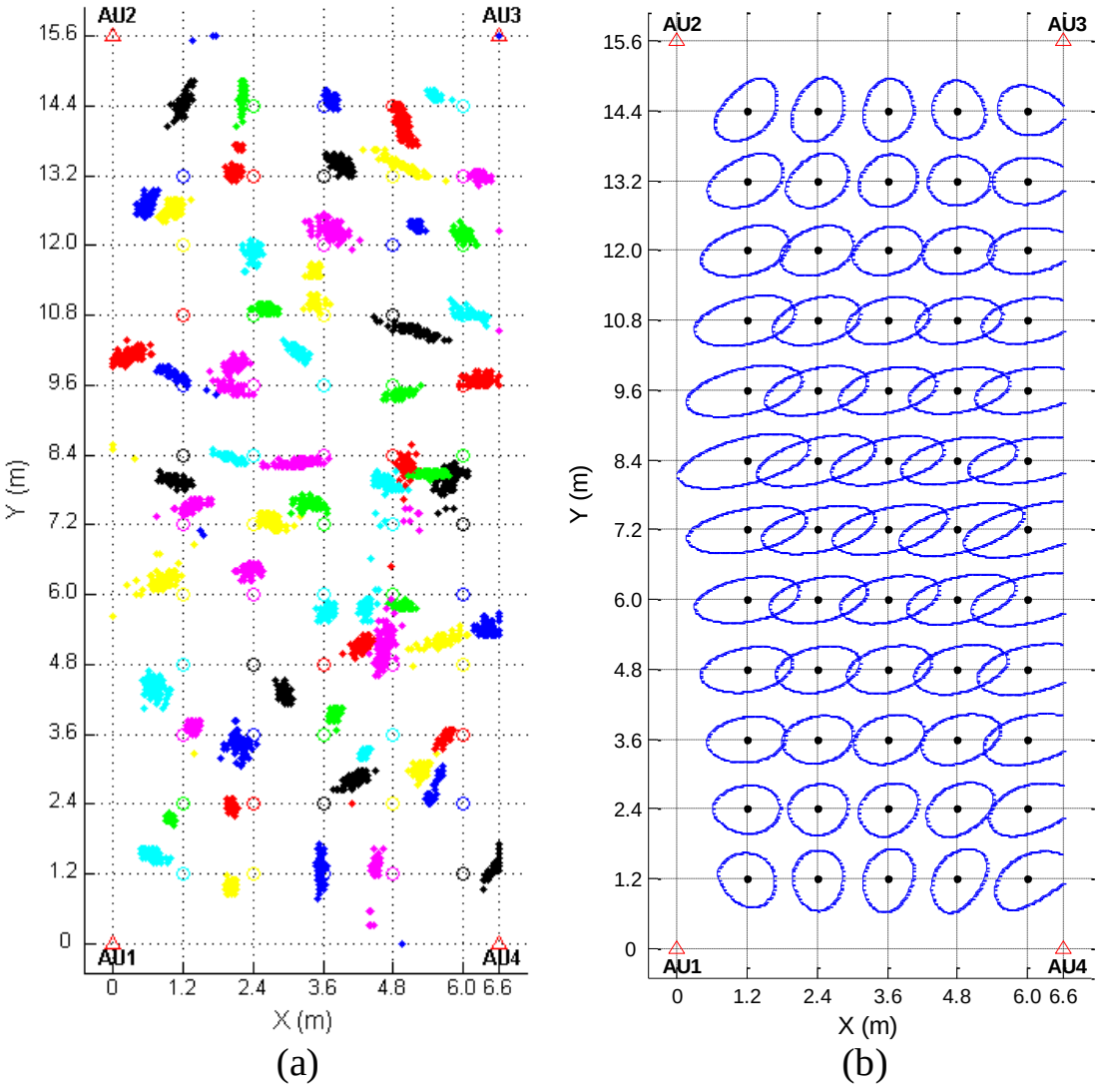


**Figure 6-24 Trial 3: (a) 2-D plot of estimated locations, and (b) simulated error spreading pattern using AU2-3-4 for upper half and AU1-2-4 for lower half, by setting TDOA difference to 3.3 ns.**

As explained earlier, three of the four AUs were chosen to perform location finding in each task. AU selection in this trial is also dependant on the sensor placement scheme. Usually the upper pairs, AU2 and AU3, will be chosen if the tag is in the upper half of the cell, while the lower pairs, AU1 and AU4, will be chosen when the tag is in the lower half of the cell. The third AU can be either of the AUs located at the further end. From the error spreading patterns illustrated in Figure 6-24 (b), it can be seen that the feature of this sensor scheme is that finer spreading patterns appear at the ends of the cell, other than in the centre of the cell, which is the case in Trial 2 (Figure 6-19 (b)).

With this sensor placement scheme, the $x$ direction variation $\Delta x$ of estimated locations would be greater than the $y$ direction variation $\Delta y$ when the tag is in the centre area of the cell. This is because the centre area is at the edge of either sensitive region of the AU1-4 pair or AU2-3 pair. By contrast, the $\Delta y$ is expected to be slightly greater than $\Delta x$, when the tag is near either end of the cell. This can be witnessed by the error spreading patterns of the points along $y$=1.2 m, and $y$=14.4 m (Figure 6-24 (b)).

As expected, the two tags had no problem being identified and located separately during the trial. The 30 experiments produce 60 groups of estimated location results, as plotted in Figure 6-24 (a). The $\Delta x > \Delta y$ variations are seen at positions (2.4 m, 8.4 m), (3.6 m, 8.4 m), (6 m, 8.4 m), (1.2 m, 7.2 m), (2.4 m, 7.2 m), and (3.6 m, 7.2 m), all of which are points near the centre of the cell. On the other hand, the $\Delta y > \Delta x$ variations are witnessed at positions (3.6 m, 1.2 m), (4.8 m, 1.2 m), (1.2 m, 14.4 m), and (2.4 m, 14.4 m), which are near the end sides of the cell.

The recorded statistics of the estimated locations are illustrated in the room map again as Figure 6-25. The overall location performance of this sensor placement scheme is relatively better than the results from the other two trials, as shown in the Table 6-7. The average RMS location error in this trial was 0.47 m, indicating that the location results were about 0.1 m more accurate than the other two schemes. The 95% circular error probability was reduced to 0.63 m, outperforming the results from the other two schemes. The best record came from the positions (1.2 m, 14.4 m), (2.4 m, 12 m), and (6 m, 10.8 m), at which positions the estimated locations were nearly unbiased, and their $CEP_{95}$ are about 30 cm from the respective true locations. The worst record was from the positions (1.2 m, 10.8 m), where large biased measurement is seen, making

the $CEP_{95}$ as large as 1.4 m. However, the deviation of location errors, 0.15 m, was at reasonable level for this position and was actually reflected the error spreading pattern predicted in Figure 6-24 (b).

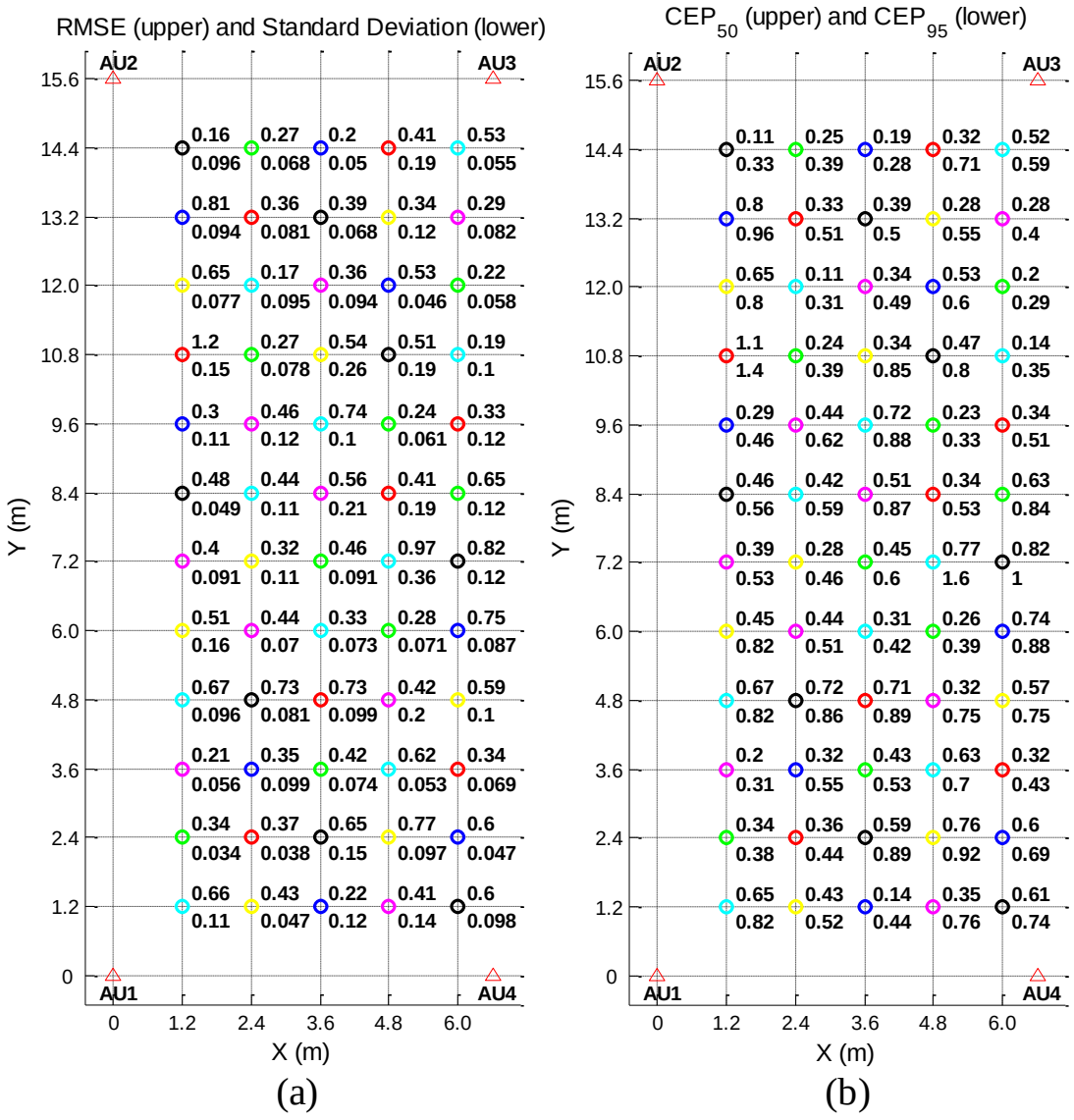


**Figure 6-25 Trial 3: (a) RMS error and the corresponding standard deviation; (b) $CEP_{50}$ and $CEP_{95}$ for the estimated locations.**

| Parameters | Values |
|---|---|
| RMS error | 0.47 m |
| $CEP_{50}$ | 0.44 m |
| $CEP_{95}$ | 0.63 m |

**Table 6-7 Trial 3: Average location performance**

To evaluate potential location accuracy with this sensor placement scheme, a ten-thousand run Monte Carlo simulation has been executed and the resulting RMS

location error against TDOA deviation curve is presented in both the Figure 6-26 and Figure 6-27. It is seen that majority of the TDOA standard deviations in the 60 experiments are at the range between 0.2 ns and 1.2 ns, which in theory shall ensure less than 0.5 m RMS location errors in all these experiments. However, due to multipath interference, the actual RMS location errors are clearly deviating from the prediction curve. Extents of these deviations suggest that the unresolved biased errors in the TDOA measurements are mainly between 0.6 ns to 2.8 ns, Figure 6-26.

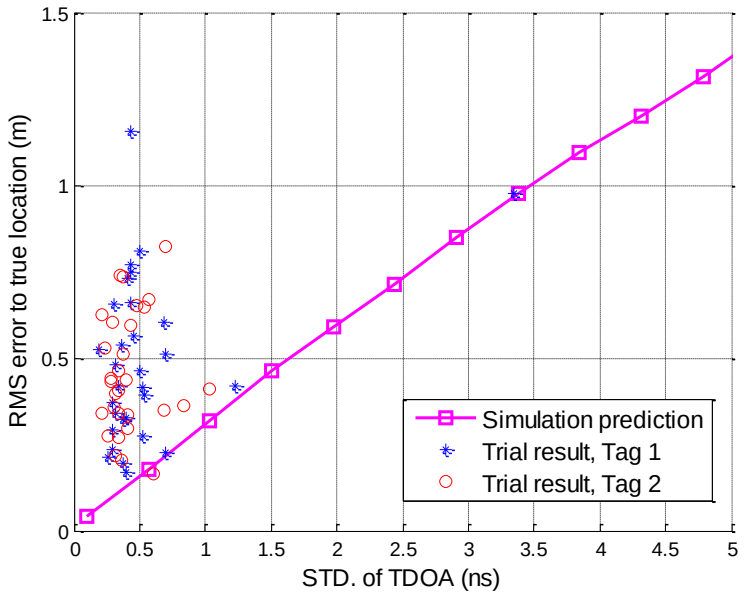


**Figure 6-26 Trial 3: RMS error with respect to true location vs. TDOA errors.**

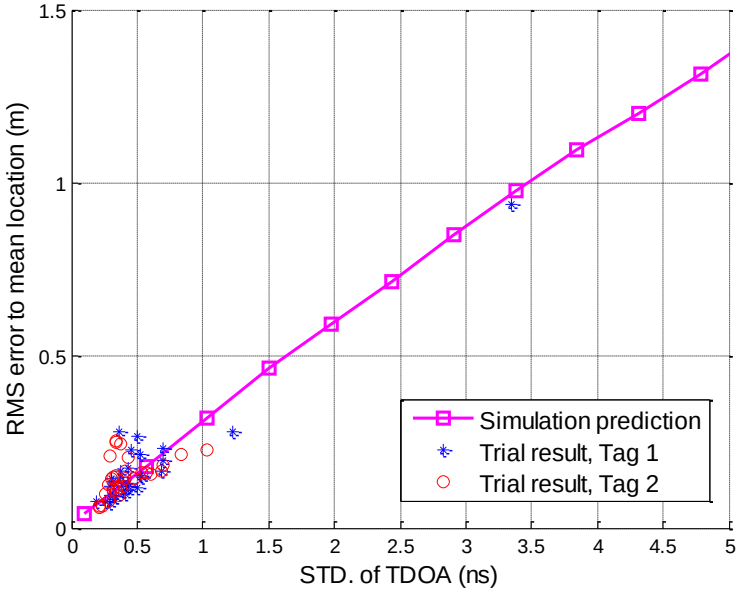


**Figure 6-27 Trial 3: RMS error with respect to mean location vs. TDOA errors.**

Since the multipath impact on the location results is in the form of additive range, causing a biased mean of estimated locations, the RMS location errors shall follow the prediction curve if these biases are removed. This is achieved by computing the RMS location errors with respect to the mean estimated location in each experiment, rather than to the true location. The results are plotted in the Figure 6-27, where measurement results and the theoretical prediction agree very well.

To summarise, the 4-AU corners placement scheme demonstrated in this trial has shown the best overall location accuracy when compared to the other two tested schemes. This is as expected by the error spreading patterns analysis (Figure 6-24) and the simulated curve (Figure 6-26). The high accuracy regions for this scheme are the end sides of the rectangular indoor cell, which is different from the 4-AU perimeters placement scheme whose high accuracy region is the central area of the cell.

## 6.6 Summary

This chapter links the theory, models, and system designs introduced in the previous chapters with real world experiments and the corresponding results. In the first section, the prototype demonstrator for the proposed indoor location system has been introduced and the installation procedure of such a system in a typical modern indoor area has also been described.

Although the final result of a location task is simply an estimated coordinate of a target, the long term performance of the location estimation depends on various conditions, e.g. signal quality, sensor placement schemes, multipath propagation, interference from other systems, and the location algorithm. Therefore, to evaluate the performance of the indoor location system, we chose and proposed four different tools, which assist us not only to find out the location error of the experiments, but also to understand the mechanism causing the results we observed. The four tools introduced in Section 6.2 are then used to interpret the trial results given in Section 6.3 to 6.5.

Three trials have been devised to demonstrate the functionality and performance of the demonstration system, which was developed according to the information given in the Chapter 5. Not surprisingly, the system has been able to deliver the better than 1 metre location accuracy as expected from the design. We have chosen 60 regularly spaced test points in the room as the known locations for experiments. One or two RFID tags were used in the trials. The estimated location results show that locations of the two tags can be resolved even when they are simultaneously transmitting. The demonstration system is able to locate the two tags with similar accuracy, as can be seen from the 2-D plot results of Trial 2 (Figure 6-19) and Trial 3 (Figure 6-24), which proves the co-existence of multiple tags.

In terms of location performance, the essential condition for good location accuracy is signal quality. If there is perfect line-of-sight propagation and the signal is not distorted by interference or noise, then any of the sensor placement schemes discussed in this Chapter would be able to deliver error-free location results. However, multipath, noise, and interference do exist in reality which causes variation of the estimated location from the true location.

The three different sensor placement schemes were tested to show how the placements of sensors can affect the possible variation of estimated locations. The types of variation can be firstly predicted using the TDOA mapping algorithm, which can produce the contour curves for specified TDOA measurement difference, namely the error spreading patterns. The error spreading patterns regarding a sensor placement scheme are dependent on the location of the measurement points. The results from the three trials have shown that estimated locations observed in these experiments deviate in a similar way to the corresponding error spreading patterns.

From these error spreading patterns, it is possible to figure out where in the indoor cell the relatively sensitive region will be for a sensor placement scheme. The concept of a sensitive region for a pair of sensors has been introduced in the Chapter 4. The sensitive region for a sensor placement scheme is an overlapping area of all or most of the sensitive regions, resulting from the available sensor pairs. Relatively finer variation of location results are expected if an RFID tag is placed in the sensitive region. As discussed in the previous sections the sensitive region is dependent on the positions of all the AUs. In Trial 1, the sensitive region was a triangular area in the

middle of the cell (Figure 6-10 and Figure 6-11). Regarding the two 4-AU schemes, their sensitive regions are also different from each other. The perimeters scheme forms its sensitive region in the centre of the cell; therefore we observed finer variation in the results recorded from the positions at the centre of the cell. By comparison, the corners scheme forms the sensitive regions at both ends of the cell, which seems to ensure better overall location performance. The overall location performance, measured by RMS location error and CEP, of the three difference schemes are summarised in Figure 6-28. It can be seen that the overall location accuracy of the 4-AU corners placement scheme is the best in terms of all the metrics used.

It has been discovered that, with 5 dBm transmitting power, the system is able to achieve good enough signal quality to induce less than 1 ns standard deviation in TDOA measurements (as referred to Figure 6-16, Figure 6-21, and Figure 6-26). However, the location accuracy achieved does not match the respective level that is predicted from the simulations. These results suggest that multipath is still the main contributor to errors in indoor location tasks, although the impact of multipath has been moderately mitigated by the frequency detection strategies introduced in the Chapter 5. Also, it is found that at a given position, the additive ranging error caused by multipath seems to behave stably over time, which results in the biased location estimations seen in Figure 6-11, Figure 6-19, and Figure 6-24.

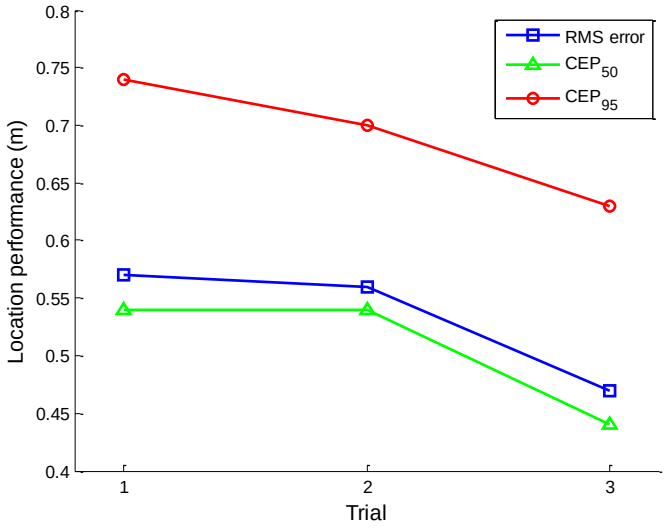


**Figure 6-28 Statistical results from the three trials.**

The discussion presented here, however, is not able to conclude that one of the sensor placement schemes will be the best in all cases, as the actual placement of sensors will depend on many practical requirements too. For example, if the potential targets usually appear in the centre of the room and rarely go to the end sides, the perimeters scheme will be preferred over the corners scheme. Therefore, the discussion above is attempting to show a way of analyzing the potential location performance from the planned sensor placements. This analysis flow has also been used in Section 6.3 to Section 6.5 and reasonably good agreement between theory and practical results has been observed. For example, the trial results presented have indicated that the simple rule of maximizing the sensitive region of the sensor pairs is applicable in practice. This can be used as a rough tool to evaluate the potential performance of a sensor placement plan. More detailed variation of estimated locations and their robustness to noise and interference can then be simulated using the TDOA mapping model. The expectable location accuracy can then be estimated using a Monte Carlo method, if the TDOA measurement deviation is given or assumed.

# *Chapter 7*

## CONCLUSION AND FUTURE WORK

In this thesis, we have presented and demonstrated probably the first indoor location system prototype using an RF-over-fibre (RoF) backbone. A novel TDOA location mapping algorithm was used to firstly estimate the location performance and also perform location finding during real-time experiments. Special signal processing techniques were used to identify and mitigate multipath effects. The achieved location accuracy in the three trials is comparable to the existing high precision indoor location systems which utilise more sophisticated communication protocols and are based on custom designed hardware. In addition, many aspects of design and implementation of an indoor location system have been studied during the research and there are multiple discoveries in this research that may be of use to future researchers.

In this chapter, these outcomes will be summarised along with a review of the conclusions drawn from this research work. Also, some potential research opportunities that have not been covered by this thesis are identified and discussed in the second section.

## 7.1 Conclusion

The research presented in this thesis is motivated by two recent technology trends. Firstly, there are growing interests in location-based applications and the location-awareness of mobile wireless systems in indoor areas, which necessitate accurate location estimation in indoor environments. Secondly, more and more wireless networks are adopting RoF as a low cost and flexible way to extend existing wireless coverage and provide multiple services. It is regarded as a future-proof technology [7] as RoF infrastructure is transparent to protocols and bit-rate. These trends trigger the pioneering idea of merging the two technologies to develop an indoor location system based on an RoF network.

This thesis firstly studies the conventional technologies discussed in the field of indoor location systems, it is found that there is lack of a system design strategy that is able to provide reliable high accuracy location performance over an infrastructure that can be shared by multiple wireless services. Some indoor location systems utilise GSM, WLAN, and other available wireless networks to perform location finding, but are usually not able to achieve good accuracy. The existing high accuracy indoor location systems either require costly stand-alone networks or have implemented abundant communications functionalities into their remote sensors to make them compatible with existing networks. These systems provide satisfying location performance for a higher price, in terms of the system complexity and cost involved in installation and maintenance of these systems.

On the other hand, by understanding the advantages of a RoF infrastructure and wireless location technologies, a novel and compact architecture for a TDOA measurement based location system using LFM chirp signals is proposed in this thesis. The TDOA location method chosen does not require synchronisation between user terminals and location sensors, and thus allows a simplification of the active RFID tag to a transmit-only design.

Another superior feature of the proposed system is that, the RoF infrastructure supports centralised RF signal processing, which allows simultaneous time difference measurement be implemented directly at the analog-to-digital conversion stage. Moreover, the wideband characteristic of an optical fibre link enables utilisation of a wideband LFM chirp signal as the tag transmitted waveform, which enables reliable time difference measurement.

The LFM chirp is adopted by the proposed TINA indoor location system to perform location finding through TDOA measurements. We have also studied the time delay determination technique using a LFM chirp and a deramping approach is used in the demonstration system.

During this study, a novel parameter, fractional slope variation (FSV), which describes the linearity of the chirp signal, has been derived so that the TDOA measurement resolution and required chirp linearity can be related. The practical use of this parameter has been shown in the Chapter 5. Considering the 83.5 MHz

bandwidth and 28 m maximum detection range specifications, it can be found that a fractional slope variation of 6.4% is required to ensure a non-distorted (with nonlinearity coefficient $a \leq 1$) point target response in the deramp process. With this conclusion, we realized that it cannot be readily met by typical VCO chips but may be fulfilled by carefully designed VCO-based chirp generator. However, frequency drift due to temperature change may cause potential uncertainty at the time measurement stage. On the other hand, DDS is able to provide not only the require linearity but also ease of configuration. Consequently, the highly linear DDS-based chirp generator is chosen as the signal source of the TINA user tag. With the signal source that produces linear chirp signals, the desired TDOA measurement can be performed and TDOA information between multiple sensor pairs of the system are determined.

The problem of solving the signal source location from the measured TDOAs (Chapter 4) was then encountered. A novel numerical algorithm called TDOA mapping is developed and its performance is compared with two existing algorithms. It is found that the proposed new method is able to produce results that approach theoretical bounds in the near field situation. The TDOA mapping algorithm is not only robust to TDOA measurement errors but also is easy to implement. It has been implemented in the demonstration system and the performance has been validated in the trials presented in Chapter 6. Furthermore, this algorithm is able to predict the error spreading pattern of the TDOA location finding method if the time error level is specified. This feature is used to analyse the relation between location finding errors and the placement scheme of location sensors. The concept of a sensitive region for TDOA sensors is proposed and it has been used to successfully predict the location spreading patterns in the three indoor location trials.

The complete indoor location system has been developed and the system design, from the RFID user tag, RoF network, to the RF receivers and central location processor, is summarised in Chapter 5. Use of a broadband optical fibre backbone simplifies system deployment by centralizing most communication hardware, e.g. base stations and servers, to a single location while the remote AUs can be designed to perform only simple transmit and receive tasks.

The impact of multipath propogation on location results has also been studied during tests of system in a real indoor environment. By analysing a great number of

deramped results and their spectra, the profile of multipath in the deramped spectrum, where the crucial time information is determined, have be modeled. According to the characteristics of multipath components, two simple yet useful frequency detection strategies are proposed to mitigate their impacts. Simulation and real measurement results have been used to clarify the correctness and performance of these strategies. It is found that there is over 90% possibility that the proposed strategies are able to reduce the range detection error by about 30 cm, when there is only one significant multipath component in the deramped output. The location estimation result is then improved and sub-metre location accuracy is achieved.

Finally, we have conducted three location trials in a large café with a grid of 6.6 m by 15.6 m. The optimised location system performed robustly despite a relatively low output power of 5 dBm and the presence of a large number of physical obstacles such as chairs and tables as well as WLAN interference. Co-existence with the WLAN has also been demonstrated by streaming live video from Internet using the WLAN connection while the location system was running.

The location results have been analyzed by means of a few statistic tools and the results show that about half metre RMS location accuracy was achieved in all of the three trials. The four AUs corners placement scheme produces the best results among the three schemes used (Chapter 6) and there is a 95% probability that 0.63 m location accuracy can be achieved from this system using the corresponding sensor placement scheme.

## 7.2 Future Work

Besides the outcome summarised in the discussion above, several areas that warrant further investigation are also identified.

The current system design can be improved in several ways. Currently, the demonstration system exhibits approximately -70 dBm sensitivity, since the oscilloscope uses 8-bit sampling resolution and provides minimum 1 mV per division scale. Therefore, there is no problem for the current demonstration system to receive signals from 20 to 30 m away. However, the receiver sensitivity can simply be

increased by using an acquisition device with higher resolution. This modification enables enlargement of the cell size of the system and thus fewer sensors are needed to cover a given indoor area.

The demonstration system presented uses a digital deramping technique, which requires a received chirp signal being digitised at high sampling rate (250 MSp/s). The resultant number of data from this process is large and therefore the location process is time consuming. An update rate of about 2 Hz was achieved during the trials for locating two user tags. This problem can be eliminated by deramping the received chirp signals in an analog way, by deramping the received chirp signals with a local reference chirp by means of an RF mixer. The trade-off is that an analog deramp processor may need to detect the presence of a received chirp and thus more sophisticated hardware may be required.

As mentioned in Chapter 6, burst interference signals from time to time affect the location results. These can be easily removed by applying a target movement speed threshold. For example, a human target is impossible to move at 100 miles per hour speed. Therefore, any detected change of location that indicates physical movement beyond this speed threshold shall be ignored by the algorithm.

These alterations will make the location system suitable for more application scenarios but do not improve the fundamental location accuracy. The location accuracy is likely to be improved if a larger signal bandwidth is available, or more location methods are integrated.

It would therefore be interesting to investigate the potential location performance if hybrid location methods are employed. For example, the use of smart antenna technology in the AUs can provide additional angle of arrival (AOA) information. This information can be used together with the already implemented TDOA information to perform even more robust location estimation. With hybrid location methods, the location algorithm may be optimised as well to fully utilise all the available information and possibly reduce the estimation time for each location task.

From the application point of view, there are also challenges that are increasingly being discussed, e.g. fast establishment of a location system at a building on fire. When fire fighters are sent to save people stranded by fire, it is valuable to actively

track the location of fire fighters. In such case, a location system that works for indoor environments shall be established in a few minutes, without knowing the size and shape of the area in advance. The indoor location algorithm proposed in this research is able to fit an arbitrary shape of location cell. However, most of the location systems need to be calibrated before operation and thus it will be valuable if this process can be shortened to a minimum.

In conclusion, it is hoped that the research presented in this thesis will act as a technology option for future lighter, cheaper, and yet better indoor location systems. Since the emerging indoor location based applications are very much diverse in terms of their application environments and requirements, there will not be a single technology or solution that will suit all scenarios. The benefits of an RoF based indoor location system had been demonstrated and hopefully this system will attract further investigation that advances its development.

# Resulting Publications

This research has resulted in the following publications:

- C. P. Liu, Y. Huang, T. Ismail, P. Brennan, and A. J. Seeds, "Demonstration of an indoor real-time location system with optical fibre backbone," *Microwave Photonics, 2009. MWP '09. International Topical Meeting on* , vol., no., pp.1-4, 14-16 Oct. 2009

- P. V. Brennan, Y. Huang, M. Ash, and K. Chetty, "Determination of sweep linearity requirements in FMCW radar systems based on simple voltage-controlled oscillator sources", *IEEE Transactions on Aerospace and Electronic Systems,* being published in edition 47(3), July 2011.

- Y. Huang, P. V. Brennan, and A. J. Seeds, "Active RFID location system based on time-difference measurement using a linear FM chirp tag signal," *Personal, Indoor and Mobile Radio Communications, 2008. PIMRC 2008. IEEE 19th International Symposium on* , vol., no., pp.1-5, 15-18 Sept. 2008

- P. V. Brennan, A. J. Seeds, and Y. Huang, "RF-ID Tag Location Using RF-over-fibre Techniques", in *Proc. of Progress in Electromagnetics Research Symposium, Prague*, 2007, pp. 255-260.

# References


[1] H. Oman, "Global Positioning System, opportunities and problems," *Aerospace and Electronic Systems Magazine, IEEE*, vol. 10, no. 7, pp. 35, 37, 39, July1995.

[2] J. G. McNeff, "The global positioning system," *Microwave Theory and Techniques, IEEE Transactions on*, vol. 50, no. 3, pp. 645-652, Mar.2002.

[3] "Global Positioning System-the newest utility," *Aerospace and Electronic Systems Magazine, IEEE*, vol. 15, no. 10, pp. 89-95, Oct.2000.

[4] M. Vossiek, L. Wiebking, P. Gulden, J. Weighardt, and C. Hoffmann, "Wireless local positioning - concepts, solutions, applications", in *Radio and Wireless Conference, 2003. RAWCON '03. Proceedings*, pp. 219-224, 2003.

[5] F. Dovis, R. Lesca, D. Margaria, G. Boiero, and G. Ghinamo, "An assisted high-sensitivity acquisition technique for GPS indoor positioning", in *Position, Location and Navigation Symposium, 2008 IEEE/ION*, pp. 1350-1361, 2008.

[6] P. Gulden, S. Roehr, and M. Christmann, "An overview of wireless local positioning system configurations", in *Wireless Sensing, Local Positioning, and RFID, 2009. IMWS 2009. IEEE MTT-S International Microwave Workshop on*, pp. 1-4, 2009.

[7] T. Koonen, "Fiber to the Home/Fiber to the Premises: What, Where, and When?," *Proceedings of the IEEE*, vol. 94, no. 5, pp. 911-934, May2006.

[8] J. Zhensheng, Y. Jianjun, C. Arshad, G. Ellinas, and C. Gee-Kung, "Simultaneous Generation of Independent Wired and Wireless Services Using a Single Modulator in Millimeter-Wave-Band Radio-Over-Fiber Systems," *Photonics Technology Letters, IEEE*, vol. 19, no. 20, pp. 1691-1693, Oct.2007.

[9] W. R. Kim and D. S. Shin, "Performance estimation on the passive-picocell radio-over-fiber system using the low-detuned electroabsorption transceiver", in *Microwave Photonics, 2008. Jointly held with the 2008 Asia-Pacific Microwave Photonics Conference. MWP/APMP 2008. International Topicsl Meeting on*, pp. 229-231, 2008.

[10] R. Alemany and R. Llorente, "UMTS radio-over-fiber pico-cell interconnection employing low-cost VCSELs and multi-mode fibre", in *Transparent Optical Networks, 2009. ICTON '09. 11th International Conference on*, pp. 1-5, 2009.

[11] D. Visani, G. Tartarini, L. Tarlazzi, and P. Faccin, "Transmission of UMTS and WIMAX Signals Over Cost-Effective Radio Over Fiber Systems,"

*Microwave and Wireless Components Letters, IEEE*, vol. 19, no. 12, pp. 831-833, Dec.2009.

[12] W. H. Foy, "Position-Location Solutions by Taylor-Series Estimation," *Aerospace and Electronic Systems, IEEE Transactions on*, vol. AES-12, no. 2, pp. 187-194, 1976.

[13] Mark Weiser, "The computer for the 21st century," *SIGMOBILE Mob. Comput. Commun. Rev.*, vol. 3, no. 3, pp. 3-11, 1999.

[14] Federal Communications Commission (FCC)., "Revisioin of Part 15 of the commission's rules regarding ultra-wideband transmission systems: First report and order,"ET-Docket, Apr.2002.

[15] W. Sun, D. Xue, D. Zheng, L. H. Dong, and C. Zhou, "A study of real-time location system in logistics management based on active RFID," *Proceedings of the 4Th International Conference on Intelligent Logistics Systems*, pp. 10-16, 2008.

[16] L. Hui, H. Darabi, P. Banerjee, and L. Jing, "Survey of Wireless Indoor Positioning Techniques and Systems," *Systems, Man, and Cybernetics, Part C: Applications and Reviews, IEEE Transactions on*, vol. 37, no. 6, pp. 1067-1080, 2007.

[17] A. Boukerche, H. A. B. Oliveira, E. F. Nakamura, and A. A. F. Loureiro, "Localization systems for wireless sensor networks," *Wireless Communications, IEEE*, vol. 14, no. 6, pp. 6-12, Dec.2007.

[18] L. Xinrong, "RSS-Based Location Estimation with Unknown Pathloss Model," *Wireless Communications, IEEE Transactions on*, vol. 5, no. 12, pp. 3626-3633, Dec.2006.

[19] P. Bergamo and G. Mazzini, "Localization in sensor networks with fading and mobility", in *Personal, Indoor and Mobile Radio Communications, 2002. The 13th IEEE International Symposium on*, 2 ed pp. 750-754, 2002.

[20] N. Patwari, A. O. Hero, III, M. Perkins, N. S. Correal, and R. J. O'Dea, "Relative location estimation in wireless sensor networks," *Signal Processing, IEEE Transactions on*, vol. 51, no. 8, pp. 2137-2148, Aug.2003.

[21] A. S. Paul and E. A. Wan, "RSSI-Based Indoor Localization and Tracking Using Sigma-Point Kalman Smoothers," *Selected Topics in Signal Processing, IEEE Journal of*, vol. 3, no. 5, pp. 860-873, Oct.2009.

[22] A. Hyo-Sung and Y. Wonpil, "Environmental-Adaptive RSSI-Based Indoor Localization," *Automation Science and Engineering, IEEE Transactions on*, vol. 6, no. 4, pp. 626-633, Oct.2009.

[23] P. Bahl and V. N. Padmanabhan, "RADAR: an in-building RF-based user location and tracking system", in *INFOCOM 2000. Nineteenth Annual Joint Conference of the IEEE Computer and Communications Societies. Proceedings. IEEE*, 2 ed pp. 775-784, 2000.

[24] L. M. Ni, L. Yunhao, C. L. Yiu, and A. P. Patil, "LANDMARC: indoor location sensing using active RFID", in *Pervasive Computing and Communications, 2003. (PerCom 2003). Proceedings of the First IEEE International Conference on*, pp. 407-415, 2003.

[25] D. J. Torrieri, "Statistical Theory of Passive Location Systems," *Aerospace and Electronic Systems, IEEE Transactions on*, vol. AES-20, no. 2, pp. 183-198, Mar.1984.

[26] K. Finkenzeller, *RFID handbook : fundamentals and applications in contactless smart cards and identification* Wiley, 2003.

[27] K. Opasjumruskit, T. Thanthipwan, O. Sathusen, P. Sirinamarattana, P. Gadmanee, E. Pootarapan, N. Wongkomet, A. Thanachayanont, and M. Thamsirianunt, "Self-powered wireless temperature sensors exploit RFID technology," *Pervasive Computing, IEEE*, vol. 5, no. 1, pp. 54-61, Jan.2006.

[28] S. R. Munnangi, G. Haobijam, M. Kothamasu, R. Paily, and R. S. Kshetrimayum, "CMOS capacitive pressure sensor design and integration with RFID tag for biomedical applications", in *TENCON 2008 - 2008 IEEE Region 10 Conference*, pp. 1-6, 2008.

[29] K. Chang, Y. H. Kim, Y. J. Kim, and Y. J. Yoon, "Functional antenna integrated with relative humidity sensor using synthesised polyimide for passive RFID sensing," *Electronics Letters*, vol. 43, no. 5, pp. 7-8, Mar.2007.

[30] Zebra Active RFID location technologies, available at http://zes.zebra.com, 2010.

[31] FCC News Report, "New Public Safety Applications and Broadband Internet Access Among Uses Envisioned by FCC Authorization of Ultra-Wideband Technology,"docket 98-153, Feb.2002.

[32] M. Bocquet, C. Loyez, and A. larbi-Delai, "Millimeter ultra wide band positioning system", in *Wireless Technology, 2004. 7th European Conference on*, pp. 265-268, 2004.

[33] S. Gezici, T. Zhi, G. B. Giannakis, H. Kobayashi, A. F. Molisch, H. V. Poor, and Z. Sahinoglu, "Localization via ultra-wideband radios: a look at positioning aspects for future sensor networks," *Signal Processing Magazine, IEEE*, vol. 22, no. 4, pp. 70-84, July2005.

[34] Ubisense Real-Time Location System Factsheets, available at www.ubisense.net, 2009.

[35] Yanying Gu, Anthony Lo, and Ignas Niemegeers, "A Survey of Indoor Positioning Systems for Wireless Personal Networks," *IEEE Communications Surveys & Tutorials*, vol. 11, pp. 13-32, 2009.

[36] Thales Research and Technology, "Emergency Services Site Information System," available at http://www.thalesgroup.com,2008.

[37] Tima Domain, "Datasheet of the Time Domain Precision Location Ultra-wideband System," available at http://www.timedomain.com,2010.

[38] V. Otsason, A. Varshavsky, A. LaMarca, and E. de Lara, "Accurate GSM Indoor Localization," in *UbiComp 2005: Ubiquitous Computing*, 3660 ed. M. Beigl, S. Intille, J. Rekimoto, and H. Tokuda, Eds. Springer Berlin / Heidelberg, 2005, pp. 141-158.

[39] N. Tyler, "CDMA mobile station location", in *Novel Methods of Location and Tracking of Cellular Mobiles and Their System Applications (Ref. No. 1999/046), IEE Colloquium on*, pp. 5-1-5/6, 1999.

[40] J. Caffery, Jr. and G. L. Stuber, "Subscriber location in CDMA cellular networks," *Vehicular Technology, IEEE Transactions on*, vol. 47, no. 2, pp. 406-416, May1998.

[41] P.Bahl and V.Padmanabhan, "RADAR: An In-building RF based user location and tracking system", in *IEEE INFOCOM*, 2 ed pp. 775-784, 2000.

[42] Ekahau, available at www.ekahau.com, 2008.

[43] AeroScout, "AeroScout Location and visibility processing for accurate and reliable asset information," Available at www.aeroscout.com/files/AeroScout Engine Data Sheet.pdf,2008.

[44] Frank Van Diggelen, "GNSS Accuracy: Lies, Damn Lies, and Statistics," *GPS World*, vol. 18 Jan.2007.

[45] P.Steggles and S.Gschwind, "The Ubisense Smart Space Platform," Available from www.ubisense.net, 2009.

[46] G. W. Stimson, *Introduction to Airborne Radar (2nd Edition)* SciTech Publishing, 1998.

[47] N. Levanon and E. Mozeson, *Radar Signals* A John Wiley & Sons Inc., 2004.

[48] H. D. Griffiths, "New ideas in FM radar," *Electronics & Communication Engineering Journal*, vol. 2, no. 5, pp. 185-194, Oct.1990.

[49] W. S. Burdic, *Radar Signal analysis* Prentice-Hall, Inc., 1968.

[50] A. Meta, P. Hoogeboom, and L. P. Ligthart, "Signal Processing for FMCW SAR," *Geoscience and Remote Sensing, IEEE Transactions on*, vol. 45, no. 11, pp. 3519-3532, Nov.2007.

[51] W. Q. Wang, "Analysis of waveform errors in millimeter-wave LFMCW synthetic aperture radar," *Int. J. Infrared and Millimetre. Waves*, vol. 27, pp. 1433-1444, Nov.2006.

[52] S. O. Piper, "Homodyne FMCW radar range resolution effects with sinusoidal nonlinearities in the frequency sweep", in *Radar Conference, 1995.*, pp. 563-567, 1995.

[53] P. Brennan, Y. Huang, M. Ash, and K. Chetty, "Determination of sweep linearity requirement in FMCW radar systems based on simple voltage-controlled oscillator sources," 2010.

[54] "General Performance Specification for Oscillator, Crystal Controlled," Department of Defense, U.S.,2006.

[55] M. Pichler, A. Stelzer, P. Gulden, C. Seisenberger, and M. Vossiek, "Phase-Error Measurement and Compensation in PLL Frequency Synthesizers for FMCW Sensors—II: Theory," *Circuits and Systems I: Regular Papers, IEEE Transactions on*, vol. 54, no. 6, pp. 1224-1235, June2007.

[56] Y. Liu, D. Goshi, K. Mai, L. Bui, and Y. Shih, "Linearity study of DDS-based W-band FMCW sensor", in *Microwave Symposium Digest, 2009. MTT '09. IEEE MTT-S International*, pp. 1697-1700, 2009.

[57] R. Casas, D. Cuartielles, A. Marco, H. J. Gracia, and J. L. Falco, "Hidden Issues in Deploying an Indoor Location System," *Pervasive Computing, IEEE*, vol. 6, no. 2, pp. 62-69, 2007.

[58] Y. Norouzi and M. Derakhshani, "Joint time difference of arrival/angle of arrival position finding in passive radar," *Radar, Sonar & Navigation, IET*, vol. 3, no. 2, pp. 167-176, 2009.

[59] Z. Yilin, "Standardization of mobile phone positioning for 3G systems," *Communications Magazine, IEEE*, vol. 40, no. 7, pp. 108-116, 2002.

[60] Y. Norouzi and M. Derakhshani, "Joint time difference of arrival/angle of arrival position finding in passive radar," *Radar, Sonar & Navigation, IET*, vol. 3, no. 2, pp. 167-176, 2009.

[61] J. P. Van Etten, "Navigation System: Fundamental of low and very-low frequency hyperbolic techniques," *Electronics & Communication Engineering Journal*, vol. 45, no. 3, pp. 192-212, 1970.

[62] R. Bucher and D. Misra, "A Synthesizable VHDL Model of the Exact Solution for Three-dimensional Hyperbolic Positioning System," *VLSI Design*, vol. 15, no. 2, pp. 507-520, 2002.

[63] B. T. Fang, "Simple solutions for hyperbolic and related position fixes," *Aerospace and Electronic Systems, IEEE Transactions on*, vol. 26, no. 5, pp. 748-753, 1990.

[64] G. Mellen, II, M. Pachter, and J. Raquet, "Closed-form solution for determining emitter location using time difference of arrival measurements," *Aerospace and Electronic Systems, IEEE Transactions on*, vol. 39, no. 3, pp. 1056-1058, 2003.

[65] Y. T. Chan and K. C. Ho, "A simple and efficient estimator for hyperbolic location," *Signal Processing, IEEE Transactions on*, vol. 42, no. 8, pp. 1905-1915, 1994.

[66] J. Ju-Wook, S. B. Choi, and V. K. Prasanna, "Energy- and time-efficient matrix multiplication on FPGAs," *Very Large Scale Integration (VLSI) Systems, IEEE Transactions on*, vol. 13, no. 11, pp. 1305-1319, 2005.

[67] Z. Ling and V. K. Prasanna, "High-Performance Designs for Linear Algebra Operations on Reconfigurable Hardware," *Computers, IEEE Transactions on*, vol. 57, no. 8, pp. 1057-1071, 2008.

[68] W. He-Wen and Y. Shang-Fu, "Comments on "A Linear Closed-Form Algorithm for Source Localization From Time-Differences of Arrival"," *Signal Processing Letters, IEEE*, vol. 15, p. 895, 2008.

[69] W. Hahn and S. Tretter, "Optimum processing for delay-vector estimation in passive signal arrays," *Information Theory, IEEE Transactions on*, vol. 19, no. 5, pp. 608-614, Sept.1973.

[70] G. Carter, "Time delay estimation for passive sonar signal processing," *Acoustics, Speech and Signal Processing, IEEE Transactions on*, vol. 29, no. 3, pp. 463-470, June1981.

[71] C. P. Liu, Y. Huang, T. Ismail, P. Brennan, and A. Seeds, "Demonstration of an indoor real-time location system with optical fibre backbone", in *Microwave Photonics, 2009. MWP '09. International Topical Meeting on*, pp. 1-4, 2009.

[72] European Radiocommunications Committee (ERC), "The European Table of Frequency Allocations and Utilisations Covering the Frequency Range 9 kHz to 275 GHz," Dublin,2003.

[73] National Frequency Planning Group, "United Kingdom Table of Frequency Allocations,"2002.

[74] A. J. Seeds and K. J. Williams, "Microwave Photonics," *Lightwave Technology, Journal of*, vol. 24, no. 12, pp. 4628-4641, Dec.2006.

[75] W. Qixing, J. Dajie, J. Jing, L. Guangyi, Y. Zhigang, and Y. Dacheng, "Application of BBU+RRU Based Comp System to LTE-Advanced", in *Communications Workshops, 2009. ICC Workshops 2009. IEEE International Conference on*, pp. 1-5, 2009.

[76] Z. Congqing, Z. Tiankui, Z. Zhimin, L. Cuthbert, and X. Lin, "Optimal Locations of Remote Radio Units in CoMP Systems for Energy Efficiency", in *Vehicular Technology Conference Fall (VTC 2010-Fall), 2010 IEEE 72nd*, pp. 1-5, 2010.

[77] C. P. Liu, A. J. Seeds, J. S. Chadha, P. N. Stavrinou, G. Parry, M. Whitehead, A. Krysa, and J. S. Roberts, "Normal-incidence 1.56-μm MQW asymmetric Fabry-Perot modulator (AFPM) for passive picocells", in

*Microwave Photonics, 2002. International Topical Meeting on,* pp. 49-52, 2002.

[78] N. Levanon, *Radar principles* New York : Wiley, 1988.

[79] B.-G. Goldberg, "Generate digital chirp signals with DDS," Microwaves & RF,2006.

[80] M.R.Winkler, *Chirp signals for communications,* IEEE WESCON, Conv. Rec., 1962.

[81] C. E. Cook, "Linear FM Signal Formats for Beacon and Communication Systems," *Aerospace and Electronic Systems, IEEE Transactions on*, vol. AES-10, no. 4, pp. 471-478, July1974.

[82] M.L.Meade and C.R.Dillon, *Signals and Systems (Tutorial guides in electronic engineering series)*, 2nd ed 1991.

[83] Z. Bin, M. Kobayashi, and M. Shimizu, "To read transmitter-only RFID tags with confidence", in *Personal, Indoor and Mobile Radio Communications, 2004. PIMRC 2004. 15th IEEE International Symposium on,* 1 ed pp. 396-400, 2004.

[84] Z. Bin, K. Mizuno, M. Kobayashi, and M. Shimizu, "Pulse Position Modulation for Active RFID System", in *Parallel and Distributed Systems, 2005. Proceedings. 11th International Conference on,* 2 ed pp. 58-62, 2005.

[85] C. B. Dietrich, Jr., K. Dietze, J. R. Nealy, and W. L. Stutzman, "Spatial, polarization, and pattern diversity for wireless handheld terminals," *Antennas and Propagation, IEEE Transactions on*, vol. 49, no. 9, pp. 1271-1281, 2001.

[86] S. Sussman, "A matched filter communication system for multipath channels," *Information Theory, IRE Transactions on*, vol. 6, no. 3, pp. 367-373, 1960.

[87] N. W. K. Lo, D. D. Falconer, and A. U. H. Sheikh, "Adaptive equalization for co-channel interference in a multipath fading environment," *Communications, IEEE Transactions on*, vol. 43, no. 234, pp. 1441-1453, 1995.

[88] L. Qilian, "Nonlinear equalization for Rician multipath fading channel", in *Acoustics, Speech, and Signal Processing, 2003. Proceedings. (ICASSP '03). 2003 IEEE International Conference on,* 6 ed p. VI-8, 2003.

[89] E. Fishler and B. Z. Bobrovsky, "Anti multipath cellular radio location for DS/CDMA systems using a novel EKF subchip RAKE tracking loop", in *Military Communications Conference Proceedings, 1999. MILCOM 1999. IEEE,* 2 ed pp. 1328-1332, 1999.

[90] G. L. Turin, "Introduction to spread-spectrum antimultipath techniques and their application to urban digital radio," *Proceedings of the IEEE,* vol. 68, no. 3, pp. 328-353, 1980.

[91] T. Ywh-Ren and C. Jin-Fu, "The feasibility of combating multipath interference by chirp spread spectrum techniques over Rayleigh and Rician fading channels", in *Spread Spectrum Techniques and Applications, 1994. IEEE ISSSTA '94., IEEE Third International Symposium on,* pp. 282-286, 1994.

[92] H. Farrokhi, "TOA Estimation using Music Super-Resolution Techniques for an Indoor Audible Chirp Ranging System", in *Signal Processing and Communications, 2007. ICSPC 2007. IEEE International Conference on,* pp. 987-990, 2007.

[93] M. Bocquet, C. Loyez, and A. larbi-Delai, "Using enhanced-TDOA measurement for indoor positioning," *Microwave and Wireless Components Letters, IEEE,* vol. 15, no. 10, pp. 612-614, 2005.

[94] G. Feng-Xiang, S. Dongxu, P. Yingning, and V. O. K. Li, "Super-Resolution Time Delay Estimation in Multipath Environments," *Circuits and Systems I: Regular Papers, IEEE Transactions on*, vol. 54, no. 9, pp. 1977-1986, 2007.

[95] Y. Song, Y. Zhuo, and L. Wang, "A Fast Estimation of Multipath Delay Using Chirp Signal", in *Communications and Mobile Computing (CMC), 2010 International Conference on,* 2 ed pp. 510-514, 2010.